

57185
P.178

NASA CONTRACTOR
REPORT



NASA CR-4

N63-22806

NASA CR-4

EXPLORER VI AND PIONEER V DATA

VOLUME II: A COMPENDIUM OF
EXPLORER VI DATA

by Alan Rosen and Edward J. Smith

Prepared under Contract No. NASw-270 by
SPACE TECHNOLOGY LABORATORIES, INC.
Redondo Beach, California
for

NATIONAL AERONAUTICS AND SPACE ADMINISTRATION • WASHINGTON, D.C. • OCTOBER 1963

CONTRACTOR REPORT CR-4

**EXPLORER VI AND PIONEER V DATA
VOLUME II: A COMPENDIUM OF
EXPLORER VI DATA**

By Alan Rosen and Edward J. Smith

**Prepared under Contract No. NASw-270 by
SPACE TECHNOLOGY LABORATORIES, INC.
Redondo Beach, California**

for

NATIONAL AERONAUTICS AND SPACE ADMINISTRATION

CONTRACTOR REPORT CR-4

EXPLORER VI AND PIONEER V DATA
VOLUME II: A COMPENDIUM OF
EXPLORER VI DATA

By Alan Rosen and Edward J. Smith
Space Technology Laboratories, Inc.

ABSTRACT

The data obtained from the scintillation counter experiment and the search coil magnetometer experiments on the Explorer VI satellite are presented graphically. A compendium of data on the field magnitude and phase angle is included. Such data should be of value to scientists studying the properties of the exosphere in the period of August 7 and October 6, 1959.

NATIONAL AERONAUTICS AND SPACE ADMINISTRATION

TABLE OF CONTENTS

	Page
CHAPTER I A Compendium of Data Obtained from the Scintillation Counter Experiment on the Explorer VI Satellite by Alan Rosen	1
Part A Introduction	1
Part B A Compendium of Data Taken with the Explorer VI Scintillation Counter	8
CHAPTER II A Compendium of Data Obtained from the Explorer VI Search Coil Magnetometer by Edward J. Smith	97
Introduction	99
Data Compendium: Field Magnitude	111
Data Compendium: Phase Angle	141
Appendix Computation of B_{\perp} and χ	163

CHAPTER I

A COMPENDIUM OF DATA OBTAINED FROM THE SCINTILLATION
COUNTER EXPERIMENT ON THE EXPLORER VI SATELLITE

by

Alan Rosen

PART A. INTRODUCTION

The graphs in Part B represent a major fraction of the data obtained from the Explorer VI Scintillation Counter during the months of August and September 1959. The graphs are ordered chronologically. At the bottom of each is a nomograph giving the geomagnetic latitude and radial distance associated with the plotted count rate at any instant of time. These count rates have been corrected for the saturation effect inherent in the scintillation counter. The following is a description of the instrument and its efficiency for detection of various particles.

INSTRUMENTATION

The detector used in this experiment consisted of a cylindrical plastic scintillator, approximately one inch in diameter and one-quarter inch thick, cemented to a Dumont 6467 photomultiplier tube. The output pulses of the photomultiplier were amplified and fed into a binary register having a capacity of 2^{20} pulses. Voltages representing the state (on or off) of the ninth, fourteenth, and twentieth binaries were added and used to modulate a subcarrier oscillator, so that transitions between the states of these binaries could be used to determine the counting rate. The output of the 2^{20} binary was also fed into a digital register whose contents were broadcast in digital form by a second transmitter.

The detector was covered with a foil having a thickness of 3.3 mg/cm^2 . An electronic bias was used in order to count only particles losing 100 kev or more of energy in the scintillator; this bias was

adjusted by using the 624 kev electron conversion peak of Cs^{137} as an energy standard. This instrument, mounted inside the shell of the satellite, responded to radiation penetrating a 3.3 mg/cm^2 foil-covered window, and to more energetic particles passing through the payload shell. The minimum energy detectable, determined by the foil thickness, the permitted angle of penetration of the foils, and the electronic bias of 100 kev, was 200 kev for electrons and 2 Mev for protons.

The omnidirectional geometrical factor* of this instrument for the direct observation of electrons and protons was estimated from geometrical considerations to be approximately $2 \times 10^{-4} \text{ cm}^2$ for 200 to 500 kev electrons and 2 to 10 Mev protons. Five hundred kev electrons and 10 Mev protons could just penetrate the shell and be detected, and at these energies the omnidirectional geometrical factor was estimated to be $4 \times 10^{-2} \text{ cm}^2$. The geometrical factor rose slowly to a maximum value of 3.5 cm^2 for very penetrating particles.

The saturation characteristic of the entire detector system, including flight power supply and all flight electronics, was determined before the satellite was launched by tests made on the actual flight instrument. The results of this test are shown in Figure 1. A one millicurie source

*The omnidirectional geometrical factor G , which depends on the counter surface area and the solid angle through which radiation can reach the counter, is defined by $\epsilon G = R/J$. R is the corrected counting rate of the detector and J , the omnidirectional intensity of isotropic radiation, is the flux per unit time of particles from all directions through a sphere of unit cross-sectional area (J is measured in $\text{cm}^{-2} \text{ sec}^{-1}$). ϵ , the detection efficiency for the radiation in question, is assumed to be 100 percent for electrons and protons.

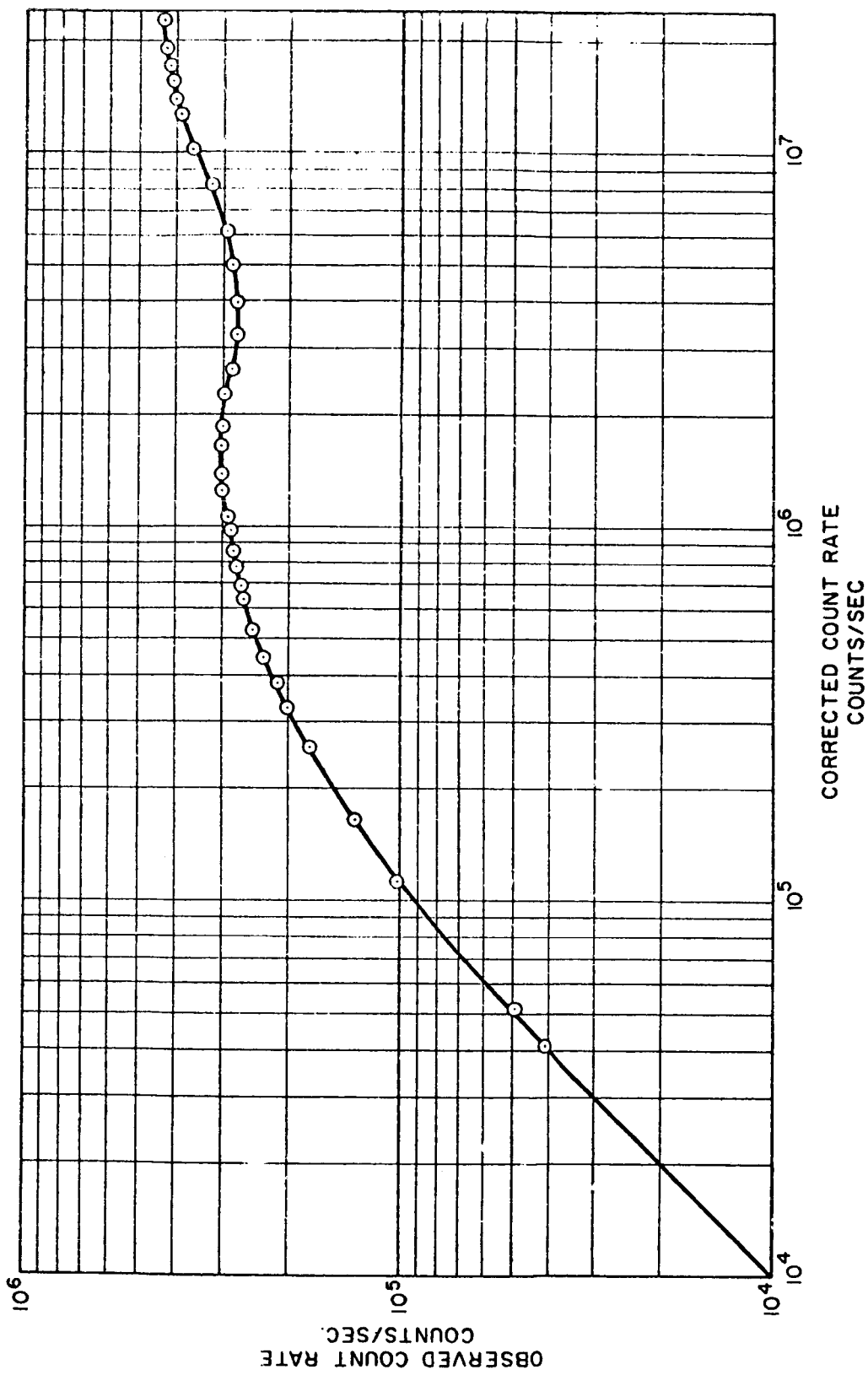


Figure 1. Observed count rate of the flight instrument as a function of incident intensity of Sr⁹⁰ source. The data points were obtained in a laboratory measurement before flight on the actual detector, power, supply, and electronics which were used in the satellite. This curve has been used to correct the count rate for saturation effects.

of Sr⁹⁰ was used for this test, and the incident intensity was increased by decreasing the source to detector distance. The observed count rate continued to rise slowly, even for very high incident intensities, because the potential across the later dynode resistors of the photomultiplier dropped, the output pulse height and width decreased, and a higher count rate could be handled by the succeeding electronic circuitry.

The scintillation counter was relatively insensitive to bremsstrahlung, and the counting rate of this instrument due to electrons of a given energy must considerably exceed the count rate due to bremsstrahlung from electrons at the same incident energy. The only photon interaction of importance in a plastic scintillator is the Compton interaction, and because of the electronic bias of 100 kev, the theoretical threshold for photon detection was about 220 kev. Electrons having energies below the threshold could not produce bremsstrahlung which would be registered by the detector. Because a plastic scintillator has a low efficiency for detection of photons above 220 kev, and because electrons having energies of several hundred kev have a small probability of producing 220 kev photons, the instrument responded principally to direct electrons at all energies.

The calculated estimates of the efficiency and geometrical factor for bremsstrahlung detection were confirmed by measurements after Explorer VI was launched on a similar instrument with the same bias level. An entire payload, identical to Explorer VI, was subjected to an electron bombardment at the High Voltage Engineering Corporation in order to

measure the response of the various radiation instruments to electrons at 1 Mev, and to bremsstrahlung from monoenergetic electrons at 500 kev, 350 kev and 250 kev. At 1 Mev the electrons were permitted to strike the payload directly, while at 500 kev, 350 kev, and 250 kev, the electron beam was absorbed in an aluminum plate placed near the payload allowing only bremsstrahlung to reach the satellite. The bombardment was made from a variety of directions, and the response was integrated over the surface of the payload to measure the product ϵG for each of these energies. These measurements represent the bremsstrahlung efficiency even at 1 Mev, for the scintillation counter was never directly in the rather narrow electron beam. These results are shown in Figure 2 together with the estimated geometrical factors for direct detection of electrons. The total response of the detector for measurement of electron flux is the sum of these two curves, and is also shown in the Figure. It is this total response curve which must be used to interpret the counting rate of the instrument in orbit.

The graphs representing the Compendium of data are labeled with a pass number. This represents the number of revolutions of the satellite around the earth numbered consecutively from the launch date. As the satellite traverses through one complete revolution around the earth, the following characteristics in the observed count rate emerge. As the satellite goes from perigee to apogee, it traverses the heart of the radiation zones and the peaks, exemplified by the first compendium figure, are observed. At apogee, as the satellite begins its return pass, the count rate is low. Furthermore, the satellite is at high enough

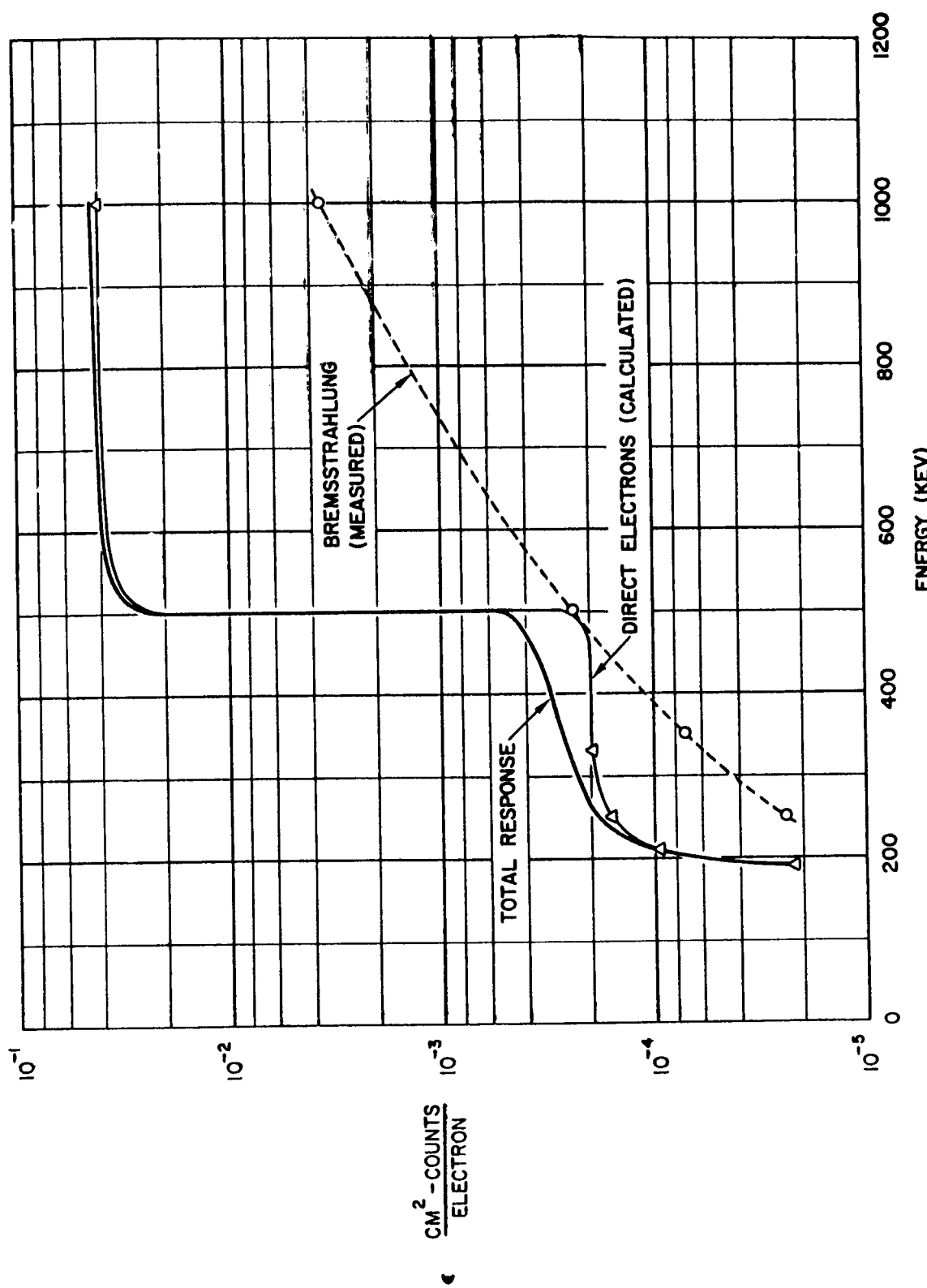
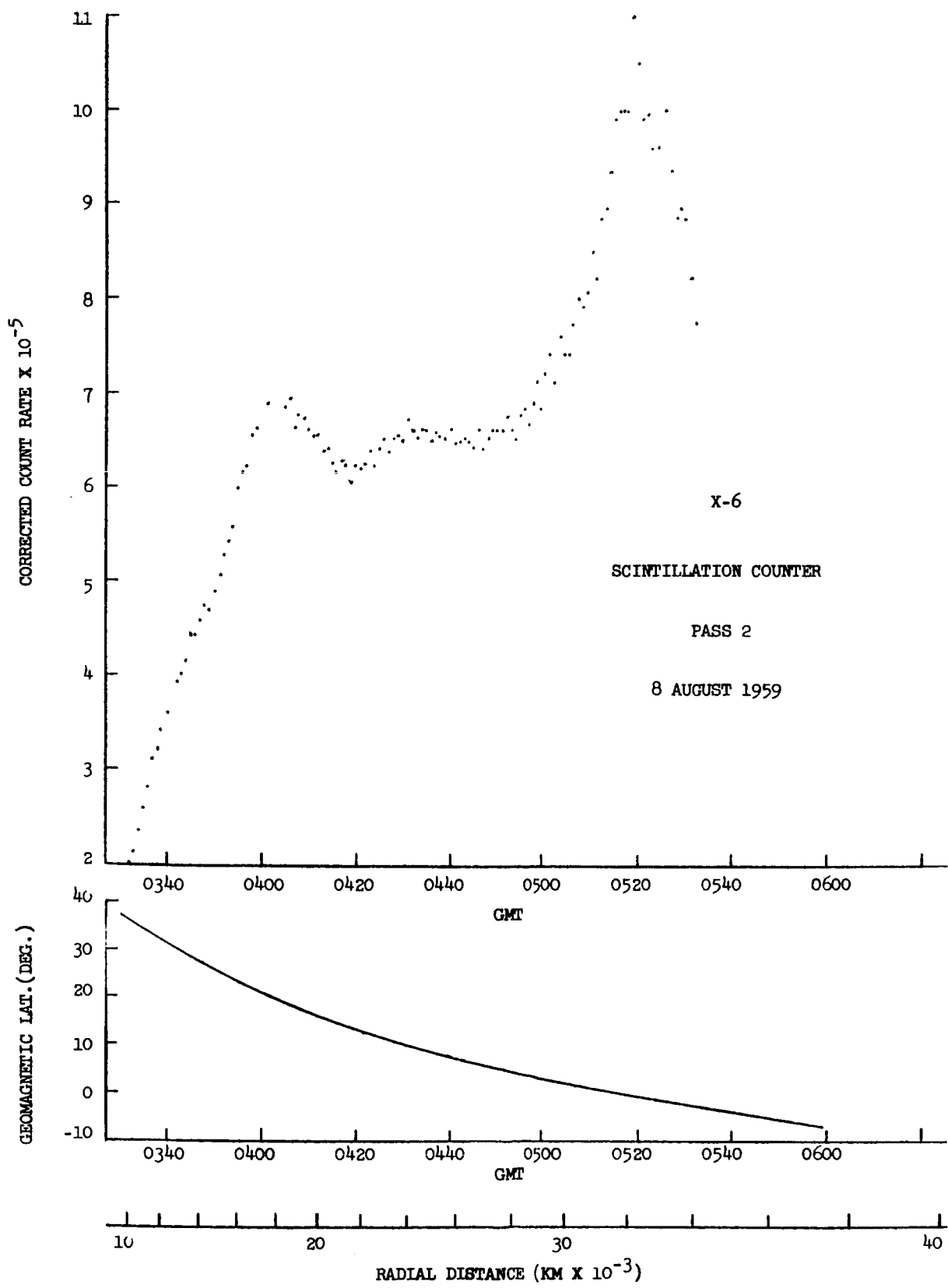


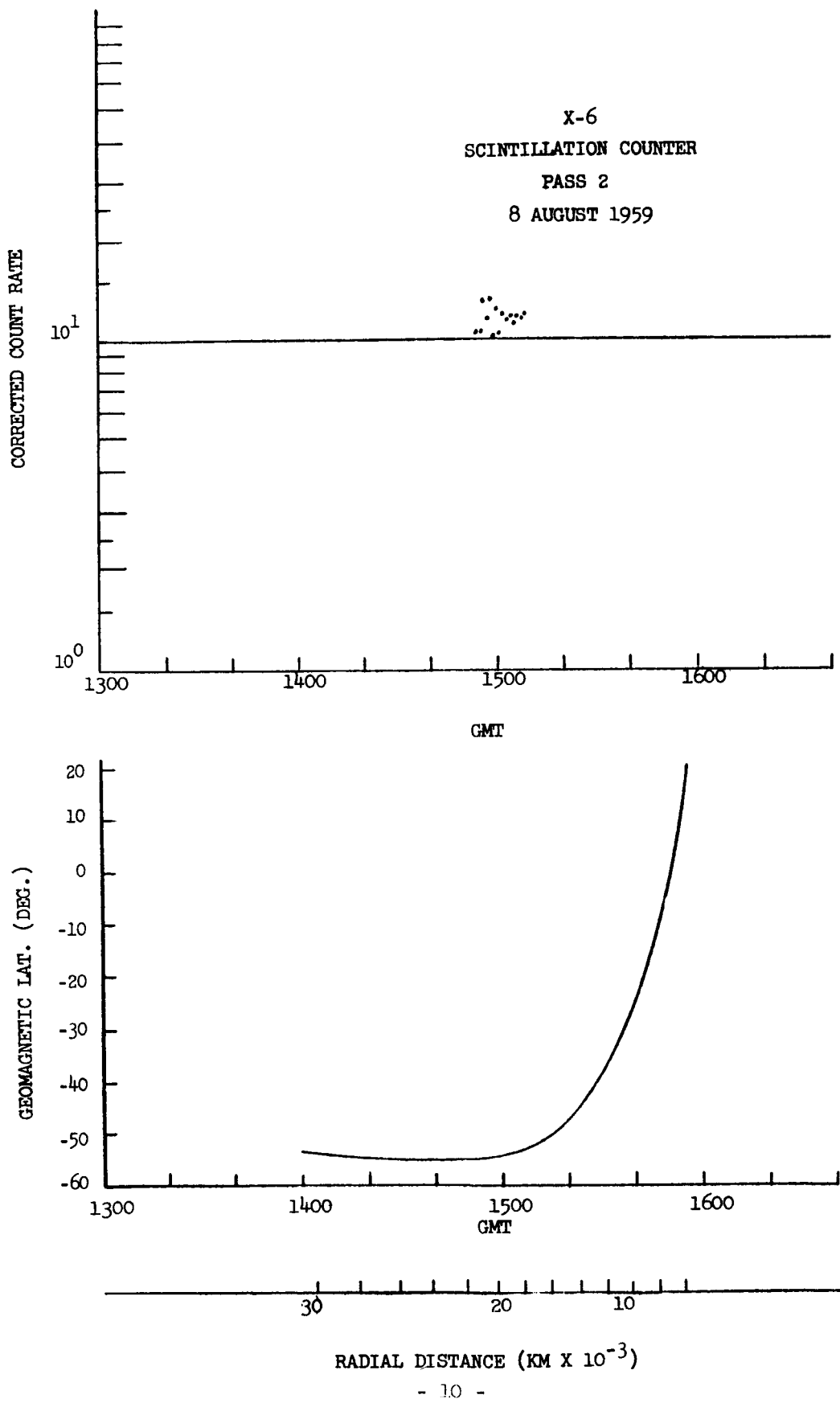
Figure 2. The Efficiency of the Scintillation Counter for the Detection of Electrons

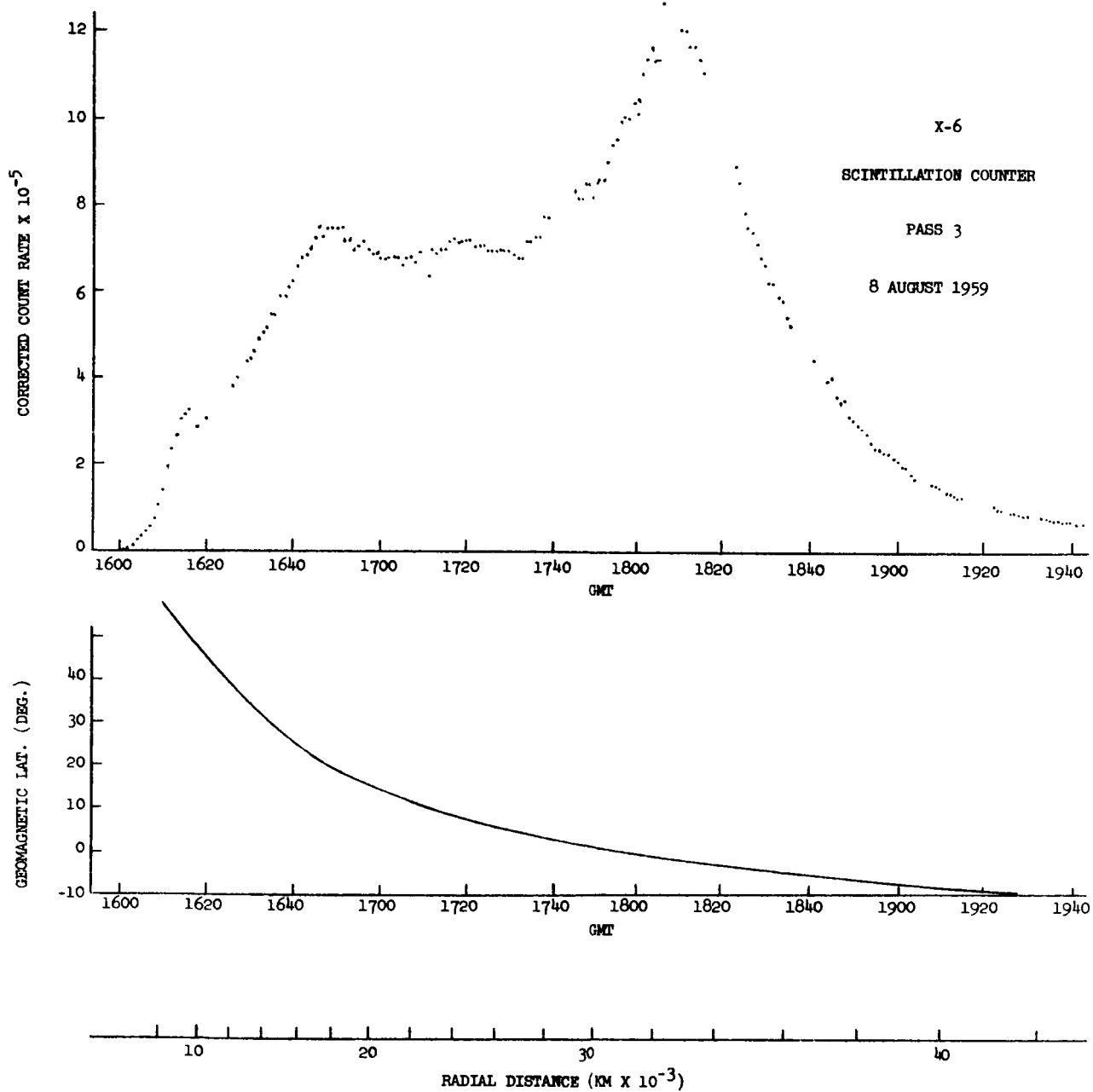
latitudes that in going from 48000 to approximately 15,000 km, it is essentially outside of the intense regions of the radiation belt, and a low count rate is generally observed (e.g. see the fifth compendium figure representing the return portion of pass 4). At altitudes below 15,000 kilometers, as the satellite approached perigee, it grazes the high latitude edge of the outer zone and a portion of the inner zone, and a peak in the count rate corresponding to that traversal may be observed (see the last section of pass 12 for example).

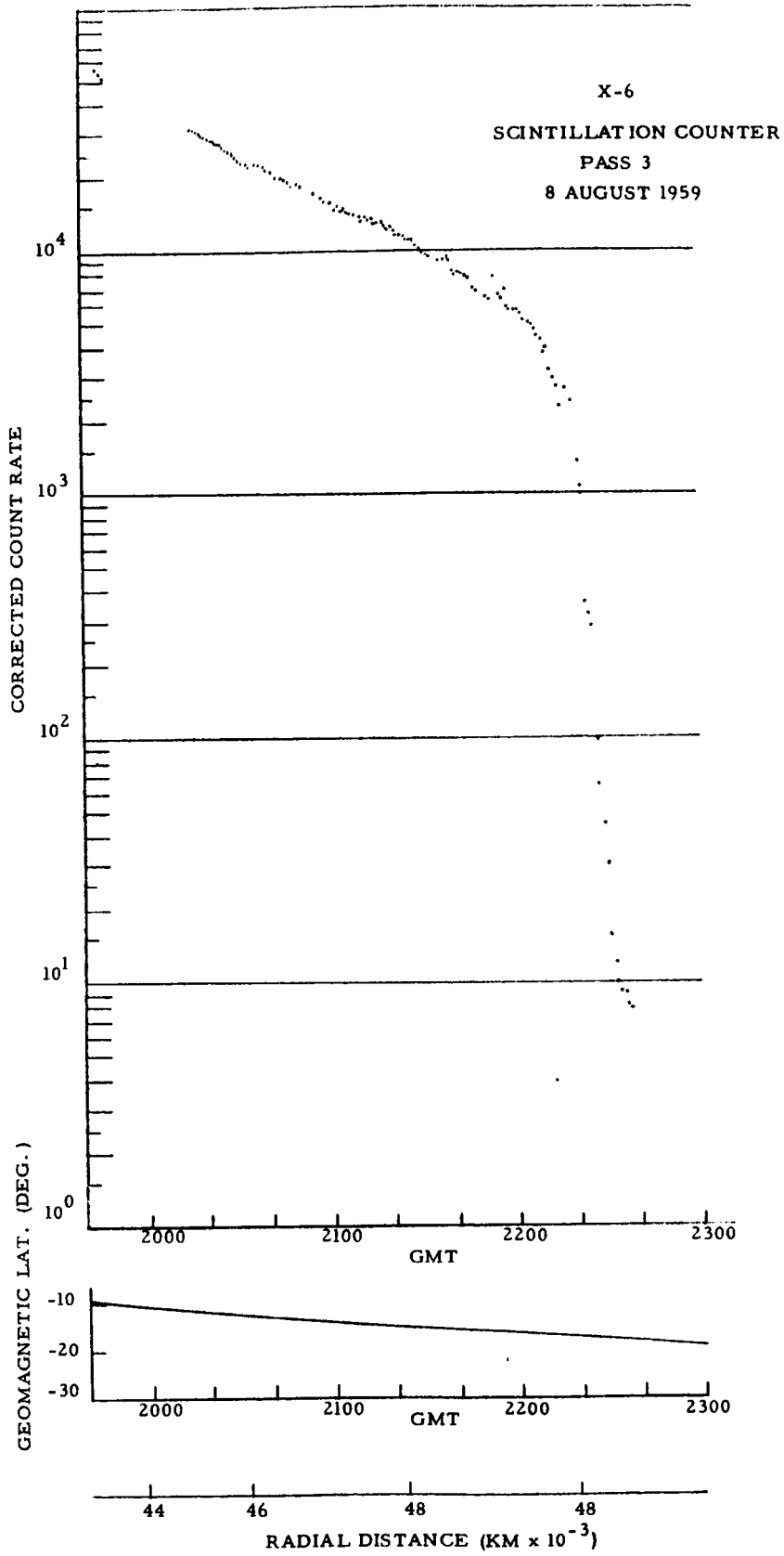
Part B

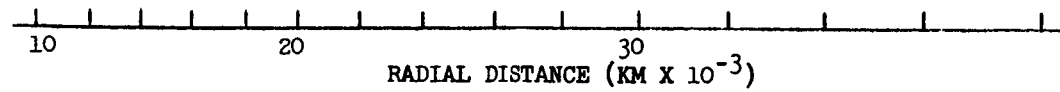
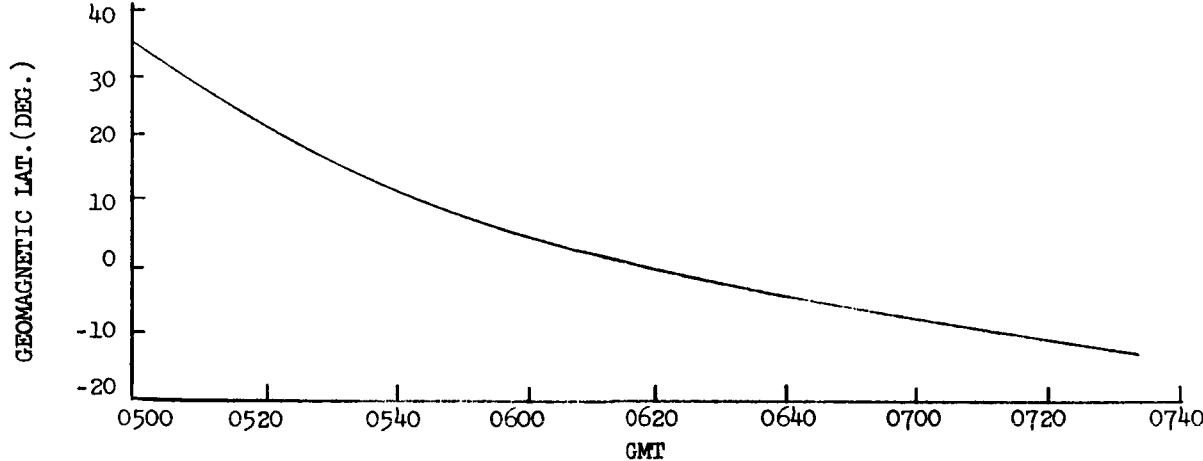
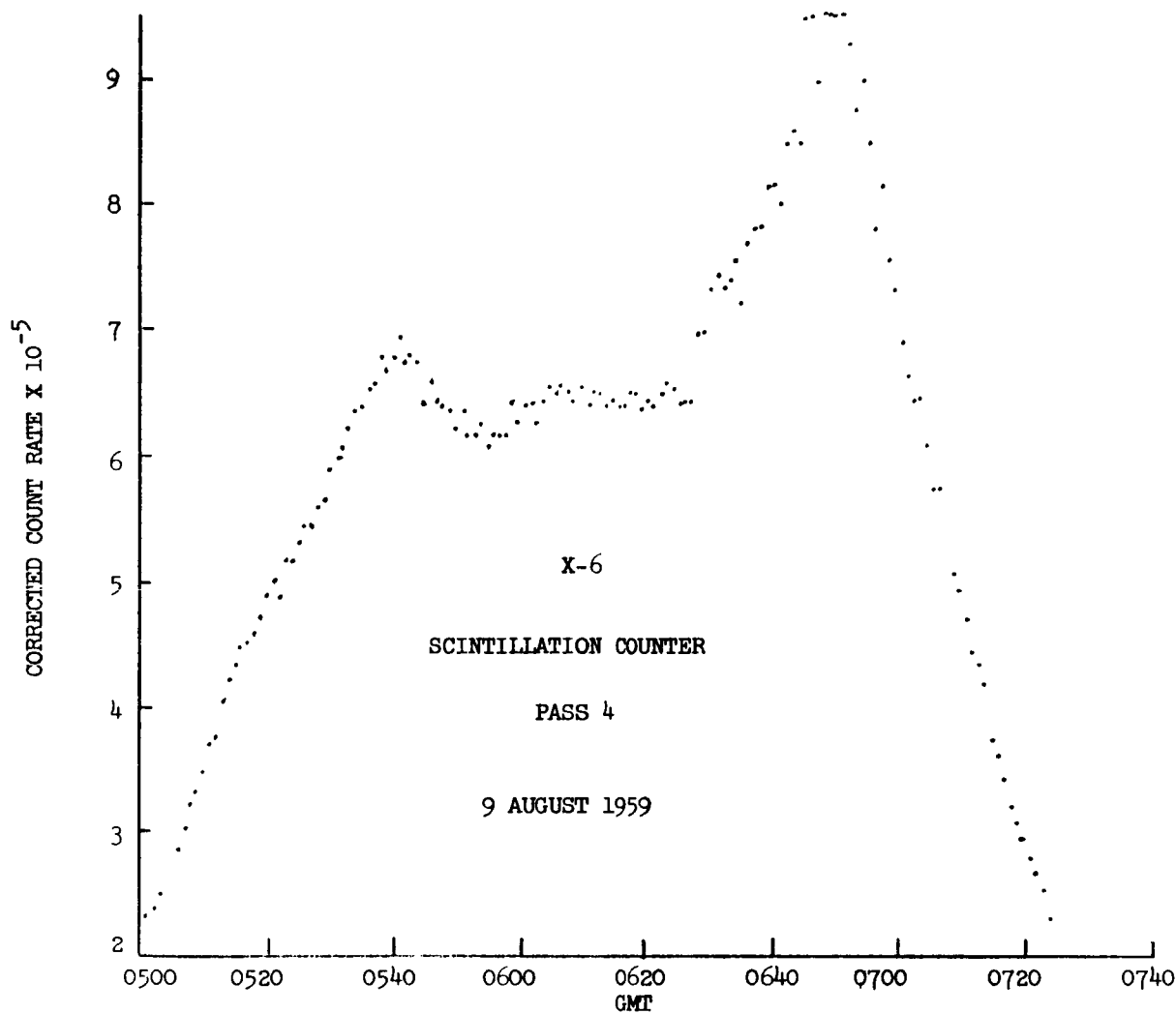
**A Compendium of Data Taken With The
Explorer VI Scintillation Counter**



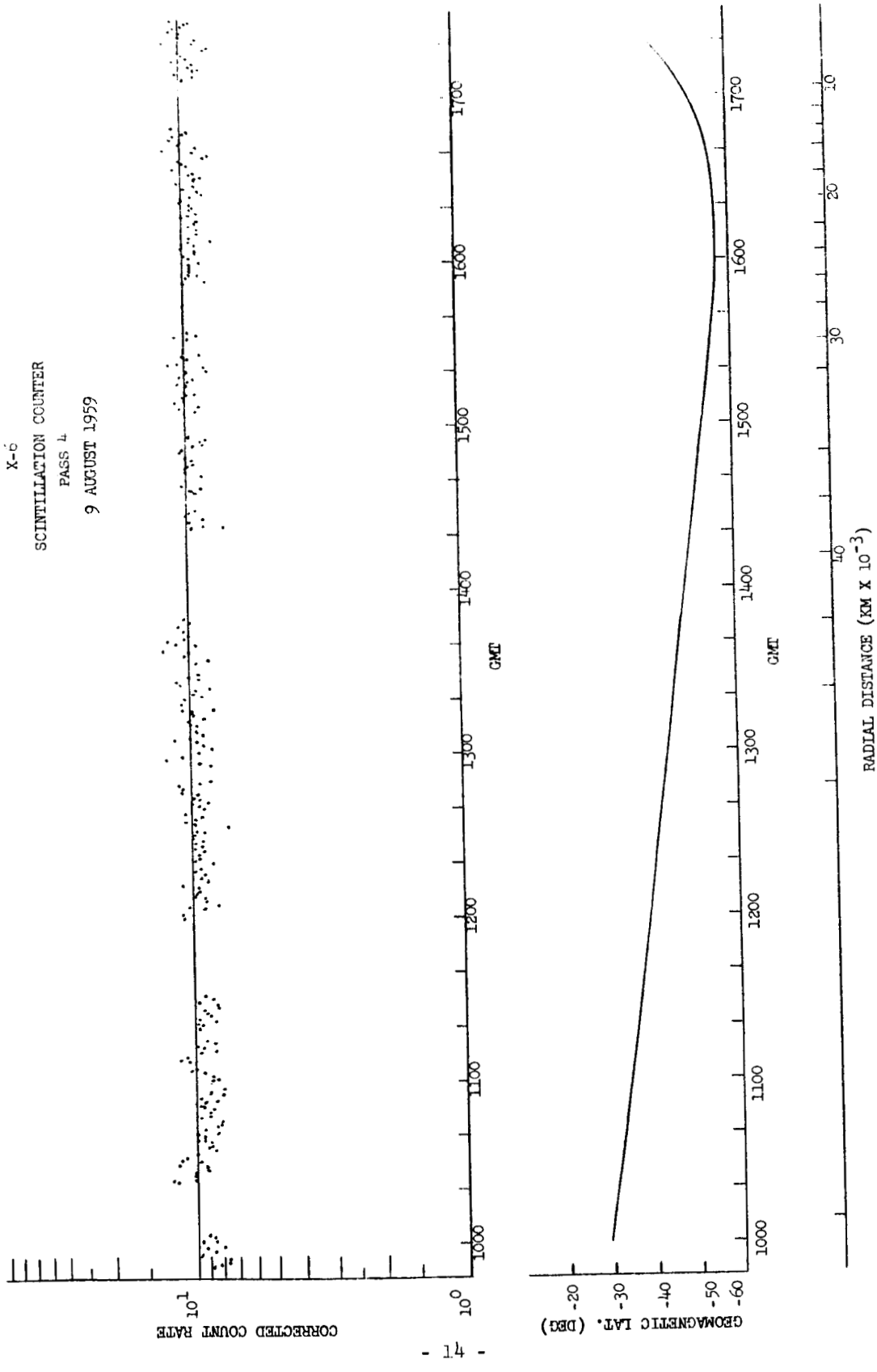


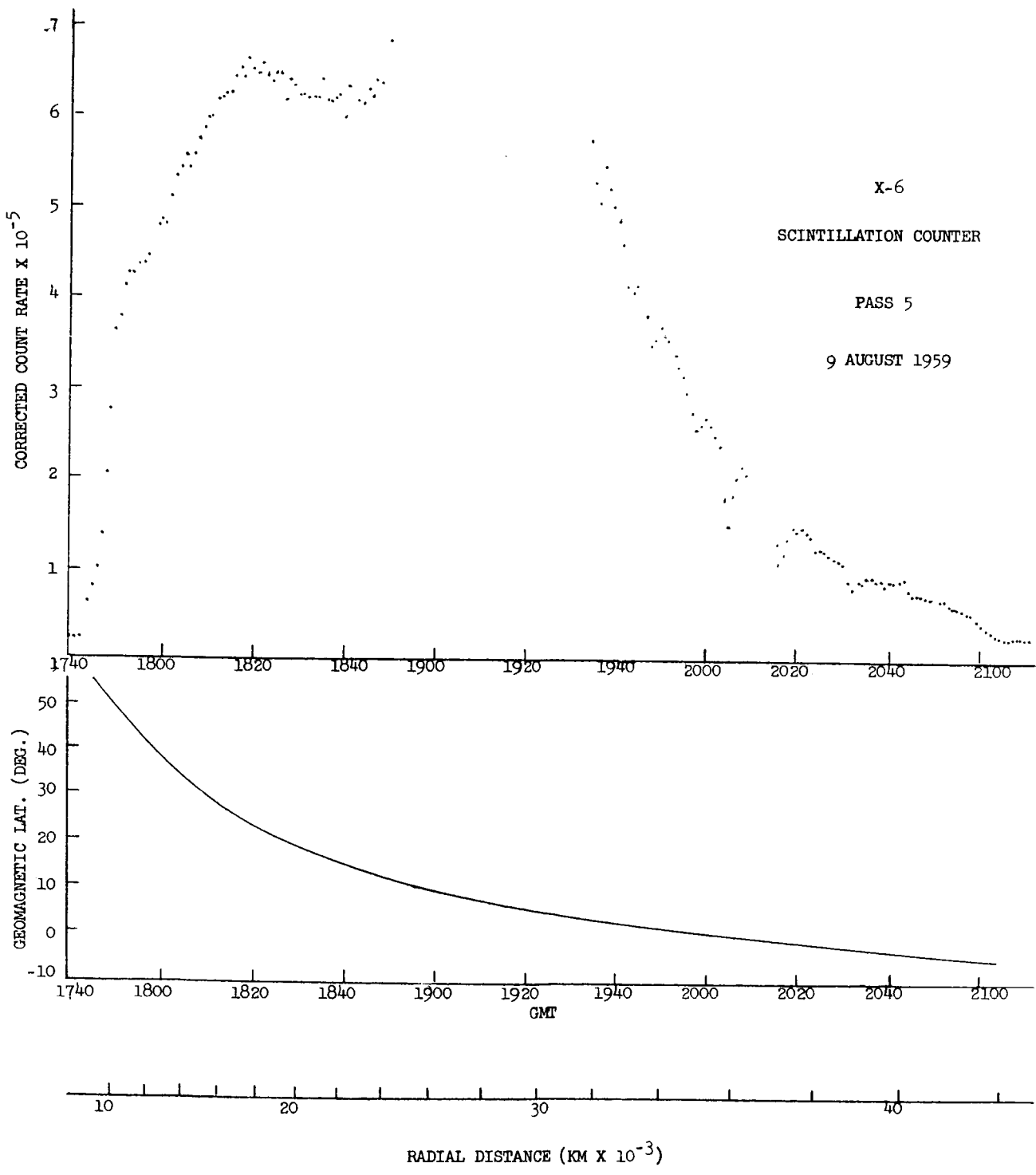






X-6
SCINTILLATION COUNTER
PAGE 4
9 AUGUST 1959



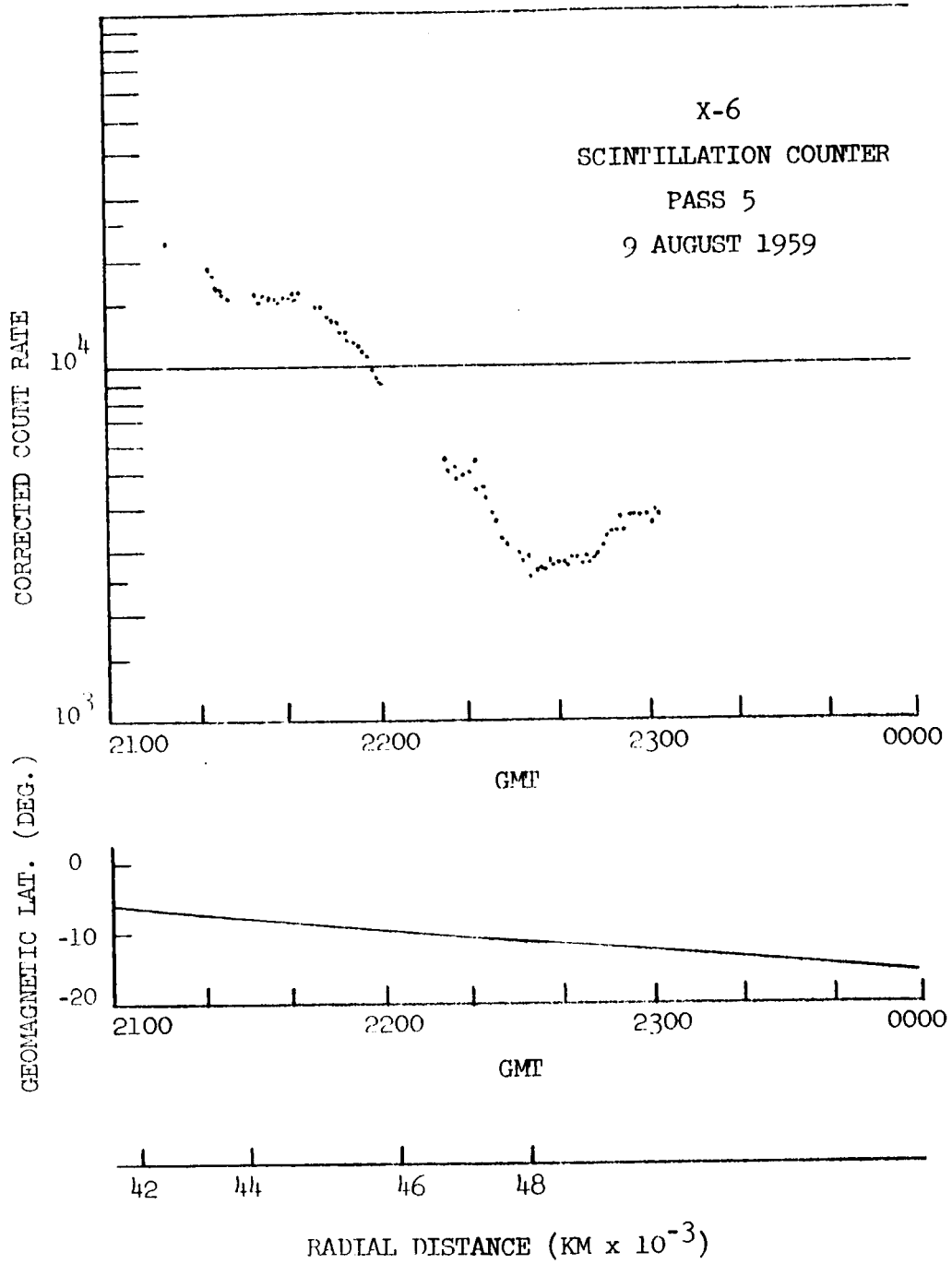


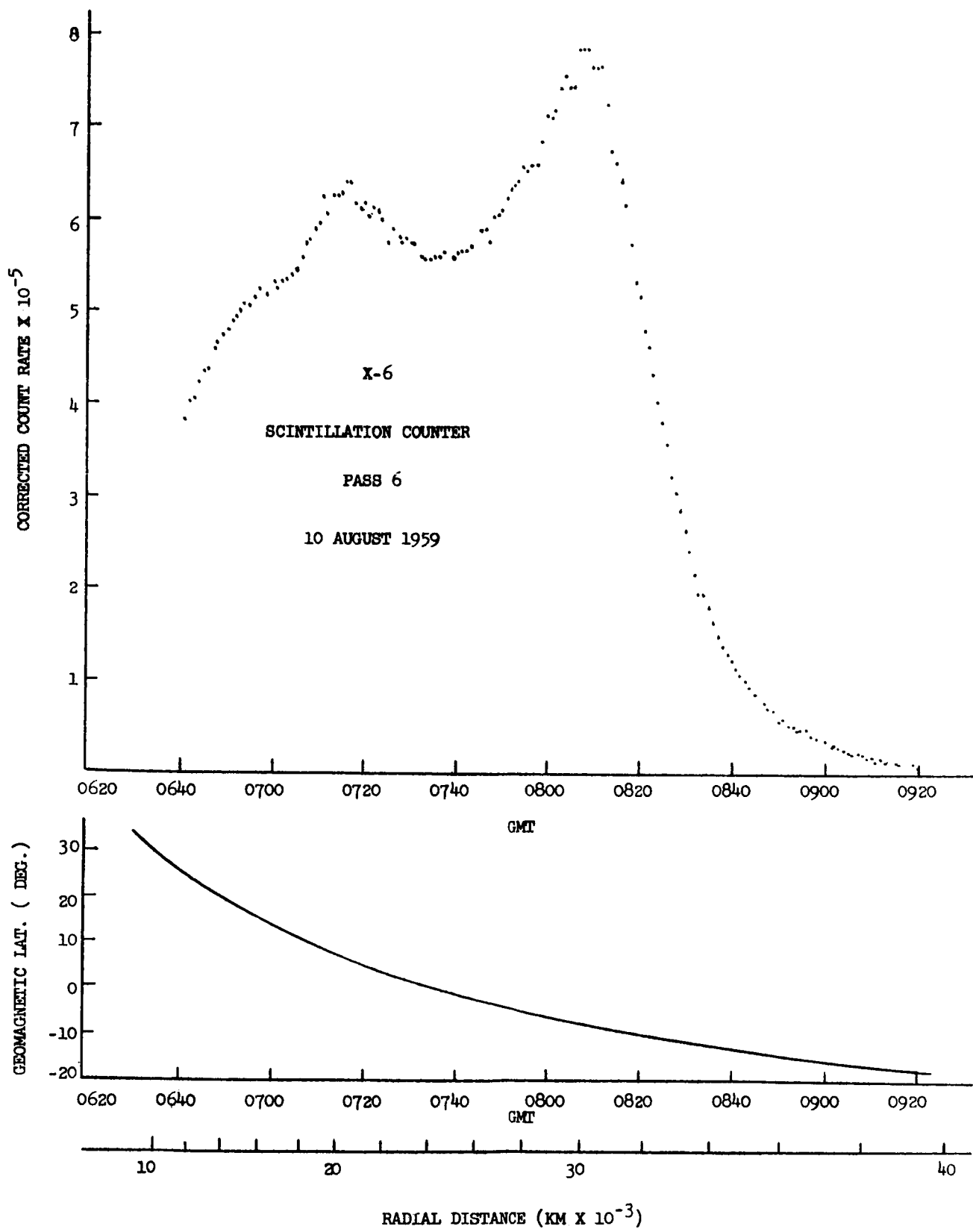
X-6

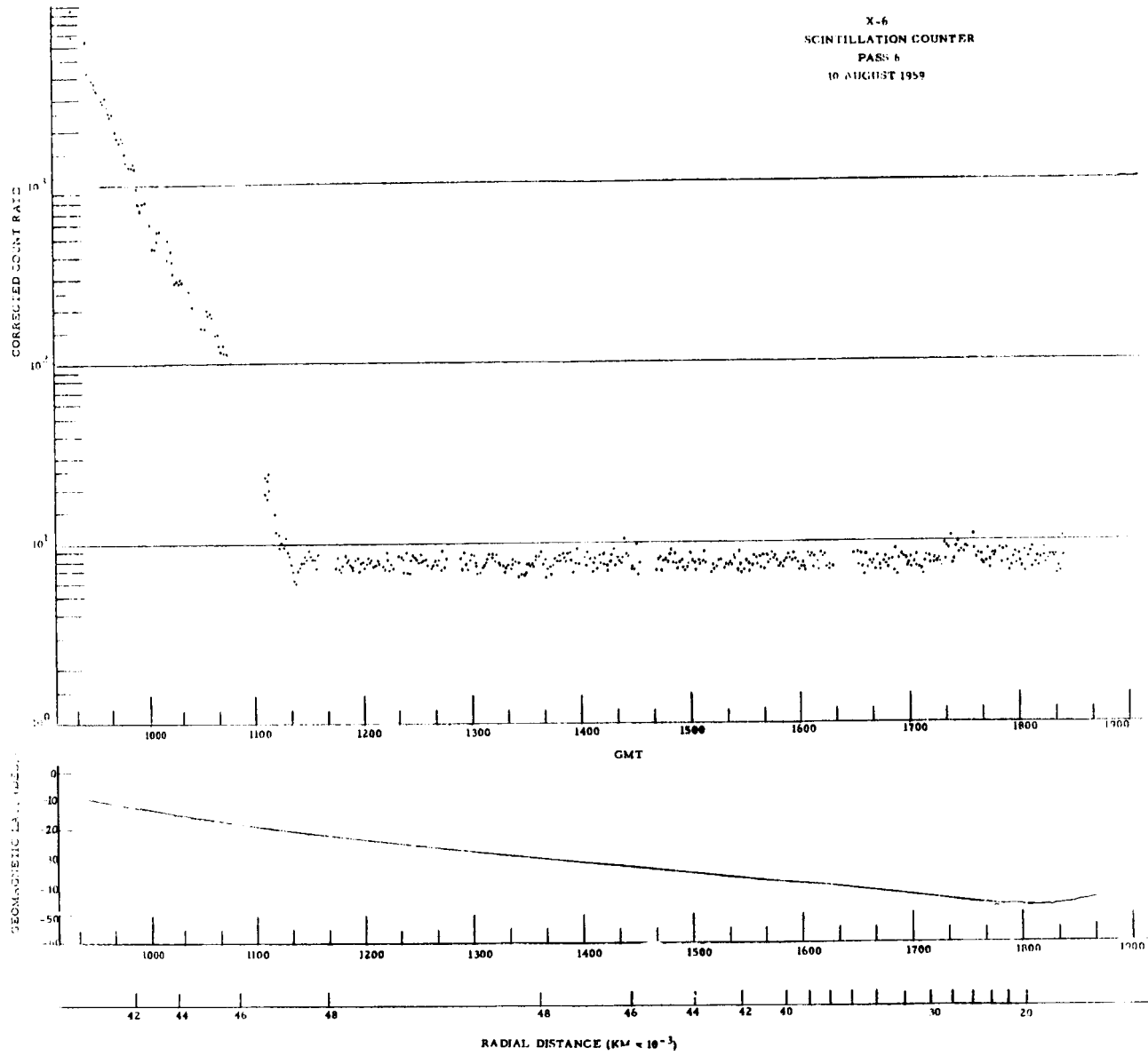
SCINTILLATION COUNTER

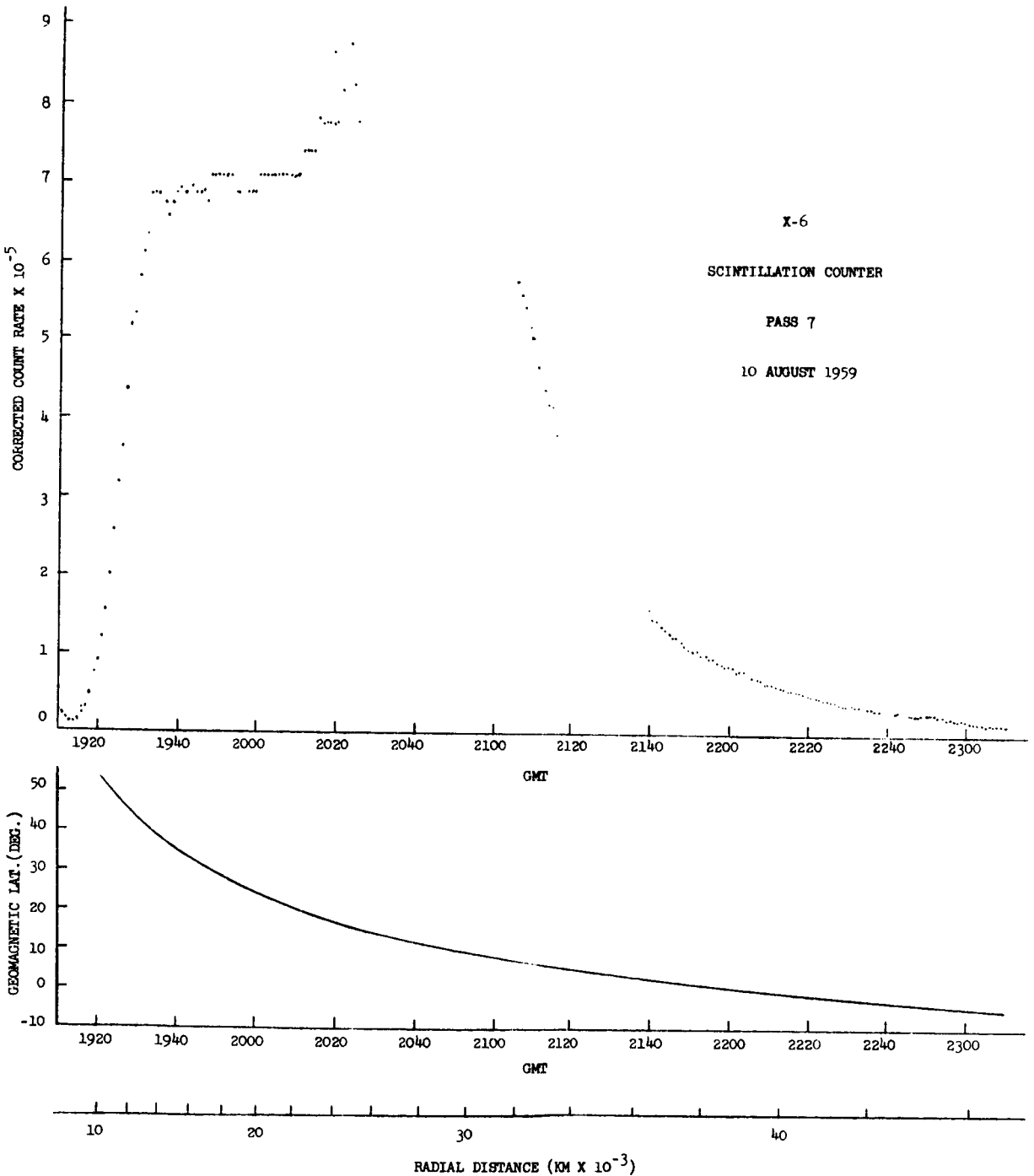
PASS 5

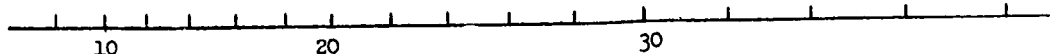
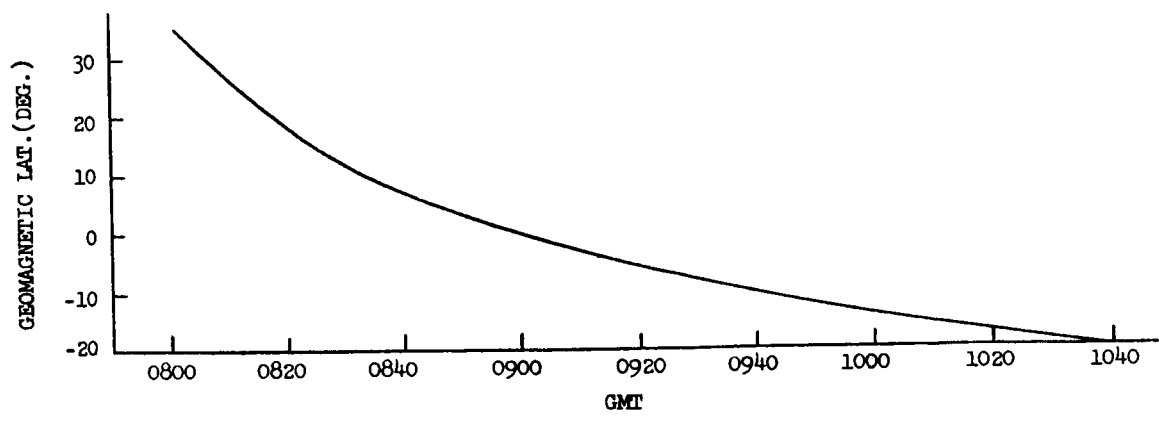
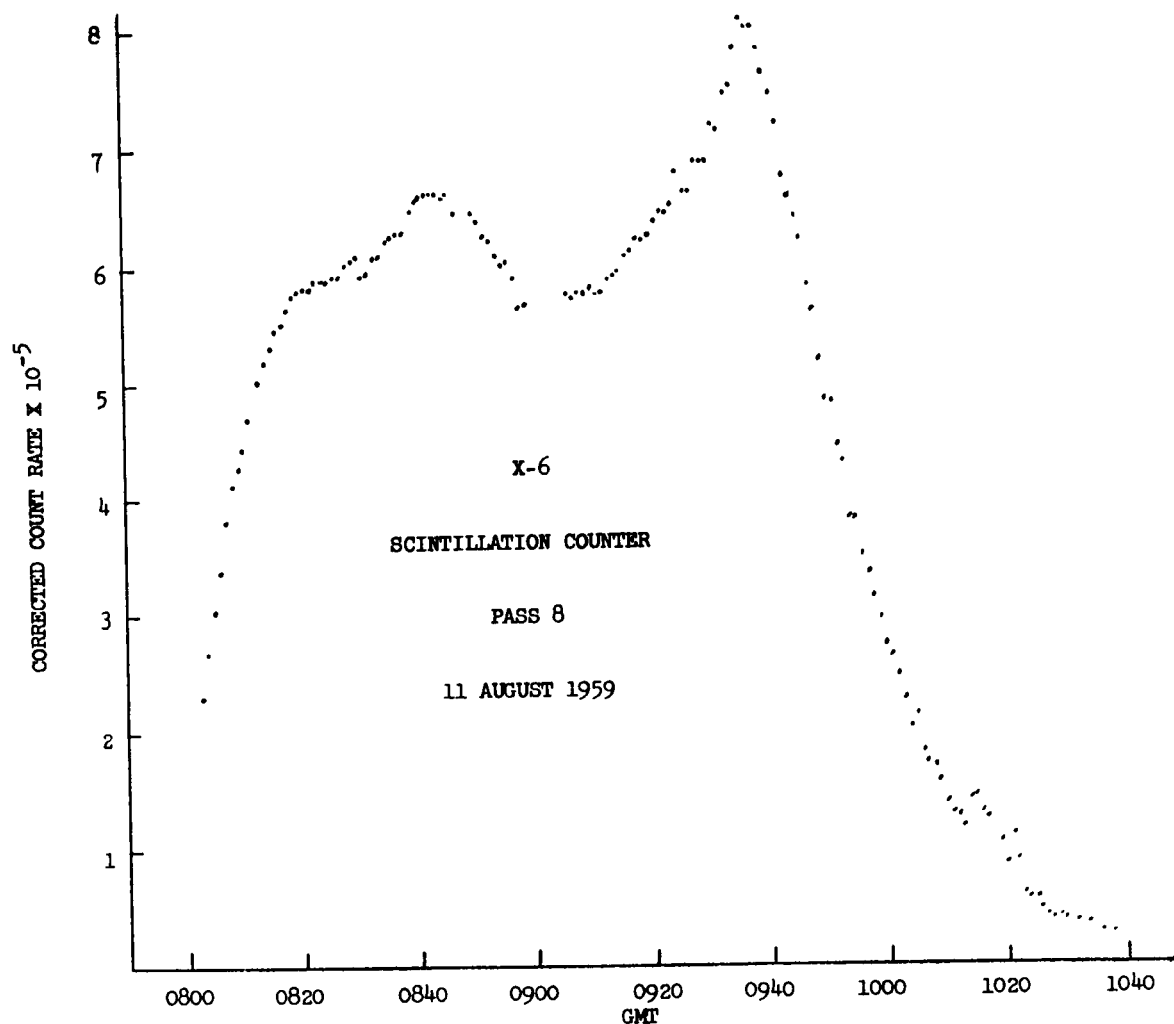
9 AUGUST 1959











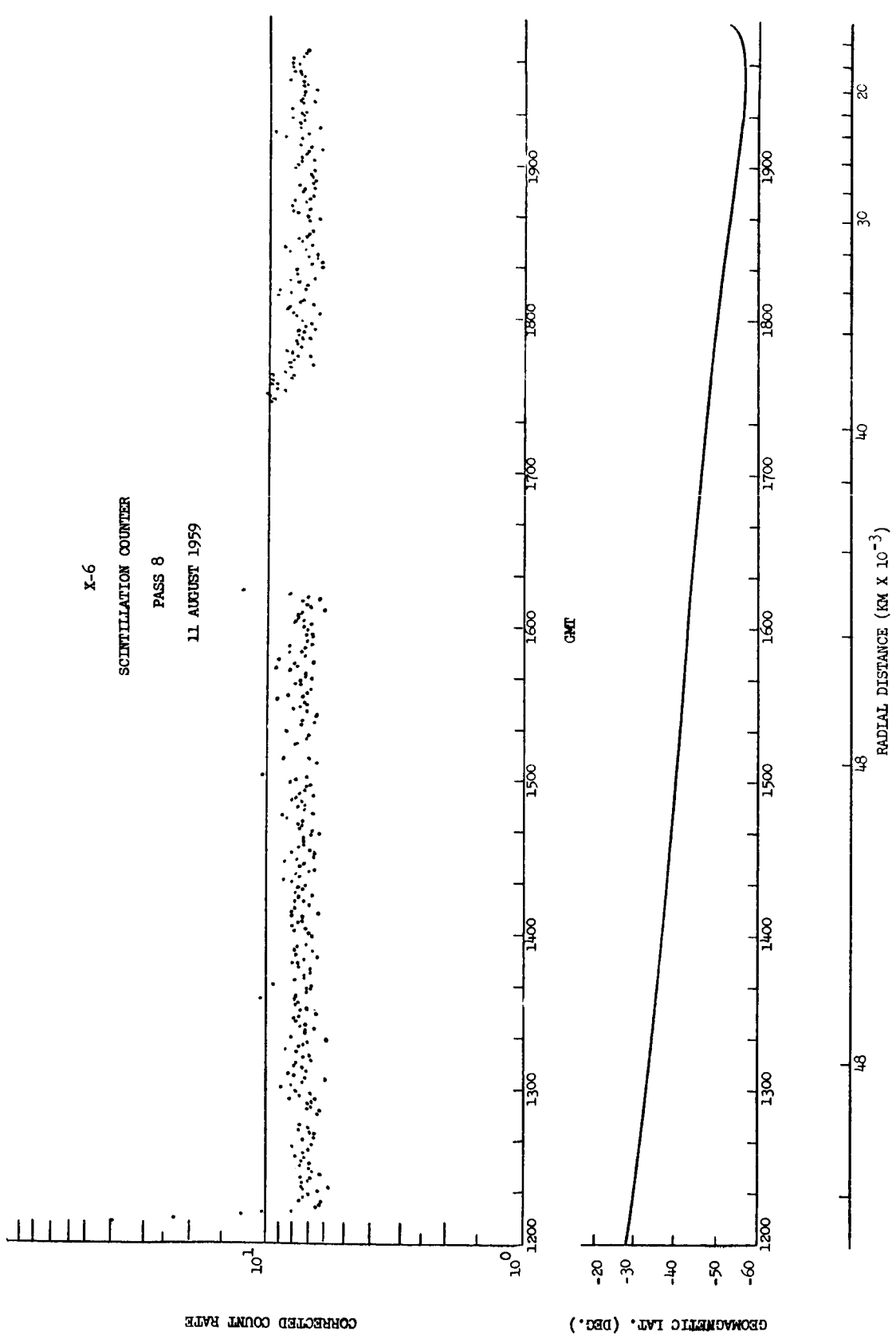
RADIAL DISTANCE (KM $\times 10^{-3}$)

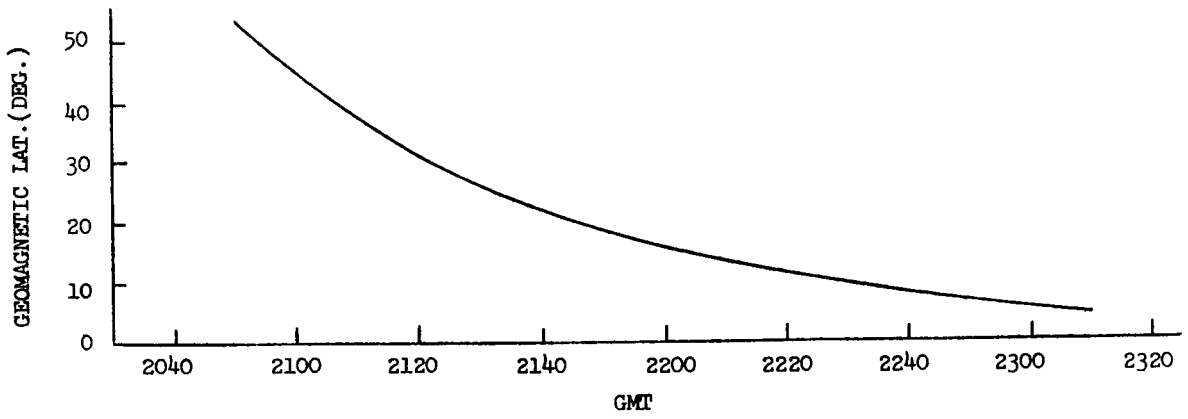
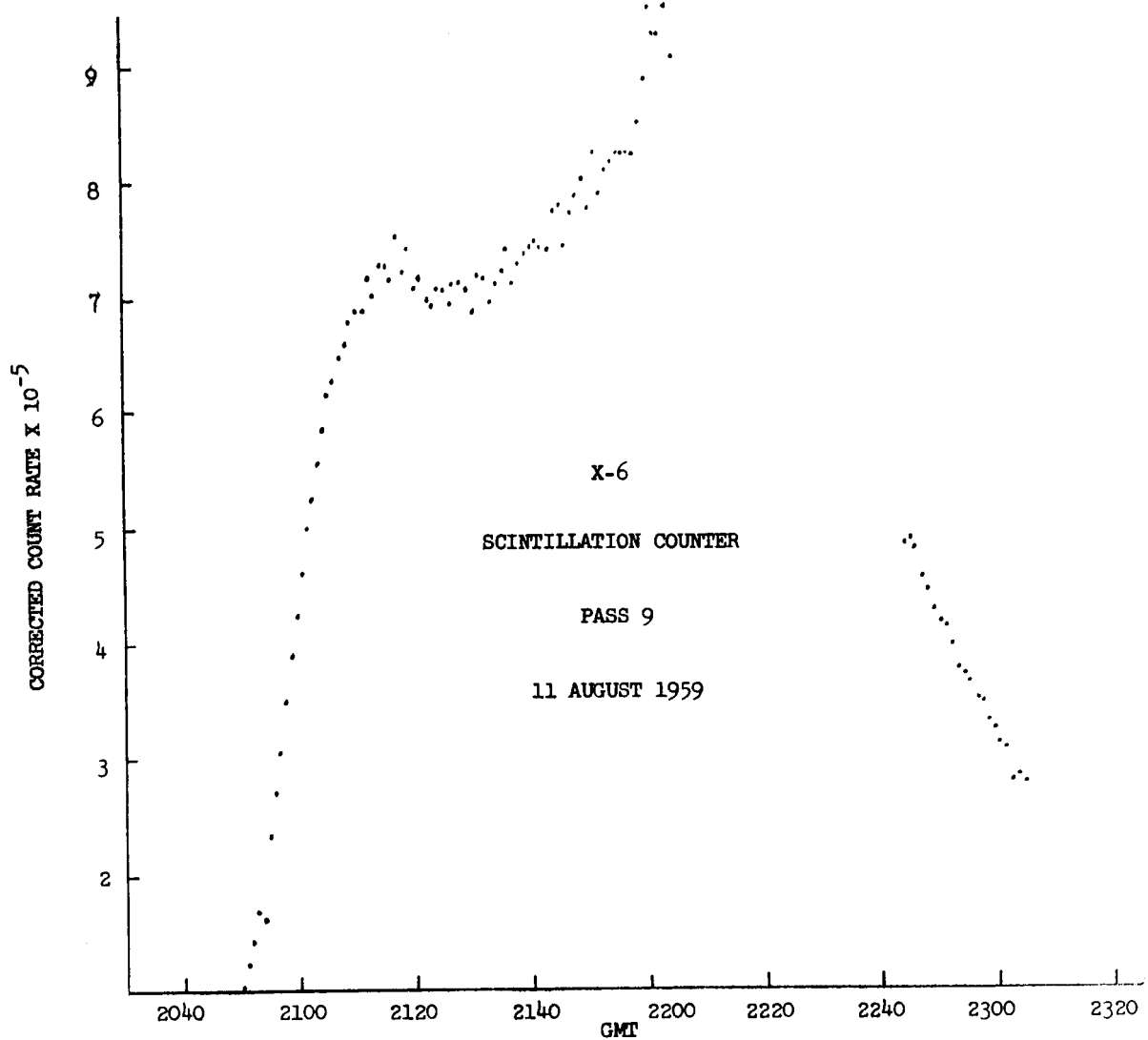
X-6

SCINTILLATION COUNTER

PASS 8

11 AUGUST 1959

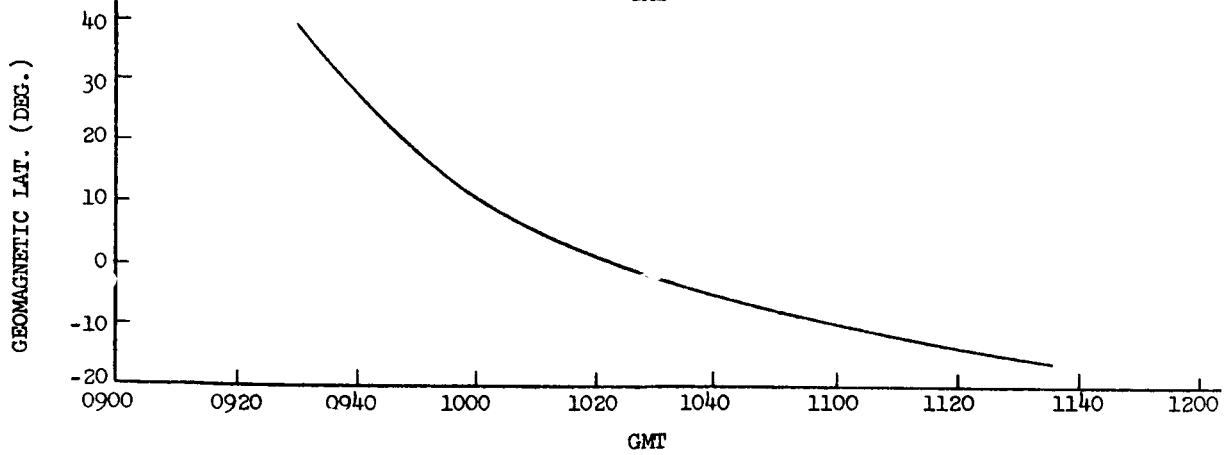
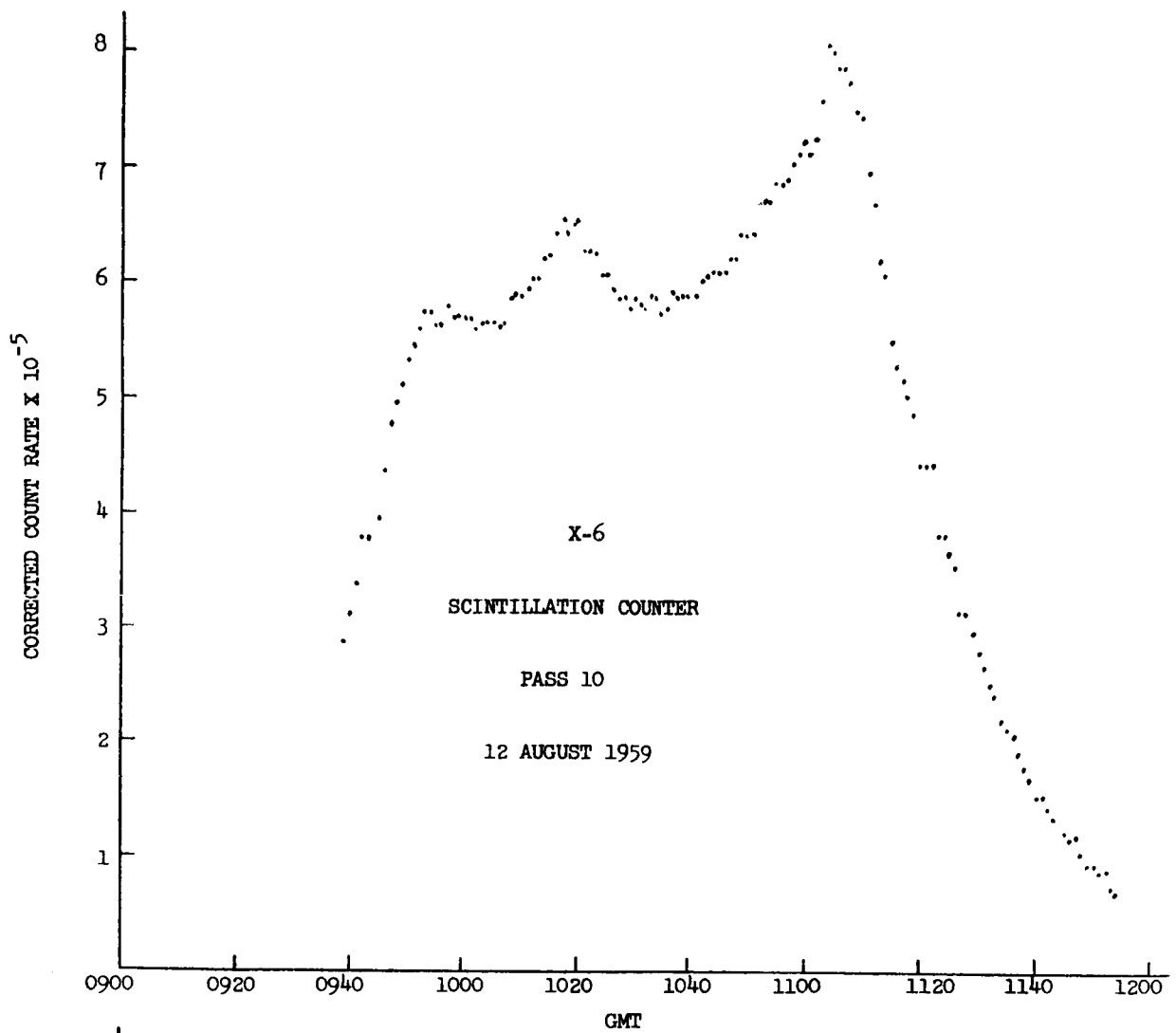




10

RADIAL DISTANCE (KM^{-3})

- 22 -



10

20

30

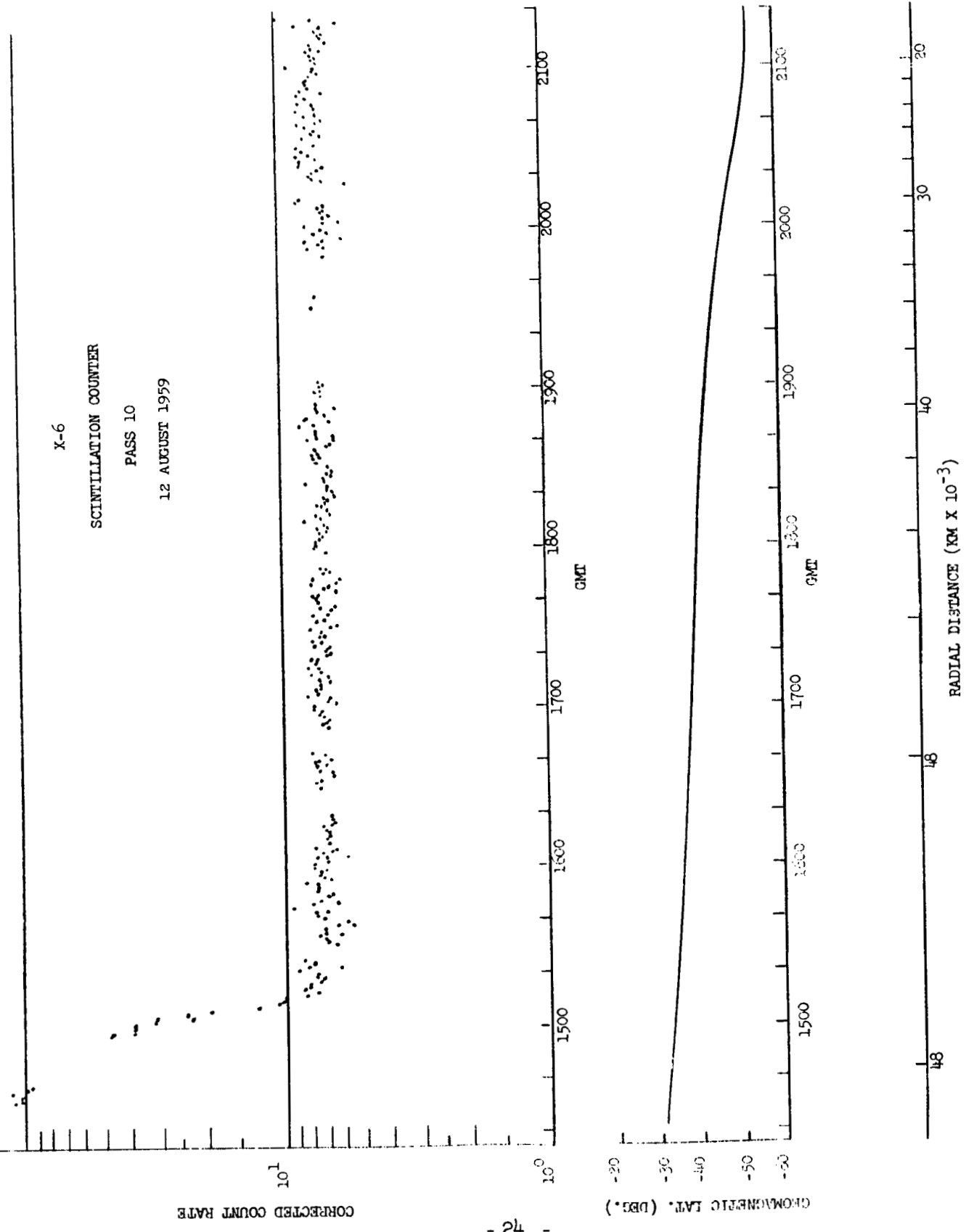
RADIAL DISTANCE (KM $\times 10^{-3}$)

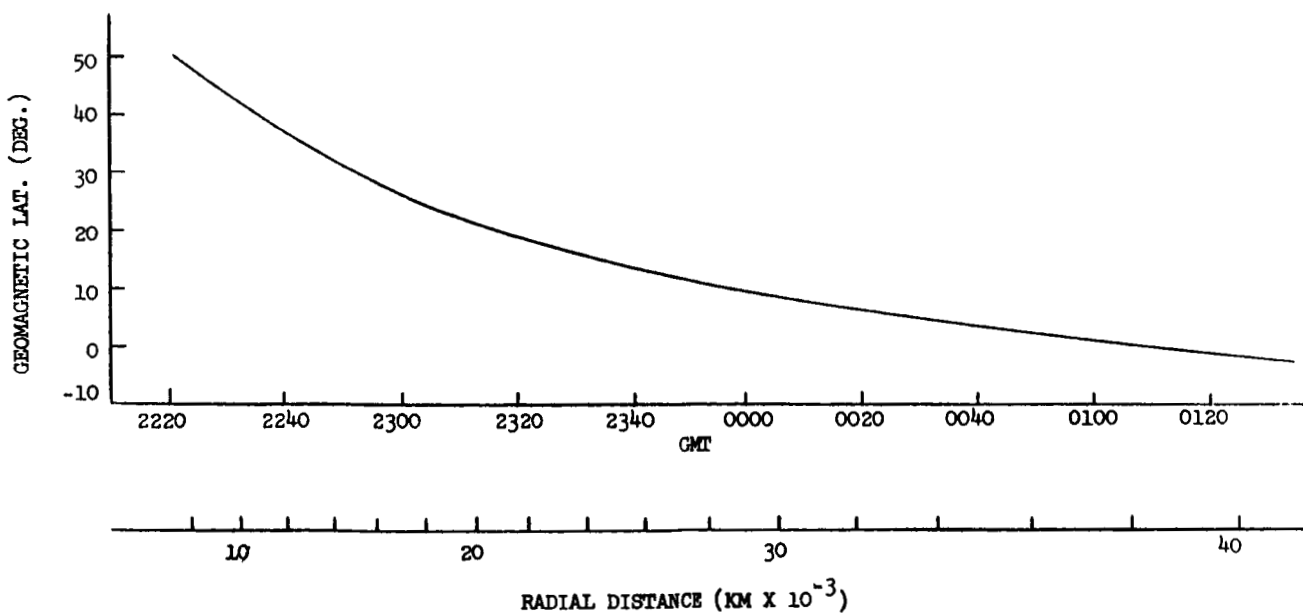
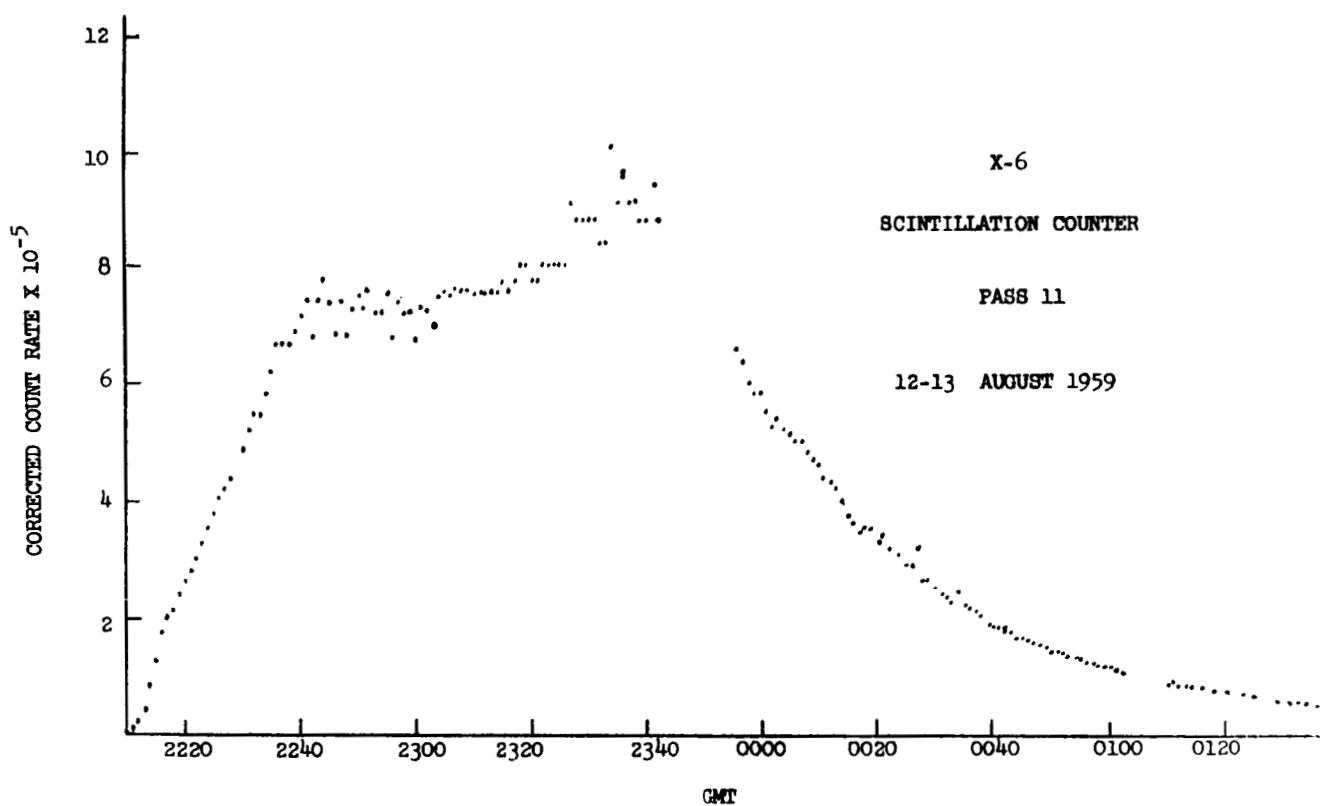
X-6

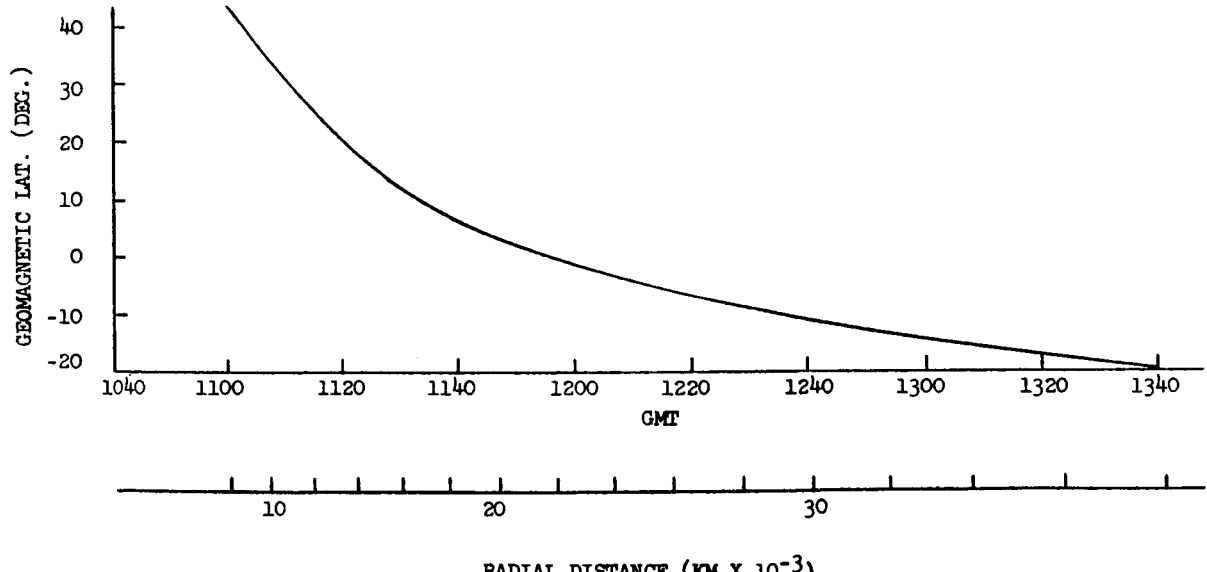
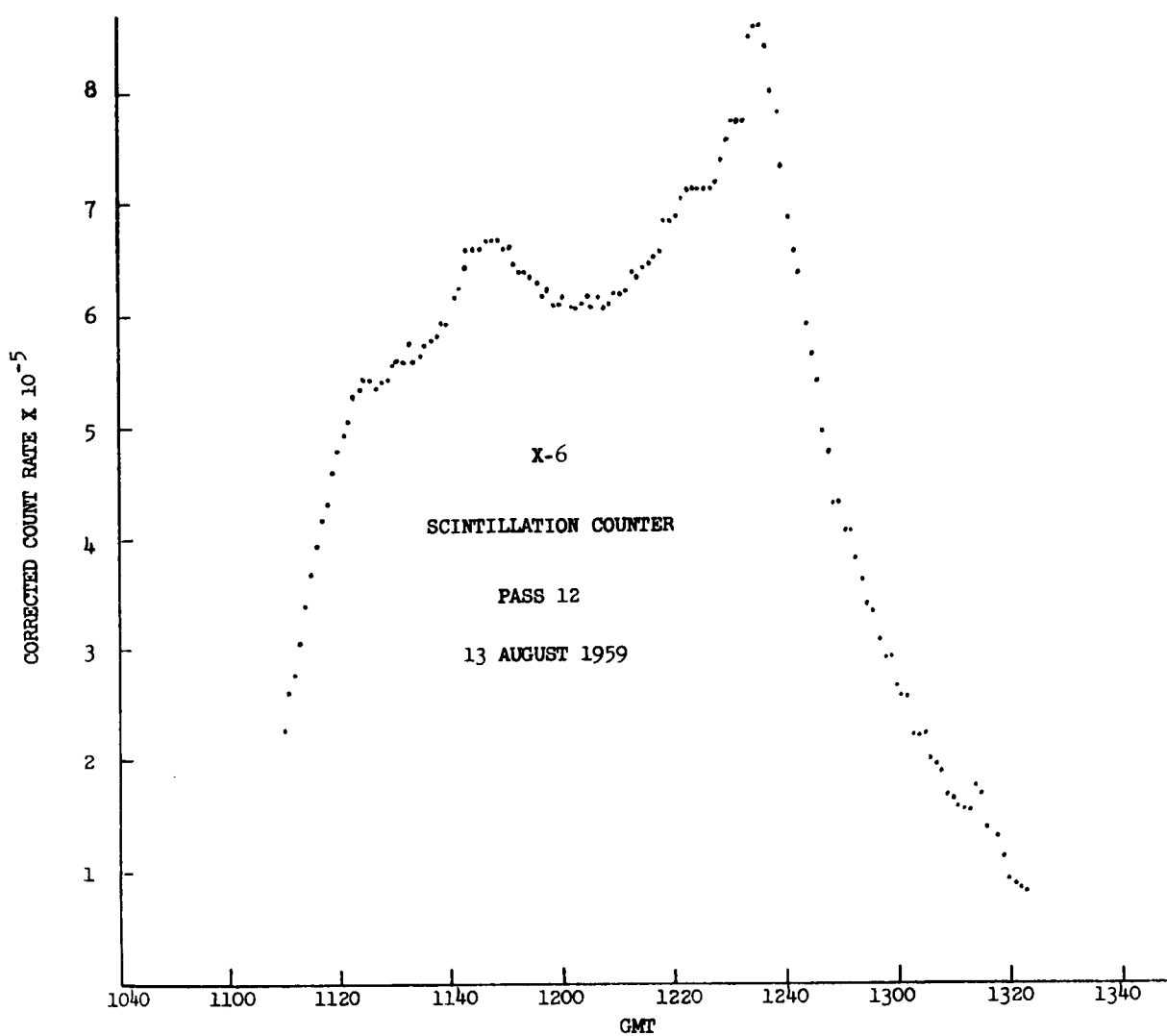
SCINTILLATION COUNTER

PASS 10

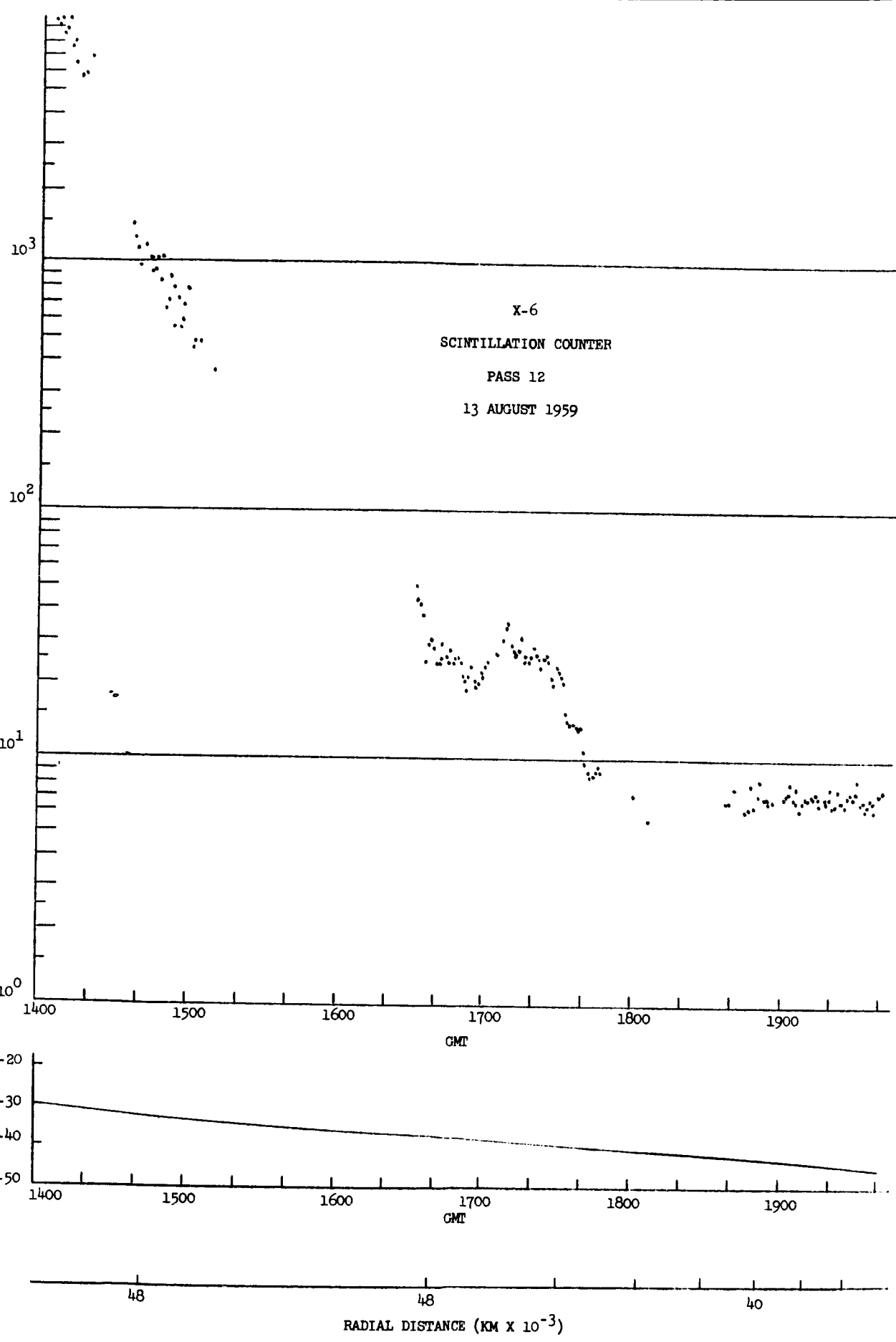
12 AUGUST 1959

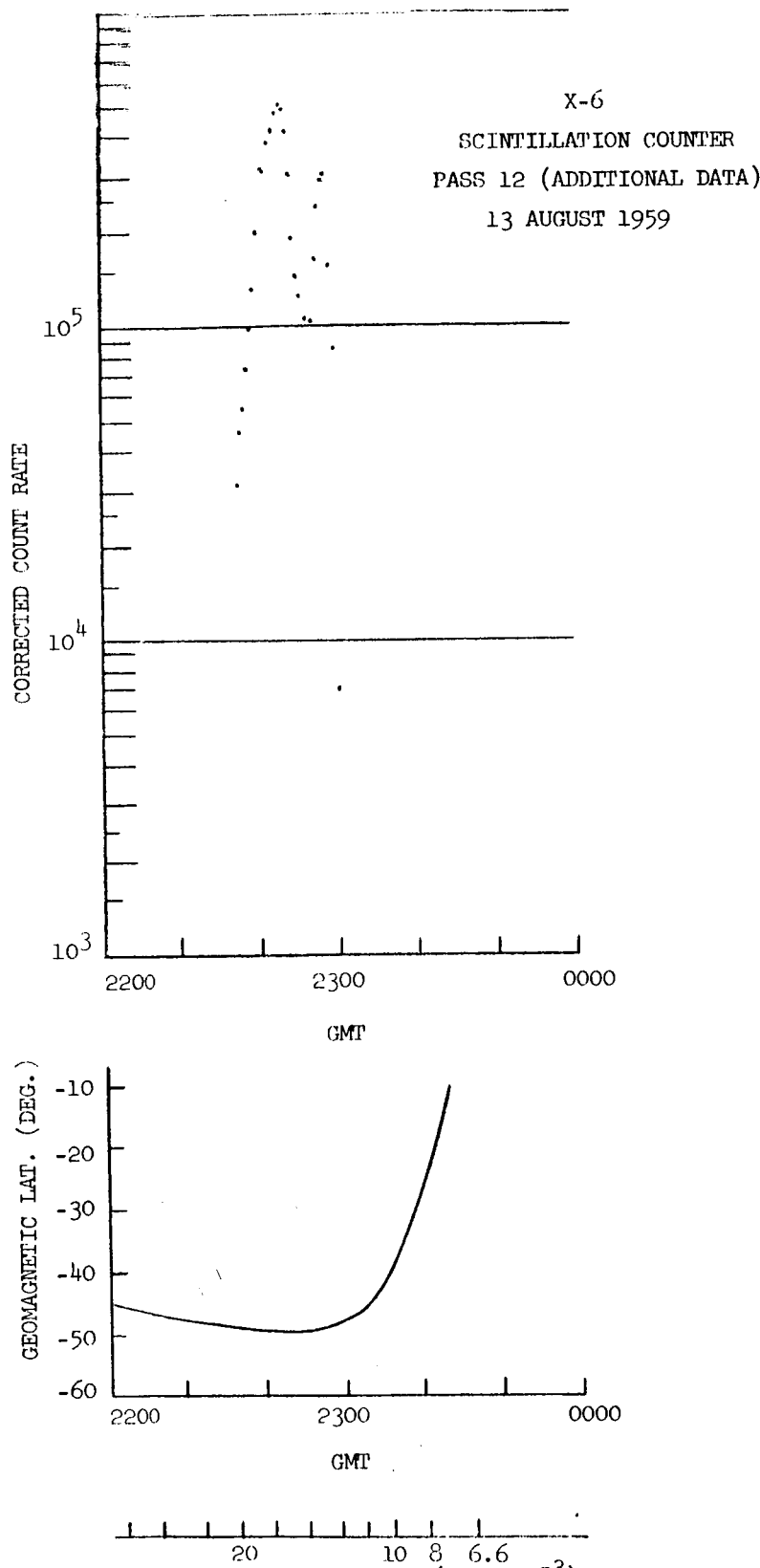


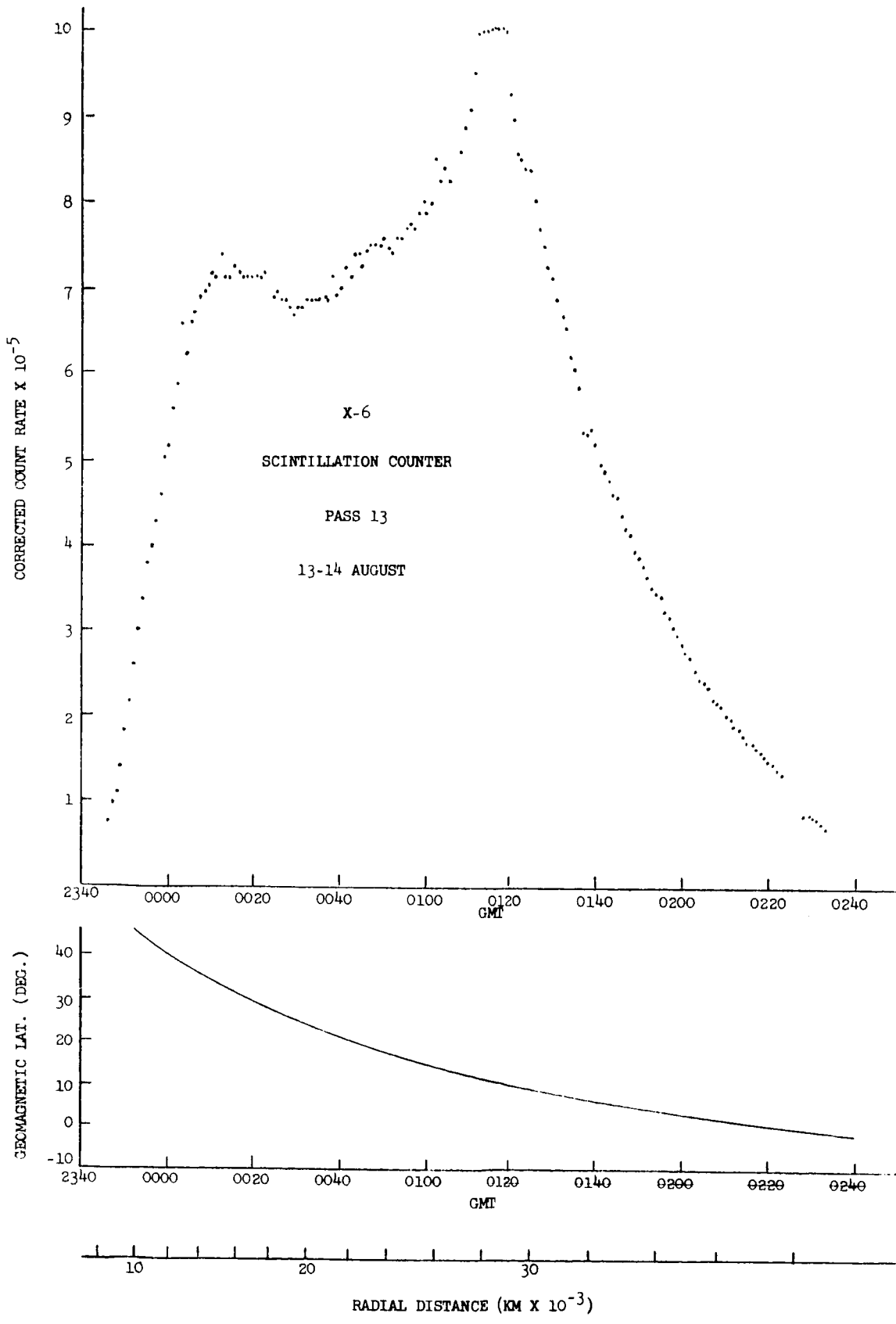


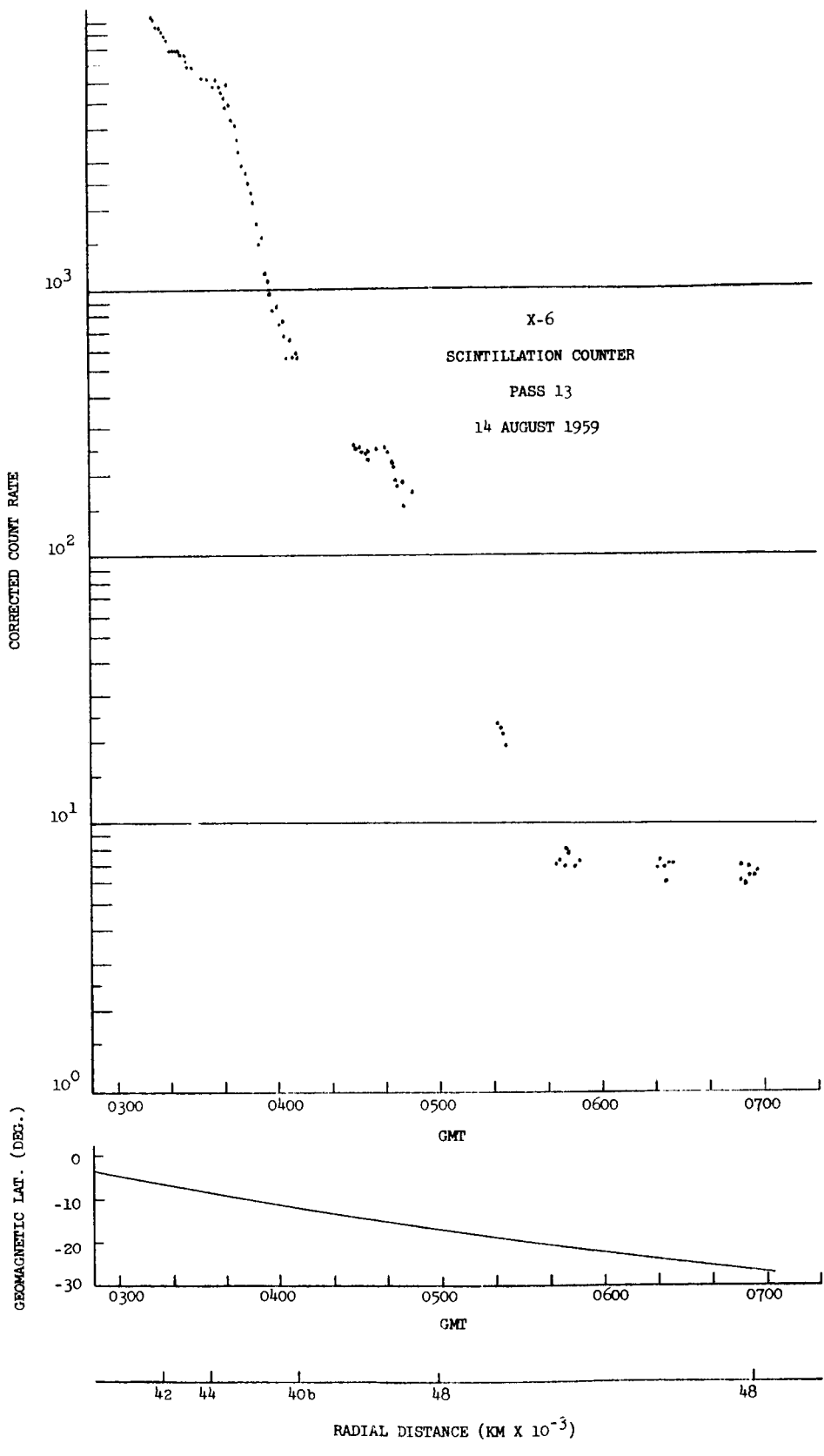


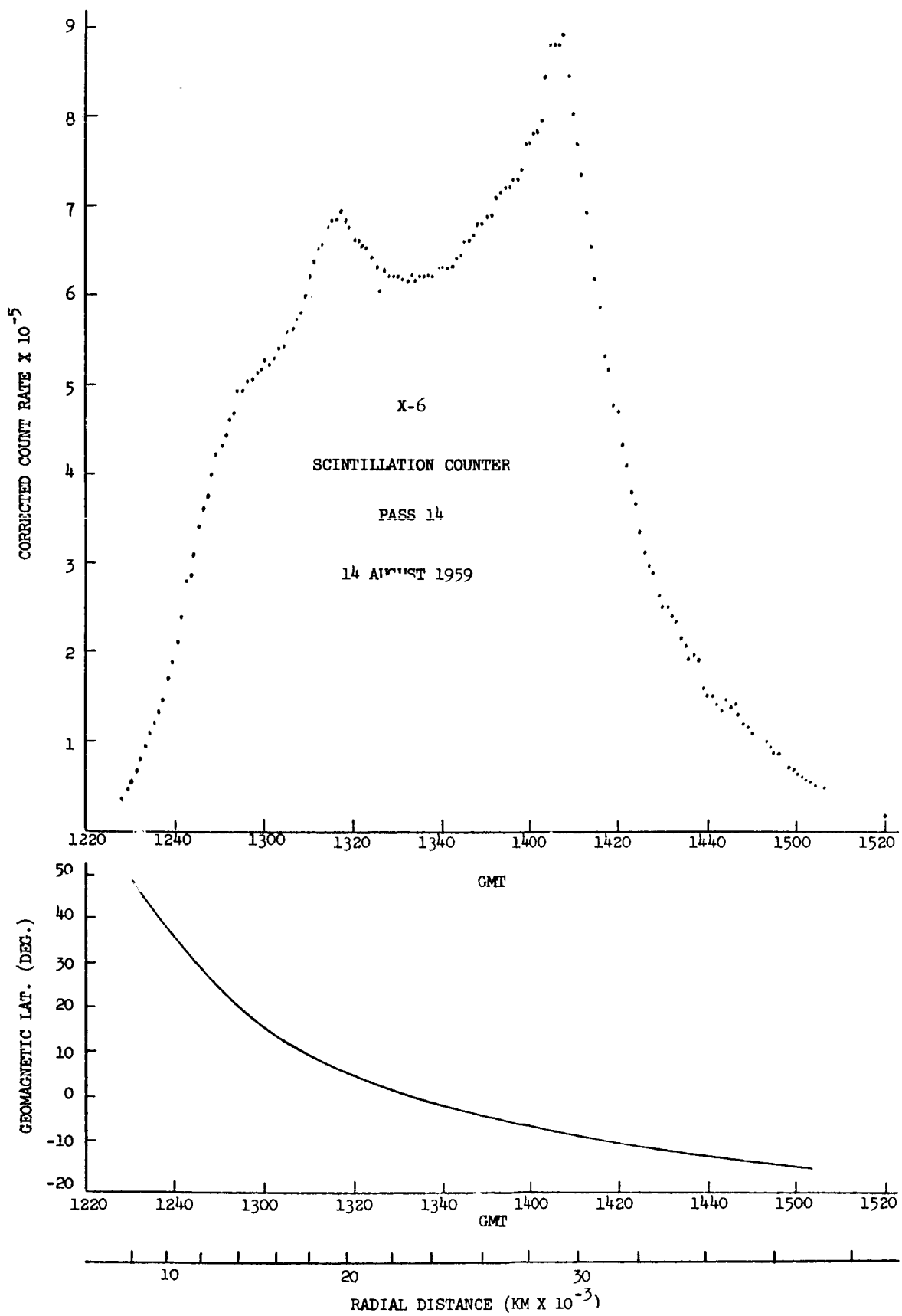
CORRECTED COUNT RATE

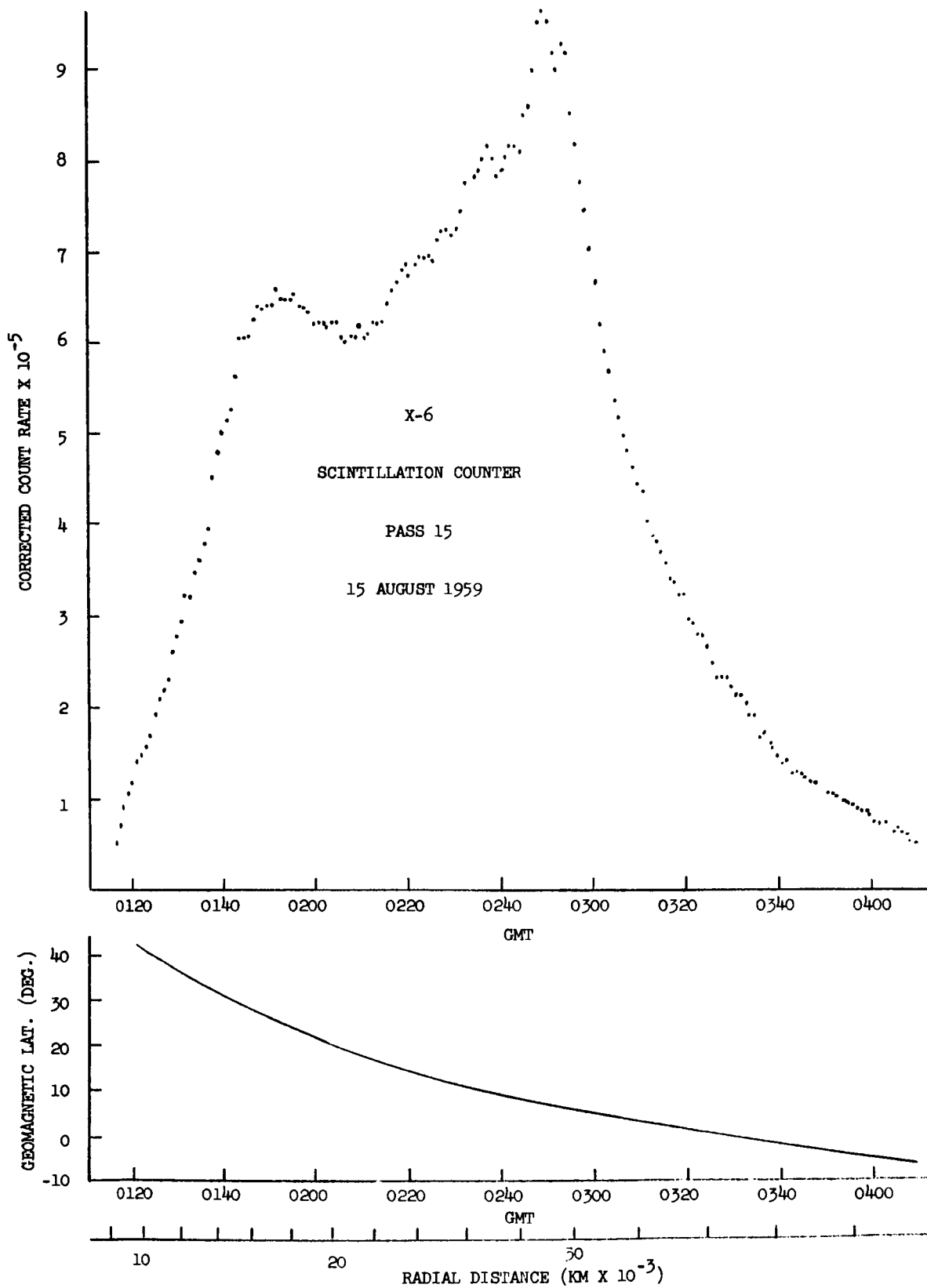


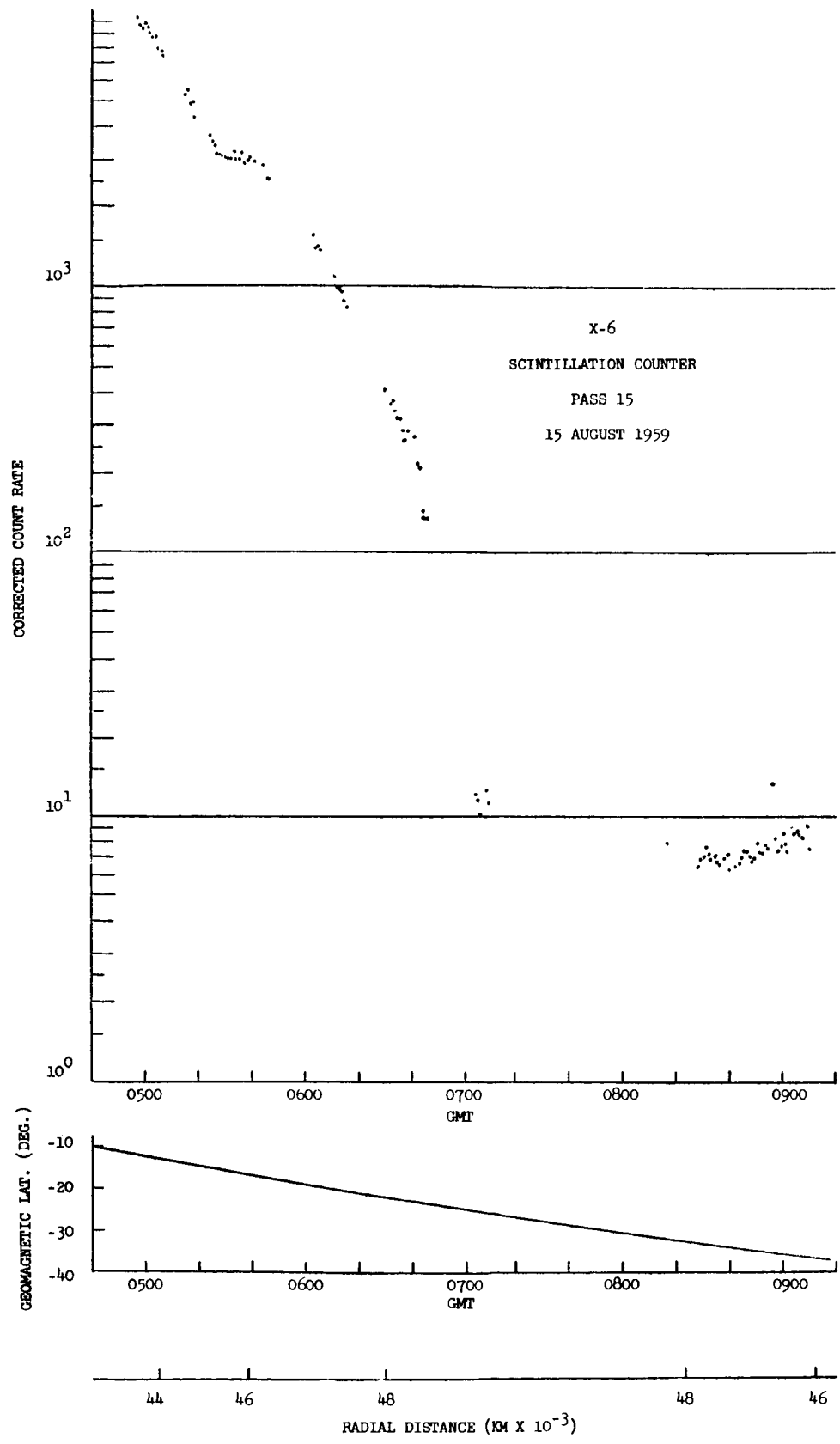


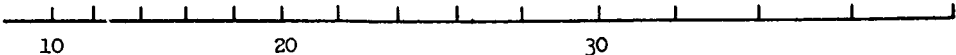
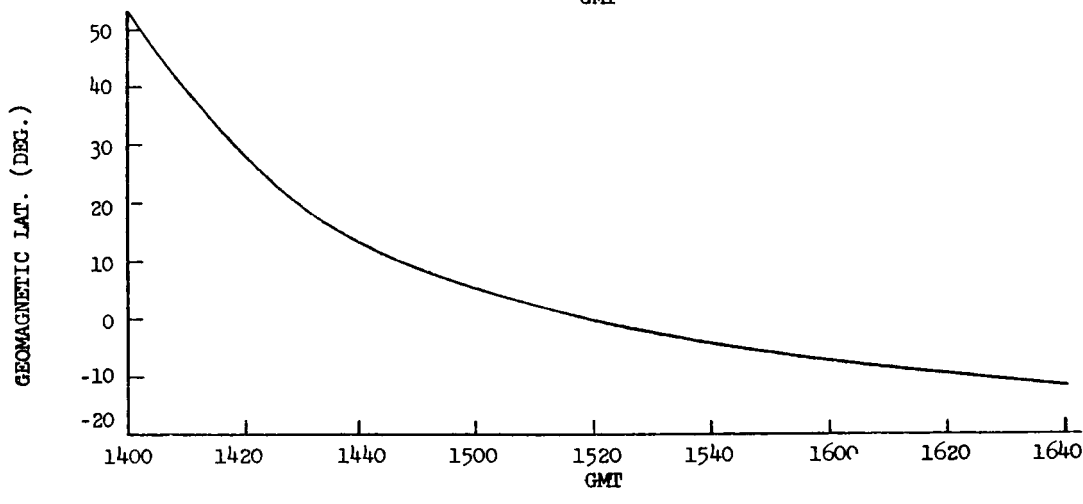
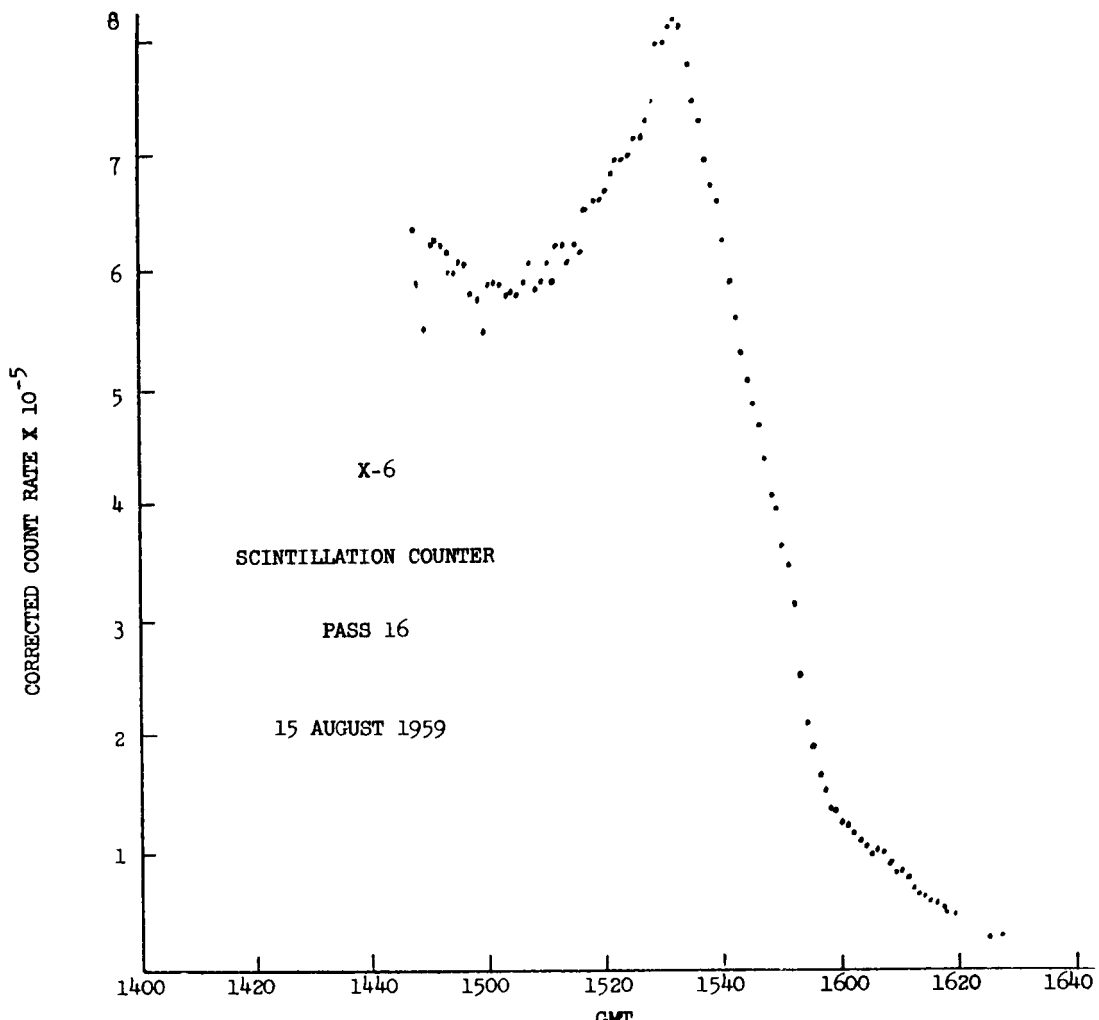


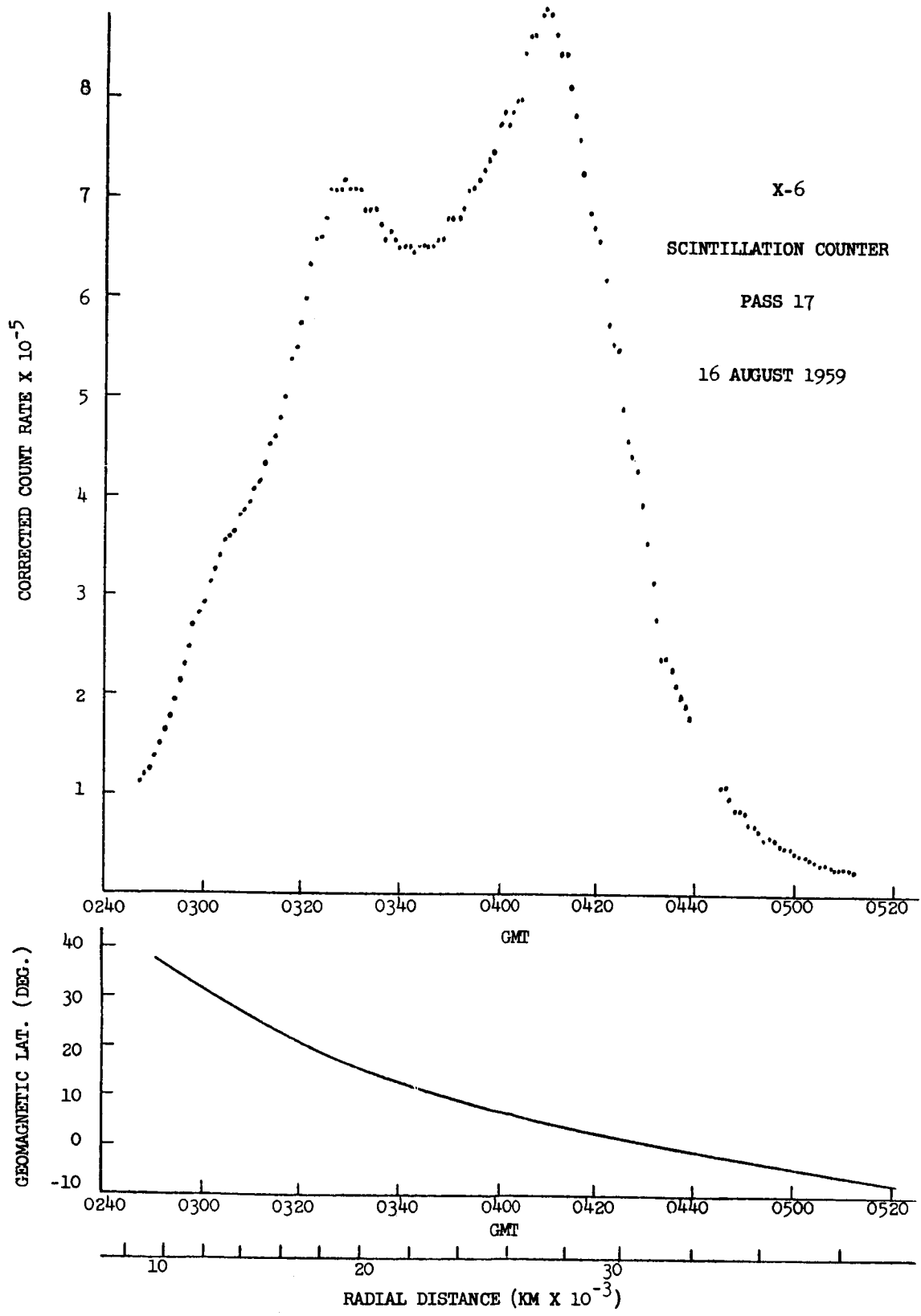




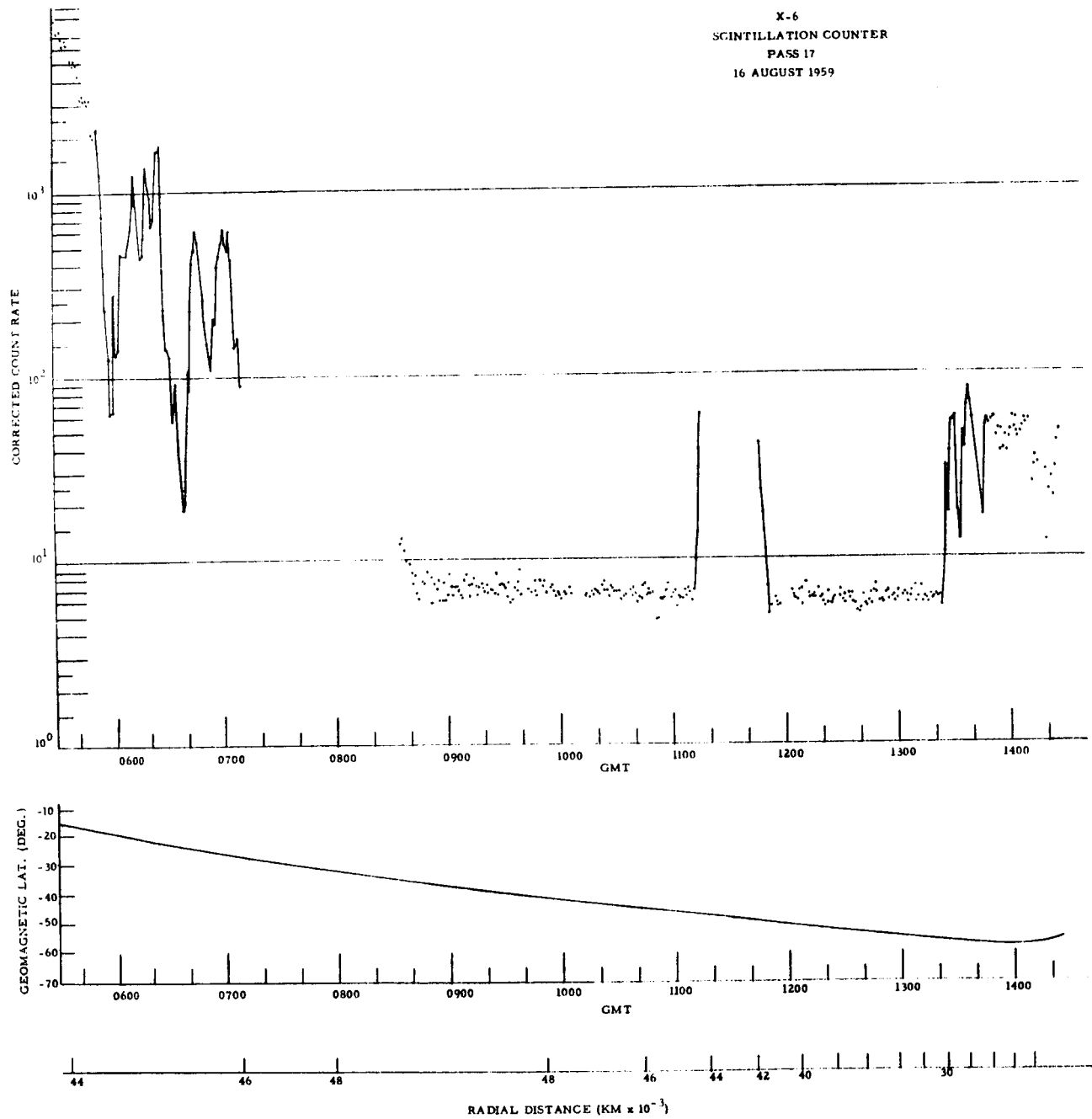


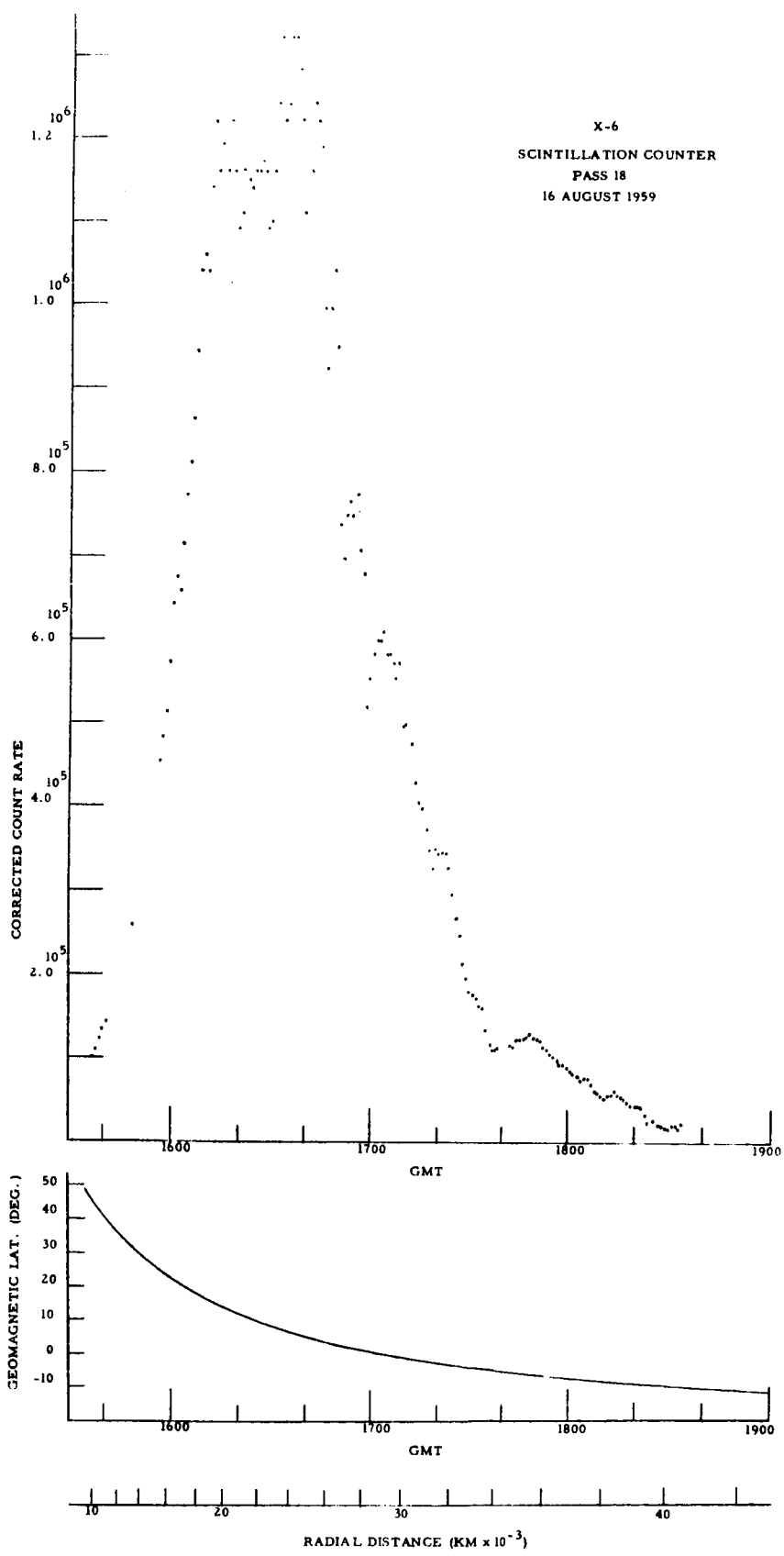


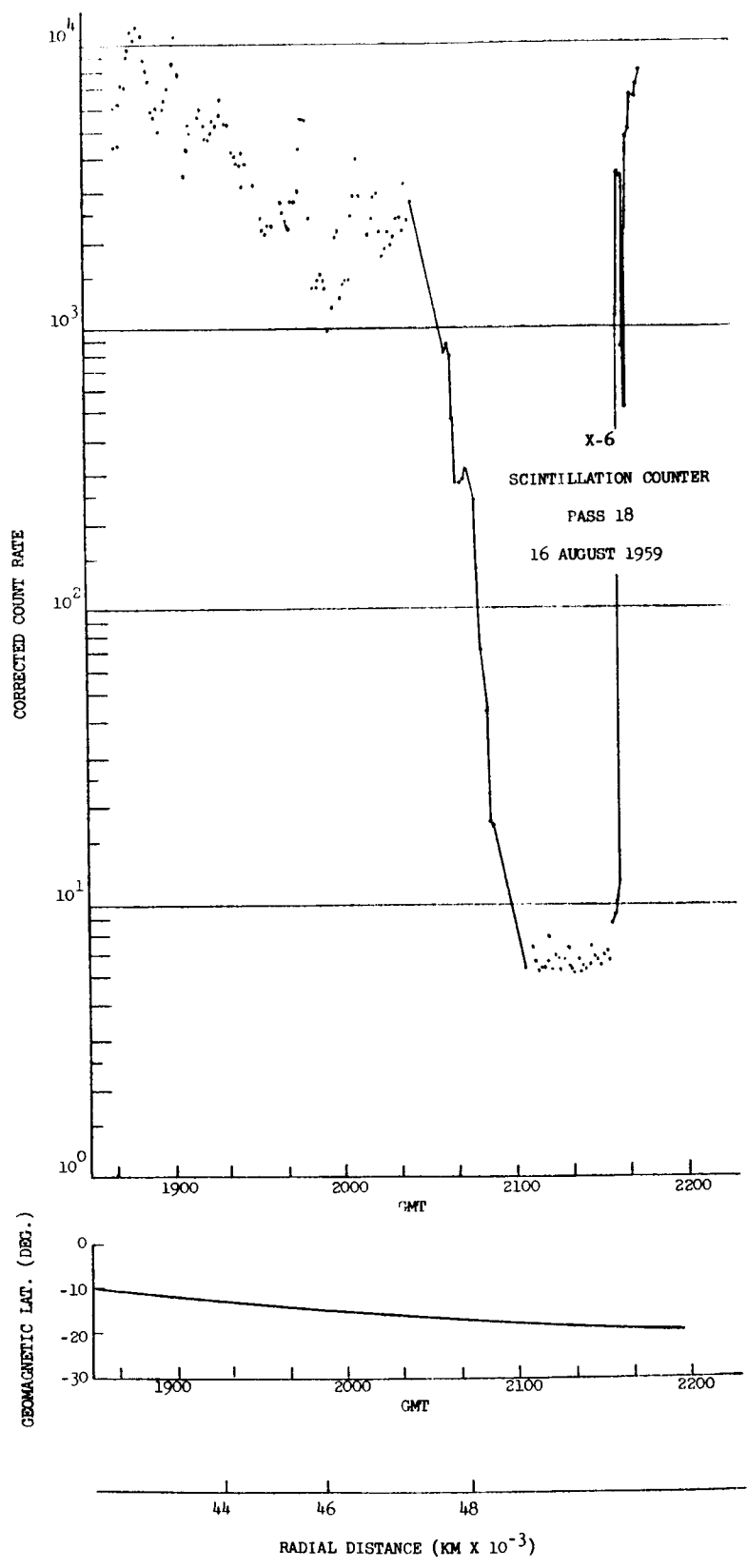


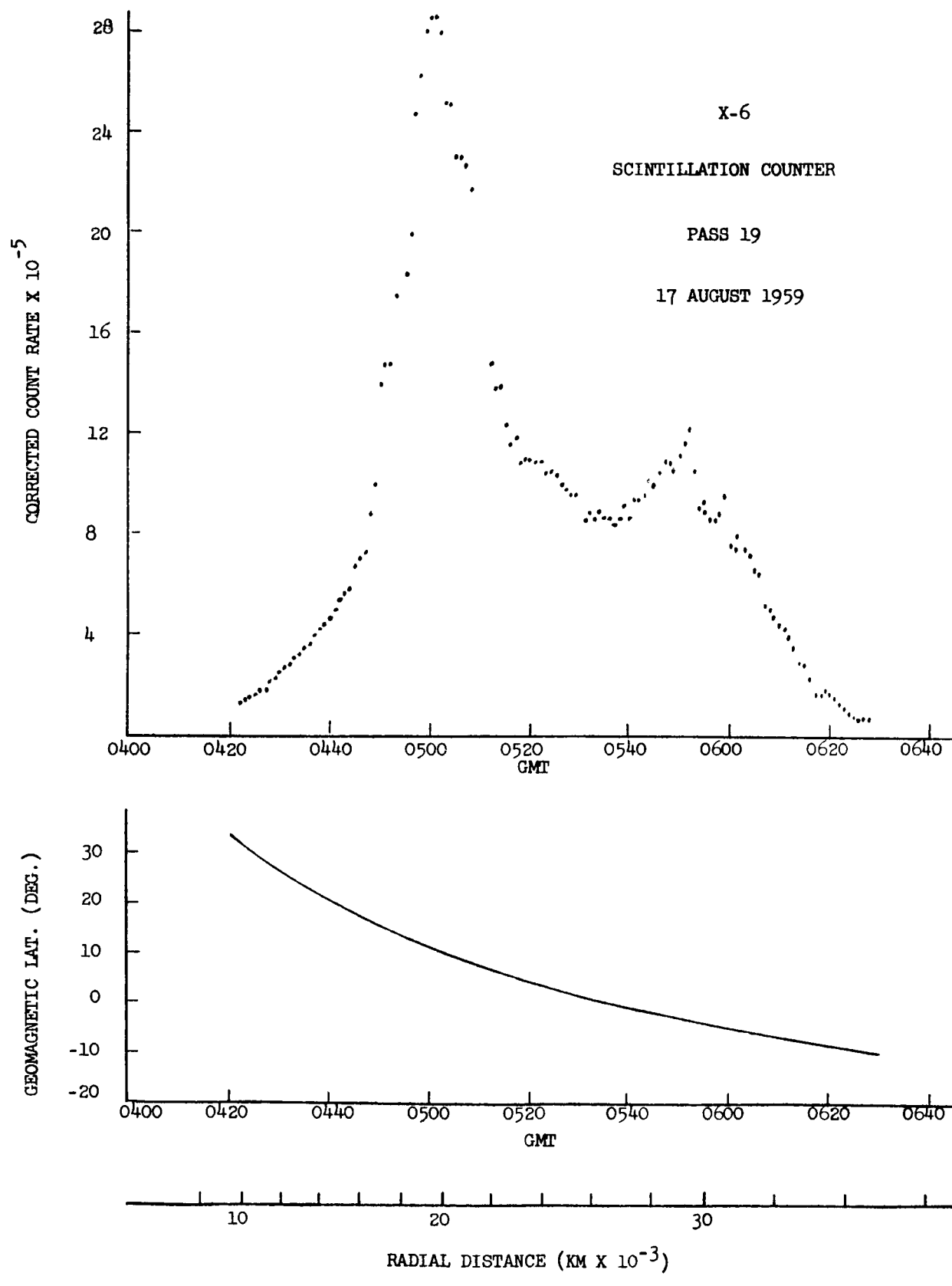


X-6
SCINTILLATION COUNTER
PASS 17
16 AUGUST 1959

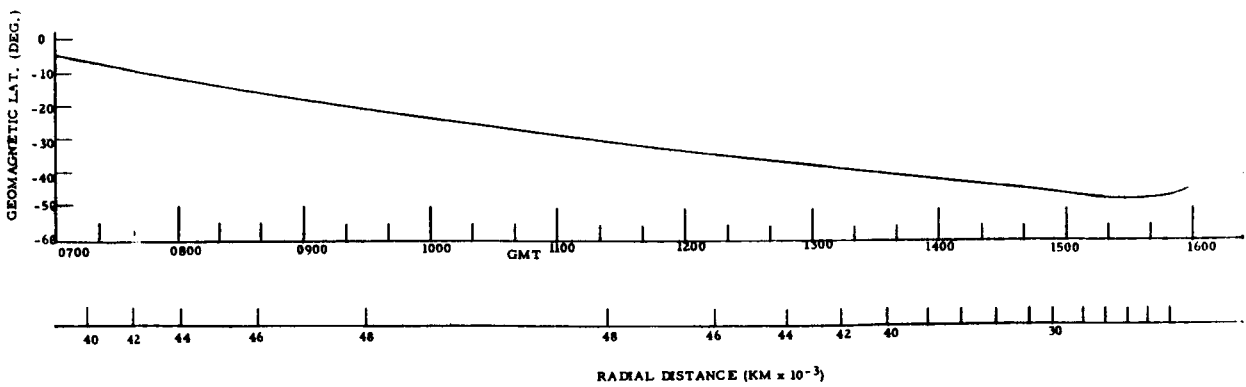
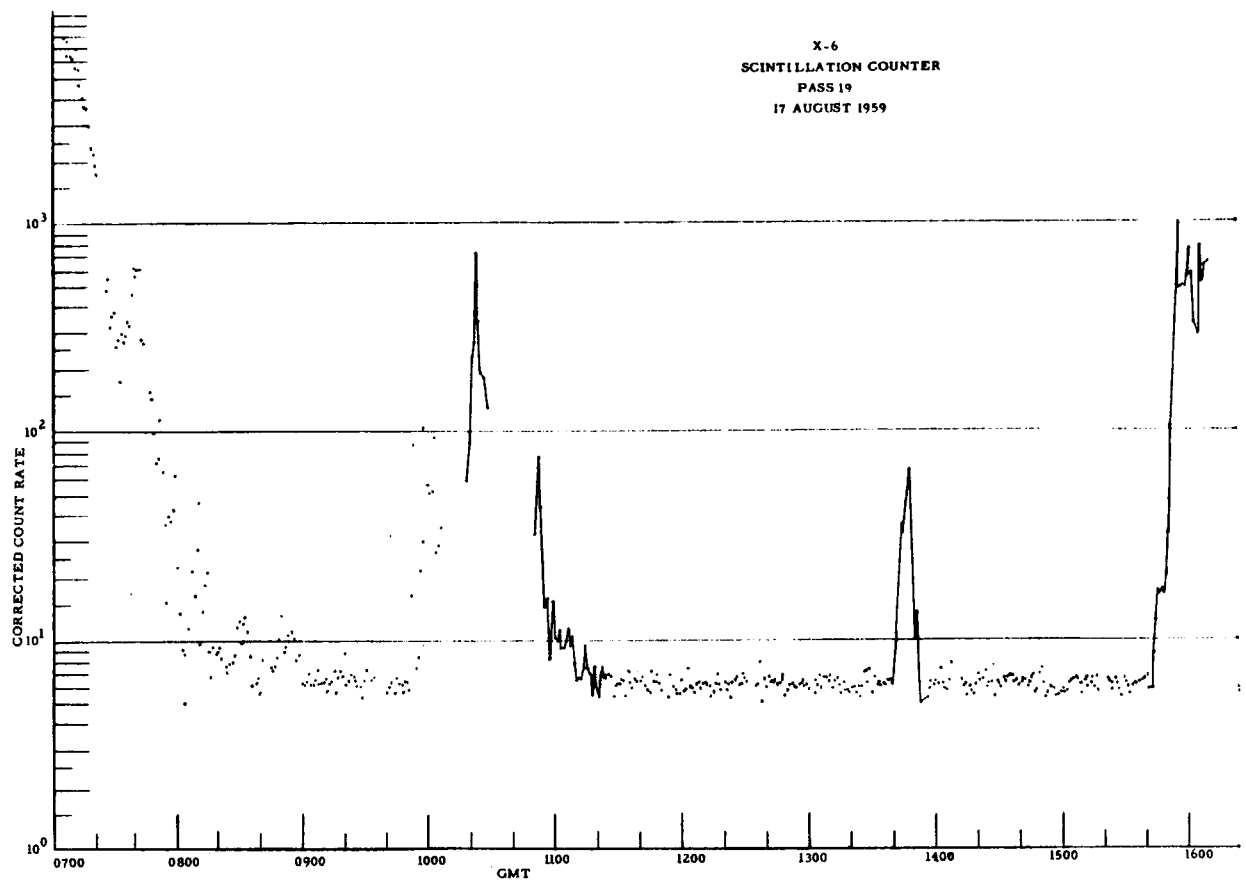


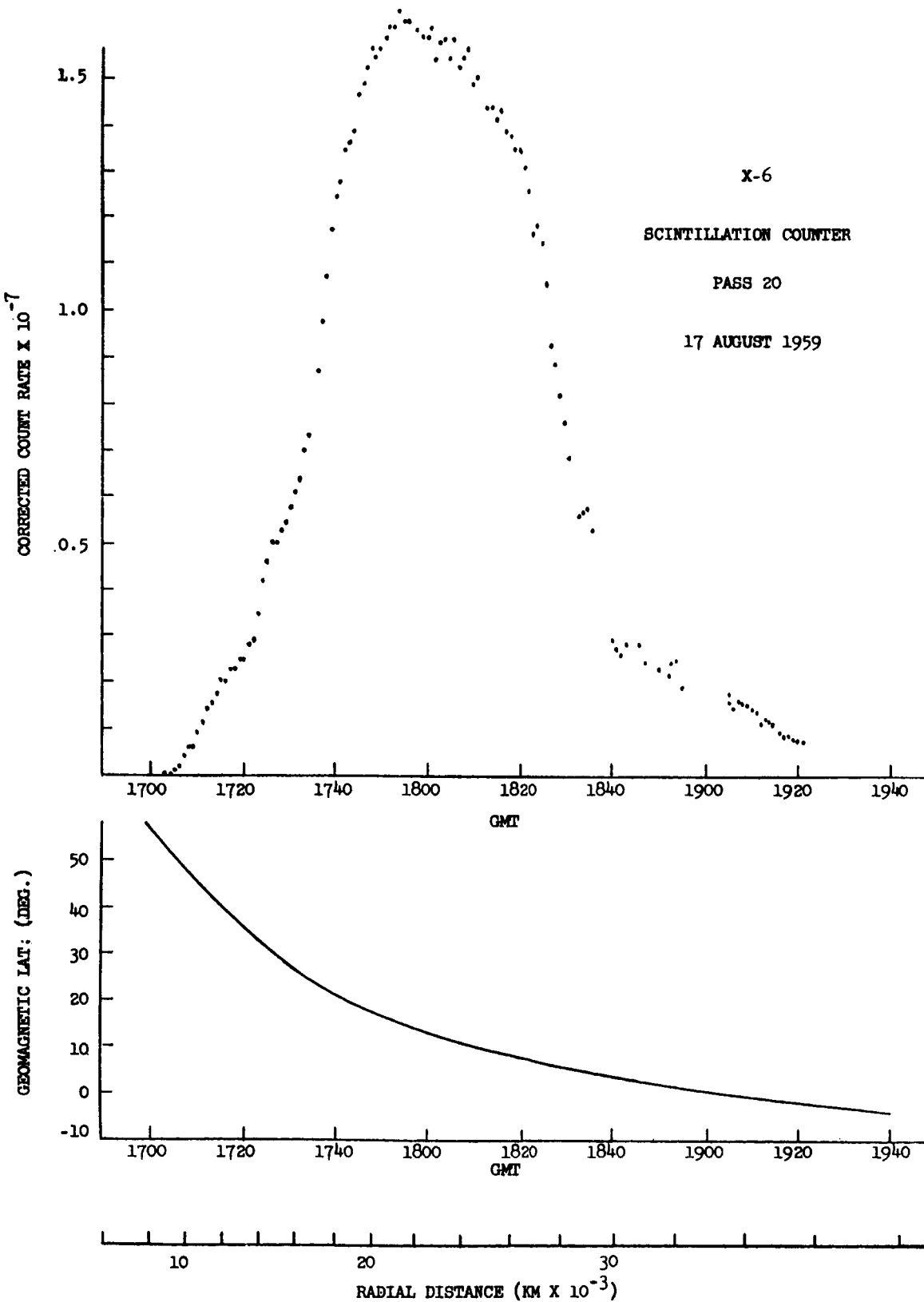


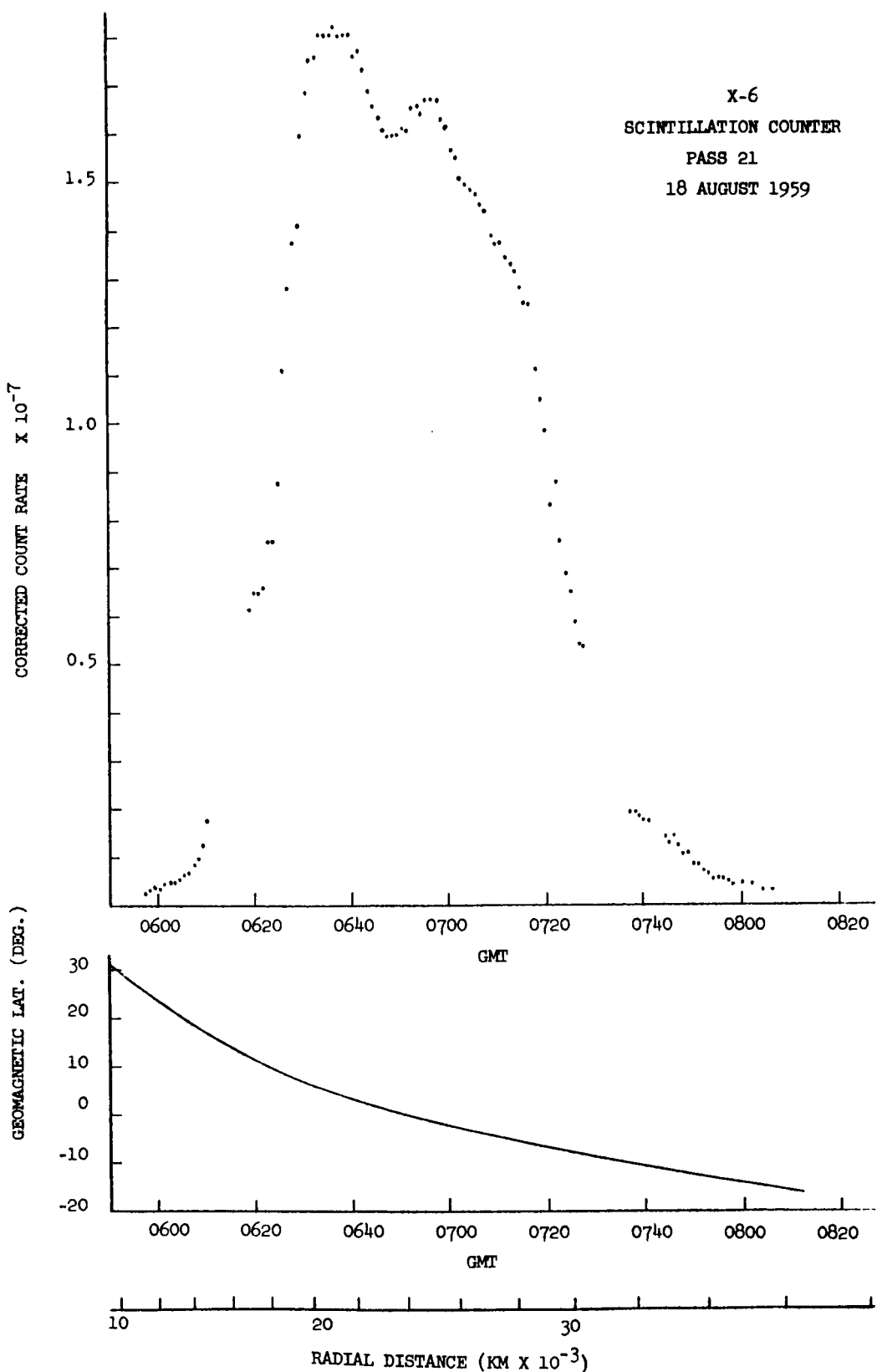


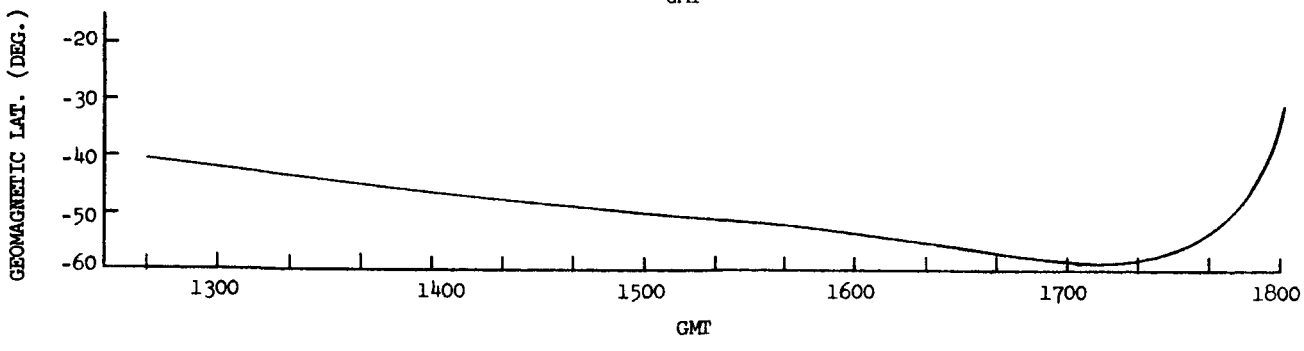
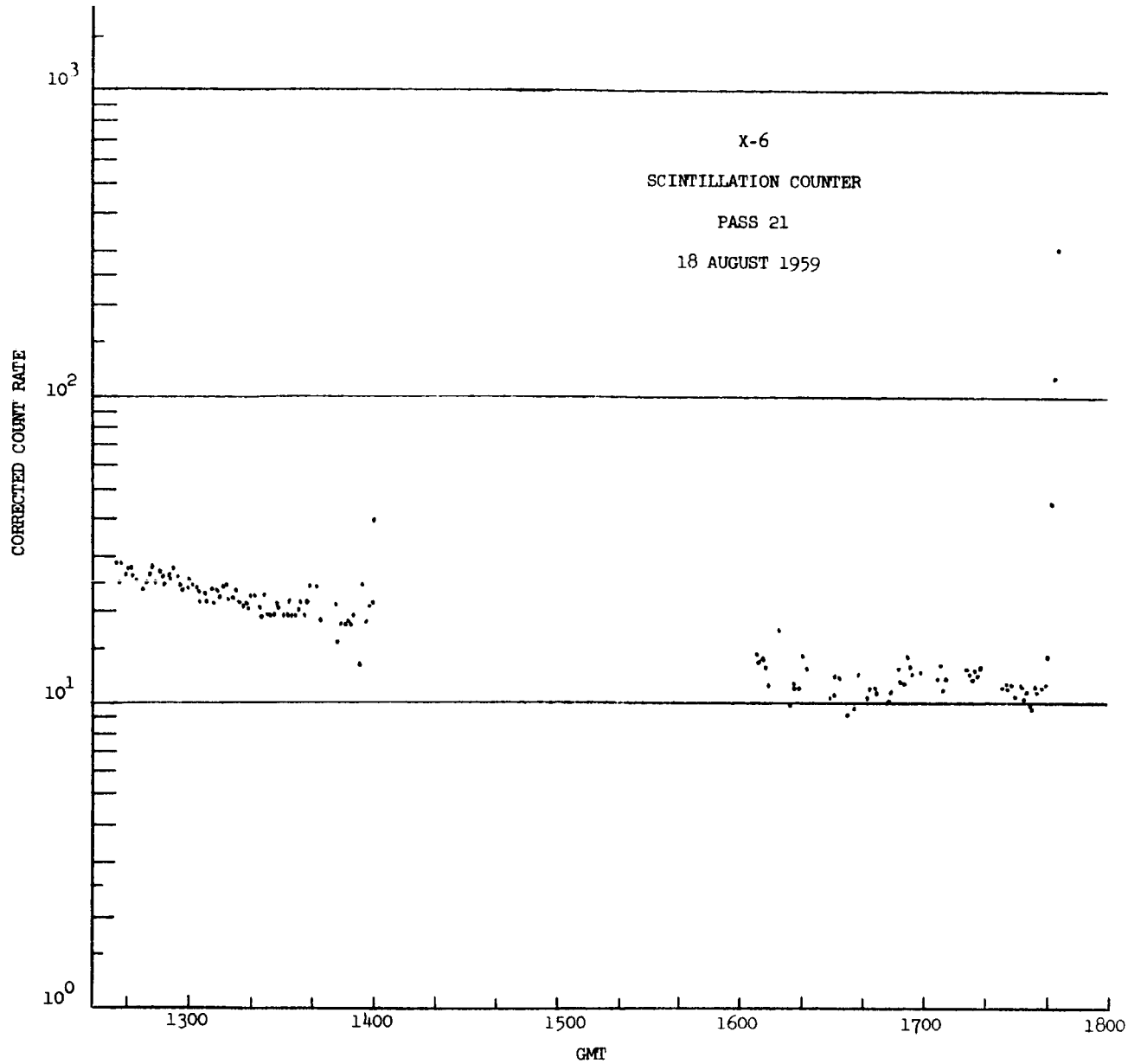


X-6
SCINTILLATION COUNTER
PASS 19
17 AUGUST 1959



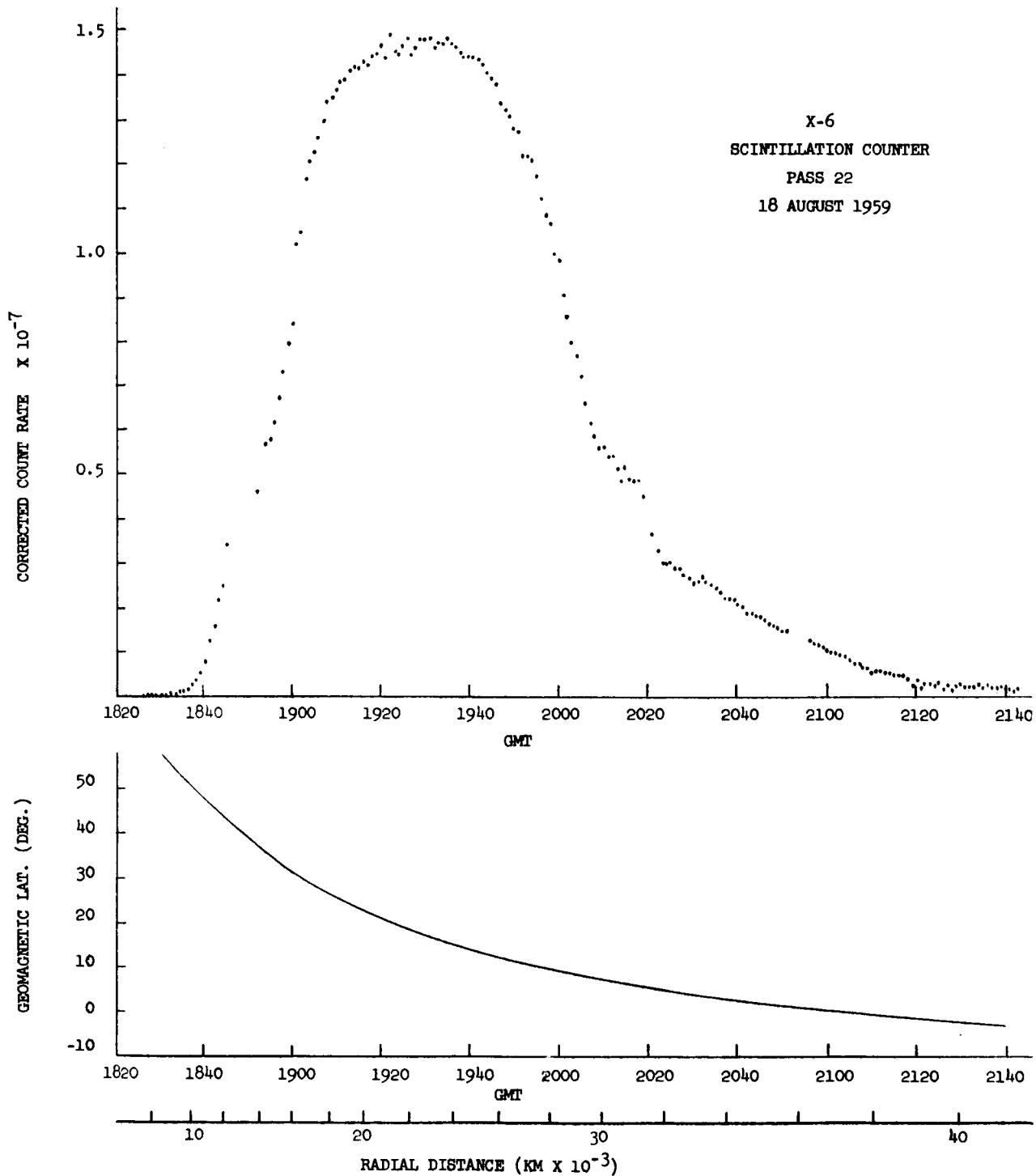


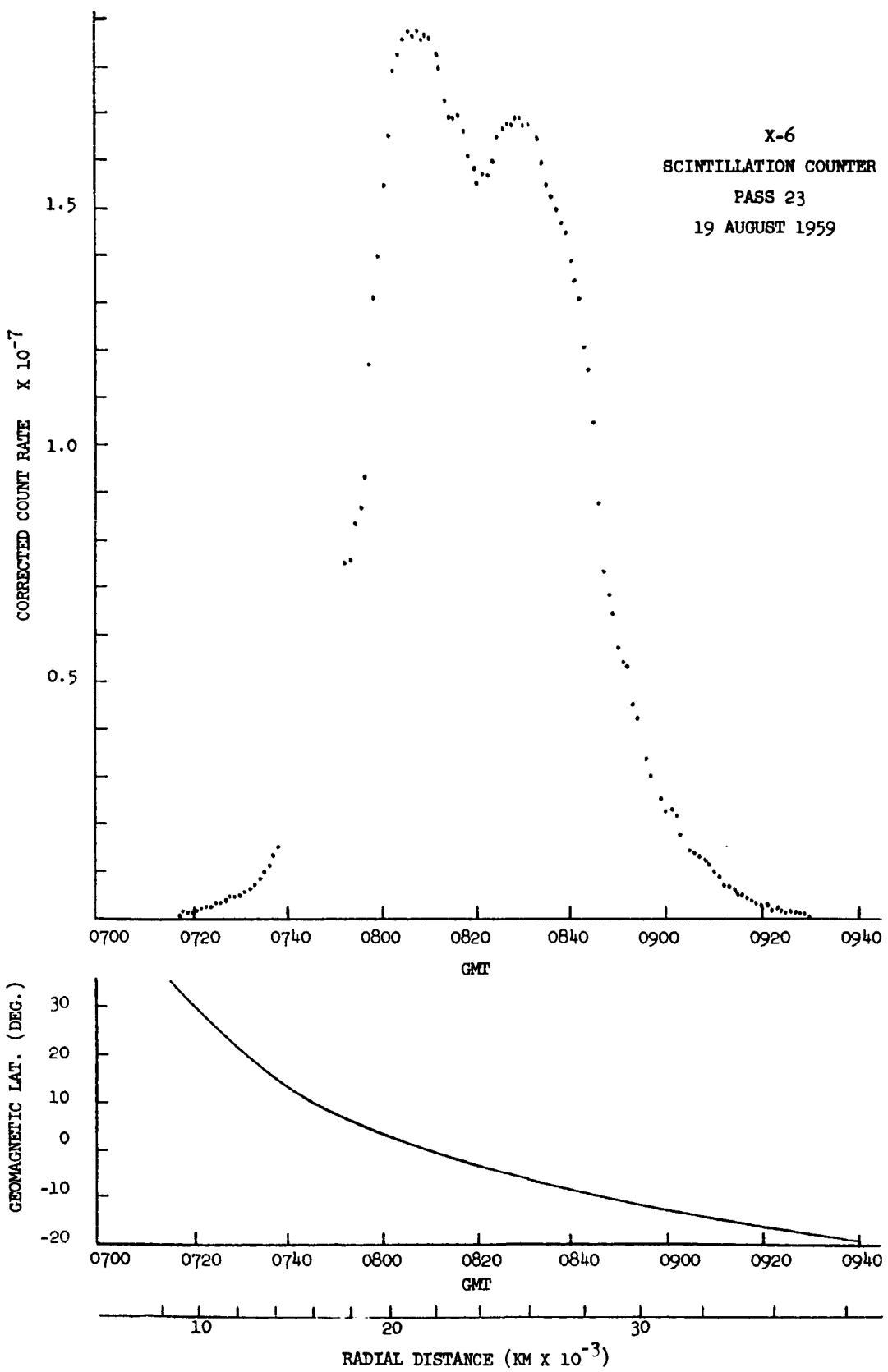


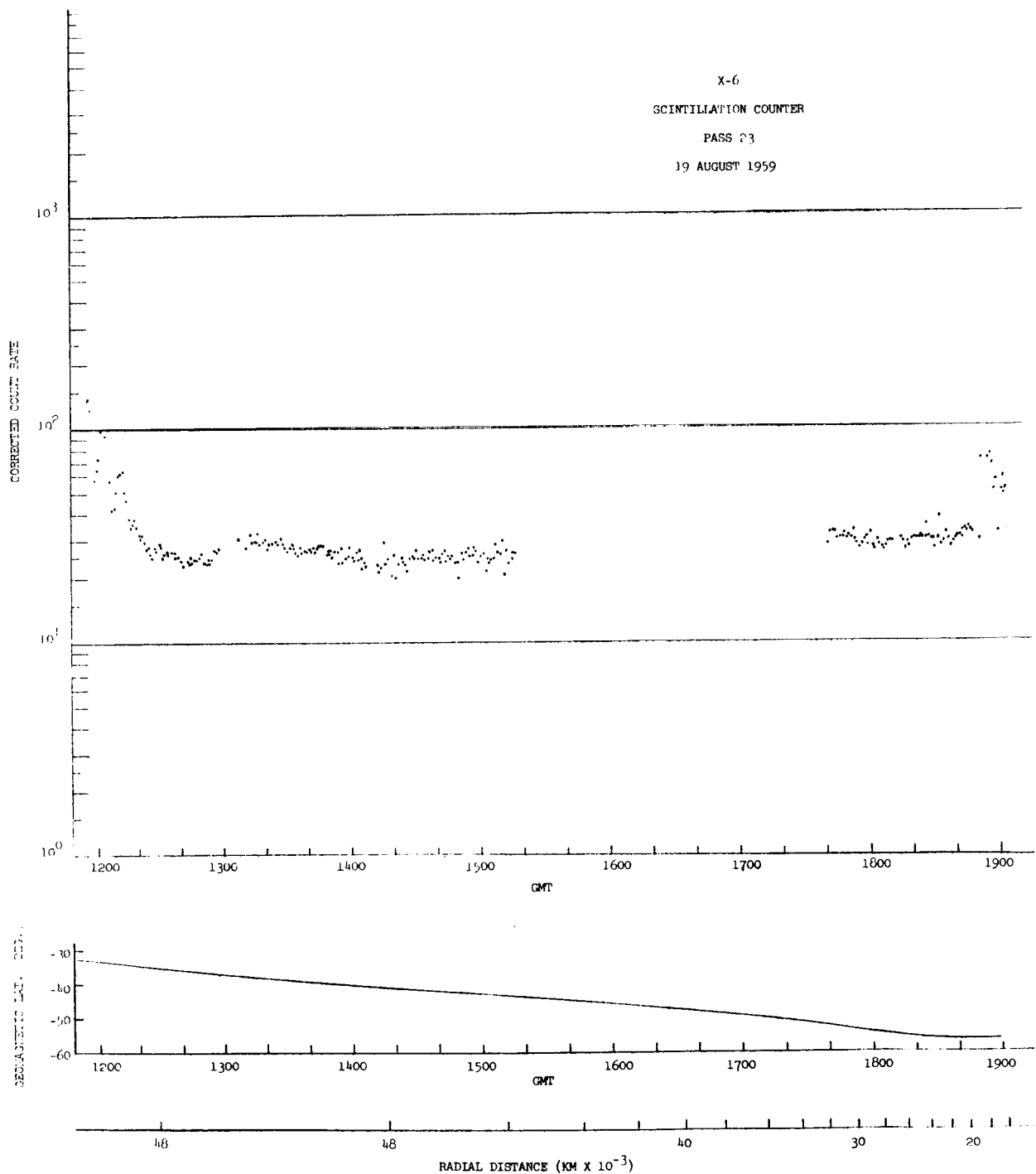


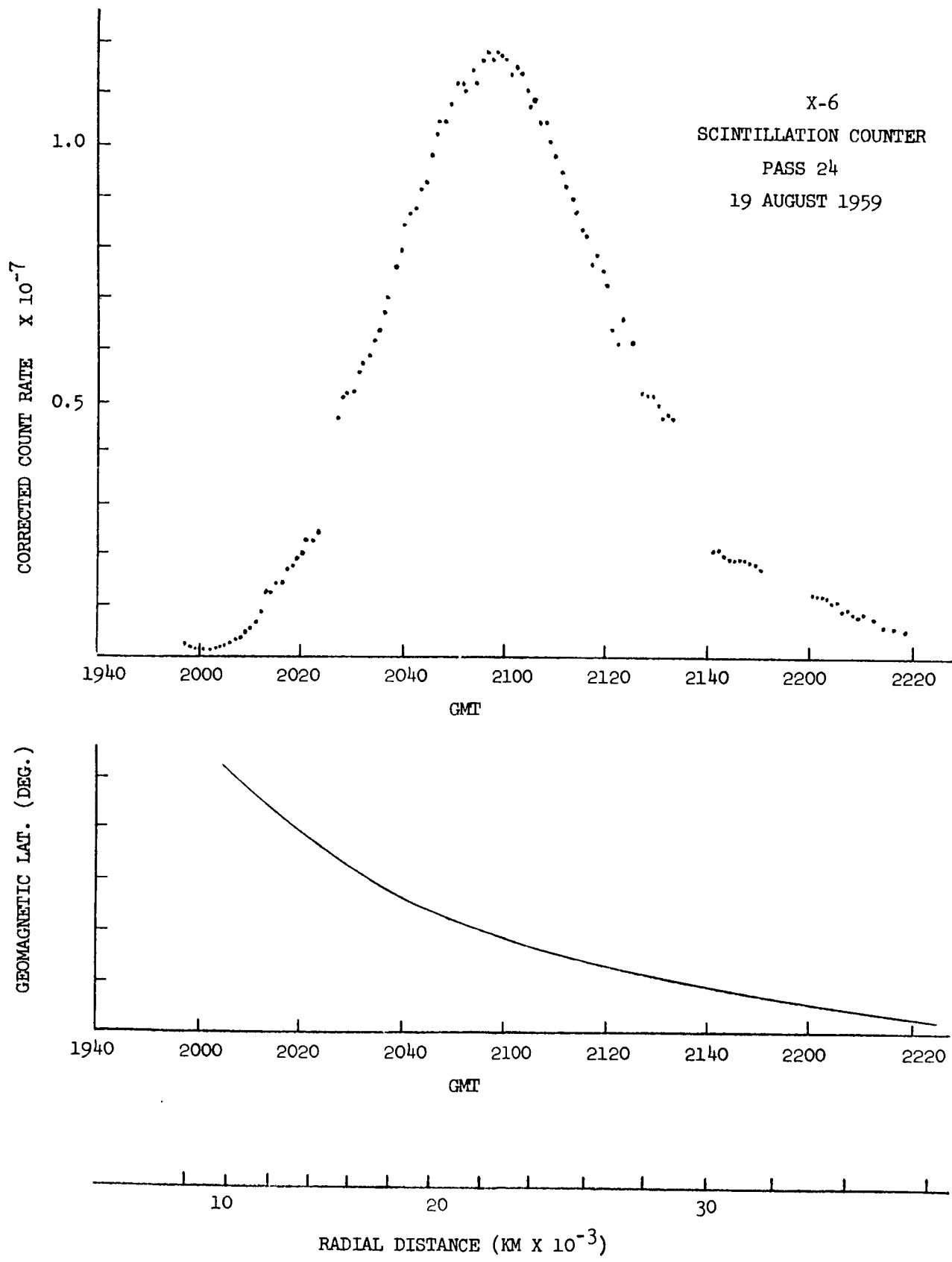
40 30 20

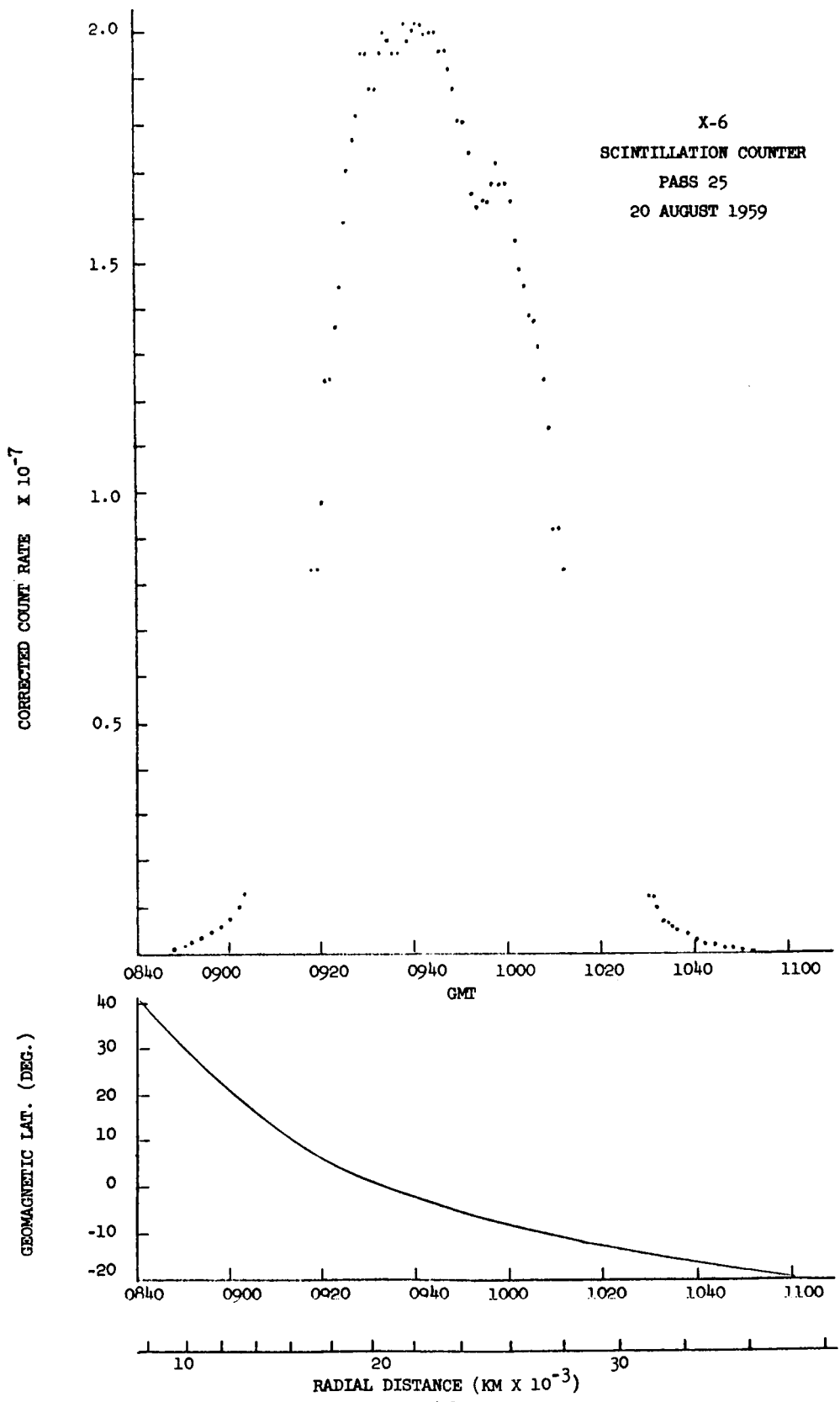
RADIAL DISTANCE (KM X 10^{-3})

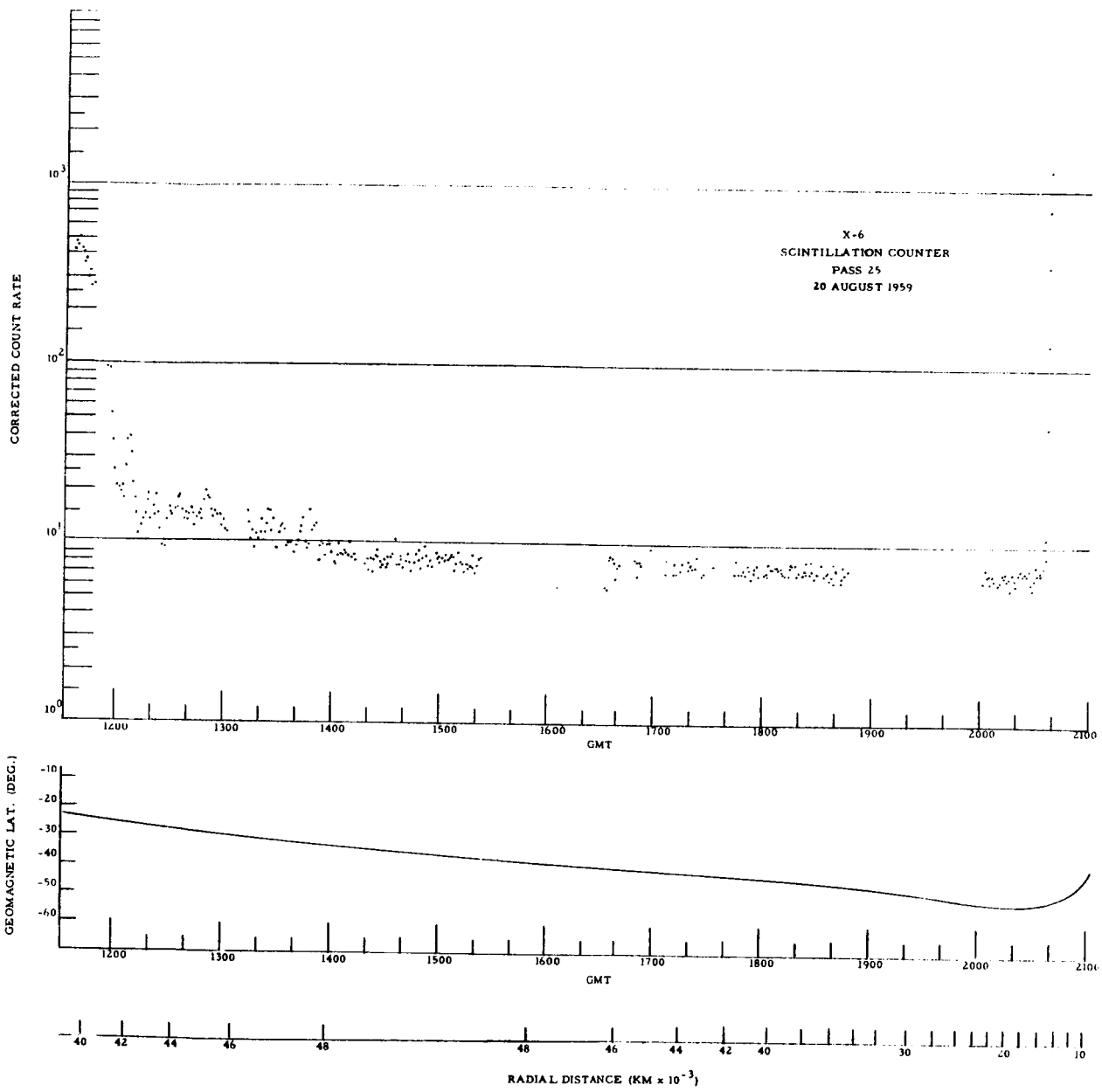


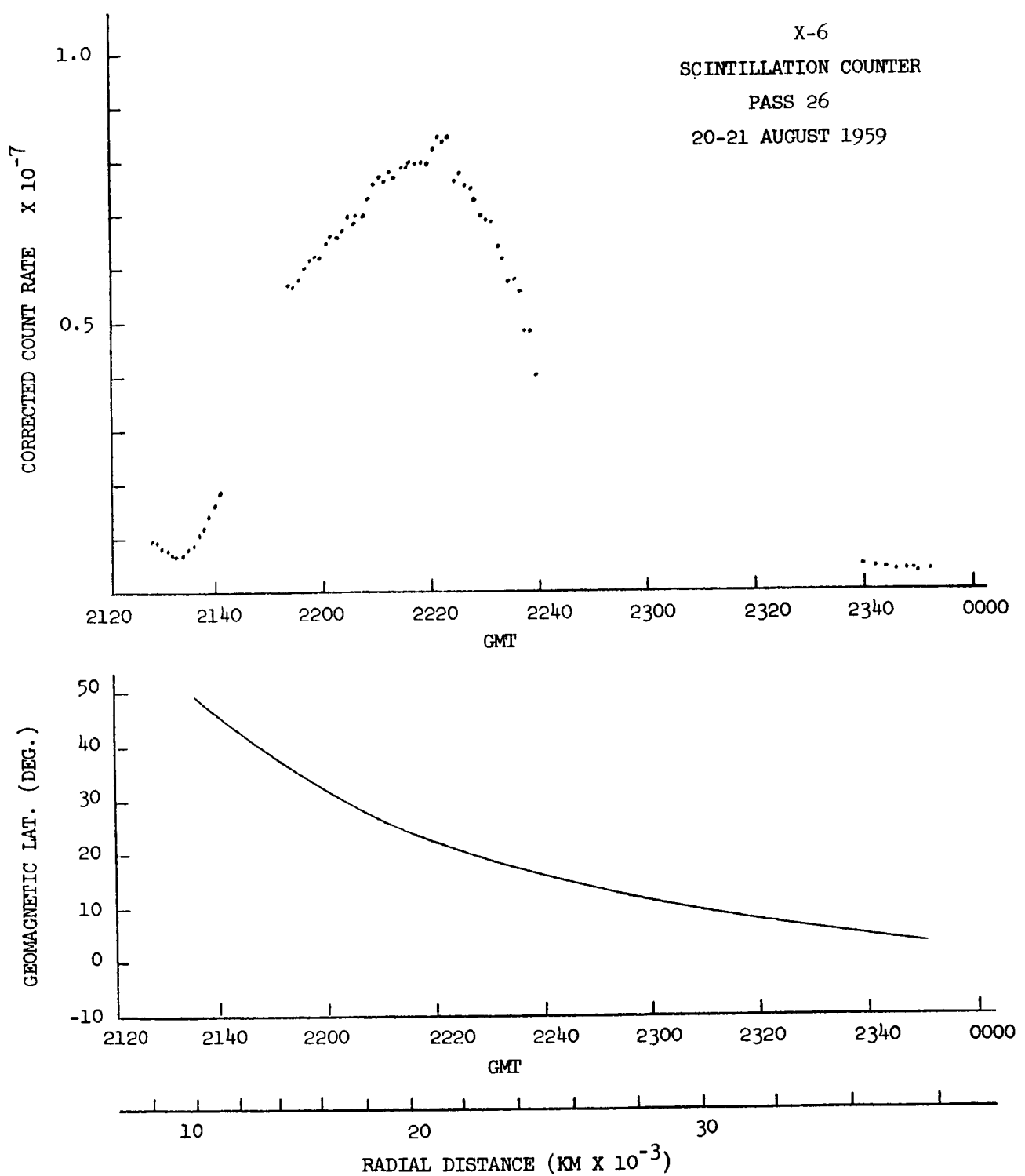


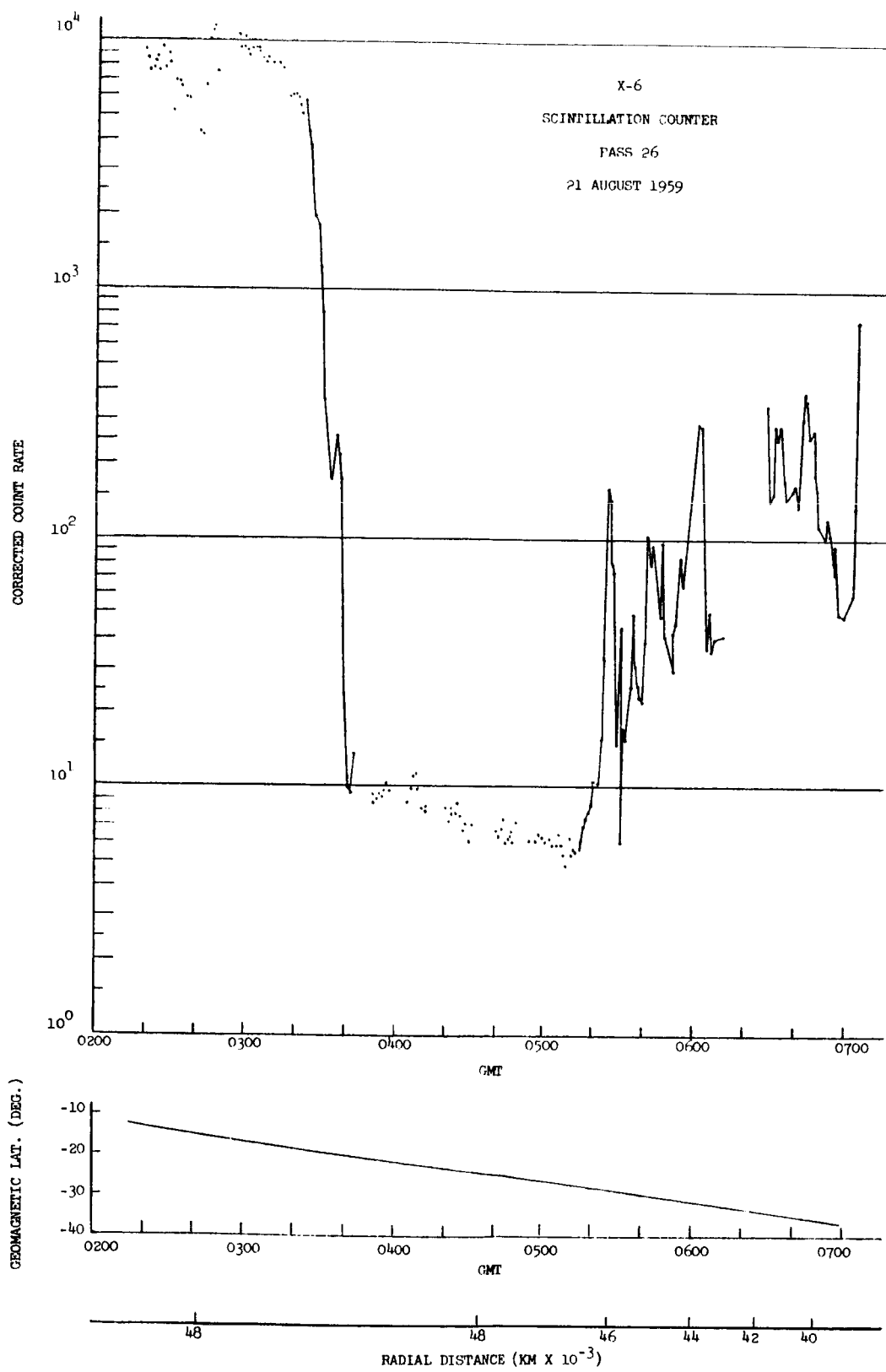


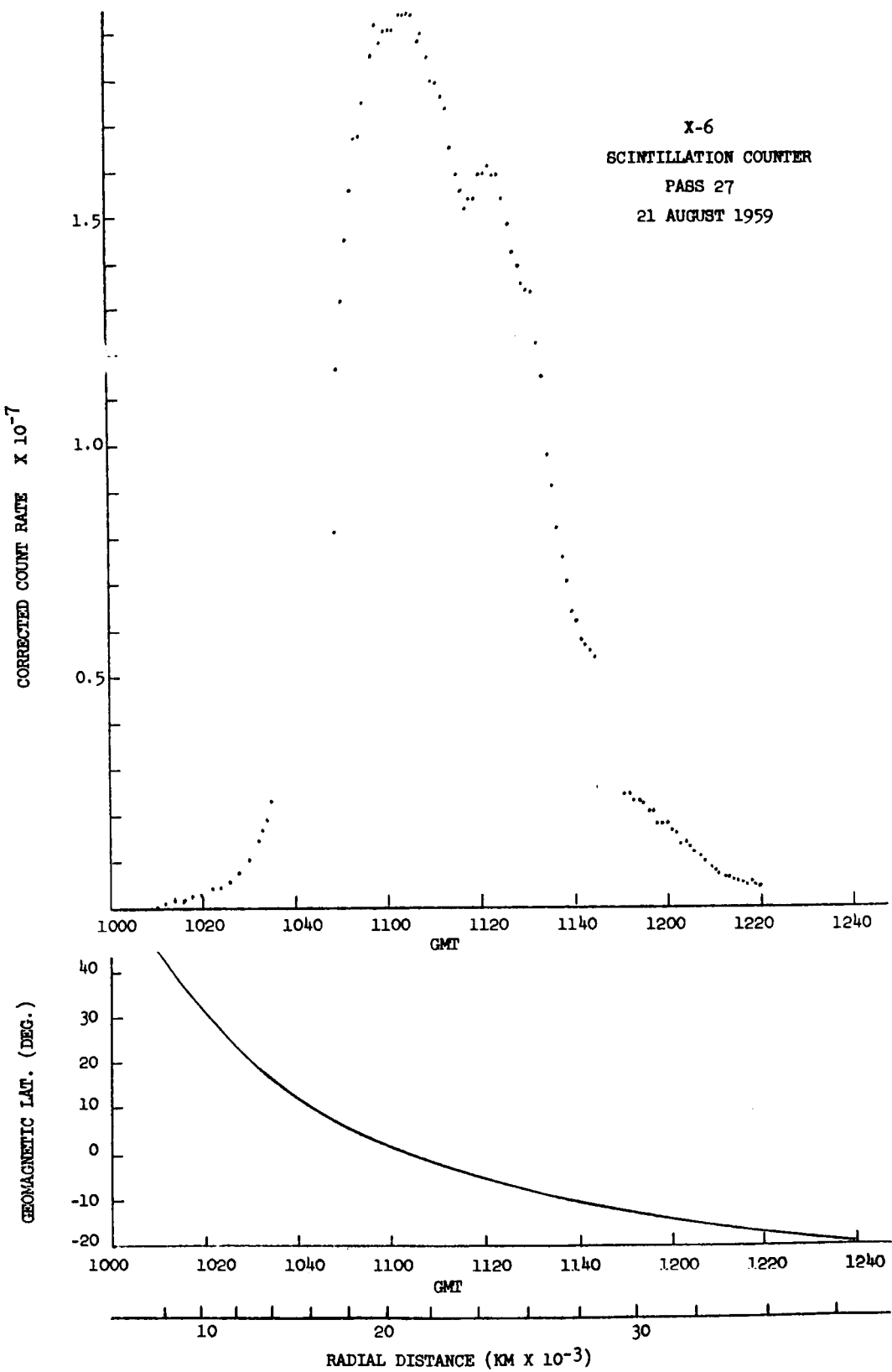


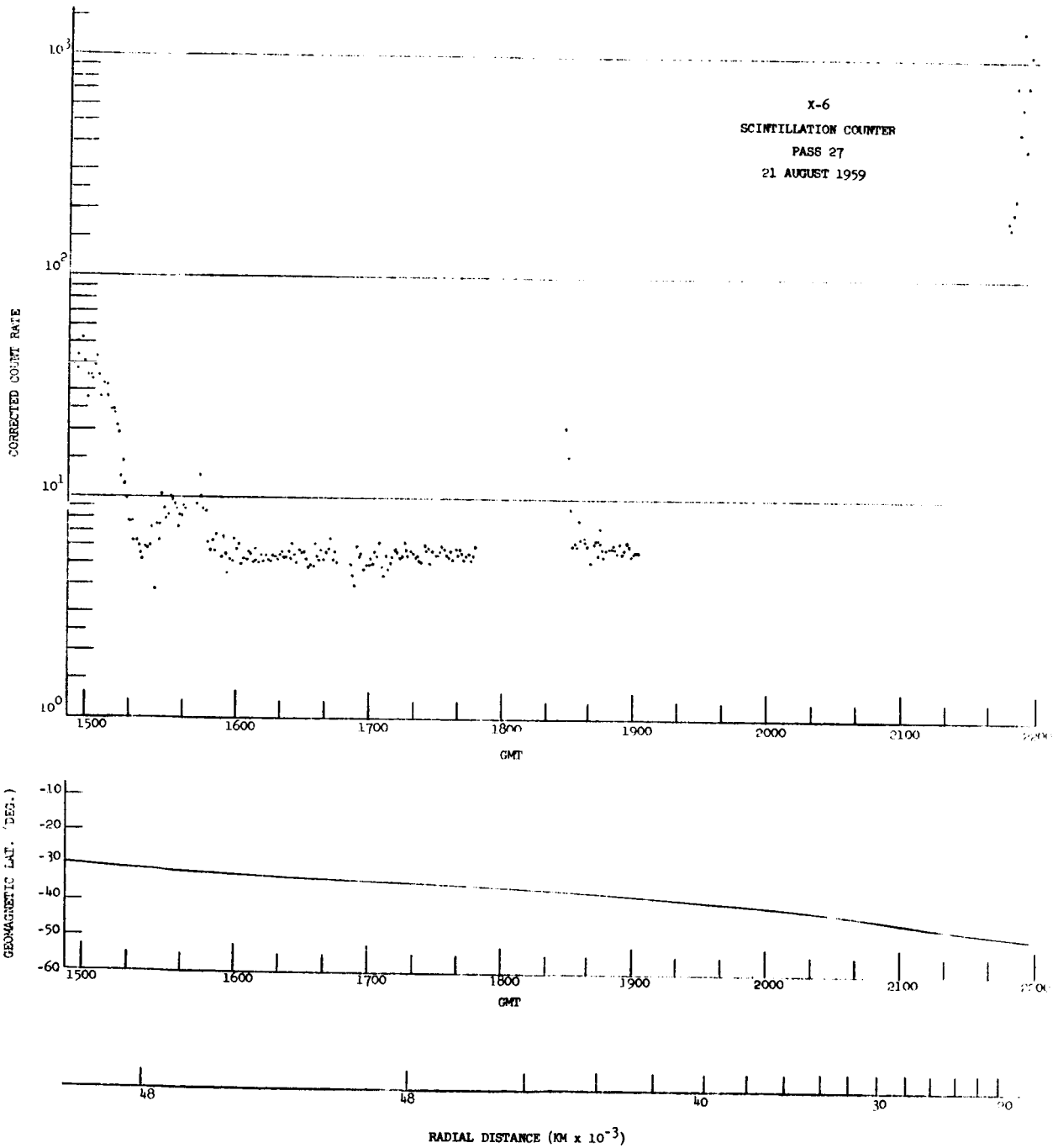


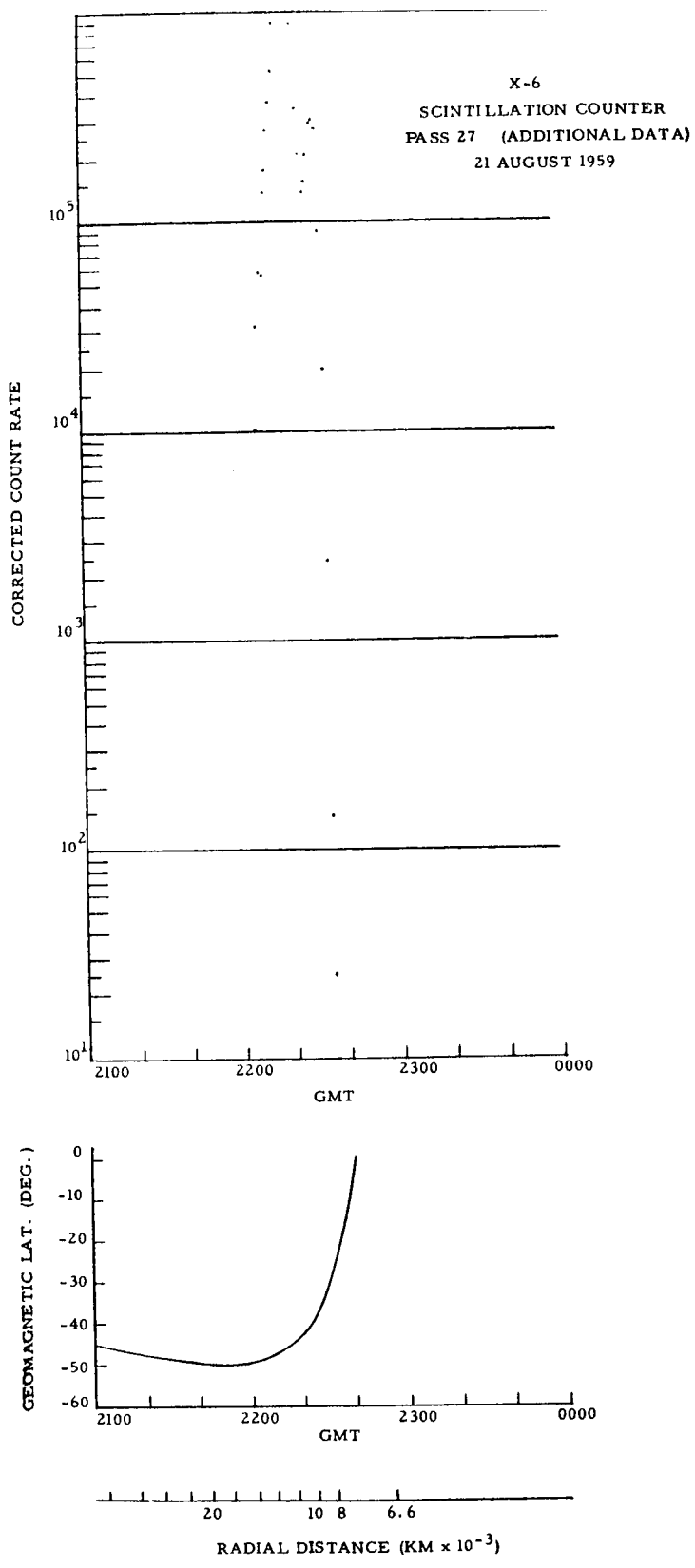


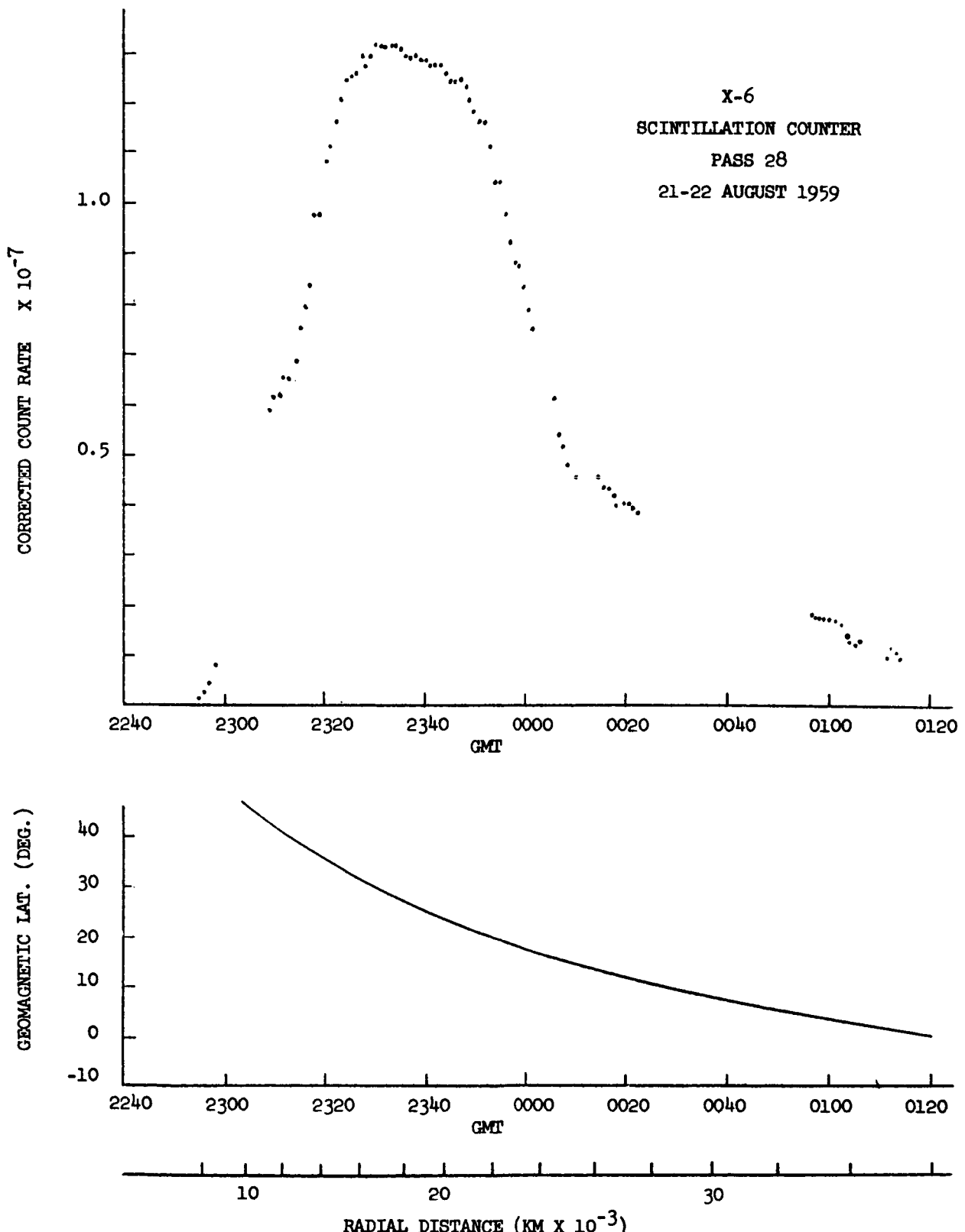


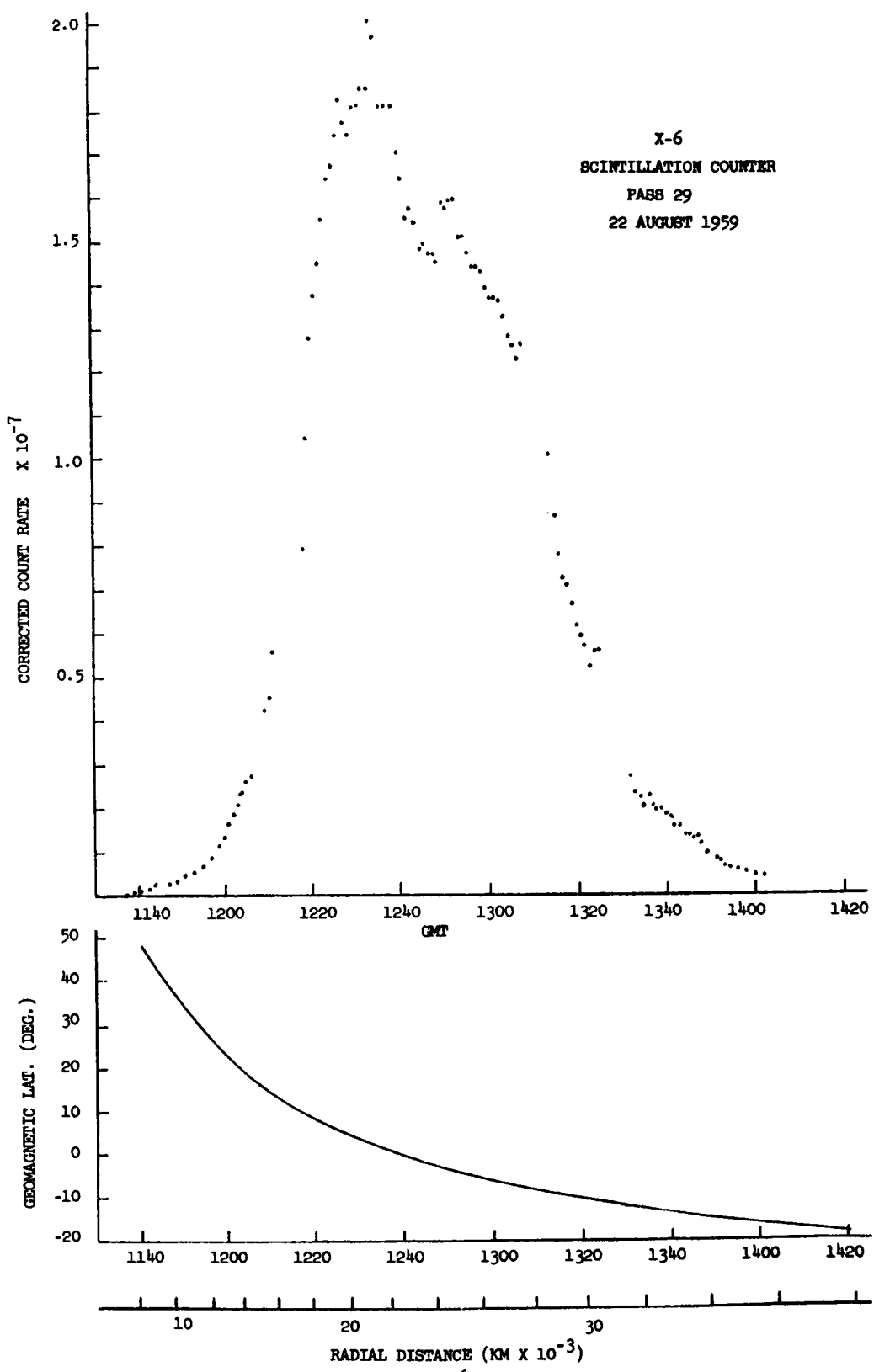












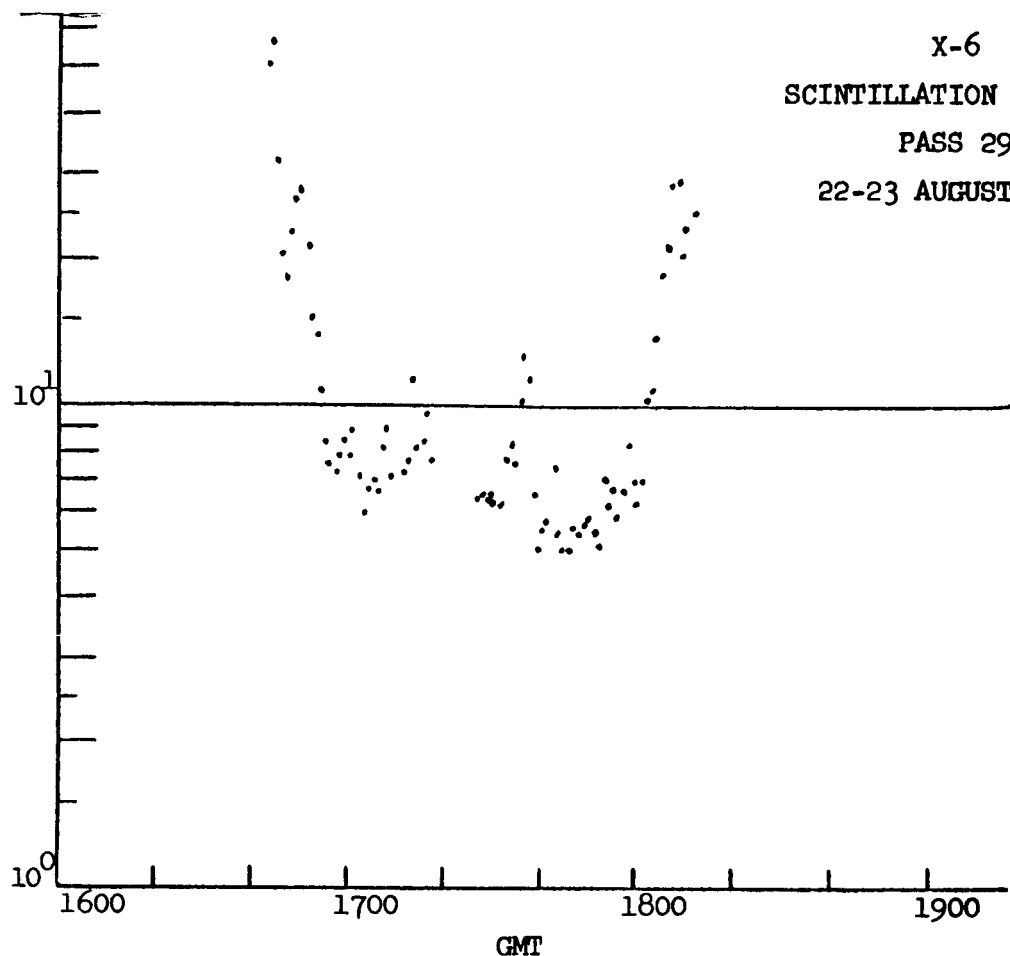
X-6

SCINTILLATION COUNTER

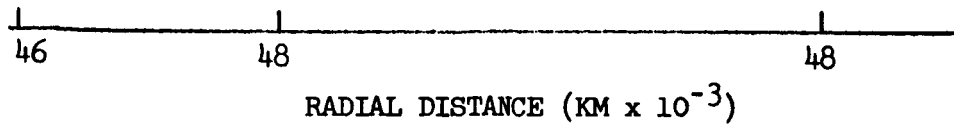
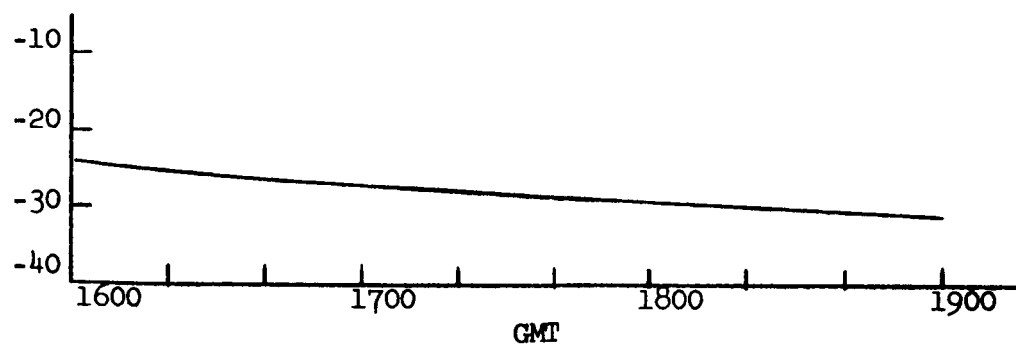
PASS 29

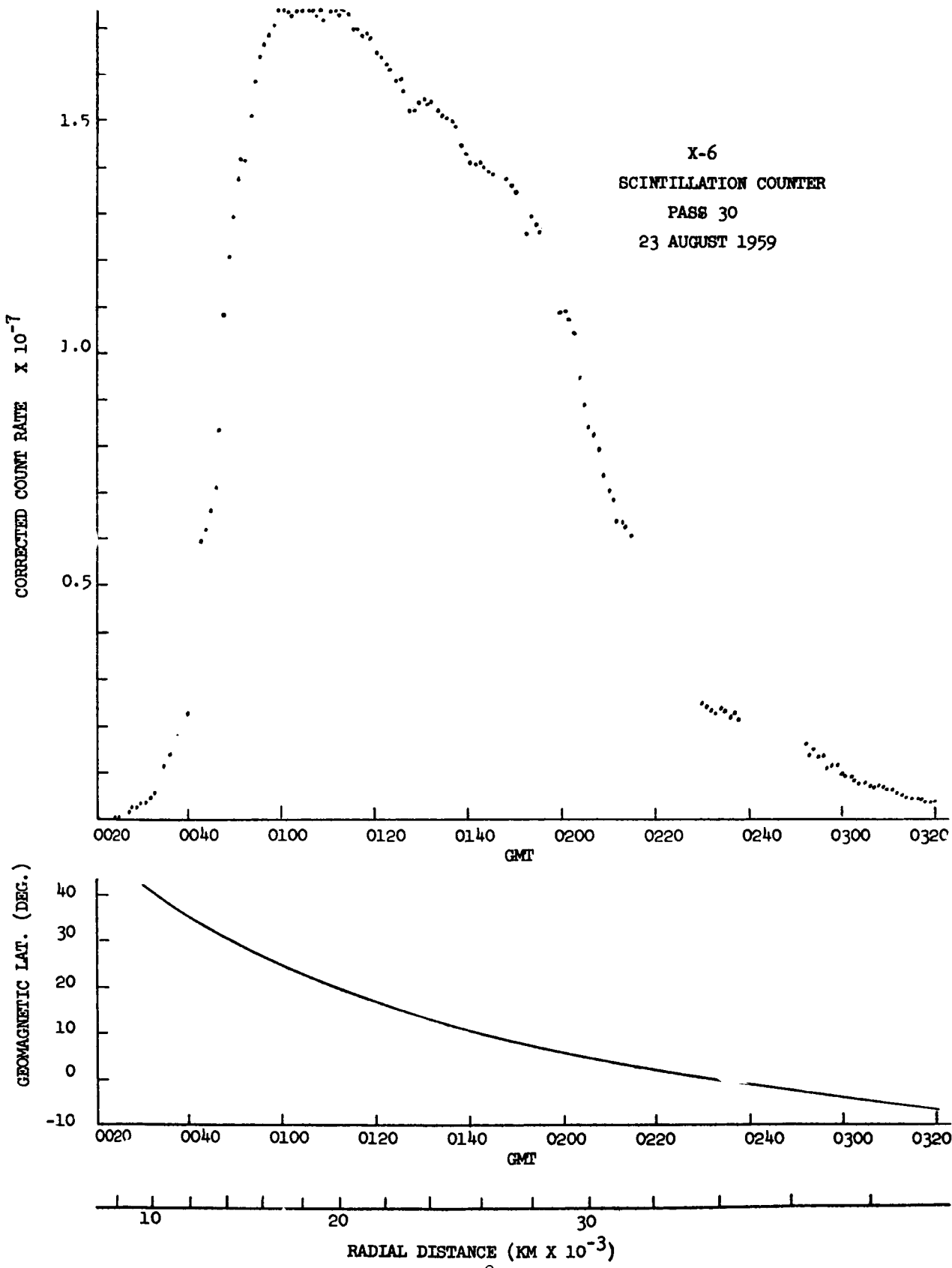
22-23 AUGUST 1959

CORRECTED COUNT RATE

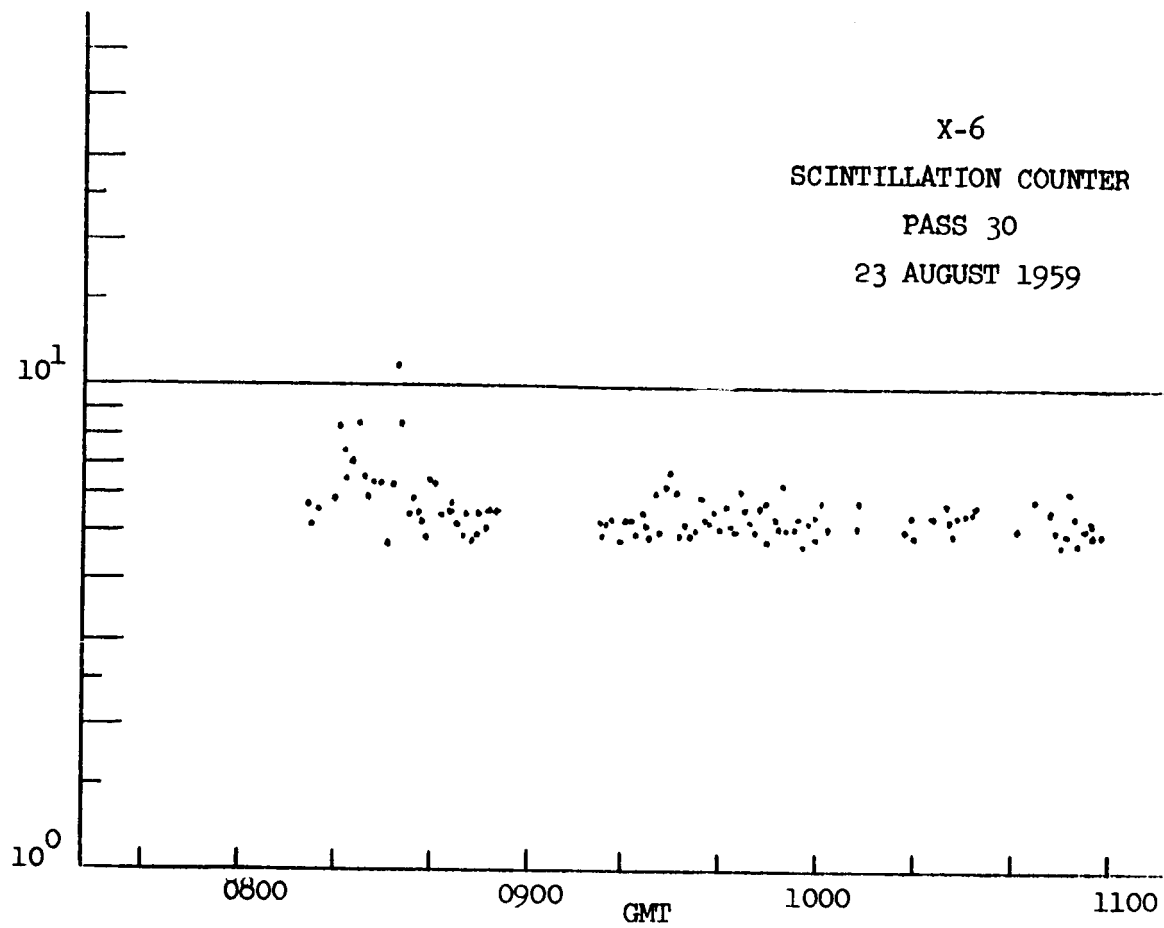


GEOMAGNETIC LAT. (DEG.)

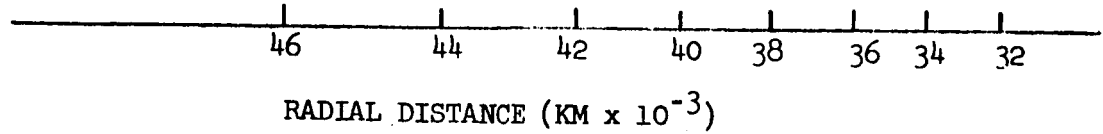
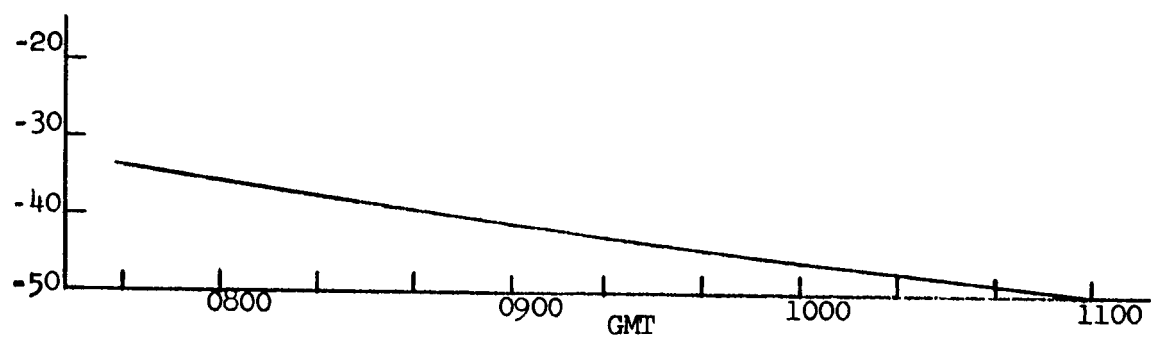


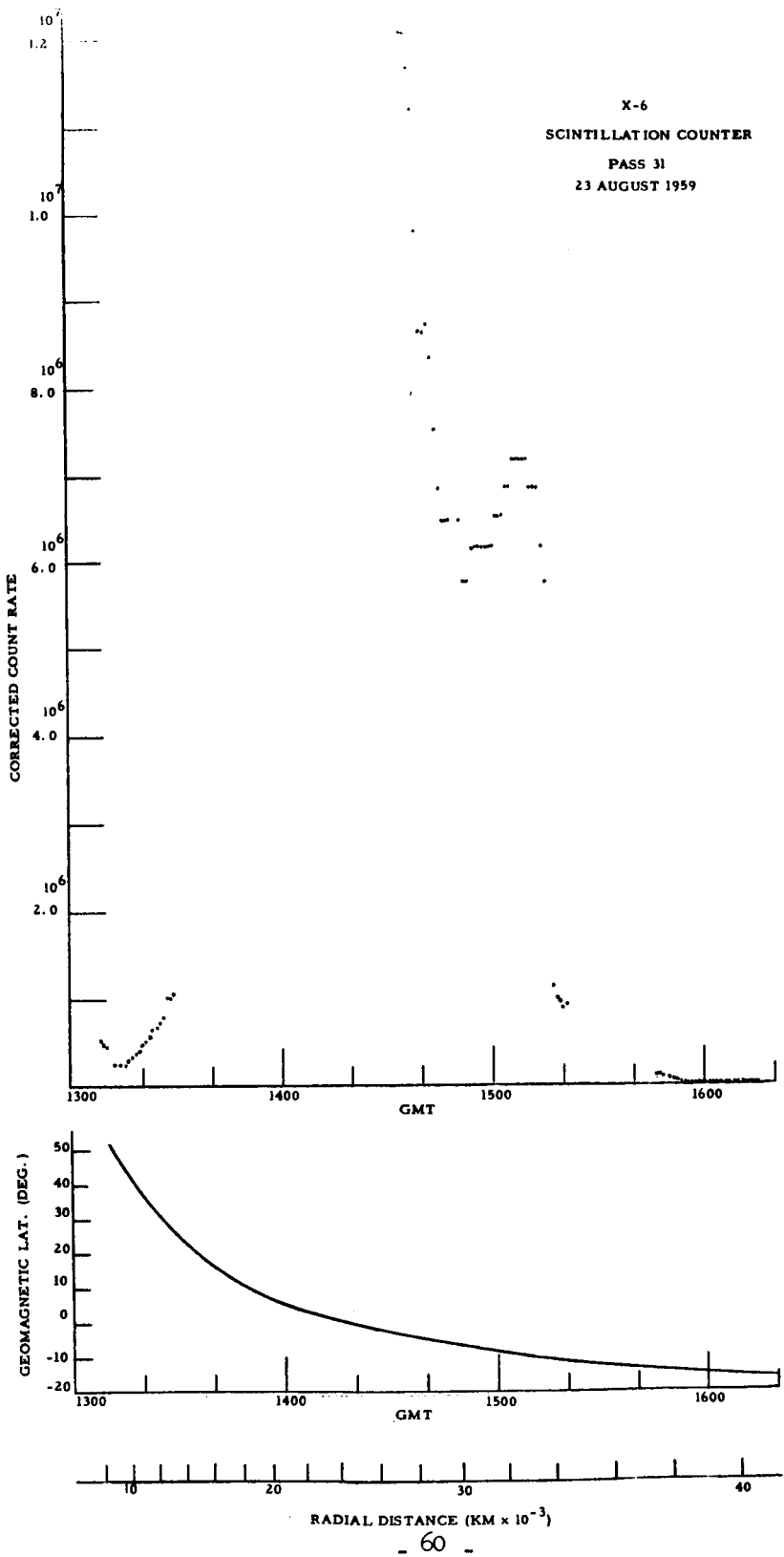


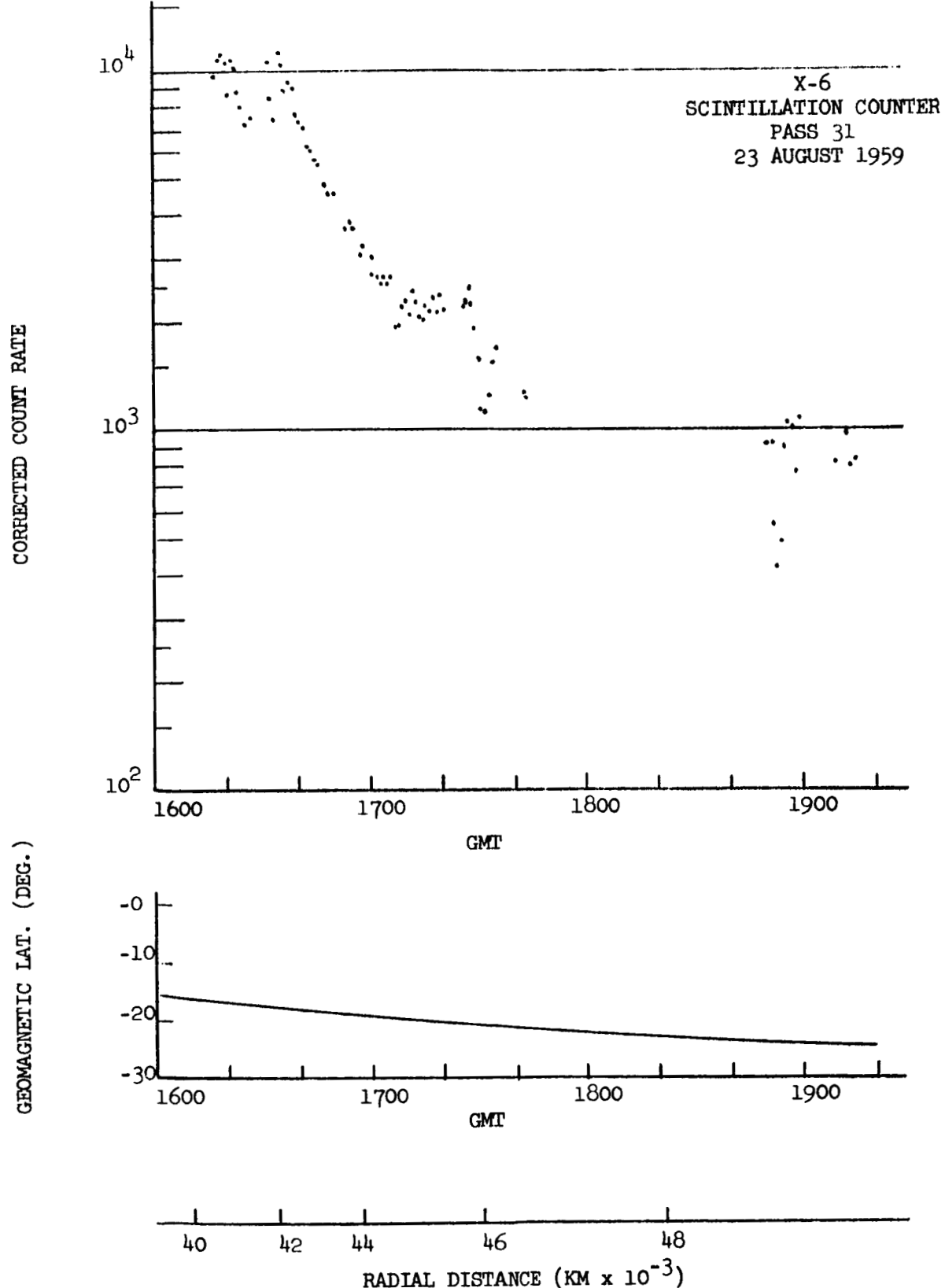
CORRECTED COUNT RATE

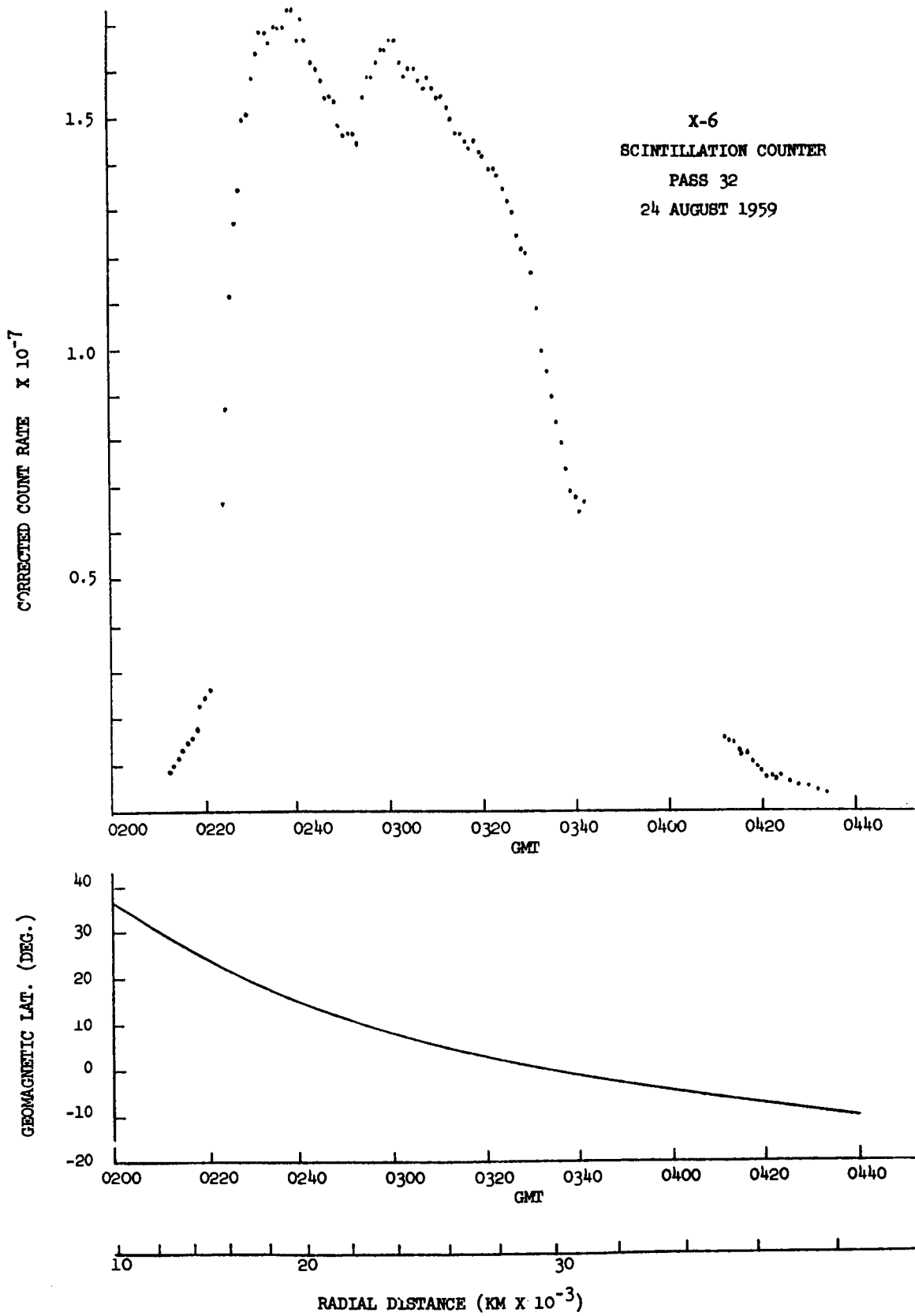


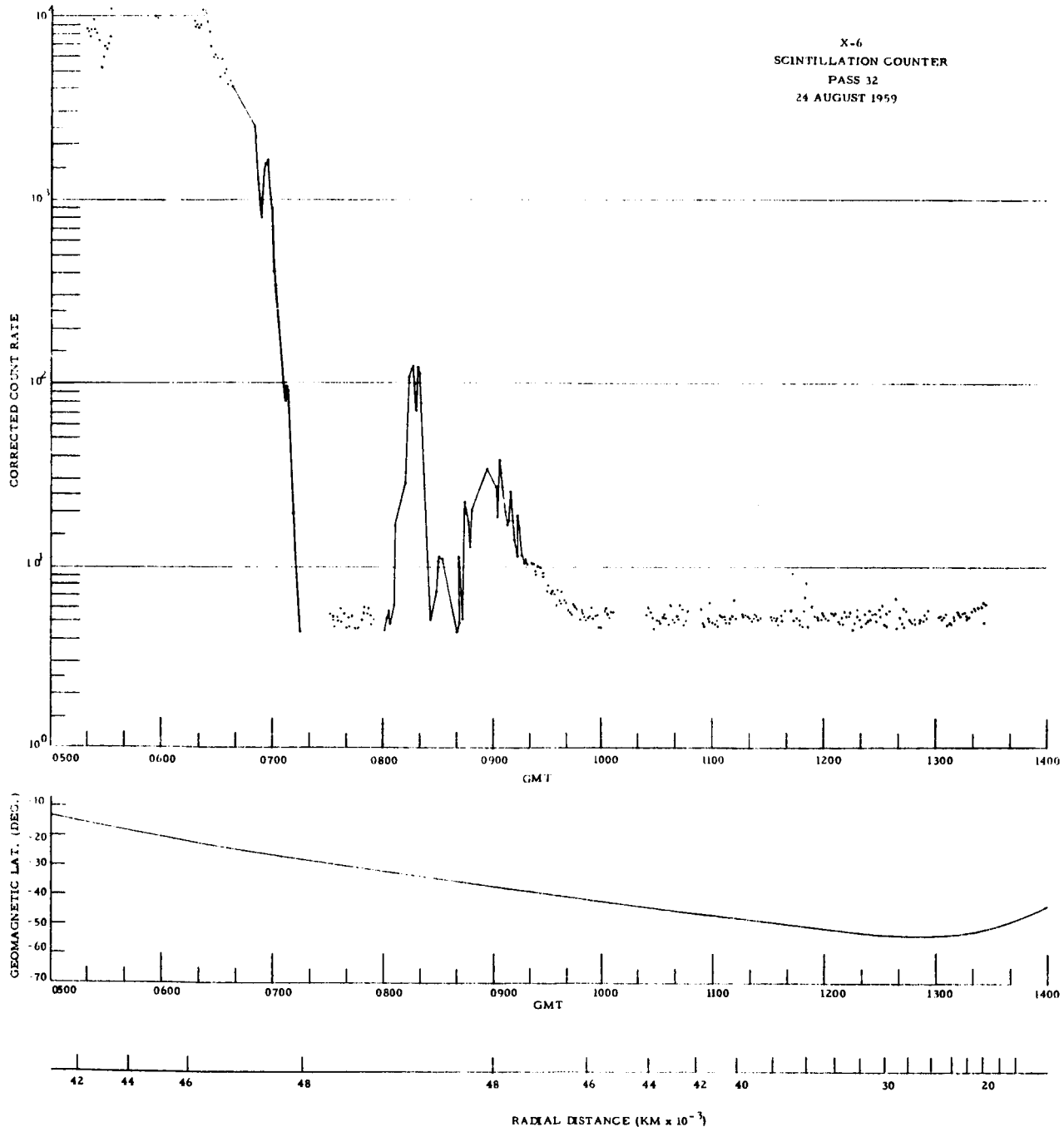
GEO MAGNETIC LAT. (DEG.)

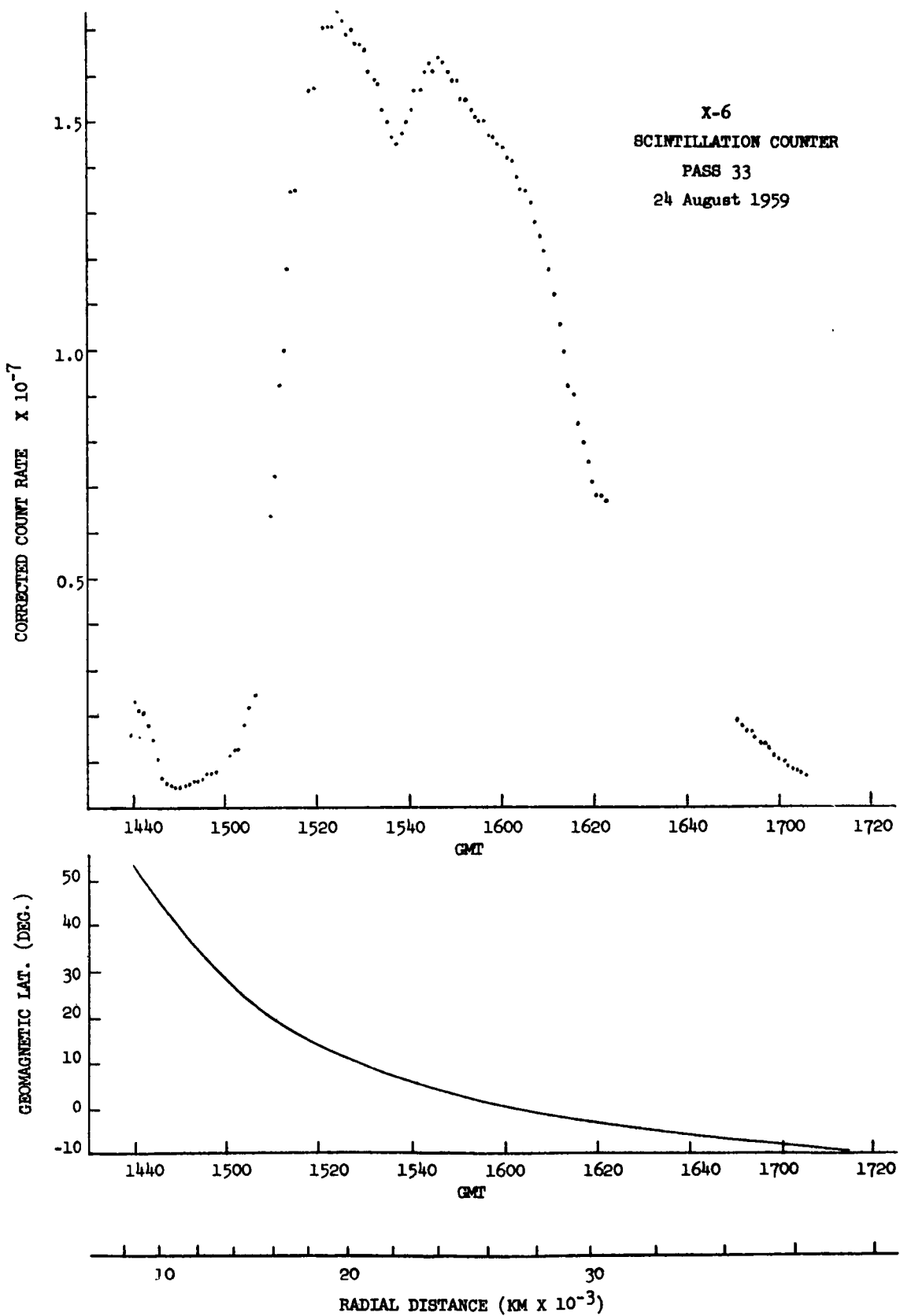


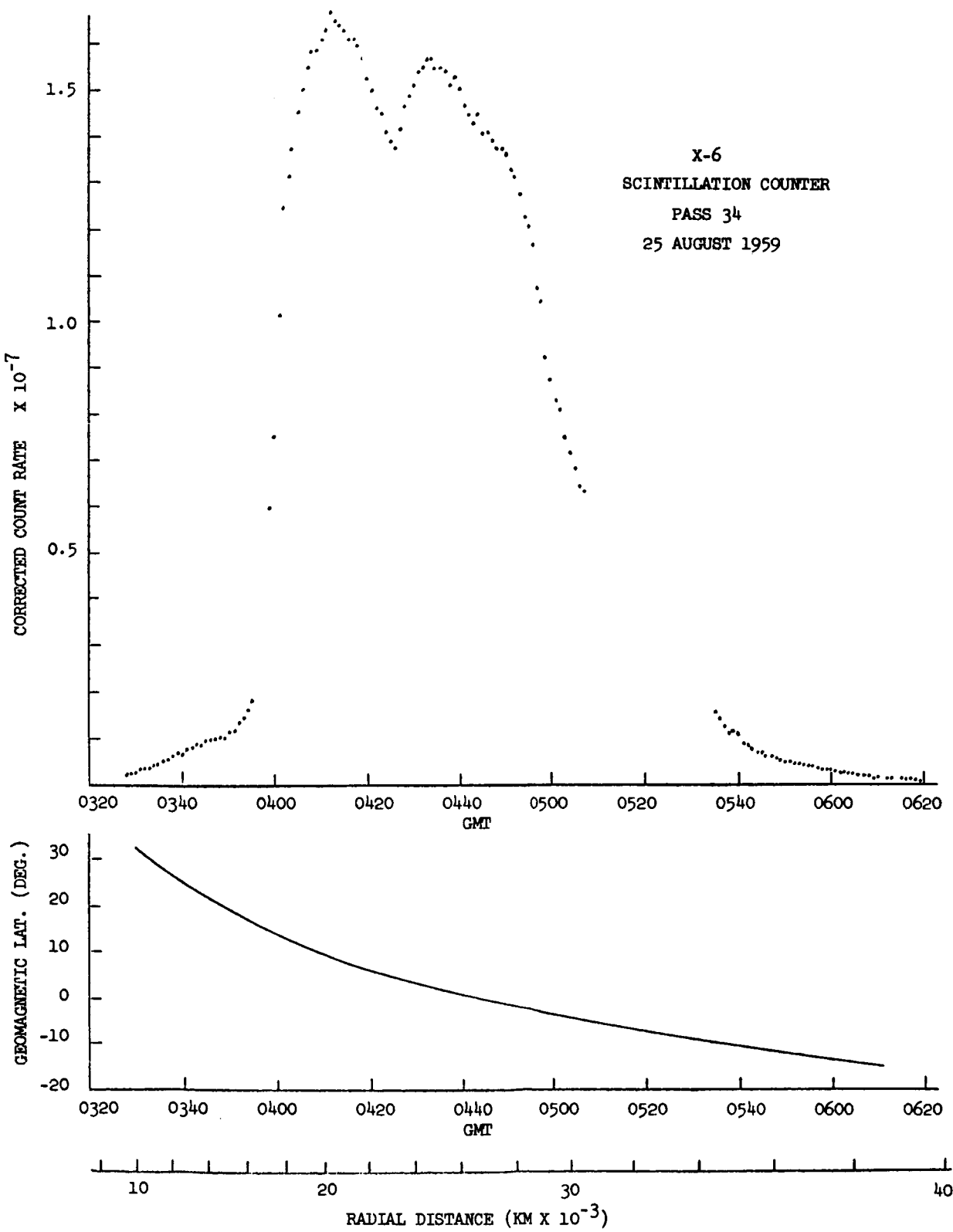




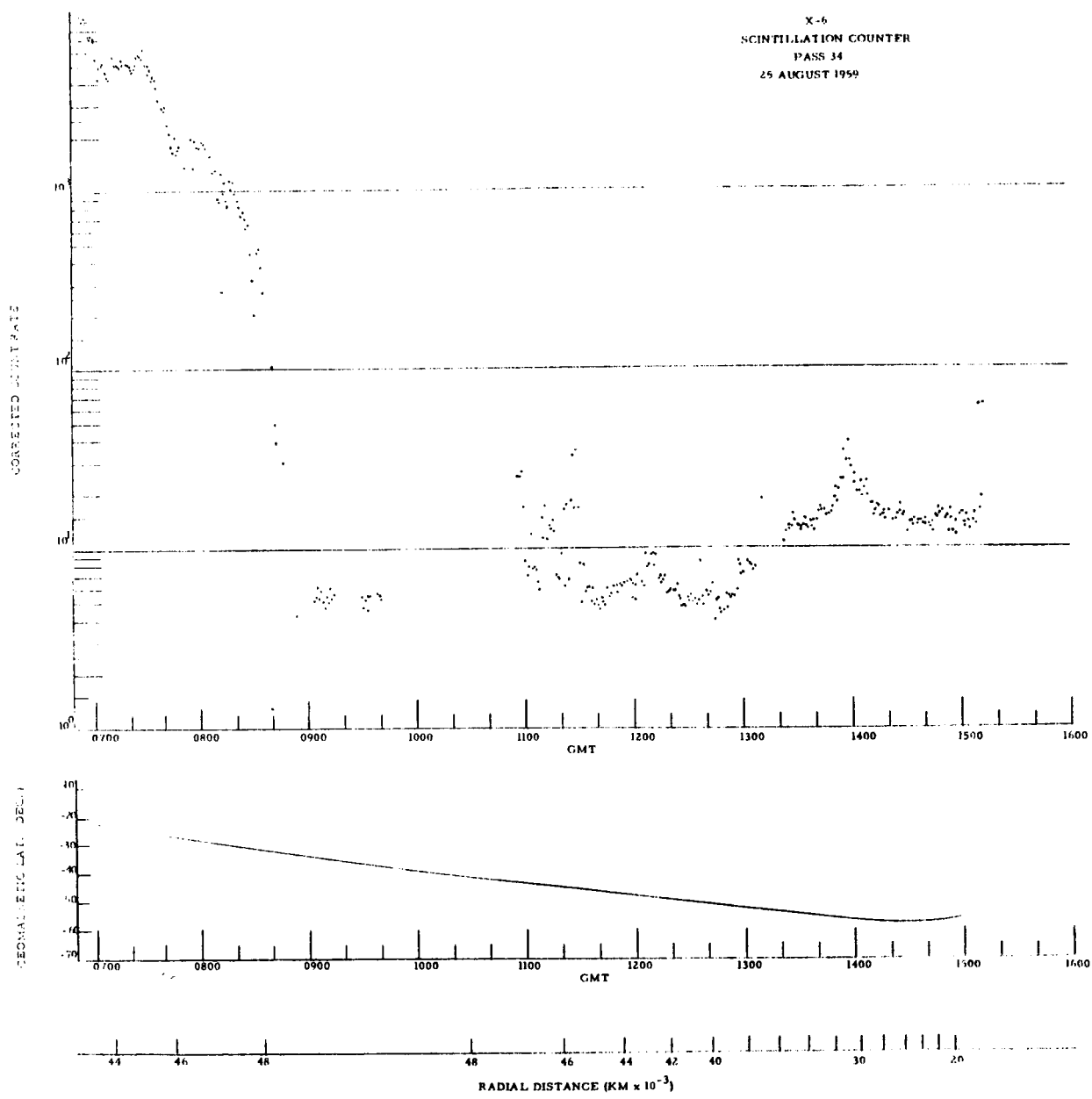


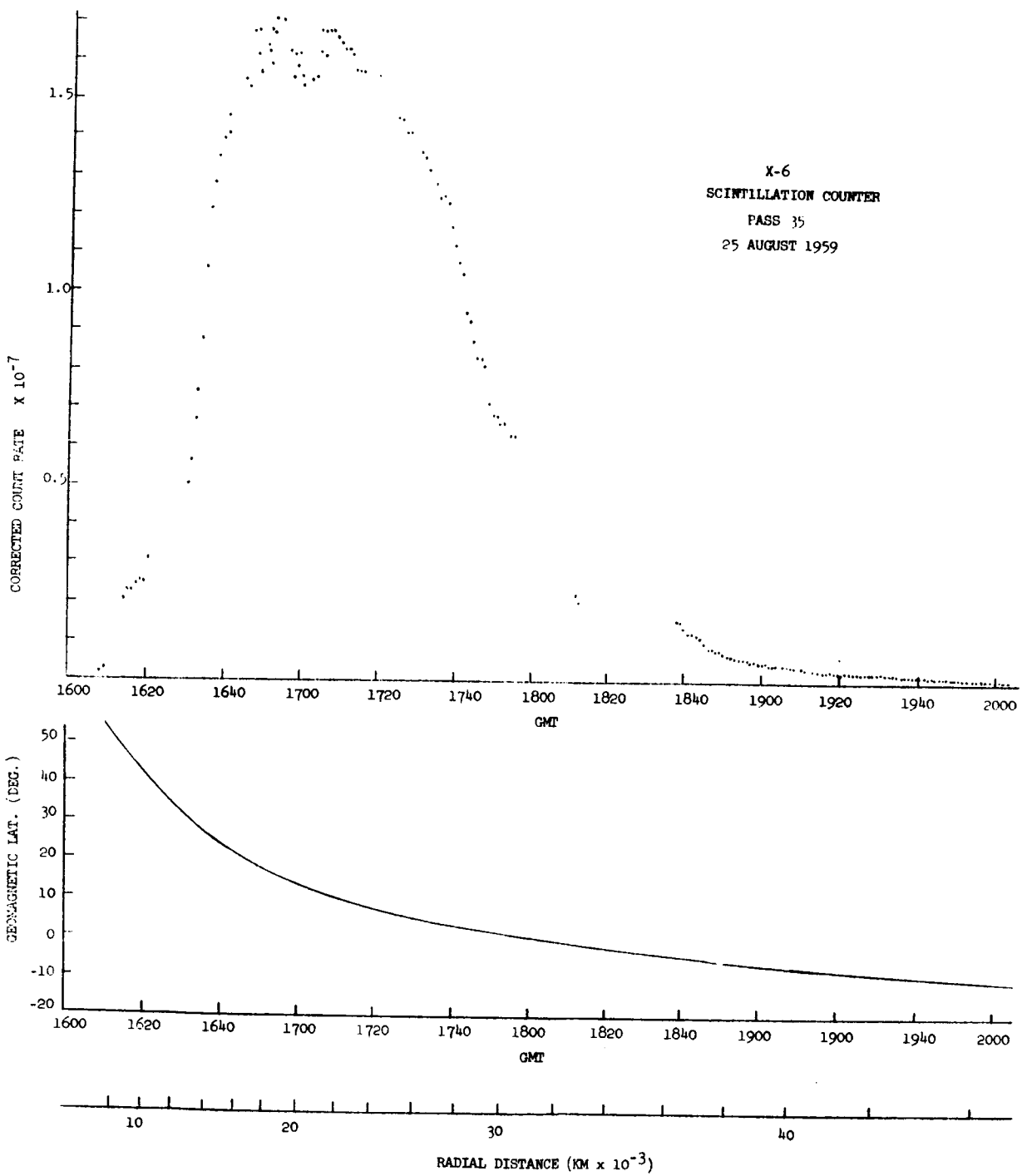


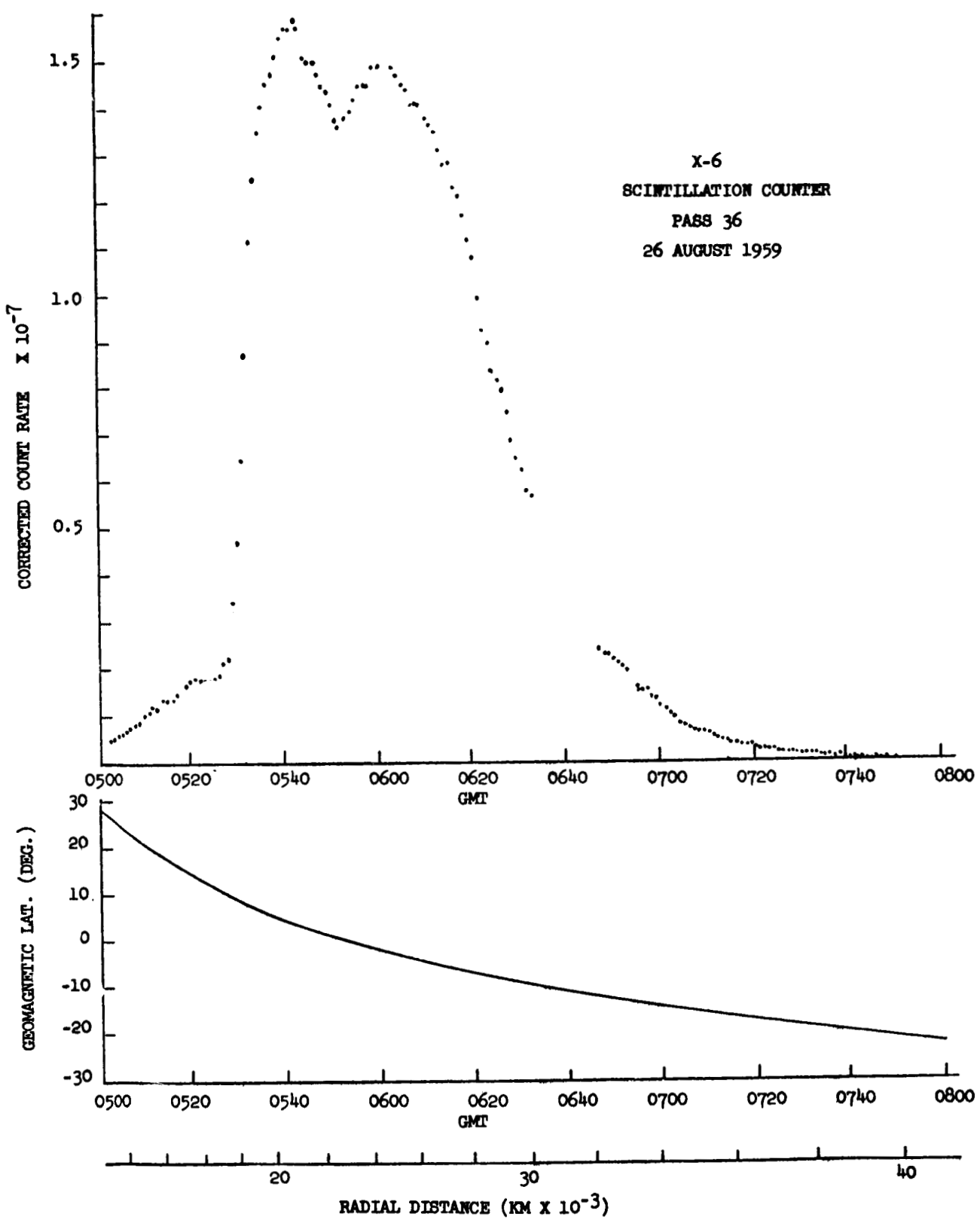




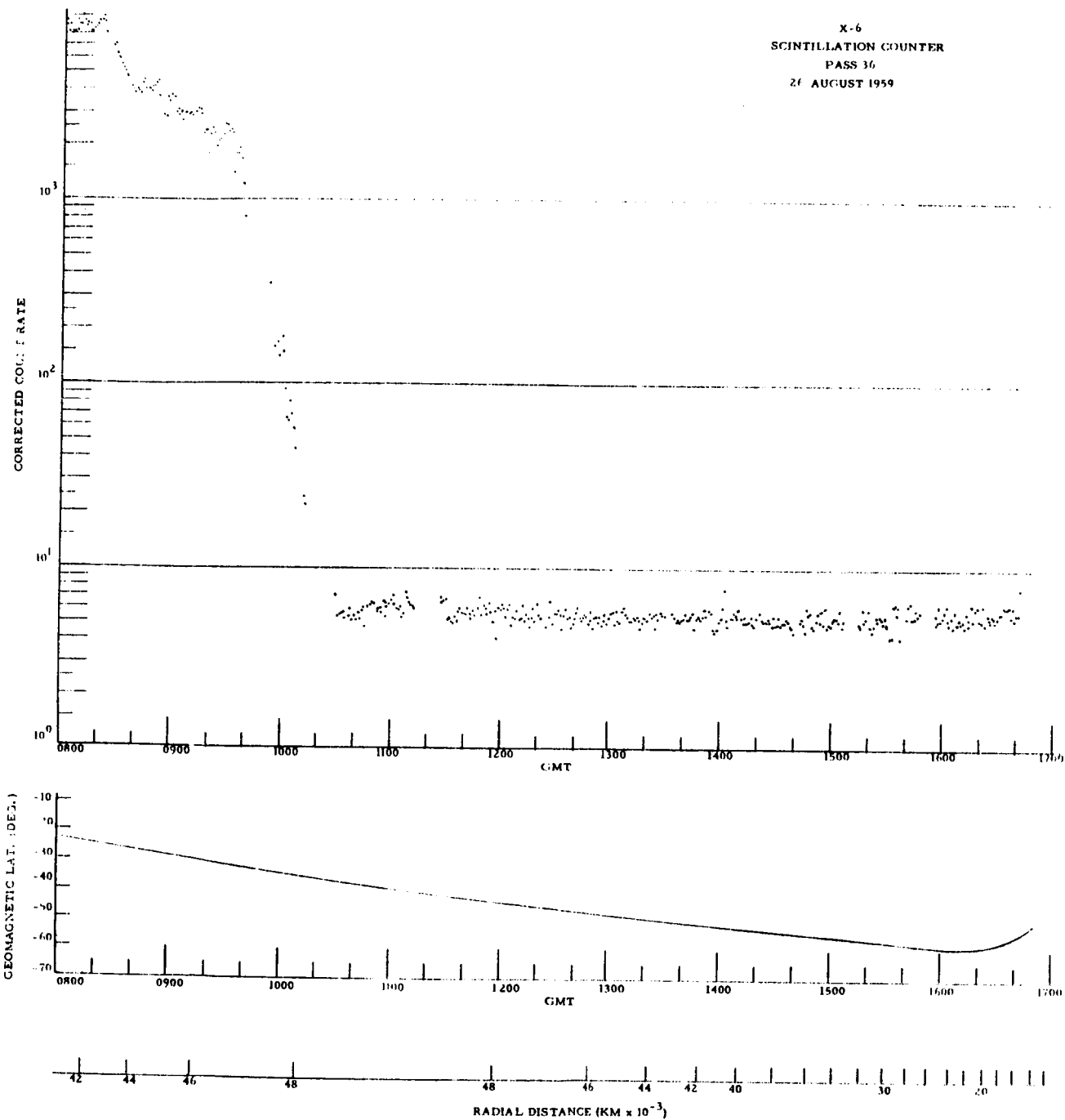
X-6
SCINTILLATION COUNTER
PASS 34
25 AUGUST 1959

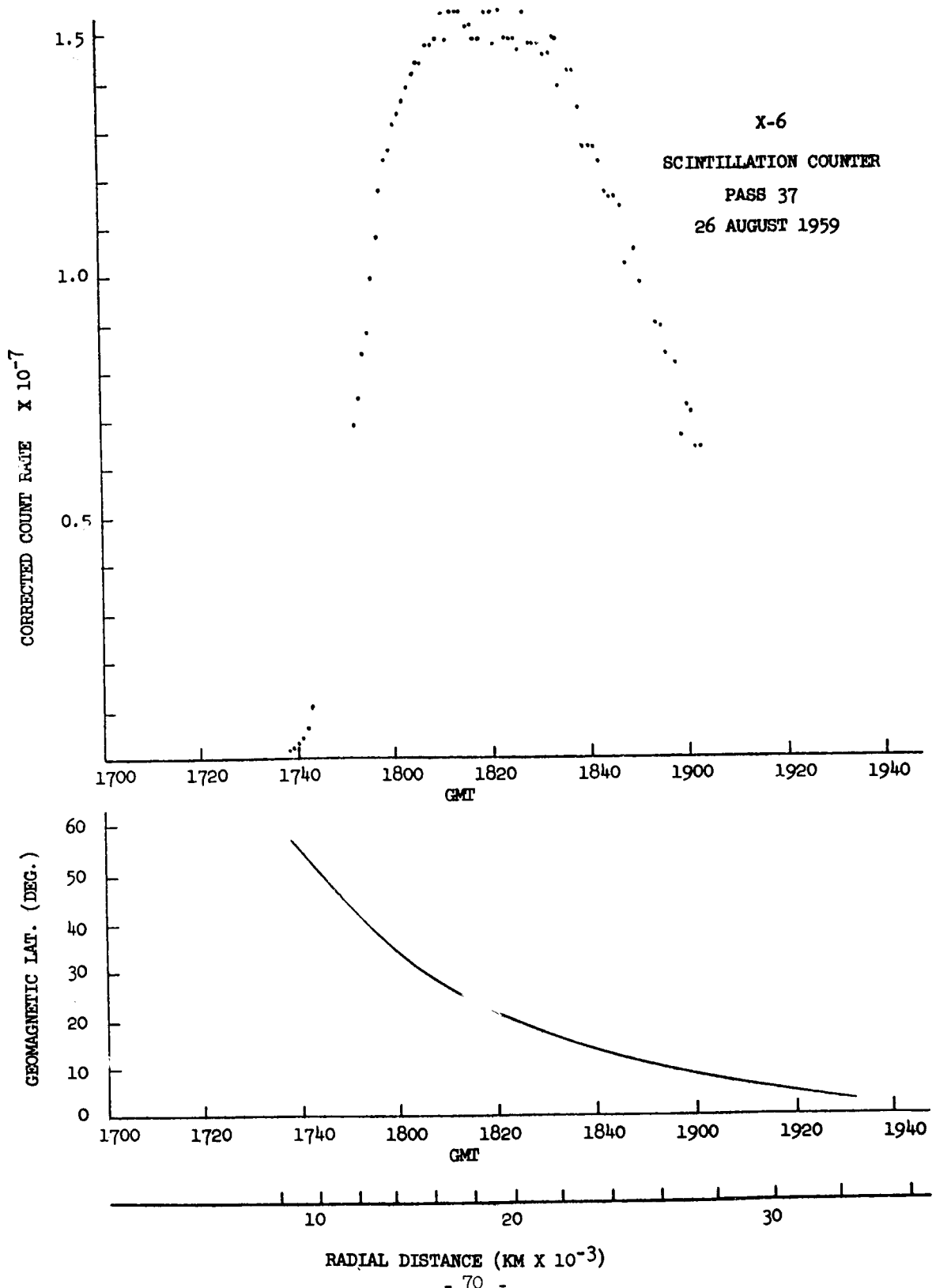


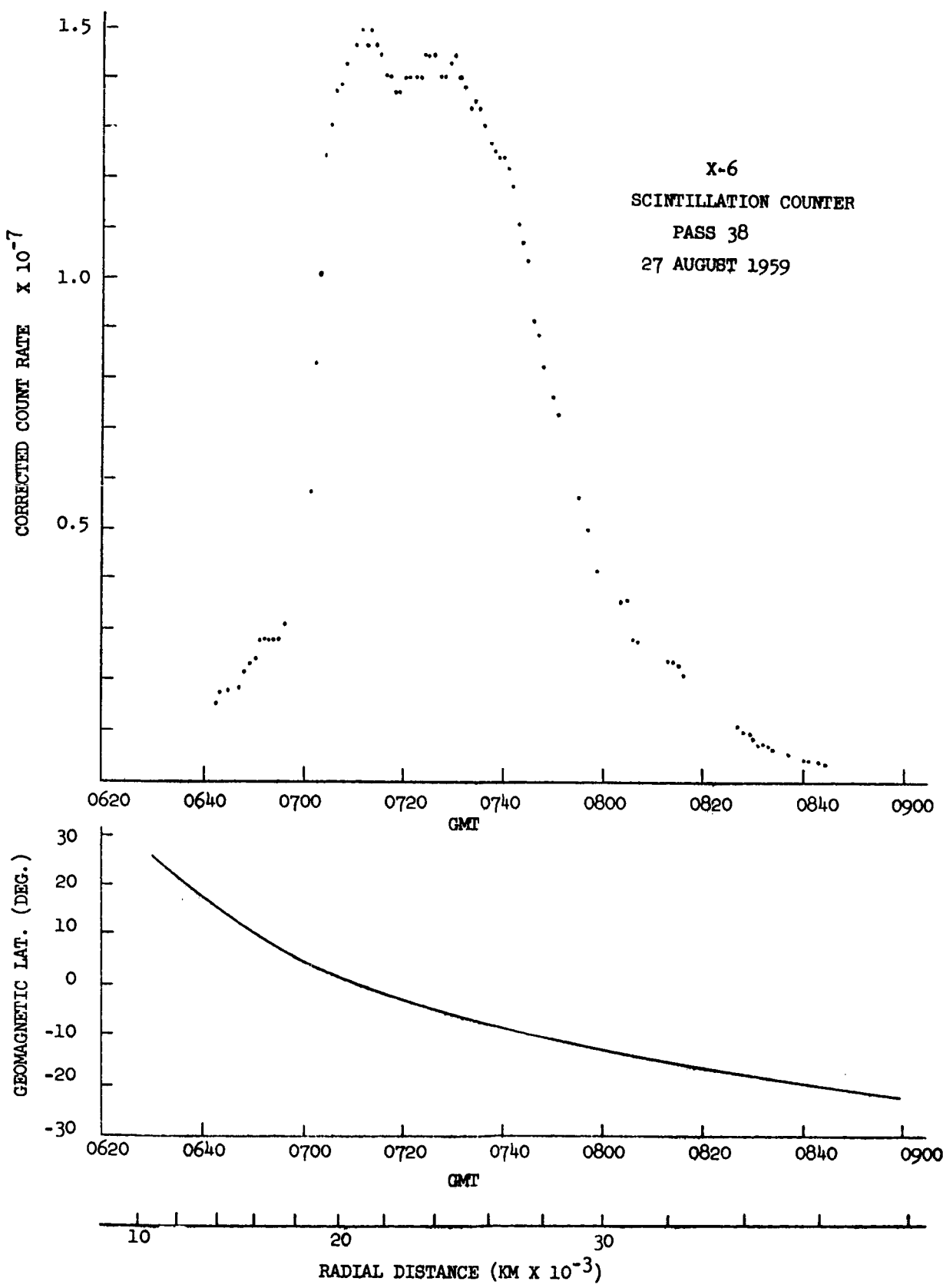


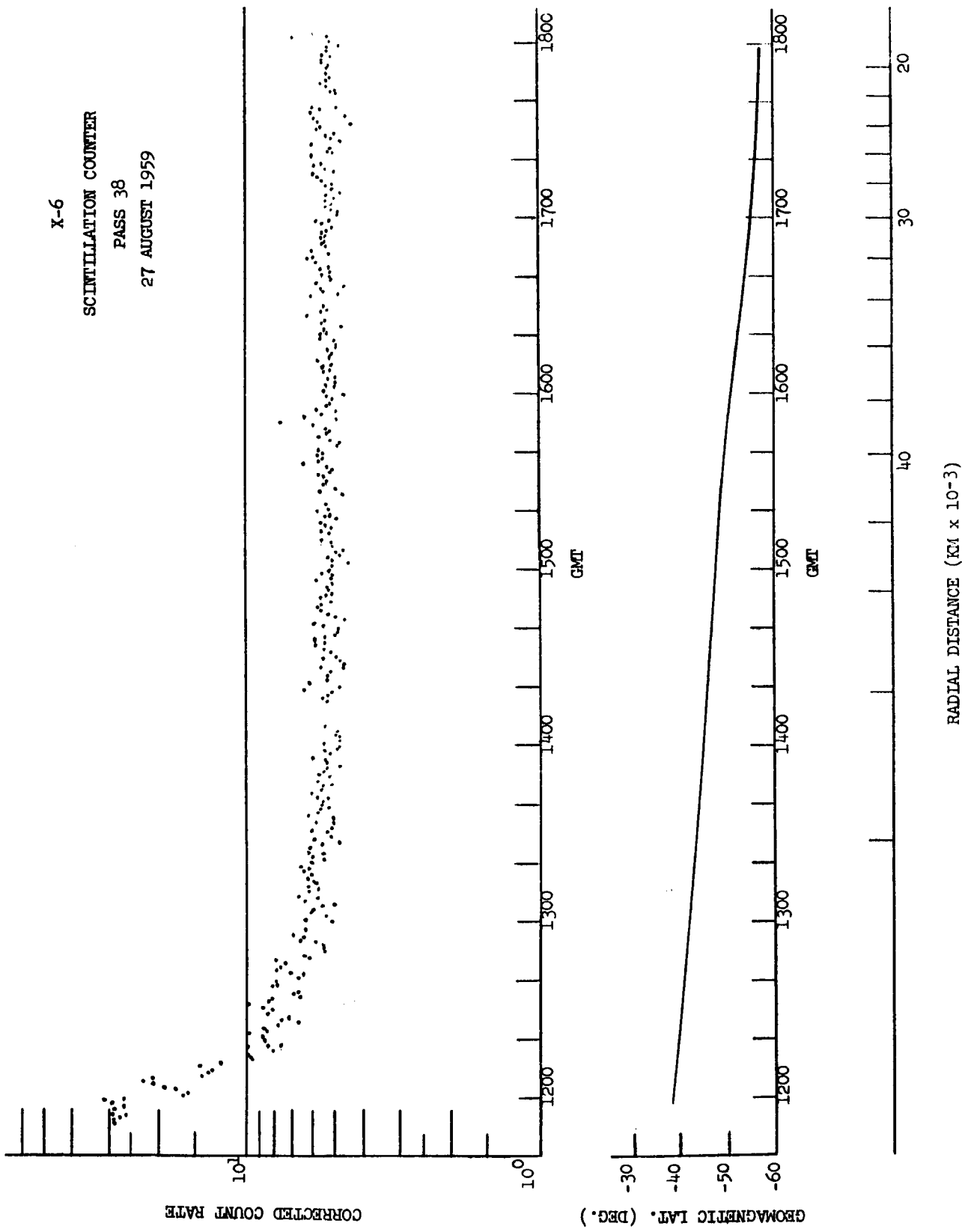


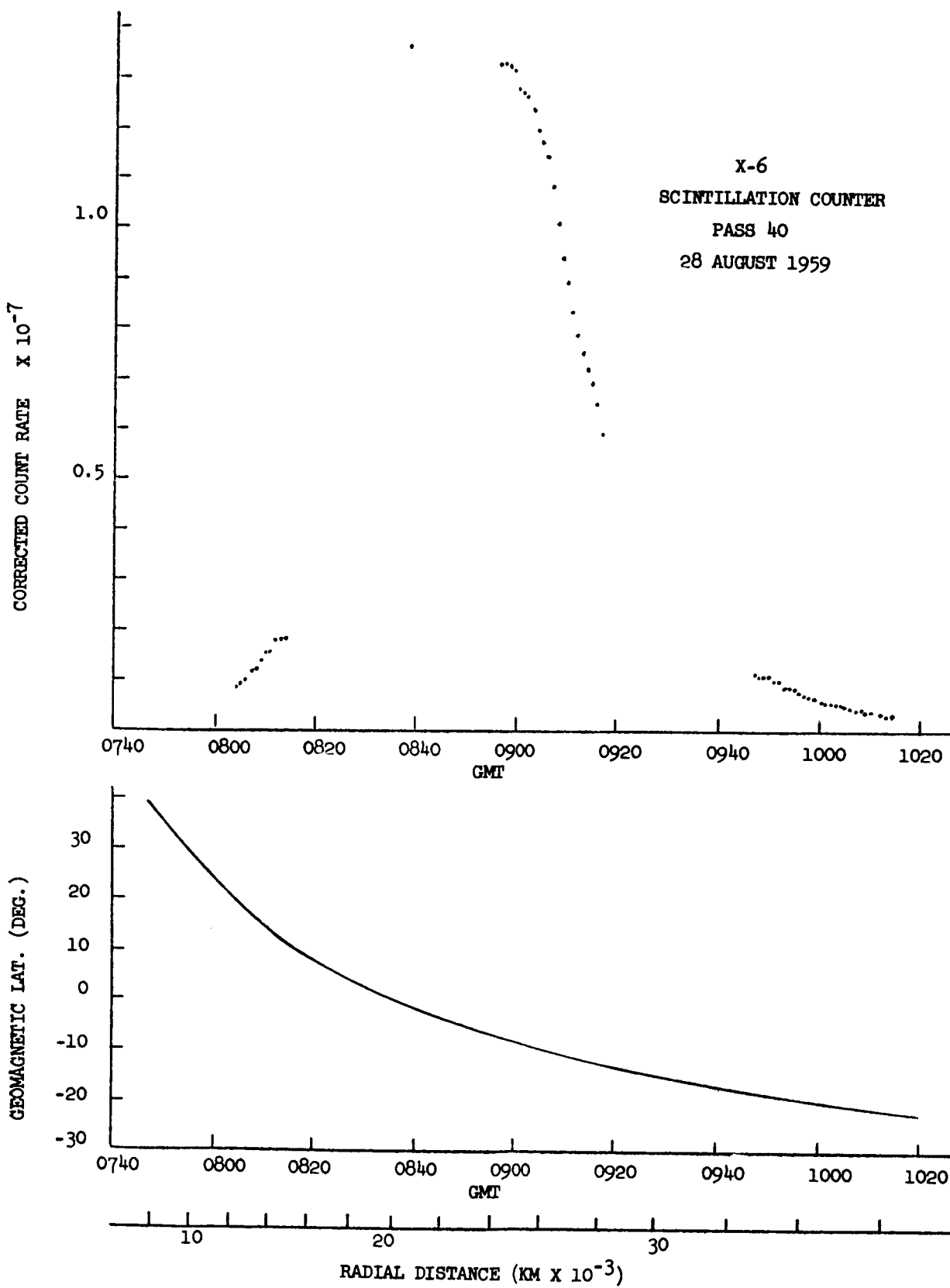
X-6
SCINTILLATION COUNTER
PASS 36
26 AUGUST 1959



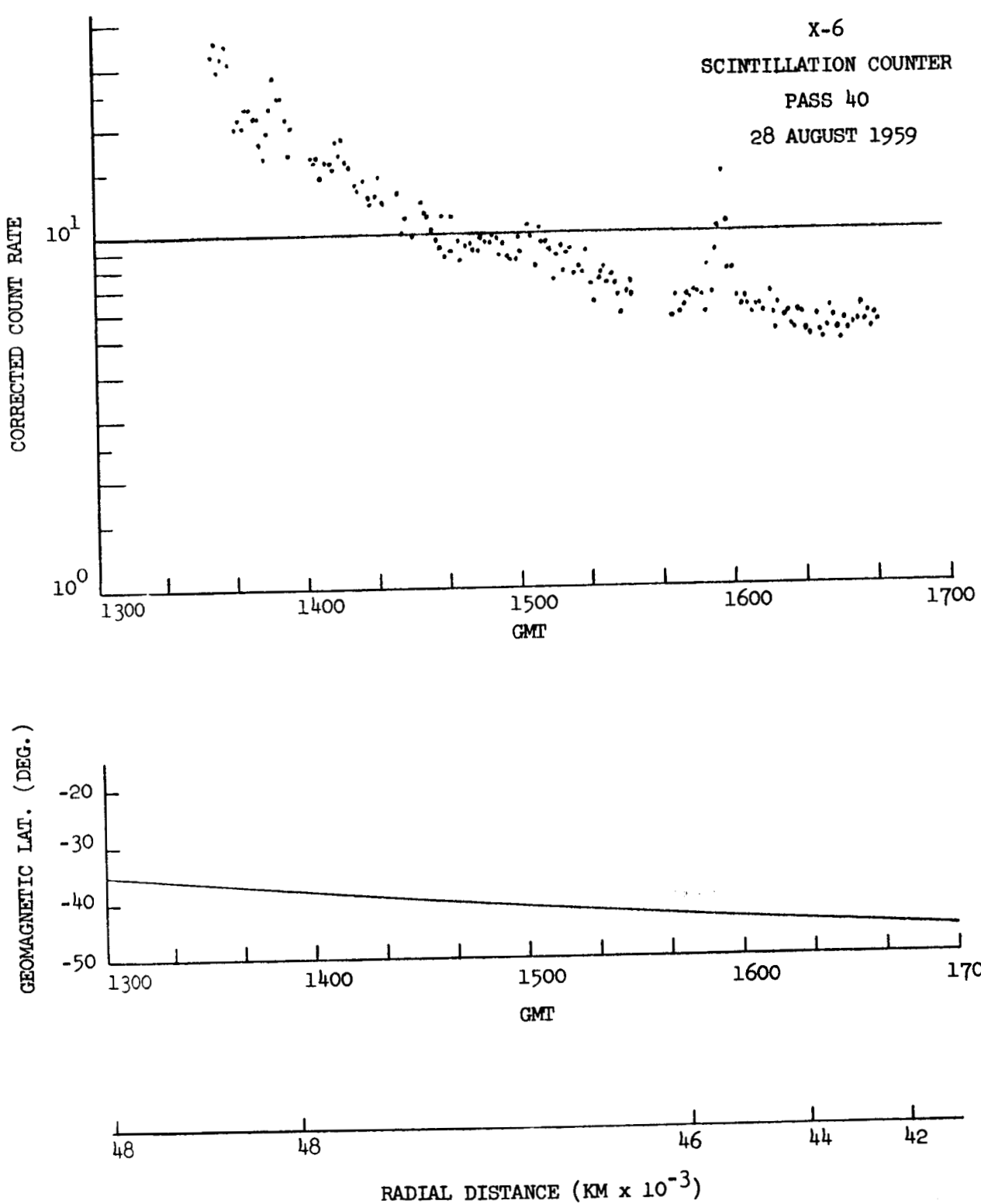


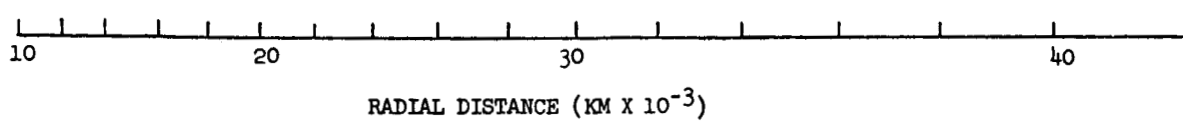
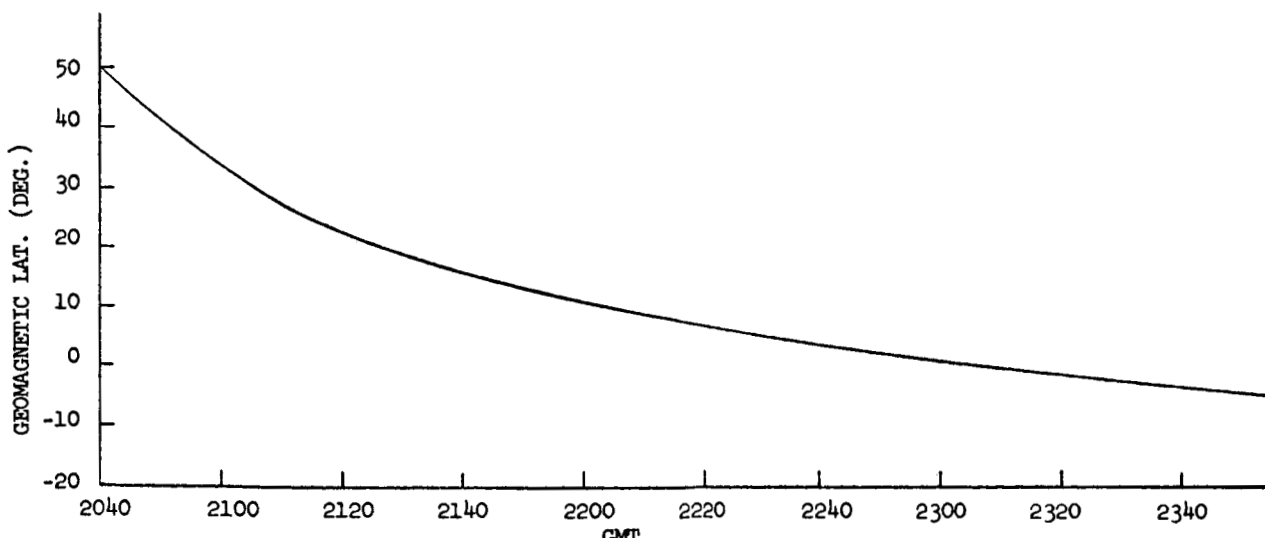
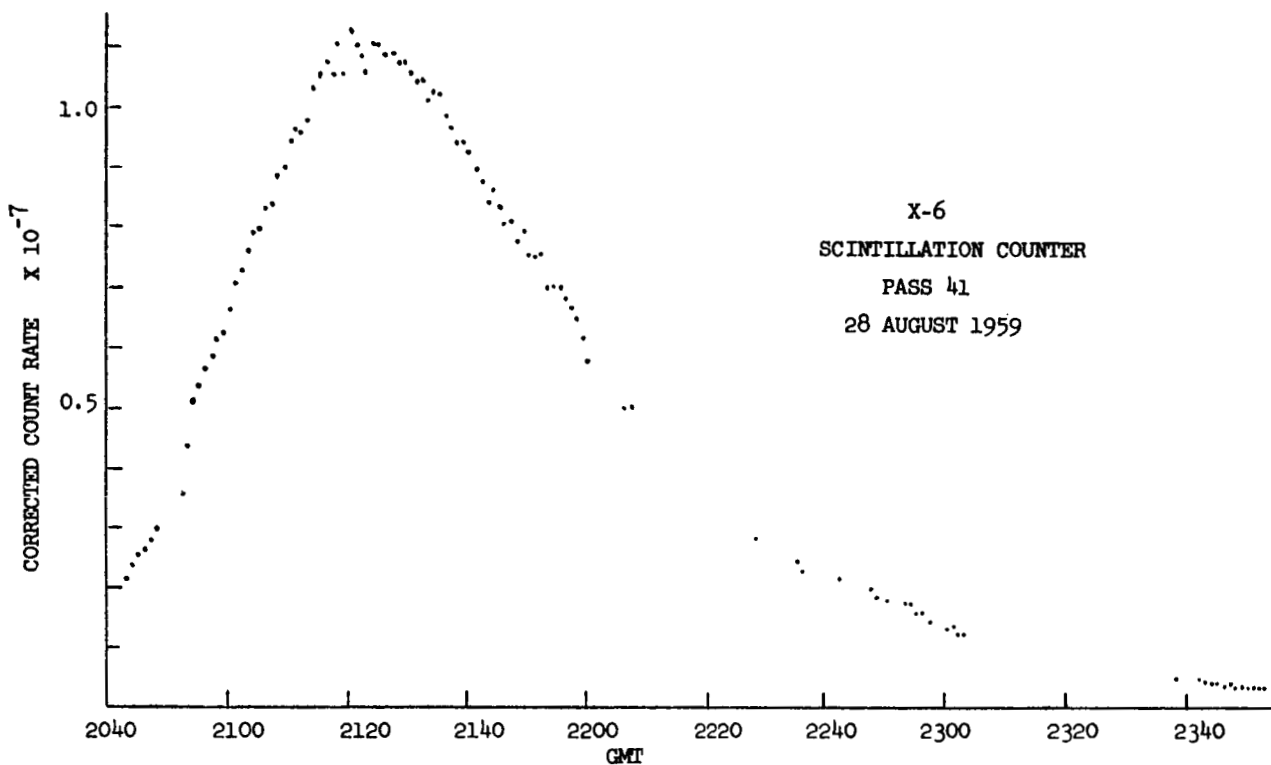


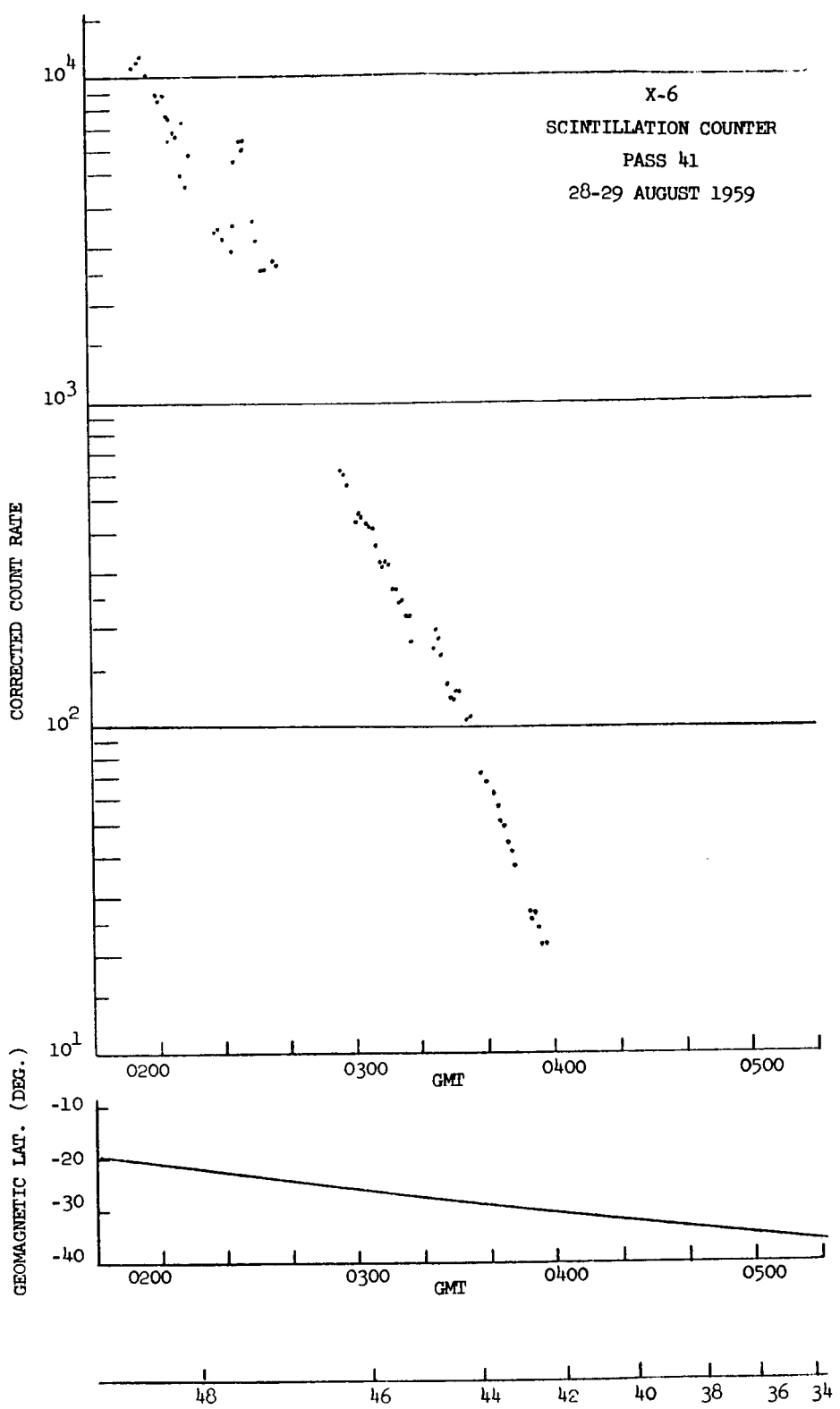


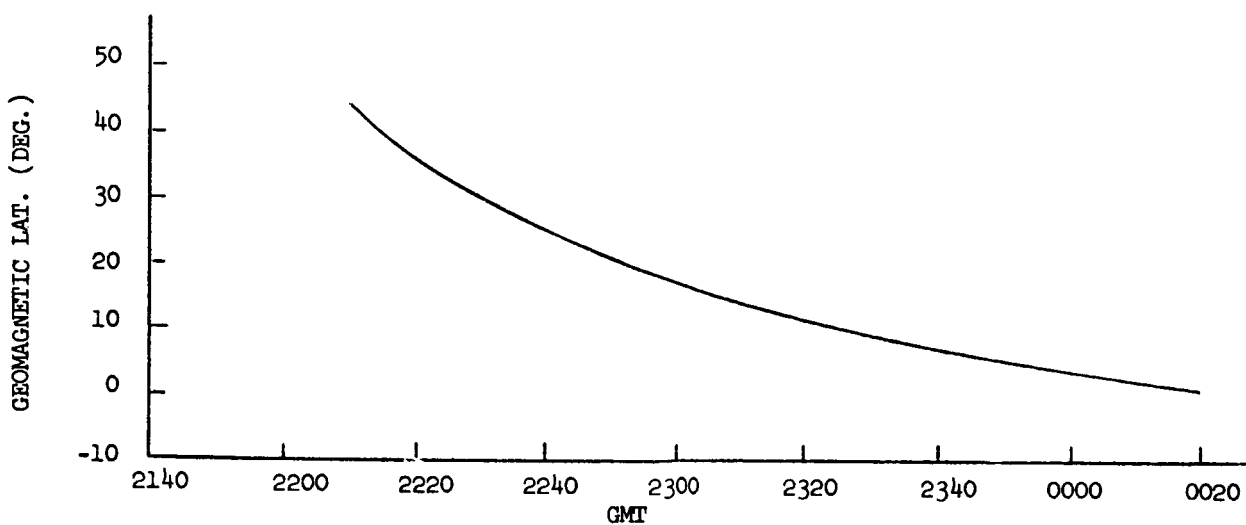
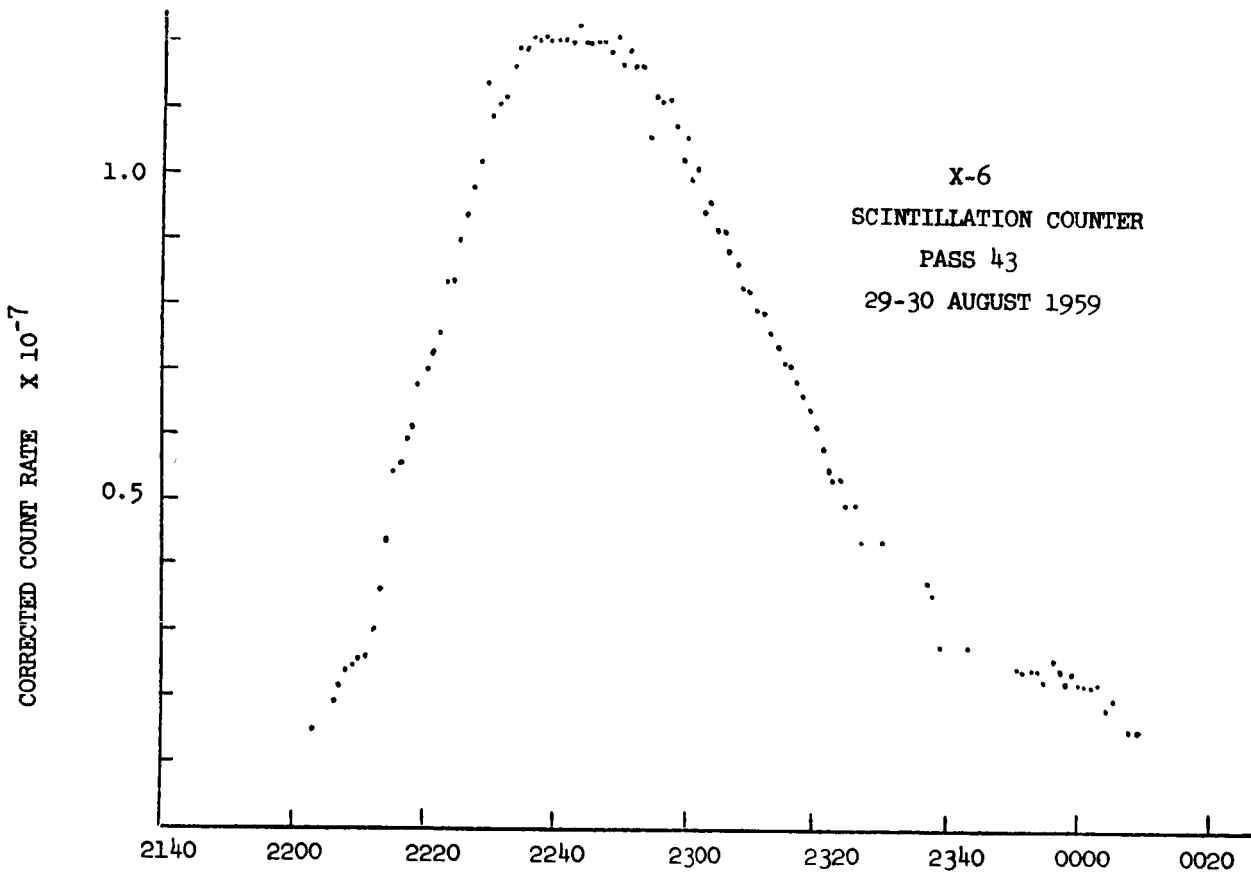


X-6
SCINTILLATION COUNTER
PASS 40
28 AUGUST 1959

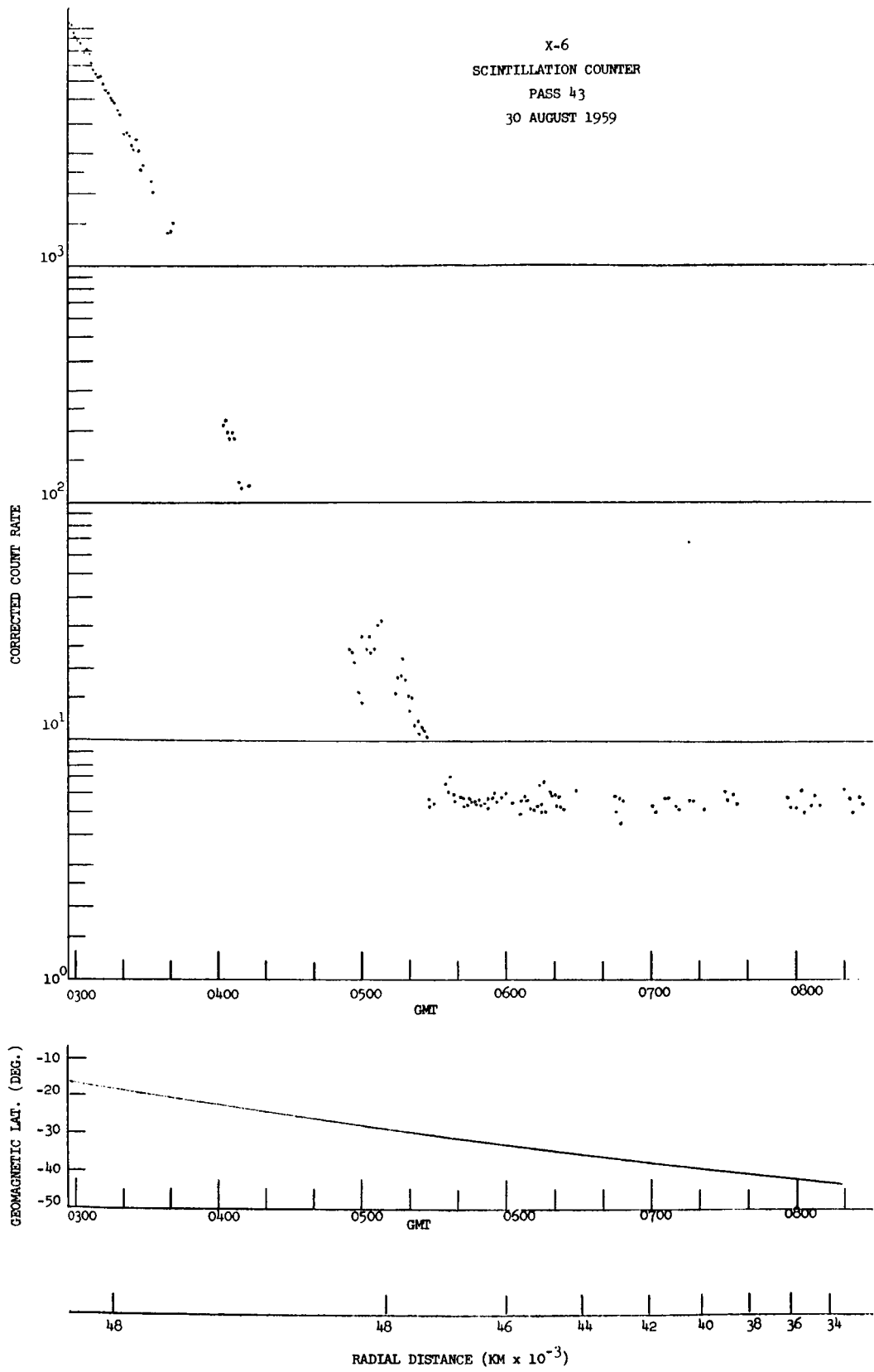


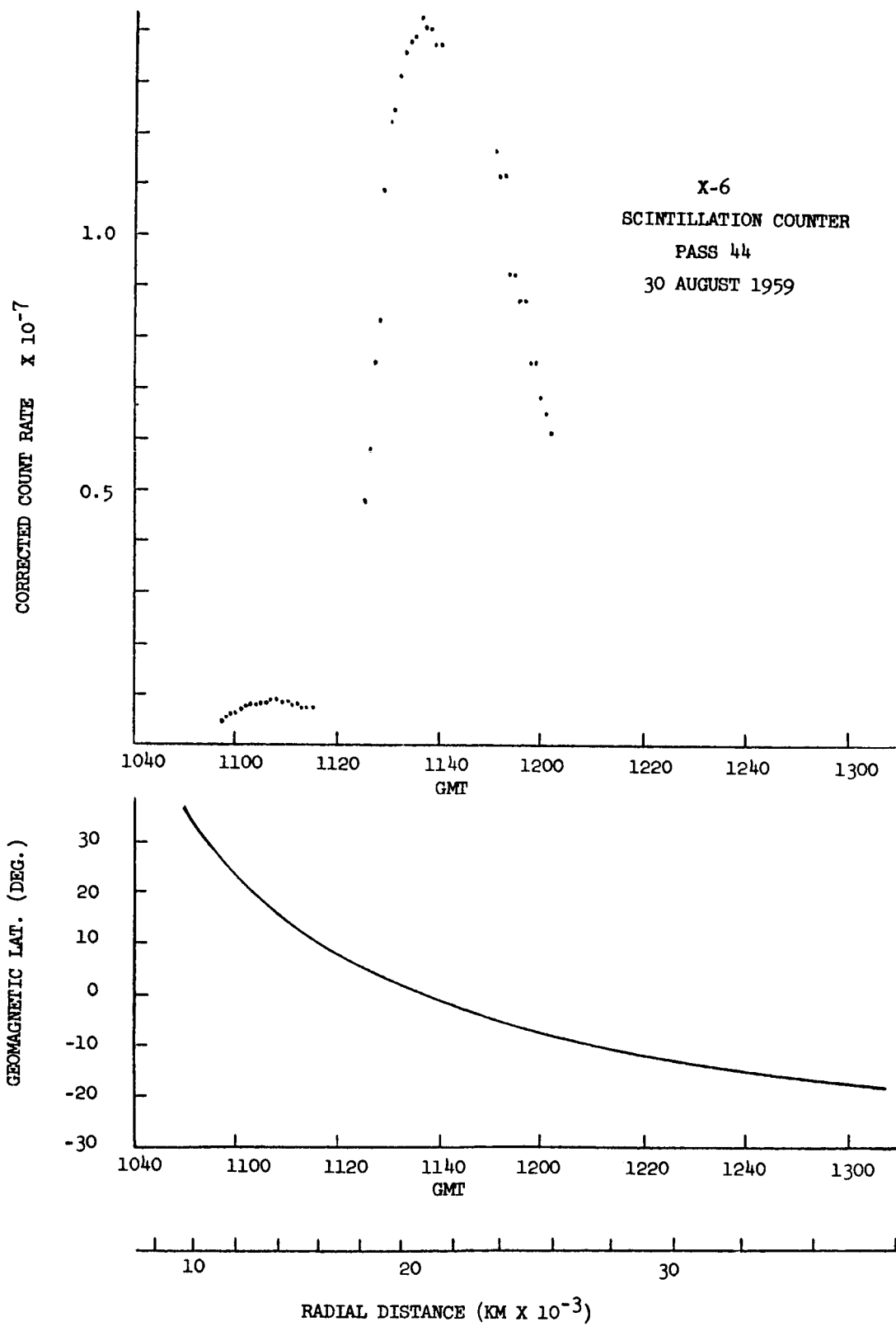


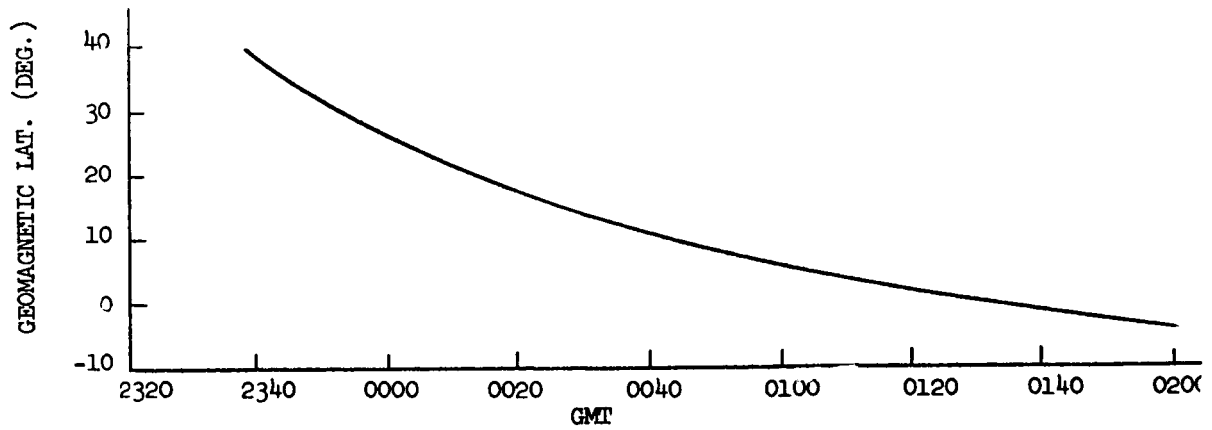
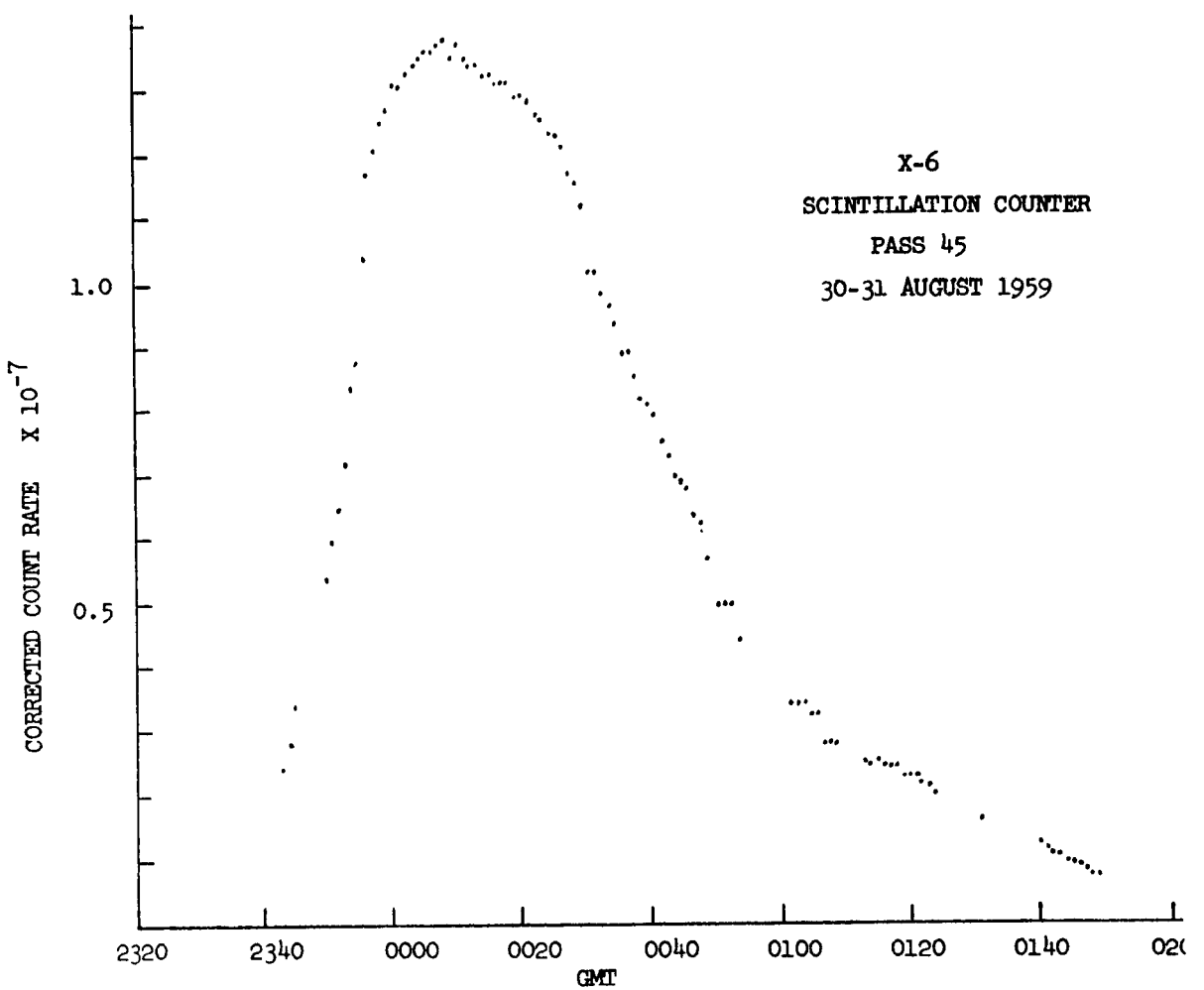




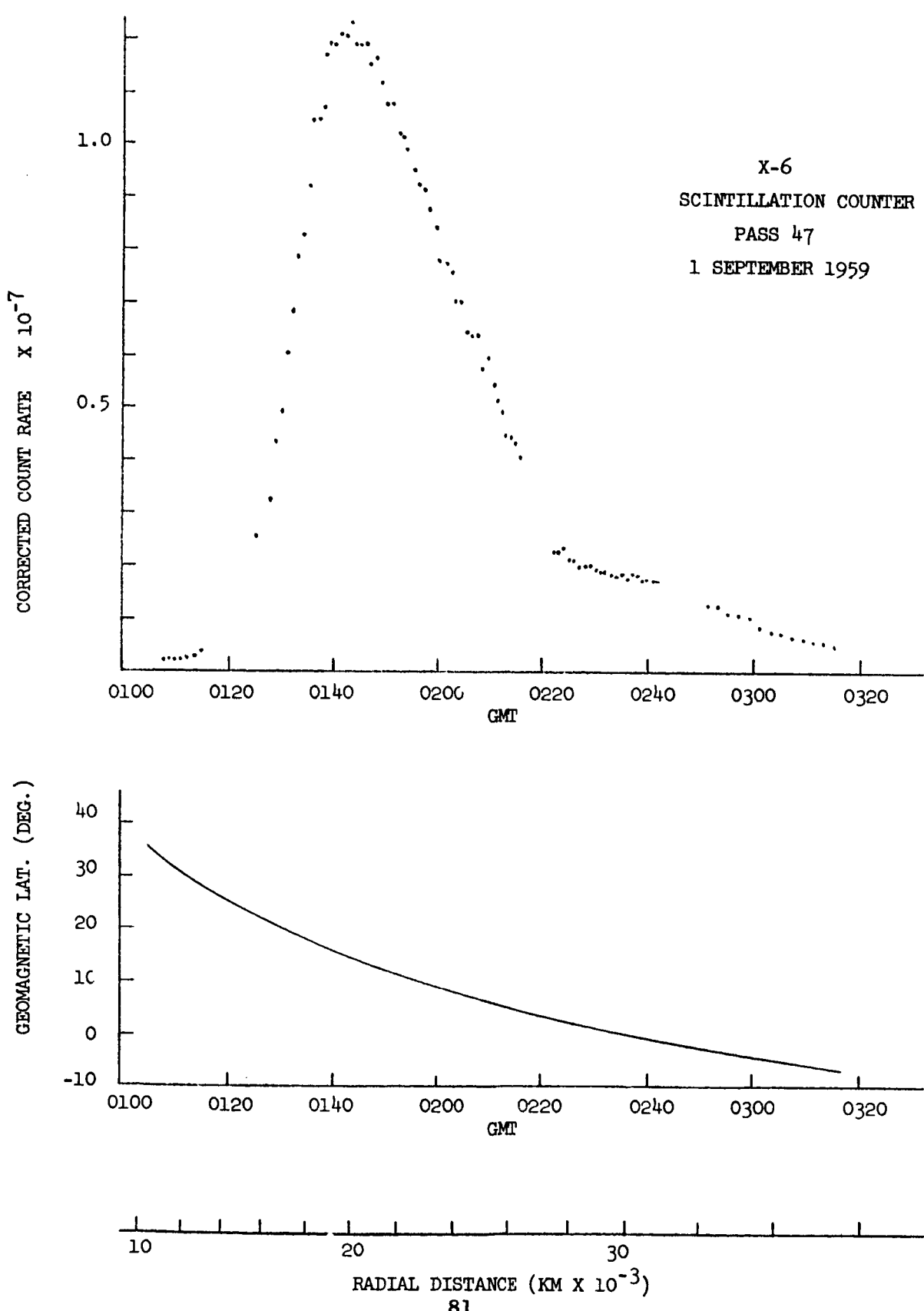
RADIAL DISTANCE (KM X 10⁻³)

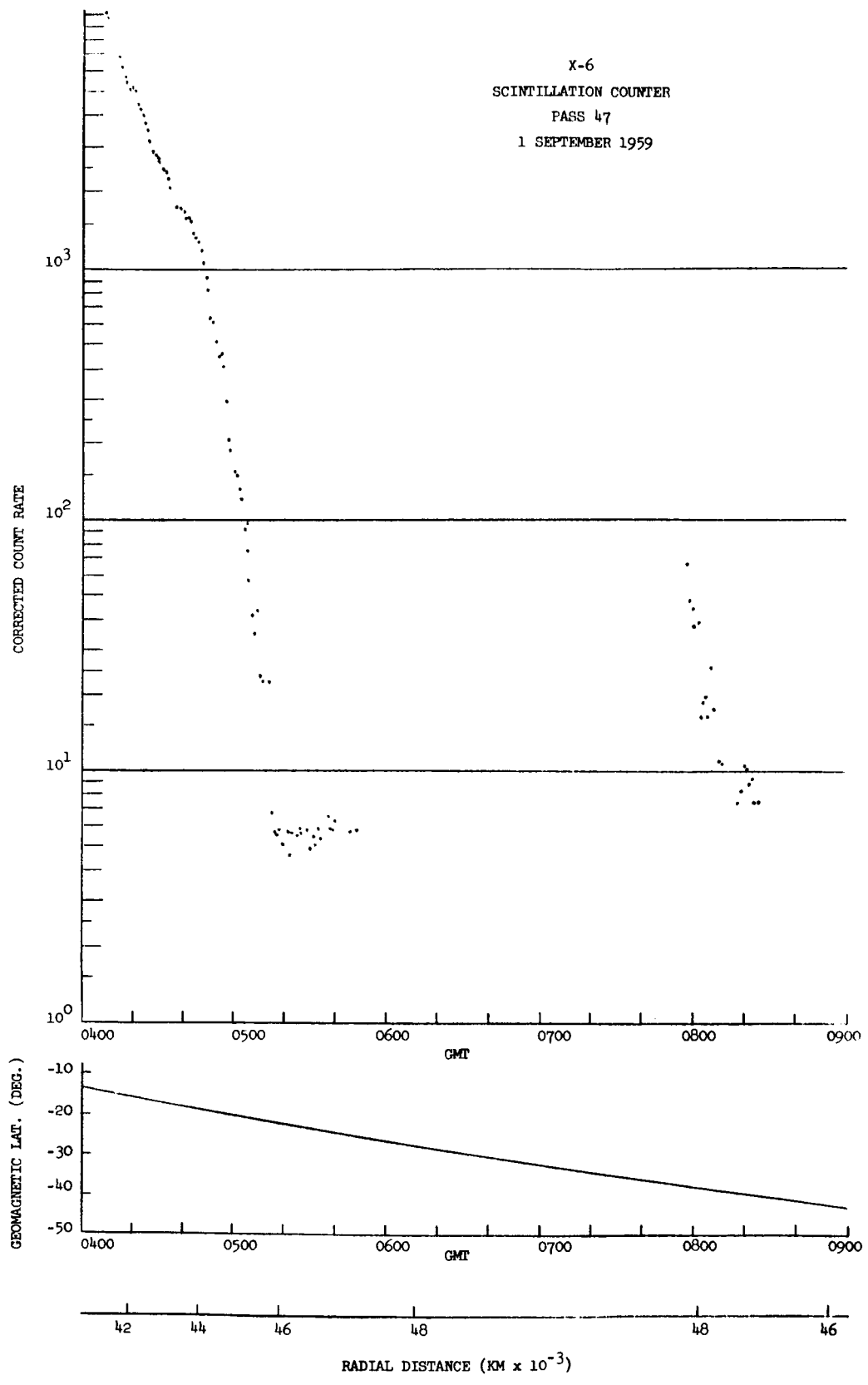


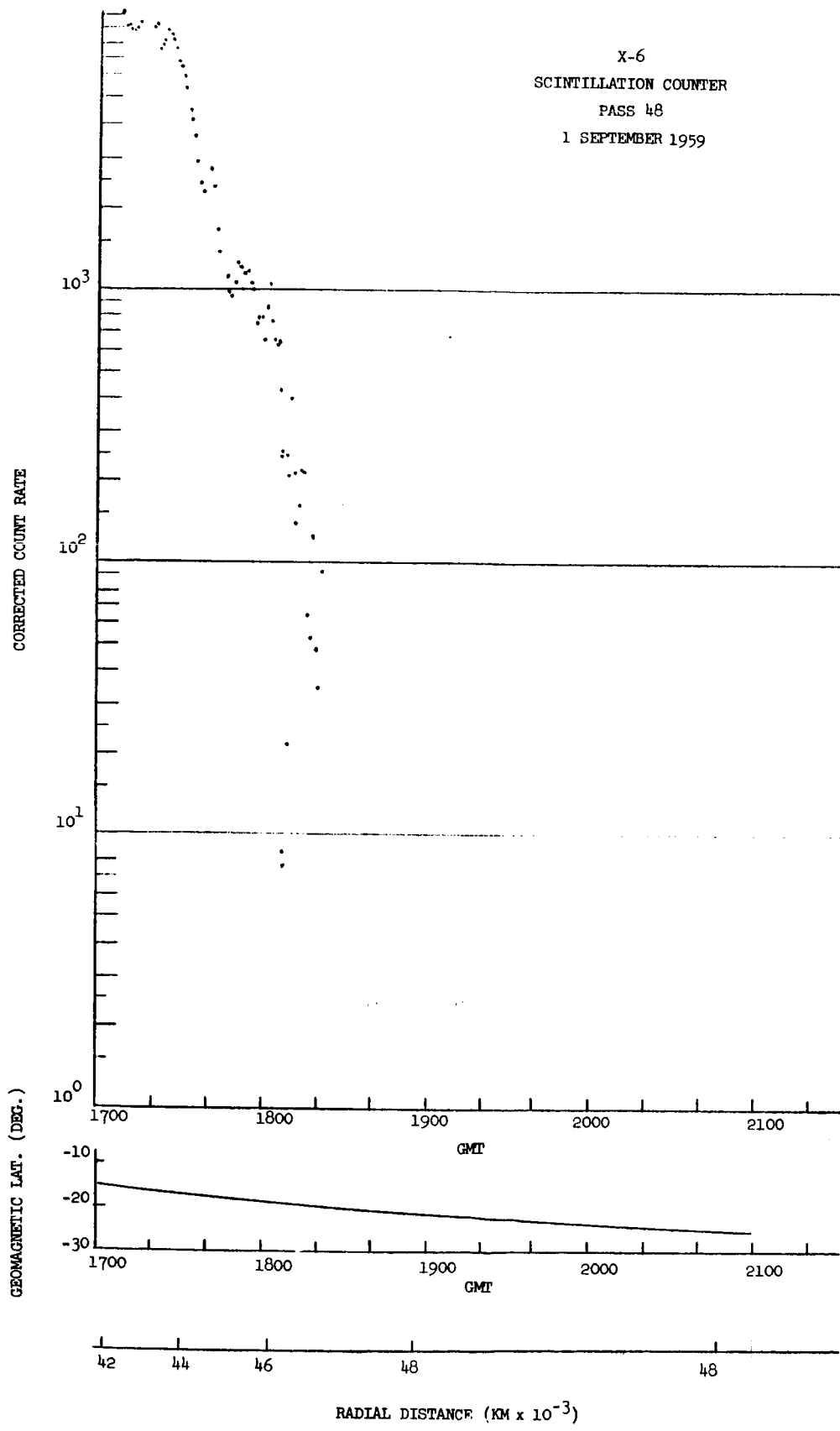


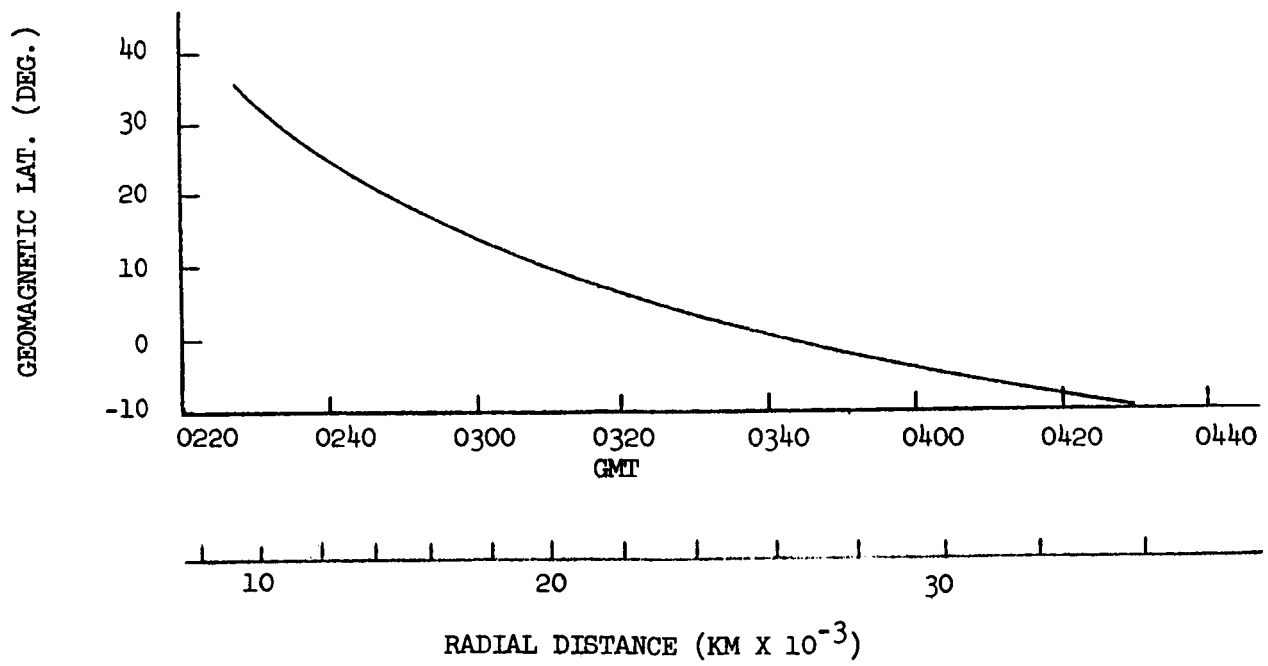
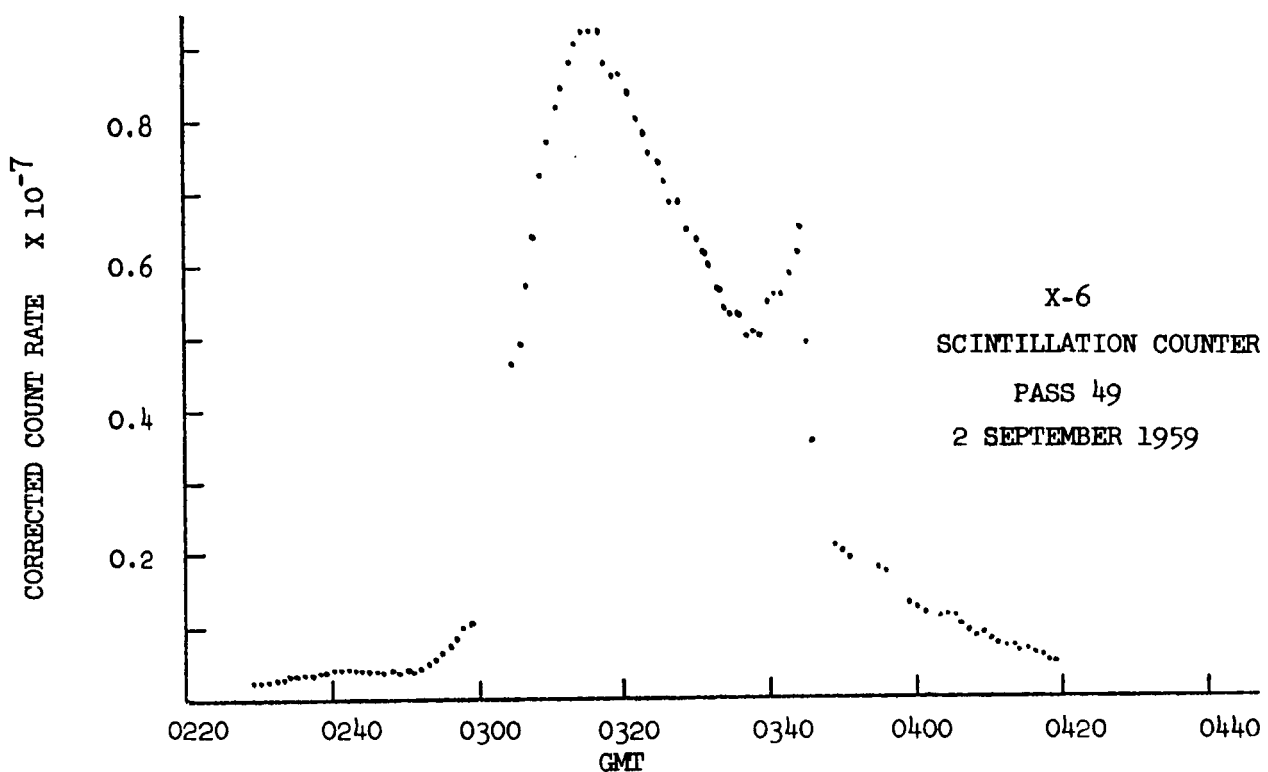


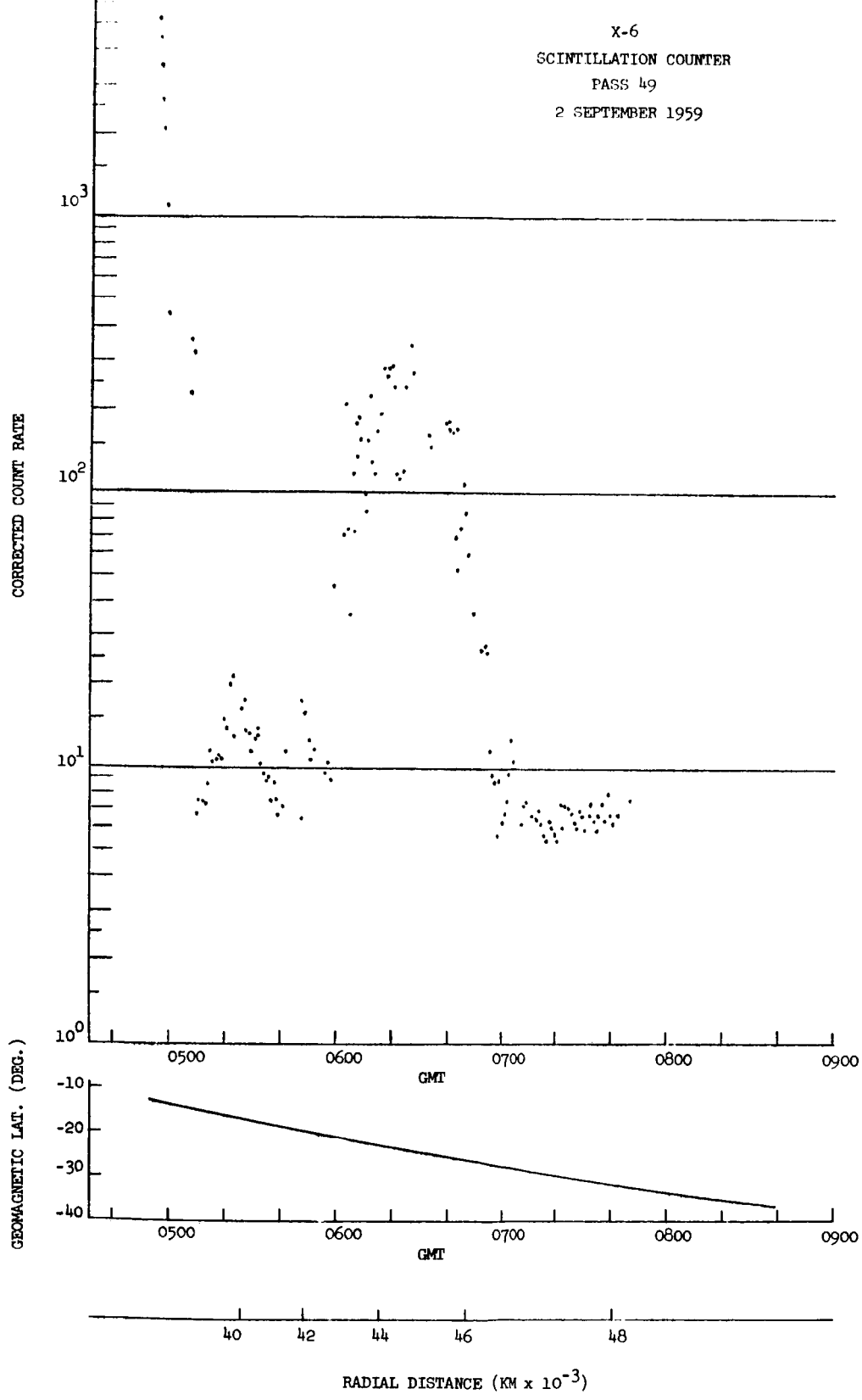
RADIAL DISTANCE (KM $\times 10^{-3}$)



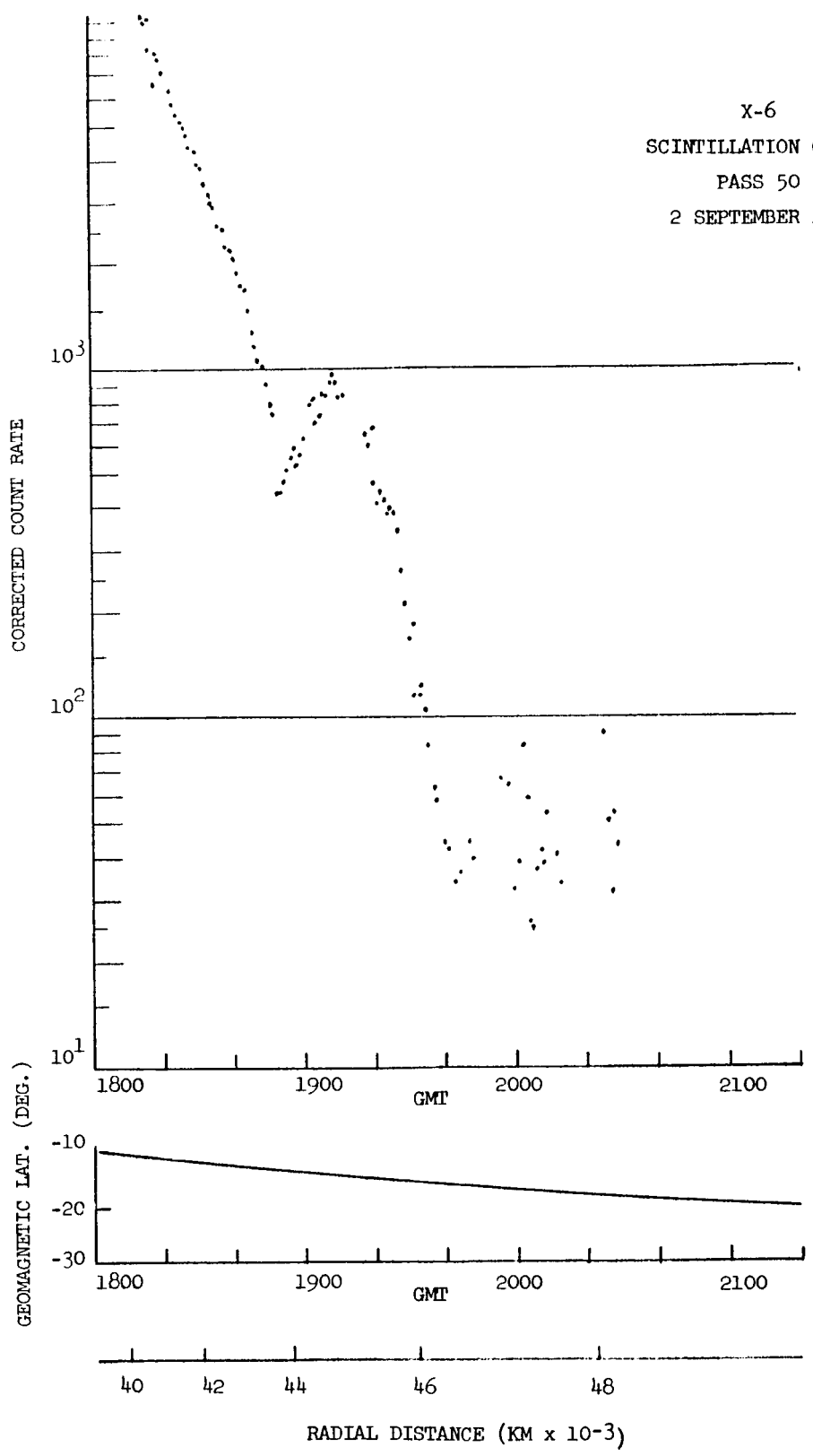


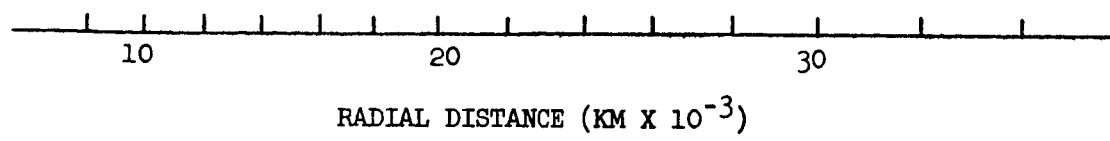
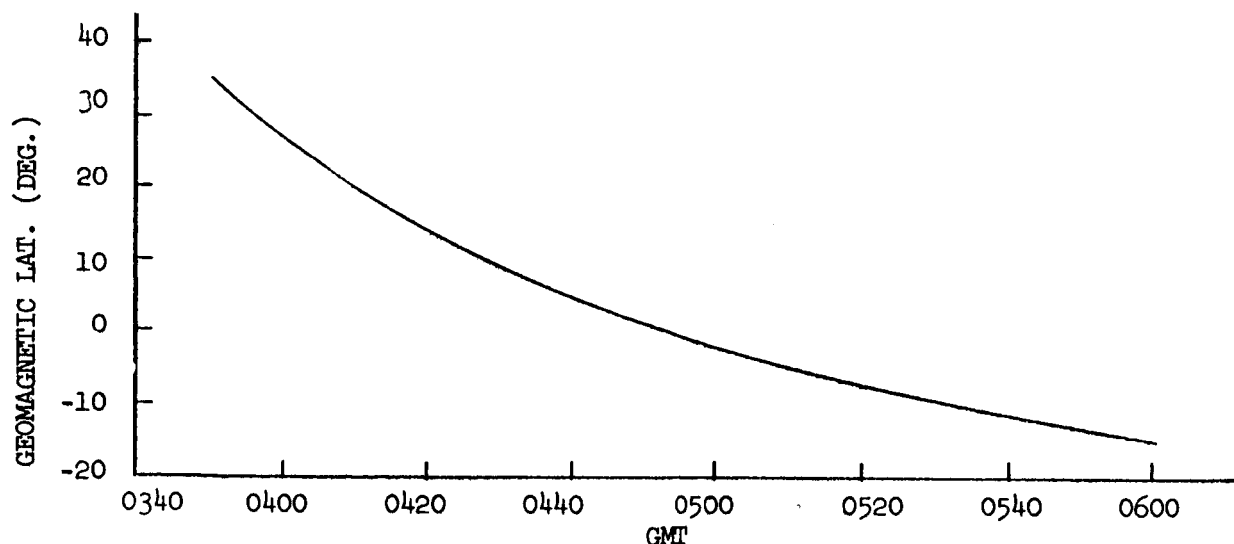
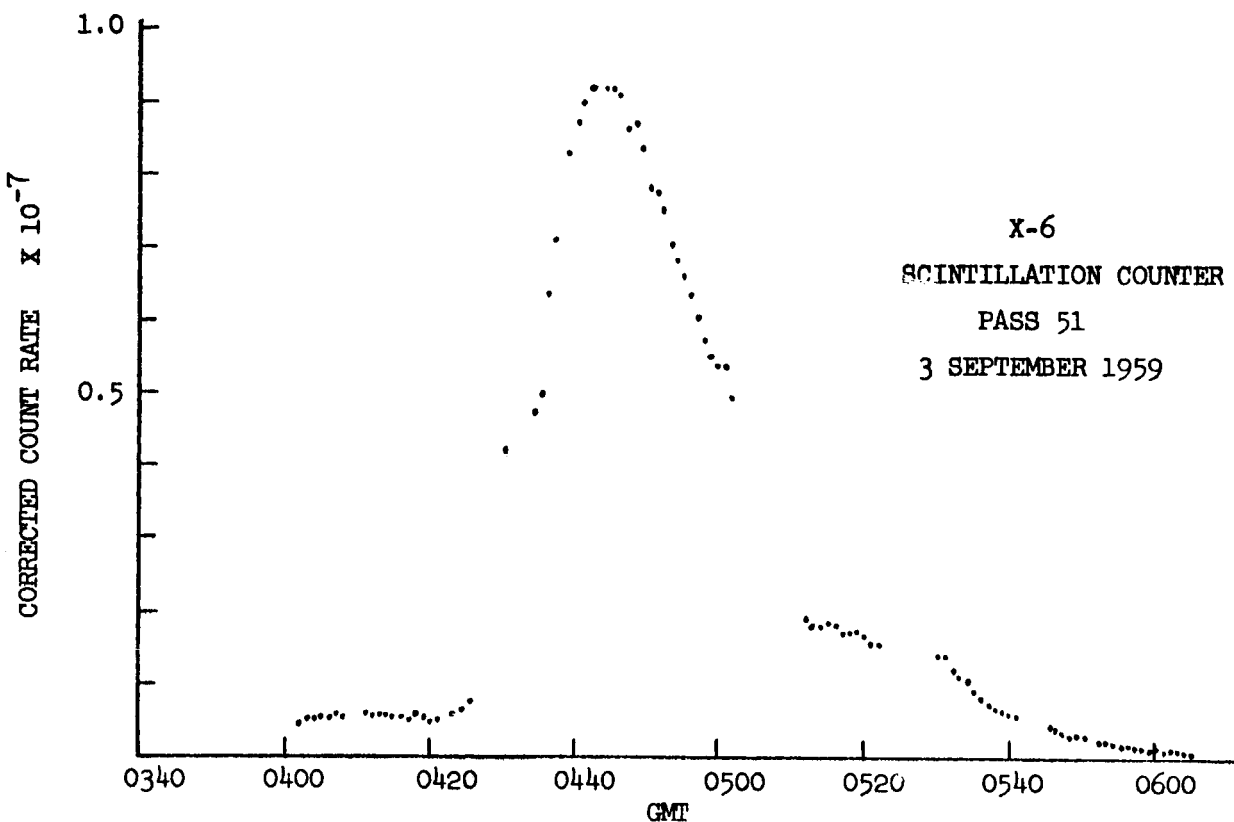


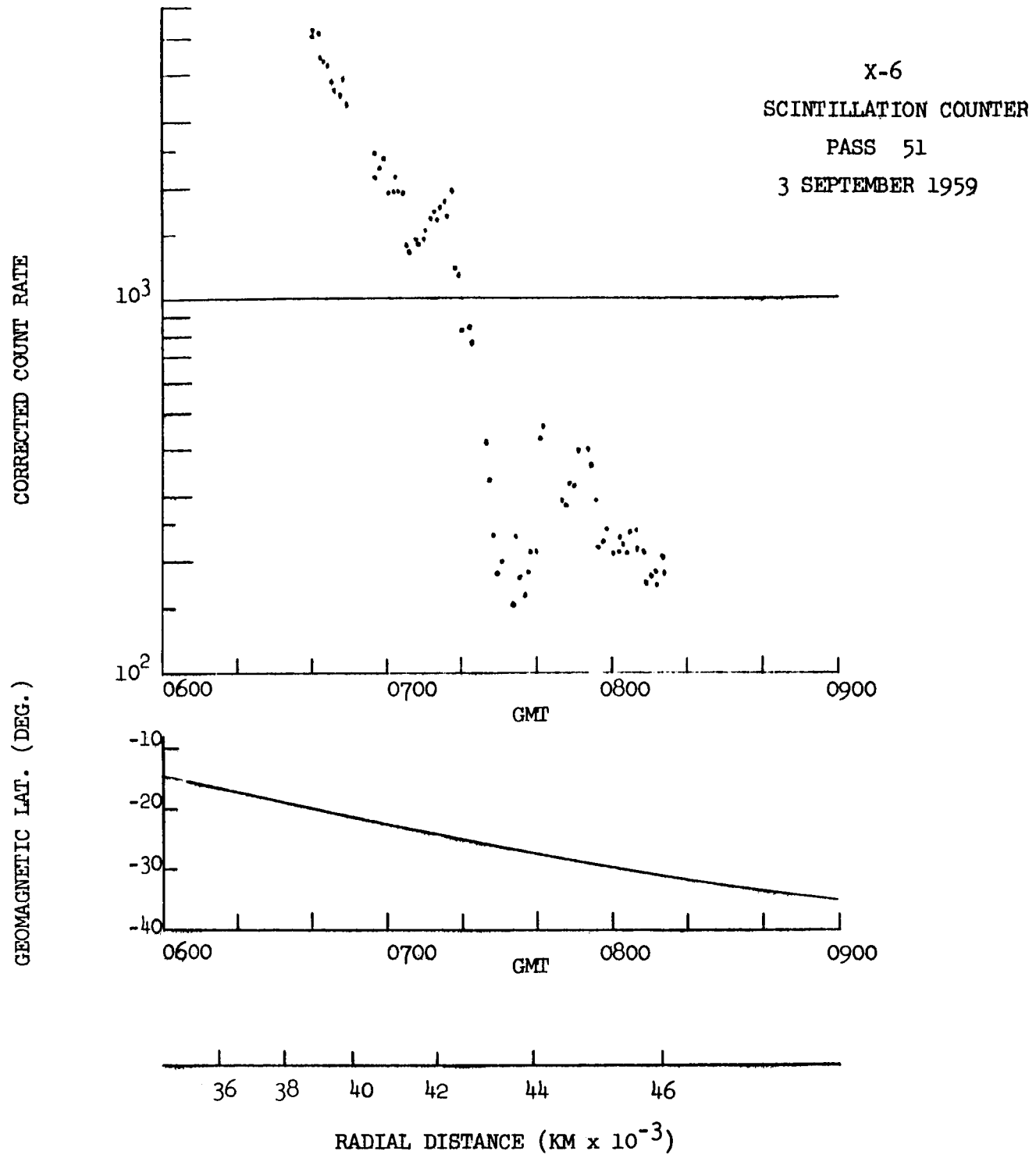


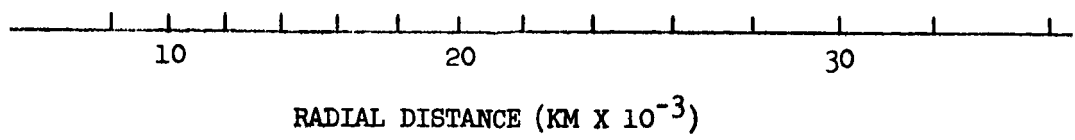
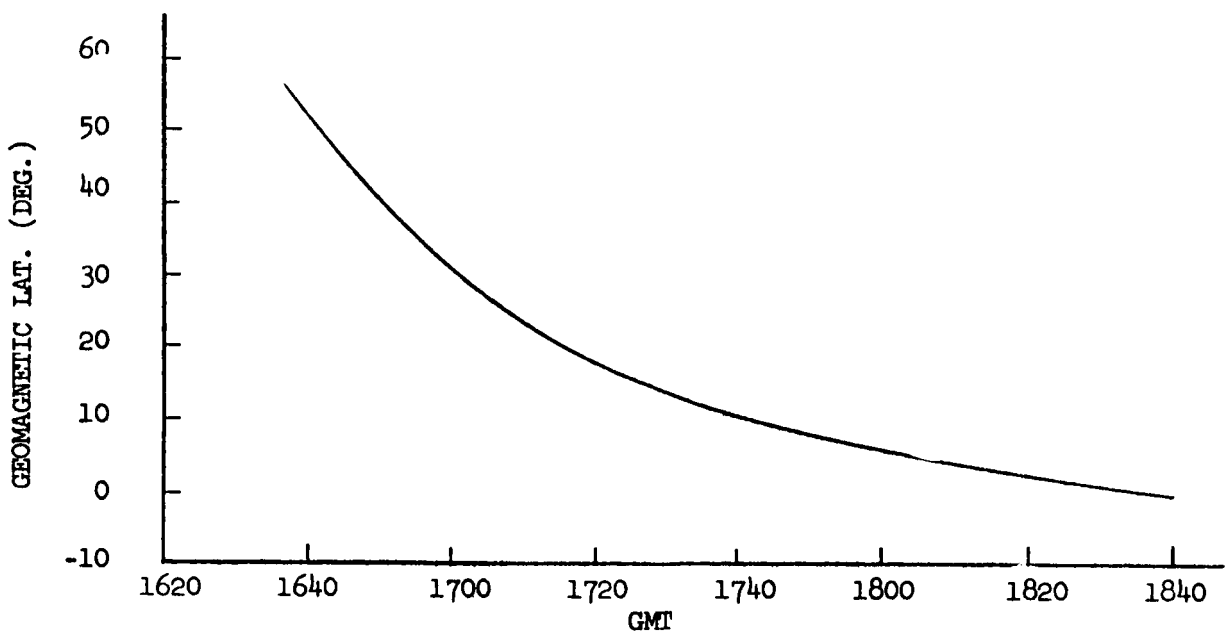
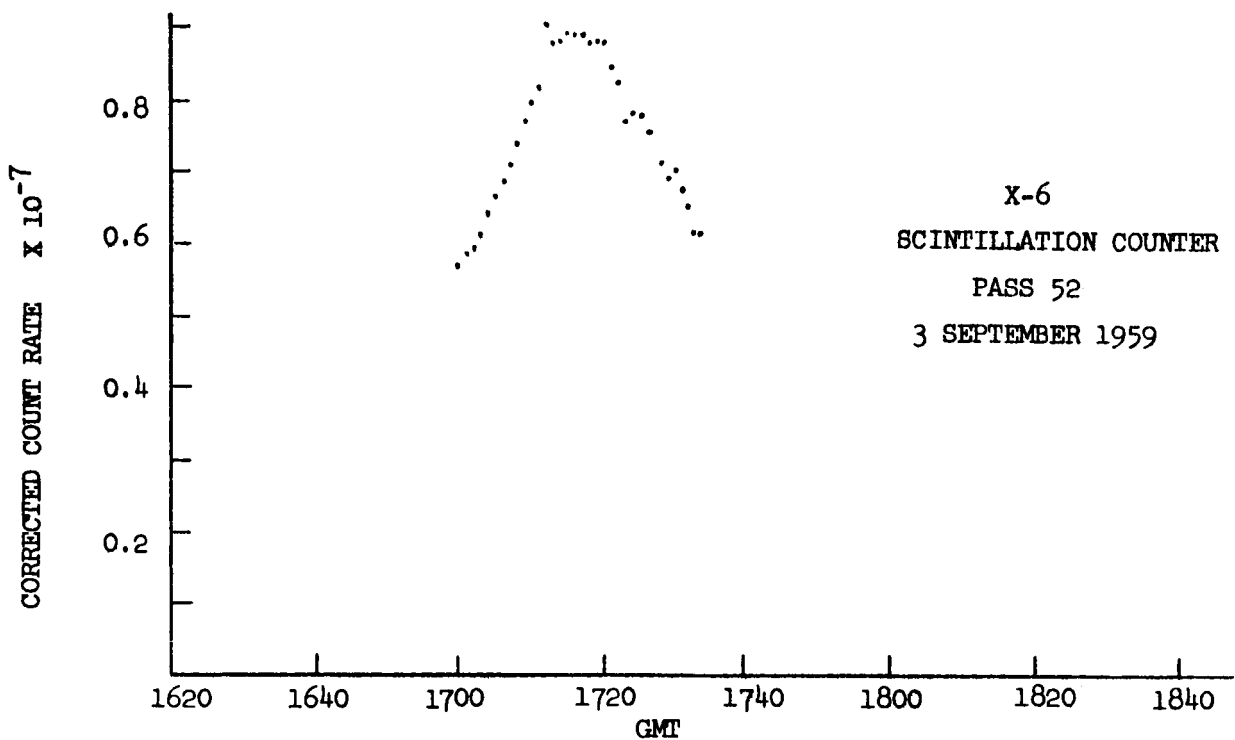


X-6
SCINTILLATION COUNTER
PASS 50
2 SEPTEMBER 1959

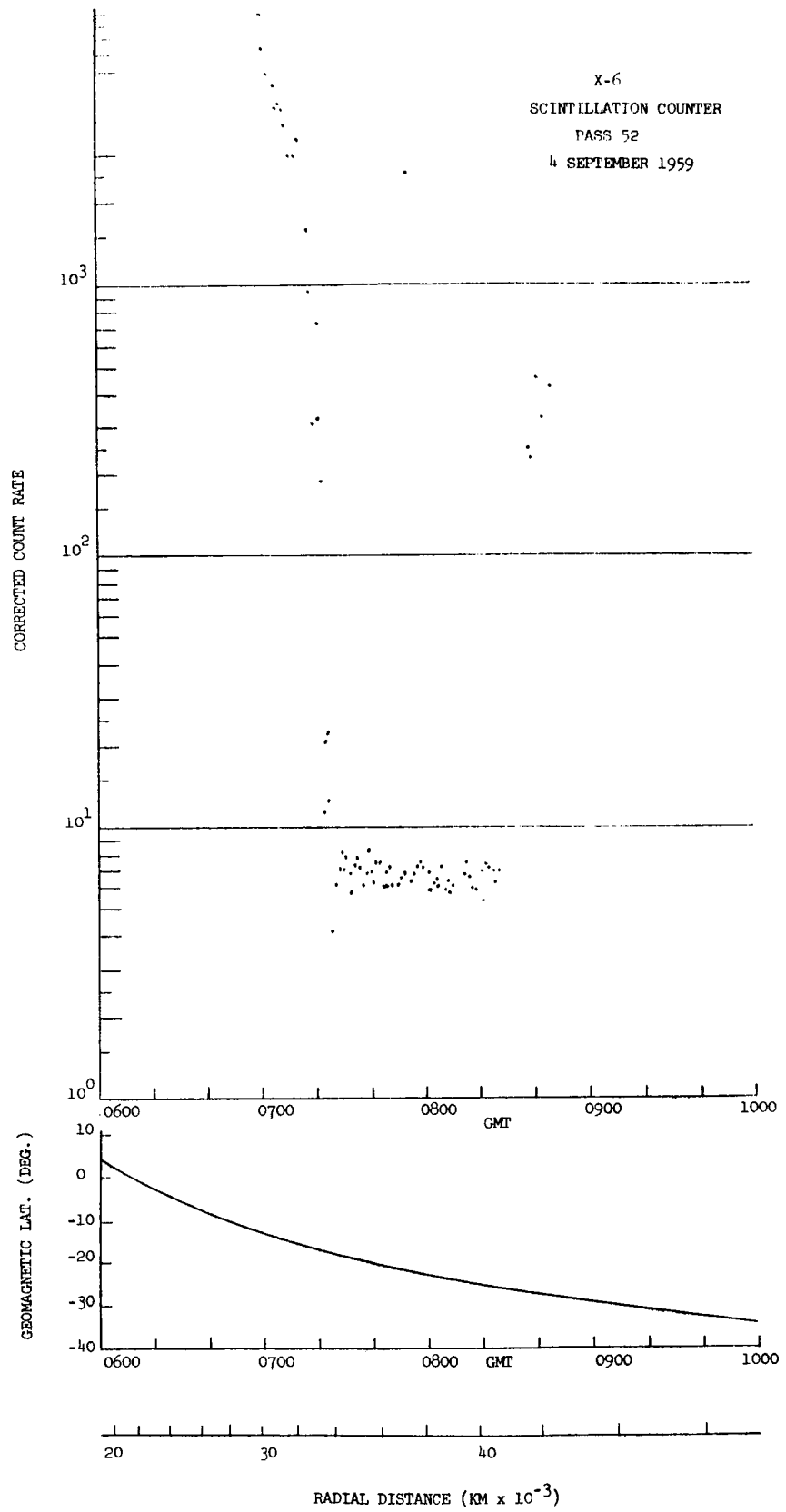


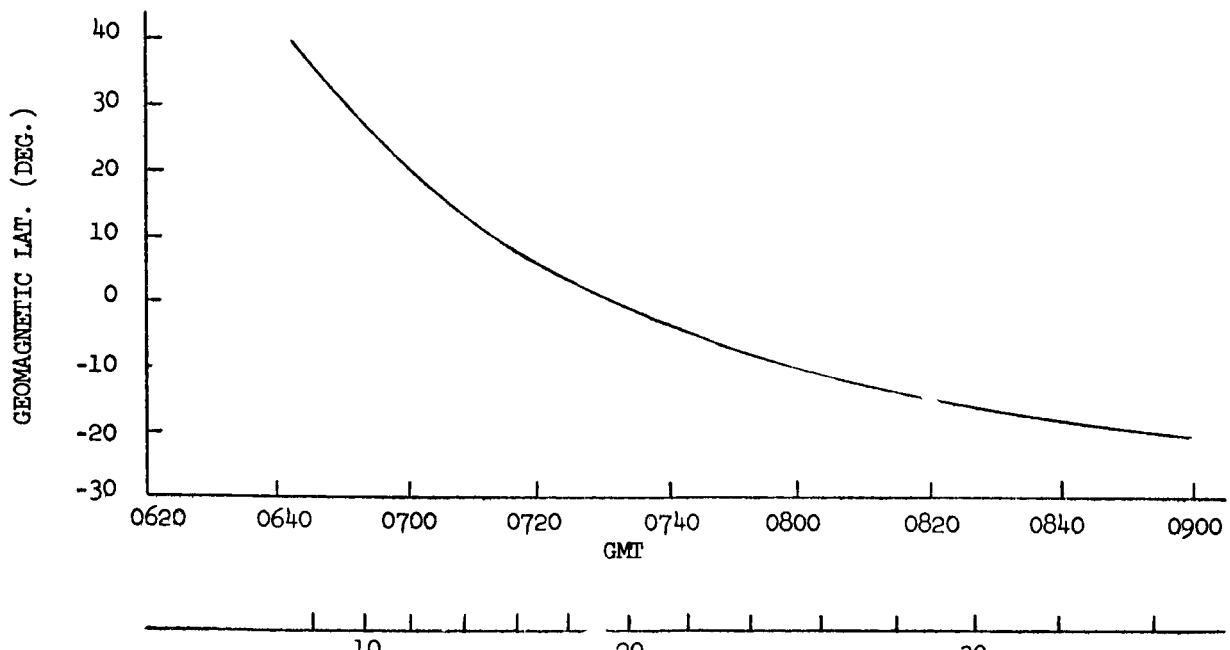
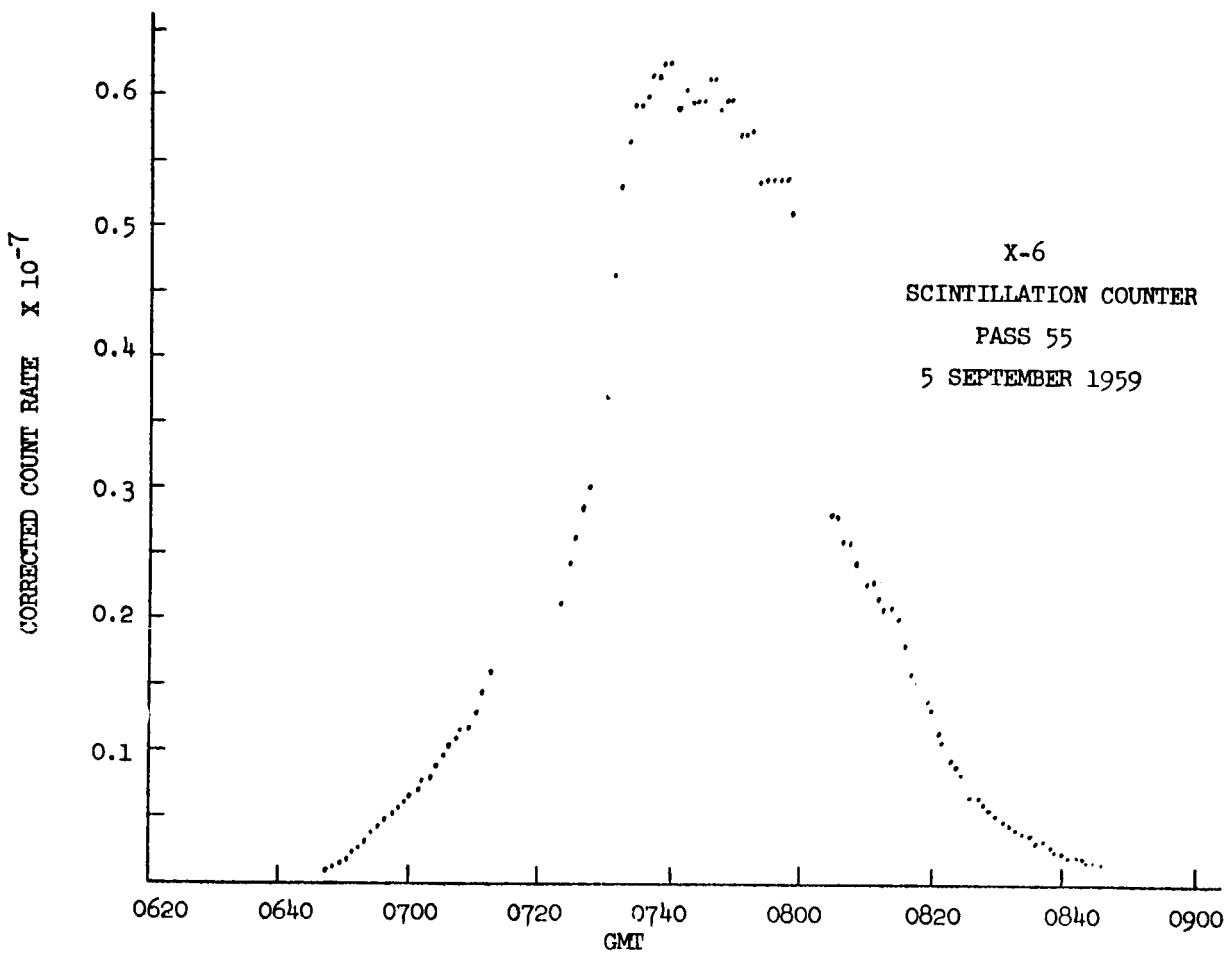






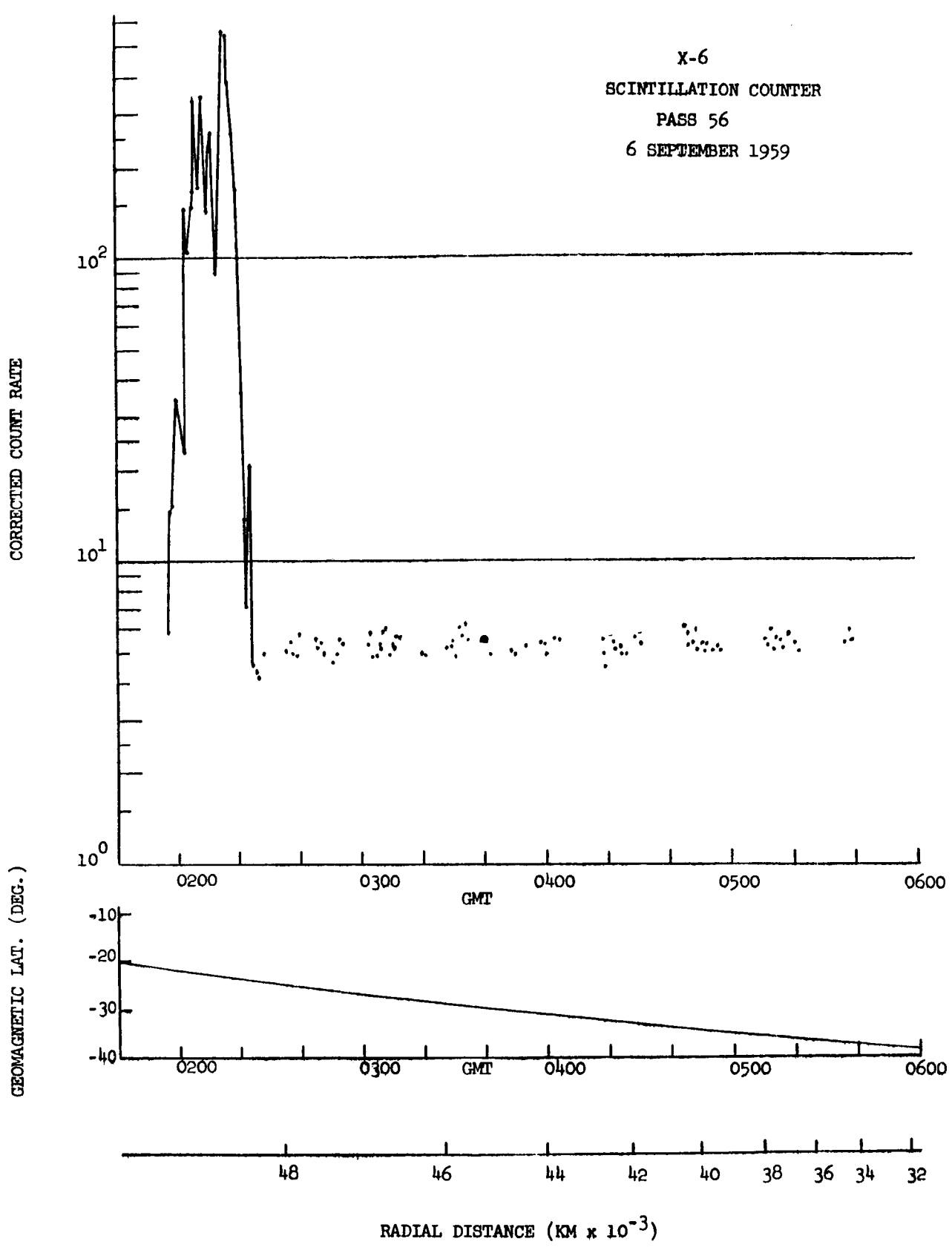
X-6
SCINTILLATION COUNTER
PASS 52
4 SEPTEMBER 1959



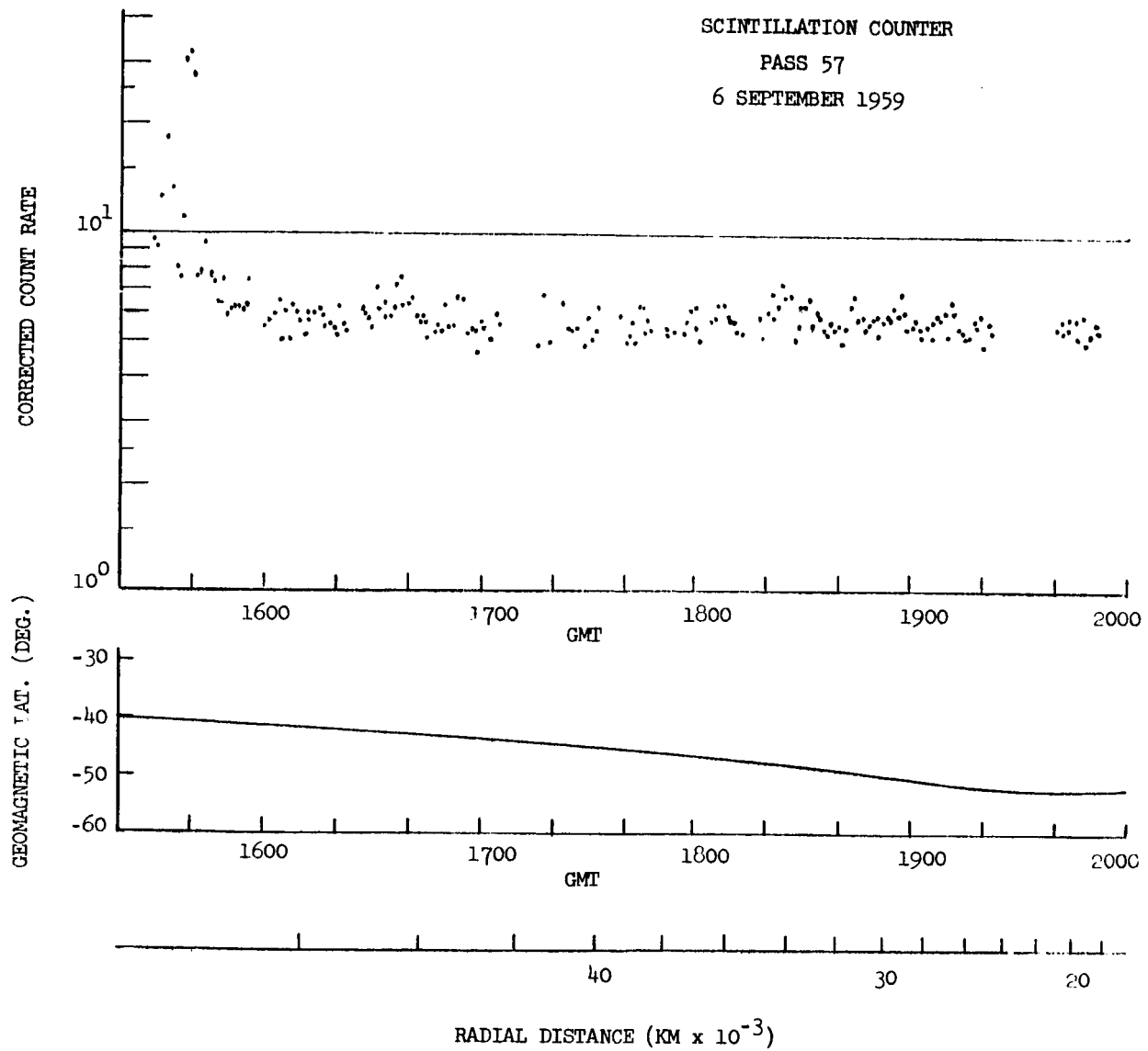


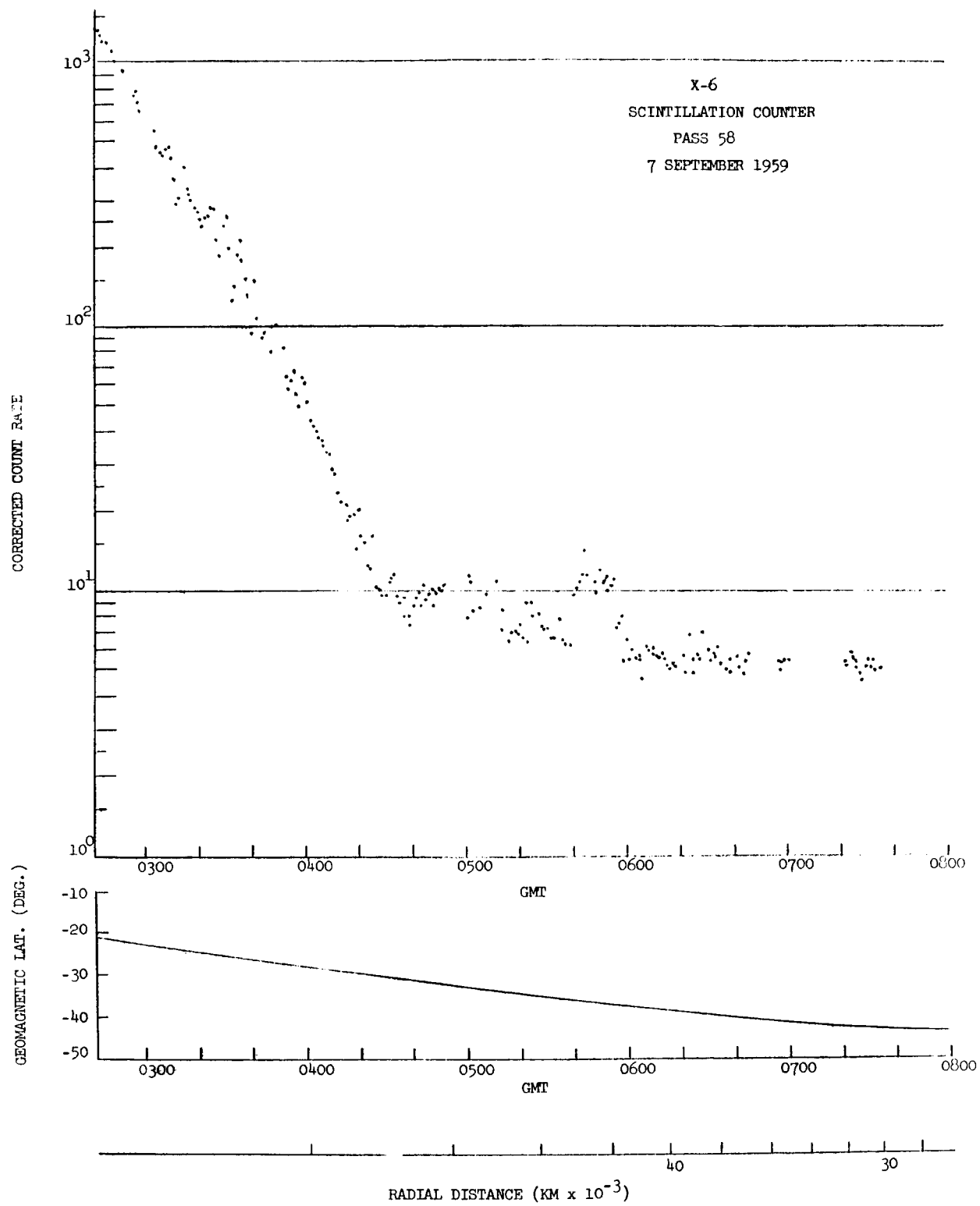
RADIAL DISTANCE (KM $\times 10^{-3}$)

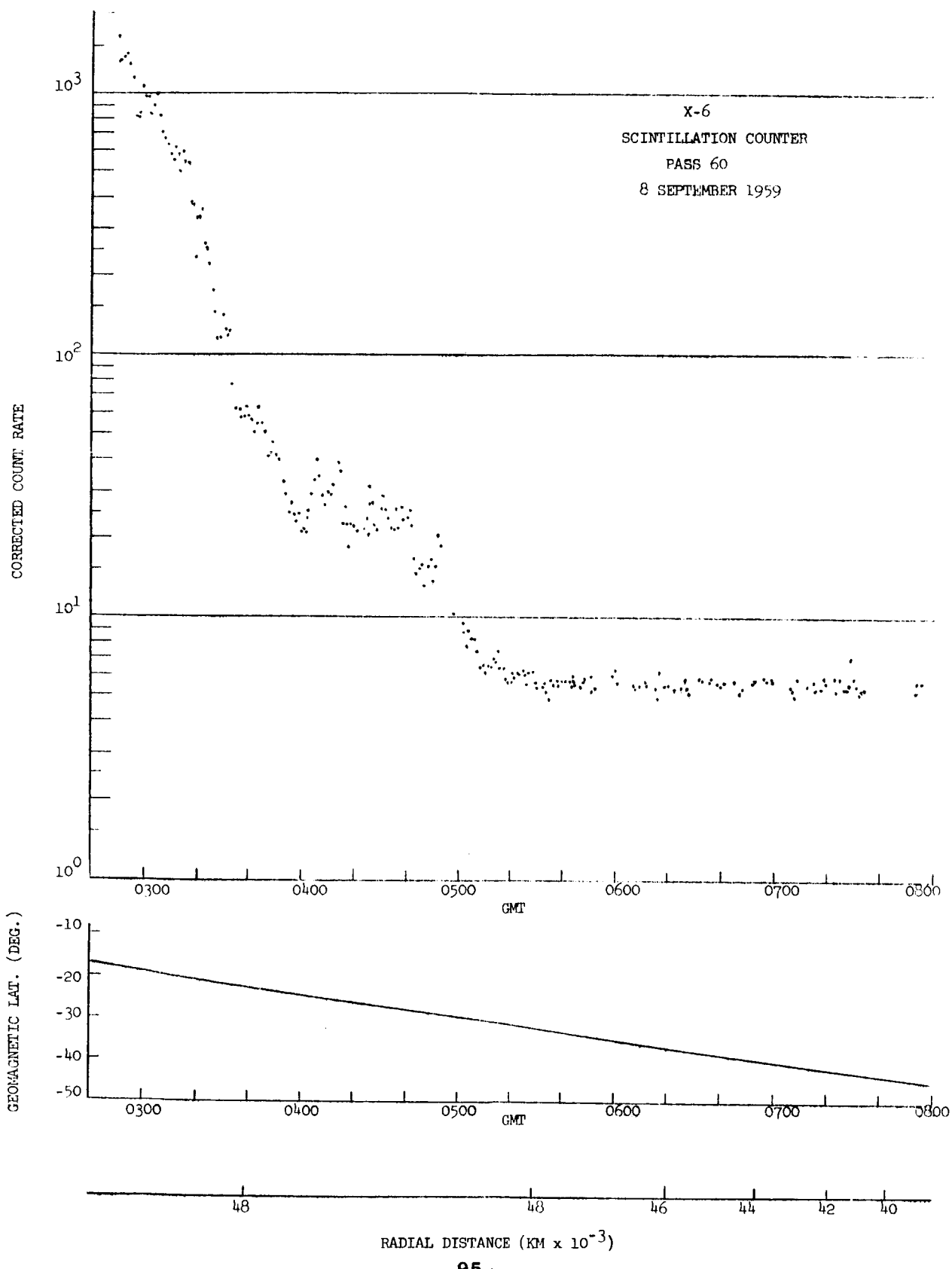
X-6
SCINTILLATION COUNTER
PASS 56
6 SEPTEMBER 1959



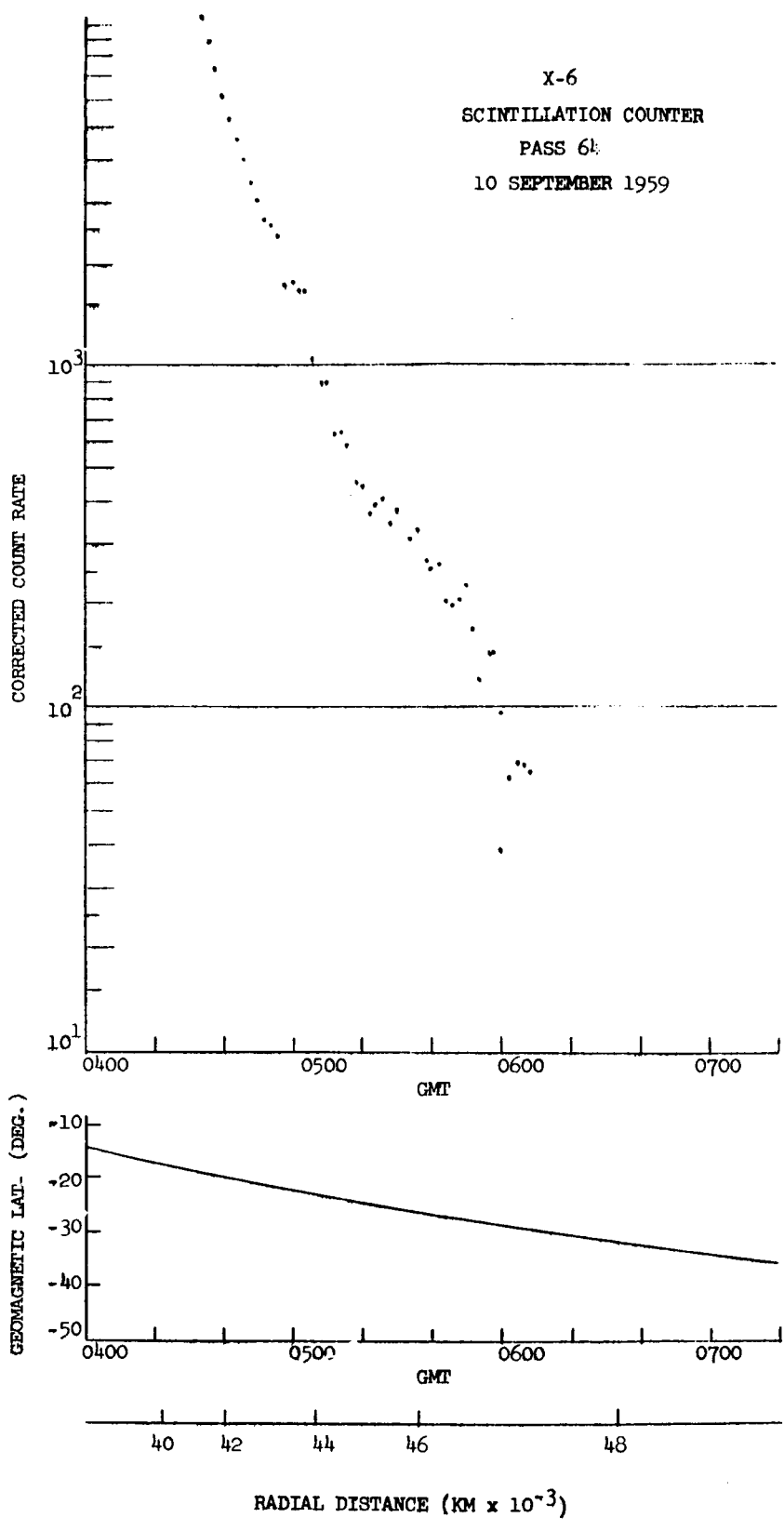
X-6
SCINTILLATION COUNTER
PASS 57
6 SEPTEMBER 1959







X-6
SCINTILLATION COUNTER
PASS 6
10 SEPTEMBER 1959



CHAPTER II

A COMPENDIUM OF DATA OBTAINED FROM THE
EXPLORER VI SEARCH COIL MAGNETOMETER

by

Edward J. Smith

Introduction

The graphs on the following pages represent all the available magnetic field data obtained by the Explorer VI search coil magnetometer. The search coil magnetometer and phase comparator (or magnetic field aspect indicator) measured two parameters of the extraterrestrial field designated B_{\perp} and ϕ . These parameters are defined, and the magnetometer described, in various publications (1). The data compilation consists of linear graphs of the phase angle, ϕ , and semi-log plots of the perpendicular field component, B_{\perp} , with universal time (i.e. GMT) as abscissa.

Two types of data appear in the figures: (a) Analog data derived from frequency modulated signals representing the output voltages of the search coil magnetometer, and (b) Digital data derived from binary numbers obtained by digital conversion of the magnetometer voltages on the spacecraft (2). In the graphs the digital data normally appear as a sequence of vertical lines (or rectangles) whose length gives the uncertainty of the measurement caused by the finite width of the digital "windows".^x There is substantially less digital data than analog data. Digital data transmissions were commanded periodically from the ground while the analog, FM transmissions were continuous. However, there are gaps in the analog data when no ground stations received the transmissions or when the quality of the demodulated data was poor ,

In addition to the magnetometer data, the graphs contain curves representing theoretical values of B_{\perp} and ϕ , called G_{\perp} and ϕ_G . These are based on an 8 coefficient, spherical harmonic expansion of the geomagnetic field (3). The mathematical formulae used to derive these quantities are given in the appendix.

* Horizontal and vertical dimensions of rectangles represent range of values giving the same binary number, and time duration, respectively. Centers of triangles are definite values corresponding to transitions between binary numbers.

The values of B_{\perp} and ϕ depend on the spacecraft spin axis orientation. The phase angle data near the earth were compared with phase angles computed for a set of spin axis directions lying on cones whose common axis was the nominal orientation. The spin axis orientation giving the most consistent agreement was used to compute the final values of B_{\perp} and ϕ . The magnitude of the geomagnetic field vector, G , is also plotted.

The values of the magnetometer output voltage representing B_{\perp} may be in error by several percent after demodulation (2 to 5%). Because of the quasi-logarithmic search coil amplifier characteristic (automatic gain control) the absolute errors at radial distances below 3 or so earth radii can be large (see figure 1). There is also a consistent difference of several percent between the analog and digital values of B_{\perp} . The reduced data, uncorrected in any way, appear in the graphs.

The values of ϕ shown in the following graphs may involve maximum errors of 2 to 3%. Since the phase comparator output voltage is a nearly linear function of ϕ , the corresponding errors in the phase angle are approximately 10 degrees. The reduced data have been adjusted by adding or subtracting a constant angle to make ϕ agree with ϕ_G near perigee passage (actually 7000 to 20,000 km, i.e. along one or both branches of the N-shaped theoretical curve) for each orbital rotation. This technique uses the data obtained near the earth, where the direction of the extraterrestrial field must be essentially the same as the direction of the unperturbed geomagnetic field within the resolution of the experiment, to check and correct the phase angle data. Note that the range of angles measured was the same at large geocentric distances and near the earth. The agreement between ϕ and ϕ_G below 20,000 km on a given pass was obtained by merely adding or subtracting a constant angle, $\Delta\phi$. $\Delta\phi$ varied, however, from

one pass to another. The same $\Delta\phi$ was subtracted from all data for a given pass. Comparison of data received simultaneously at two ground stations has shown that maximum differences of 2 to 3% did occur occasionally. Such differences must be associated with errors in the demodulation equipment at the ground stations and perhaps in the laboratory at STL.

To analyze and interpret the magnetometer data, it is essential to know the spatial position of the Explorer VI when the measurements were obtained. The plots of B_L and ϕ contain some trajectory information. The times are indicated when the Explorer VI was 20,000, 30,000, 40,000 and 48,800 kilometers from the earth's center. The phase data also contain a marker which indicates when the spacecraft crossed the geomagnetic equator (the geomagnetic latitude, δ_M , equals zero). The geomagnetic latitude of Explorer VI was computed from the geographic position using a centered dipole approximation to the geomagnetic field (4).

Figures 2 and 3 contain additional information regarding the instantaneous geomagnetic latitude of Explorer VI. The geomagnetic latitude at radial distances from 20,000 to 48,800 km in 5000 km intervals for the outgoing portion of each orbit is shown. δ_M is plotted separately for the odd-numbered and even numbered passes. Thus, to find the geomagnetic latitude at a given time, determine the radial distance and pass number from the plots of B_L and ϕ , and refer to the appropriate curve in figure 2 or 3. Trajectory information in geomagnetic coordinates is also available in the Scintillation Counter Data Compendium (Part B). For more accurate trajectory information, it will be necessary to refer to tabulations based on the Explorer VI definitive orbit (5) or to tabulations of the magnetic parameters (G_L , ϕ_G , δ_M , λ_M). These tabulations are stored at STL.

Another parameter that may be important in analysis and interpretation is the orientation of the spacecraft with respect to the earth-sun direction. The angle, λ_s , shown in figure 4, is the angle between the projections of the spacecraft-earth direction and earth-sun direction onto the geographic equatorial plane. The sun-earth-spacecraft angle at 20,000 and 48,800 km is shown as a function of pass number.

REFERENCES

1. Sonett, C. P., D. L. Judge, and J. M. Kelso, Evidence Concerning Instabilities in the Distant Geomagnetic Field: Pioneer I, *J. Geophys. Res.* 64, 941 (1959)

- Sonett, C. P., D. L. Judge, A. R. Sims, and J. M. Kelso, A Radial Rocket Survey of the Distant Geomagnetic Field, *J. Geophys. Res.*, 65, 55 (1960)

- Sonett, C. P., E. J. Smith, and A. R. Sims, Surveys of the Distant Geomagnetic Field: Pioneer I and Explorer VI, Space Research, Proceedings of First International Space Science Symposium, Edited by H. Kallman BIJL (North-Holland Pub. Co., Amsterdam, 1960), p. 921

- Sonett, C. P., E. J. Smith, D. L. Judge, P. J. Coleman, Current Systems in the Vestigial Geomagnetic Field: Explorer VI, *Phys. Rev. Letters*, 4, 161 (1960)

- Smith, E. J., P. J. Coleman, D. L. Judge, and C. P. Sonett, Characteristics of the Extraterrestrial Current System: Explorer VI and Pioneer V, *J. Geophys. Res.*, 65, 1858 (1960)

- Smith, E. J., and C. P. Sonett, Satellite Observations of the Distant Field During Magnetic Storms: Explorer VI, Proceedings of International Conference on Cosmic Rays and the Earth Storm (Kyoto, Sept. 1961) *J. Phys Soc. Japan* 17, 17 (1962)

- Smith, E. J., A Comparison of Explorer VI and Explorer X Magnetometer Data, *J. Geophys. Res.* 67, 2045 (1962)

- Smith, E. J., Theoretical and Experimental Aspects of Ring Currents, in Space Science (Ed. D. P. LeGalley) Wiley and Sons New York (1963)

2. Greenstadt, E. W., The Data Systems for Explorer VI and Pioneer V, IRE Transactions on Space Electronics and Telem., SET-6, 122 (1960)
3. Vestine, E. H., Lines of Force of the Geomagnetic Field in Space, Planet. and Space Science 1, 285 (1959)
4. Chapman, S., and J. Bartels, Geomagnetism, Oxford University Press, New York (1949)
Dessler, A. J., Geomagnetism, in Satellite Environment Handbook (ed. F. S. Johnson), Stanford University Press, Stanford, Cal. (1961)
5. Moe, K., Explorer VI Definitive Orbit, Final Report, STL Report 8650-6001-RU-000 (1962)
6. Smith, E., and C. P. Sonett, Satellite Observations of the Geomagnetic Field During Magnetic Storms, to be submitted to the J. Geophys. Res.
7. Ephemeris of the Sun, The American Ephemeris and Nautical Almanac, U. S. Nautical Almanac Office, U. S. Naval Observatory, U.S. Government printing office, Washington. (The coordinates of the sun referred to in the appendix are called X, Y, Z, e.g. see page 20-27 in the 1959 issue.)

FIGURE CAPTIONS

Figure 1. Search Coil Magnetometer Sensitivity

This figure is actually a form of calibration curve for the search coil magnetometer. B_{\perp} is plotted against radial distance for a fictitious trajectory which crudely approximates the outgoing portion of the Explorer VI orbit. Figures at the top of the graph refer to the magnetometer output voltage, given in terms of percent of full scale. The vertical lines spaced along the curve indicate (a) the field value corresponding to a given output level (i.e., the intersection between the vertical line and the curve) and (b) the range of field values corresponding to a range of one or more percent in the output level. A difference of 1 percent may represent several hundred gamma in an ambient field of several thousand gamma but only a few gamma in a 100 gamma field.

Figure 2. Explorer VI Geomagnetic Latitude: Odd-numbered Passes

The geomagnetic latitude is shown when the spacecraft was at altitudes of 20, 25, 30, 35, 40, 45, and $48.8 \cdot 10^3$ km on the outgoing portion of odd-numbered orbits.

Figure 3. Explorer VI Geomagnetic Latitude: Even-numbered Passes

The geomagnetic latitude of Explorer VI on the outgoing portion of even-numbered orbits is shown with the radial distance as a parameter.

Figure 4. Sun-Earth-Spacecraft Angle

This angle is defined in the discussion of the magnetic storm observations included in this report.⁽⁶⁾ The projections of the earth-sun vector and Explorer VI radius vector onto the geographic equatorial plane form the angle, λ_s . The value of λ_s at 20,000 and 48,800 km is shown as a function of orbit number.

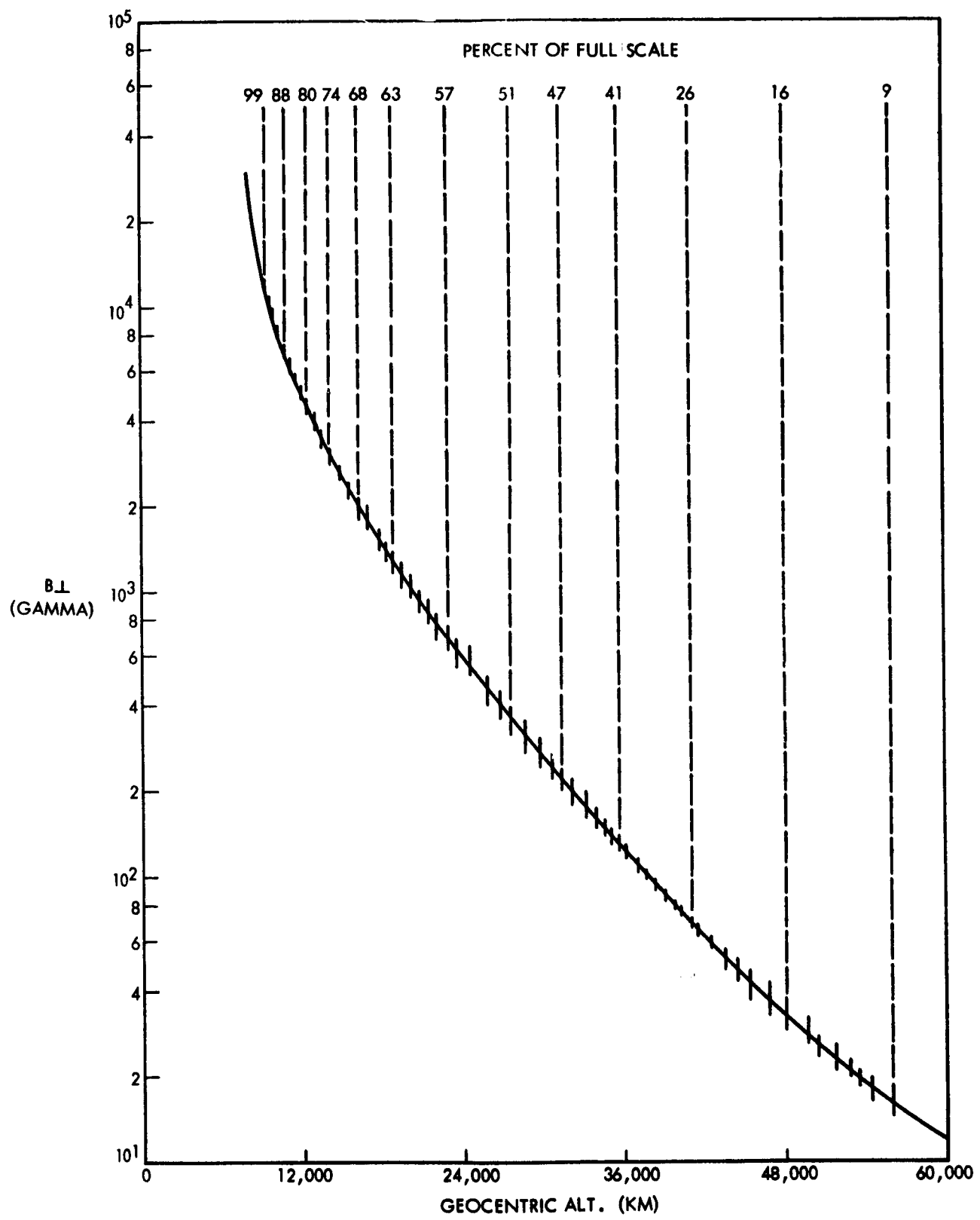


Figure 1. Search Coil Magnetometer Sensitivity

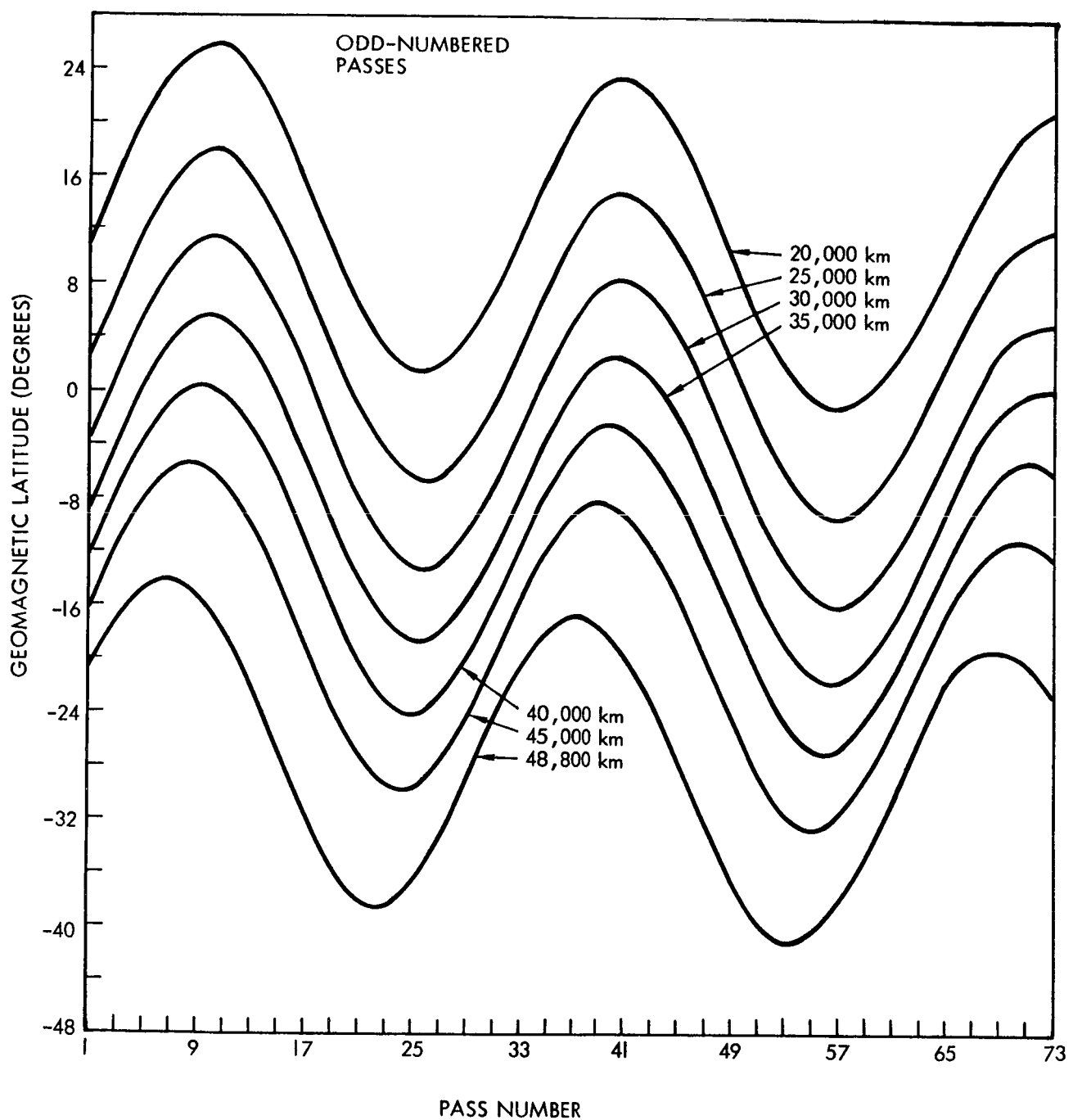


Figure 2. Explorer VI Geomagnetic Latitude: Odd-numbered Passes

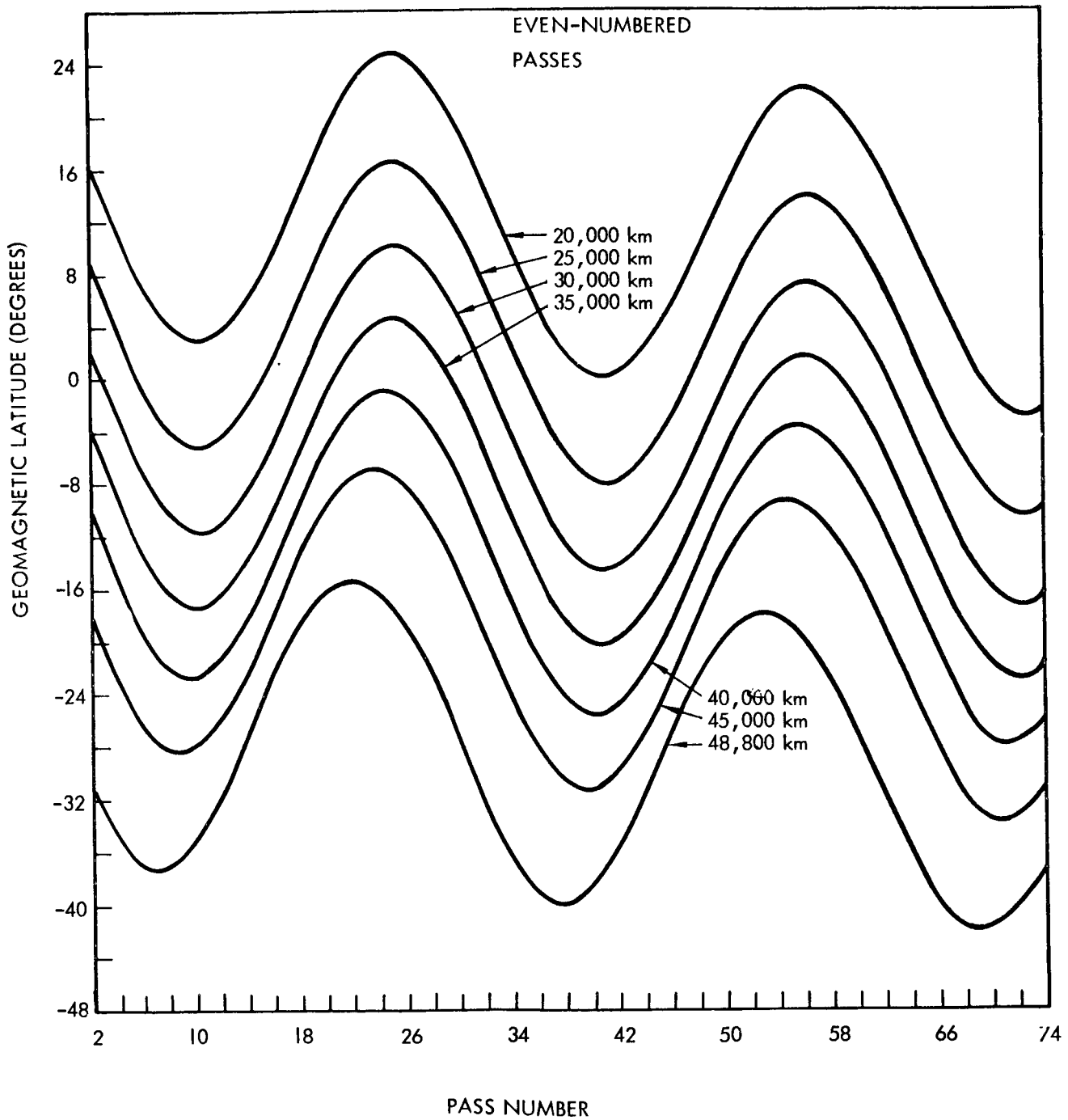


Figure 3. Explain VI Geomagnetic Latitude: Even-numbered Passes

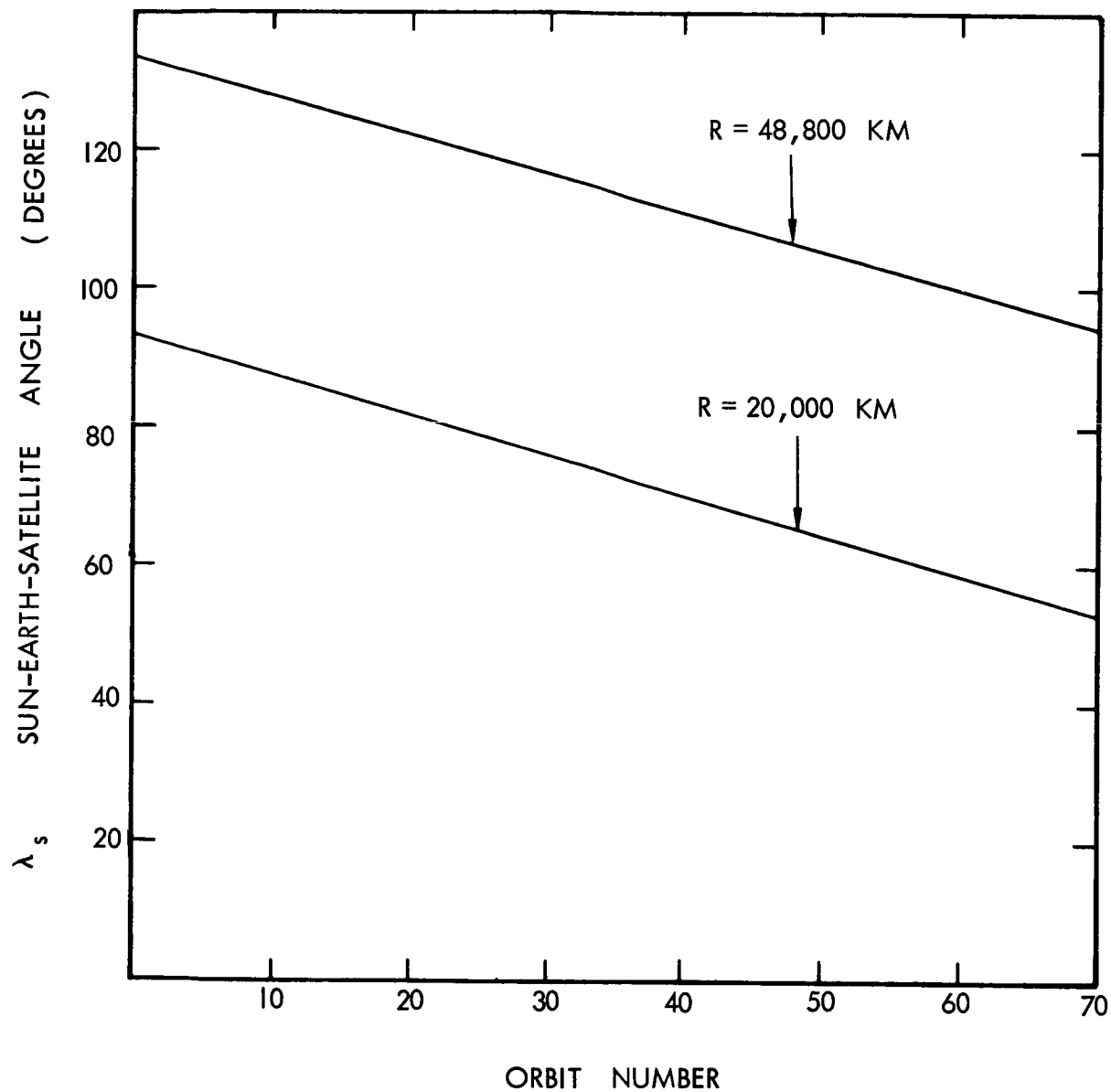
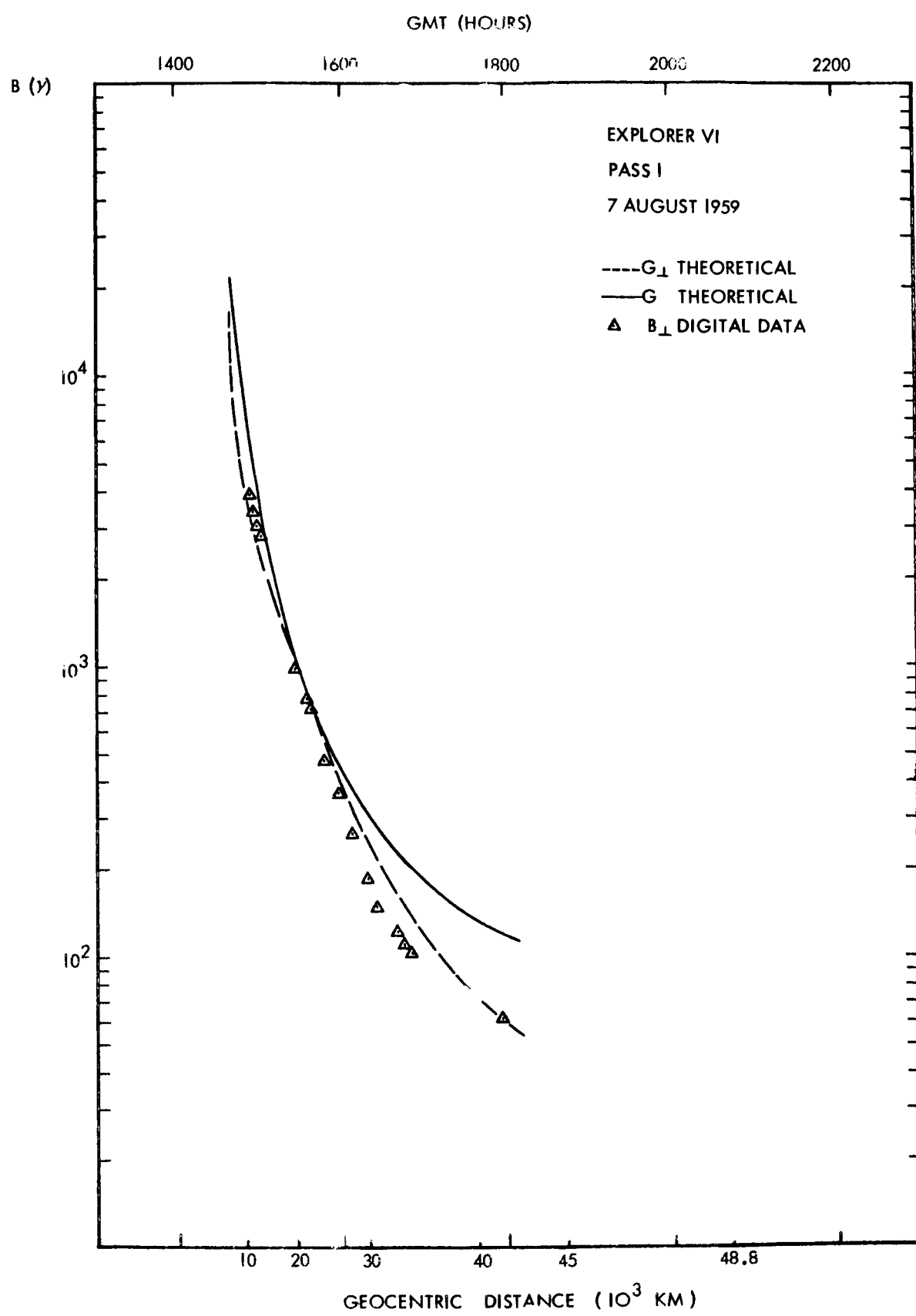
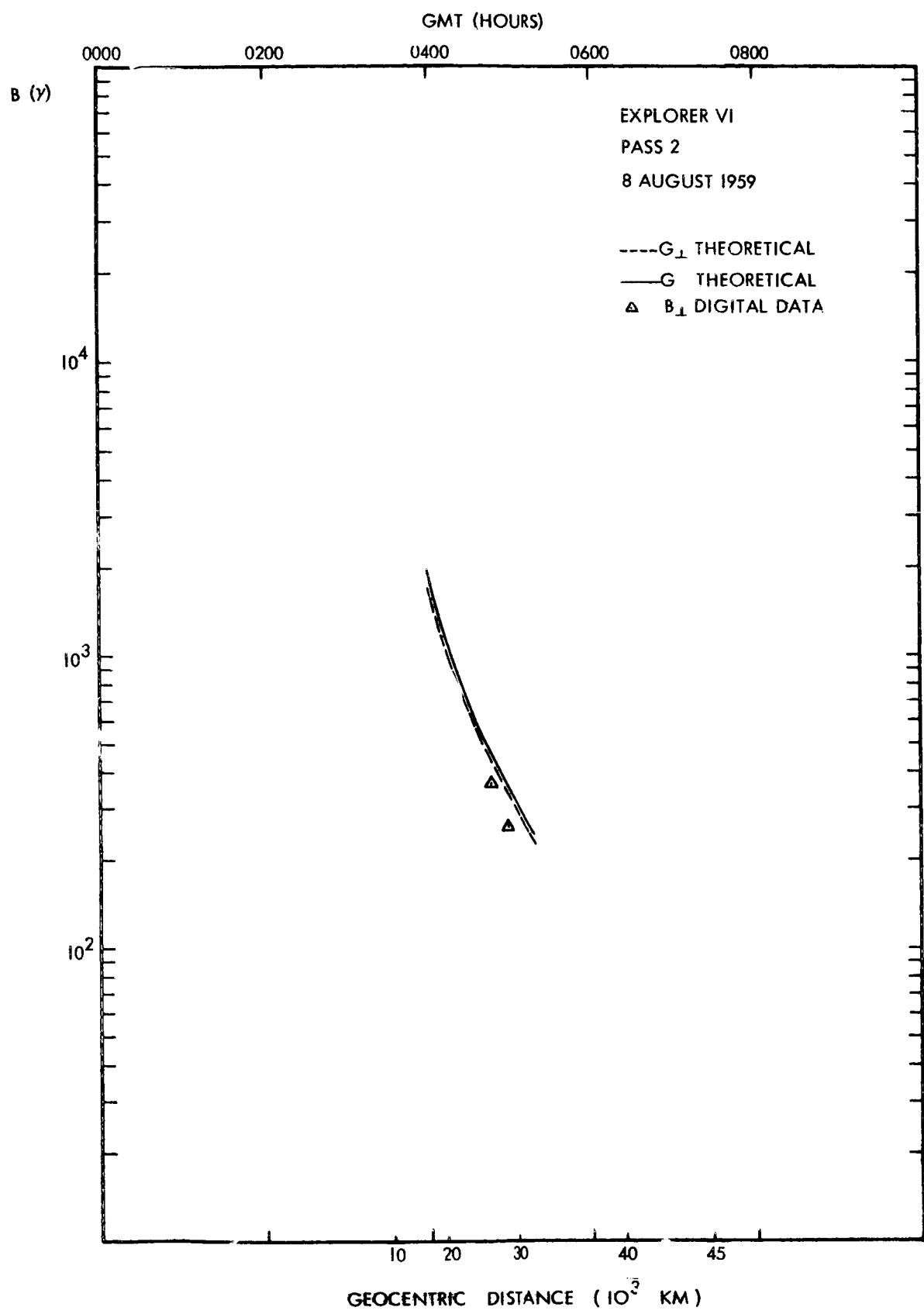
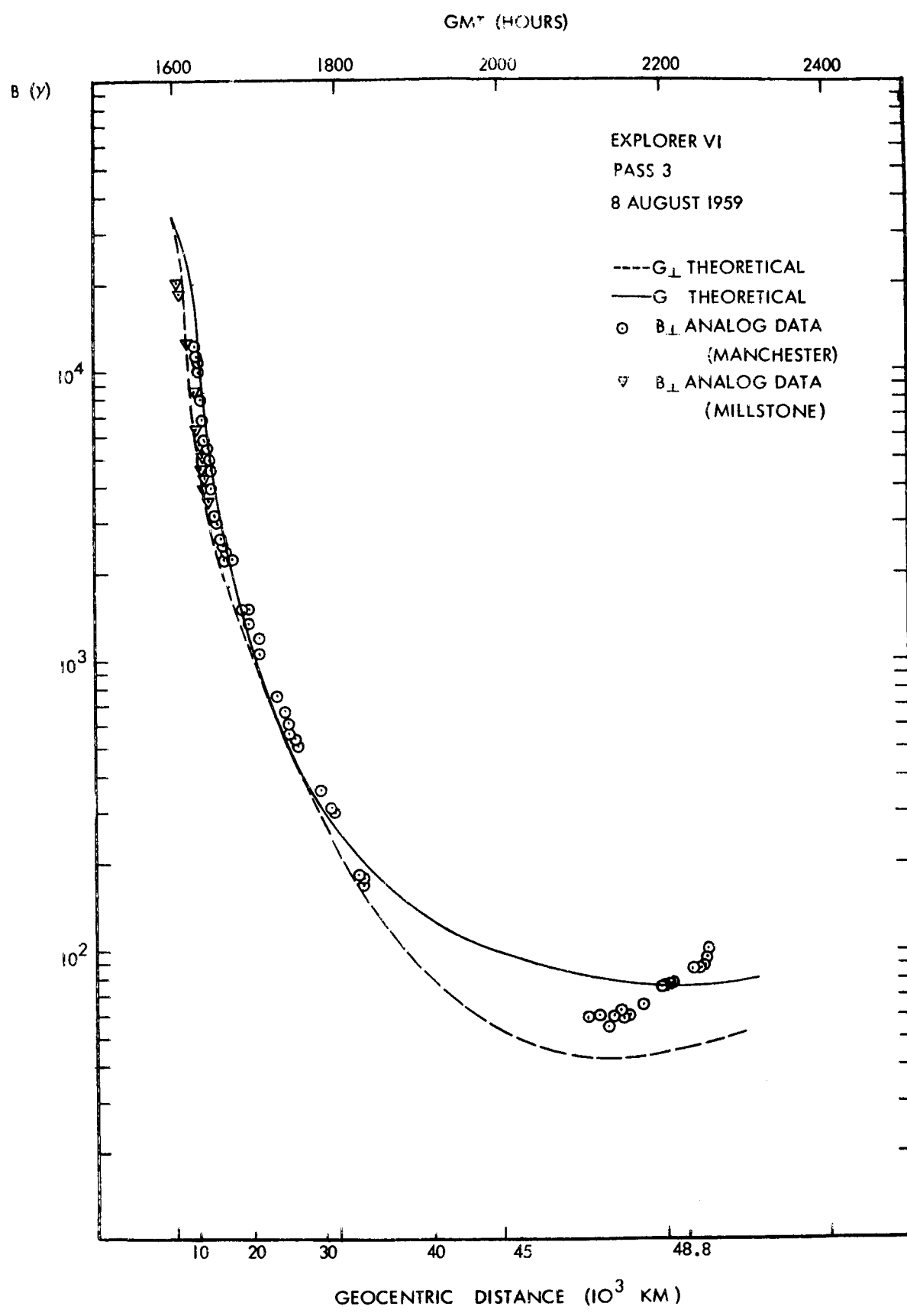


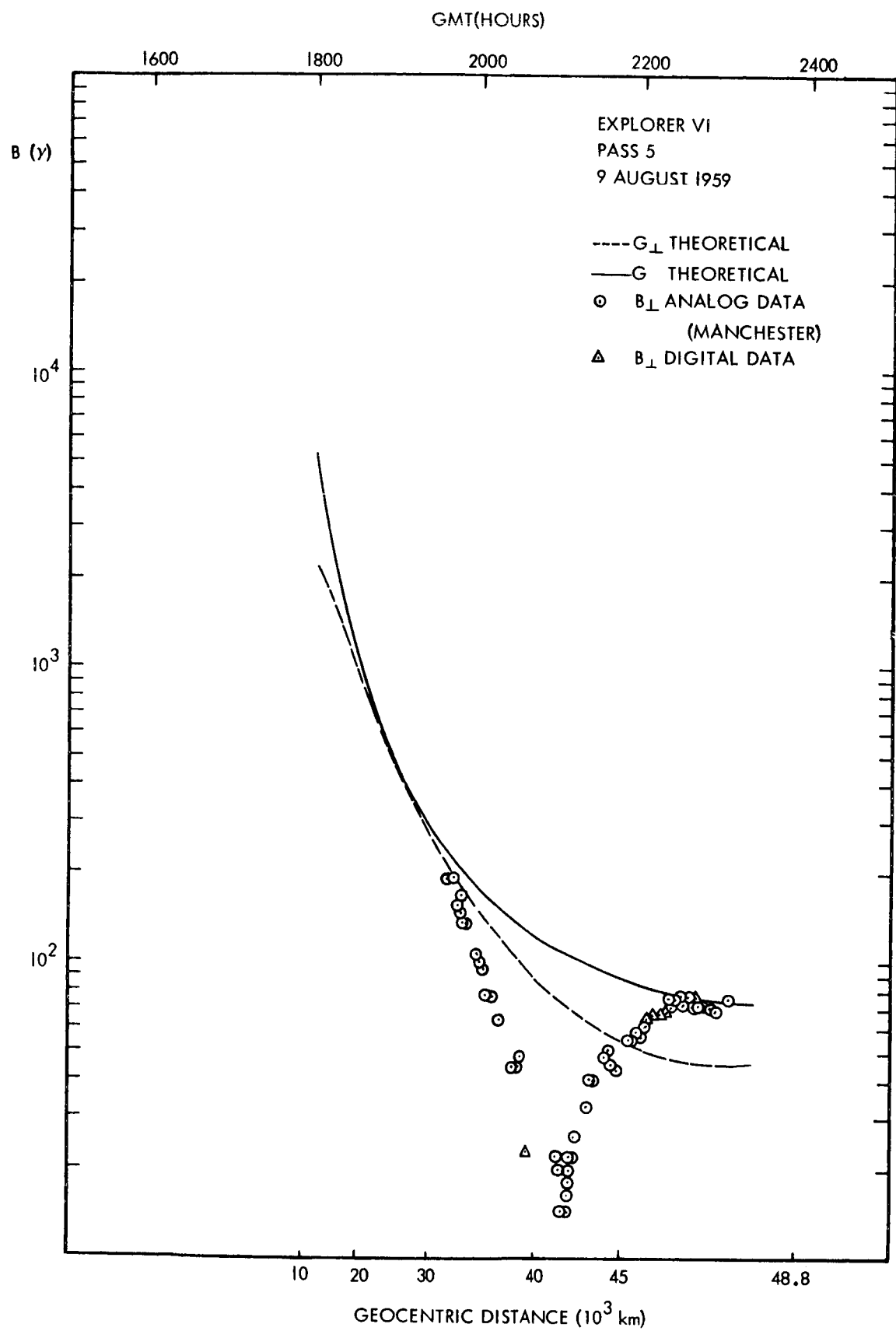
Figure 4. Sun-Earth-Spacecraft Angle

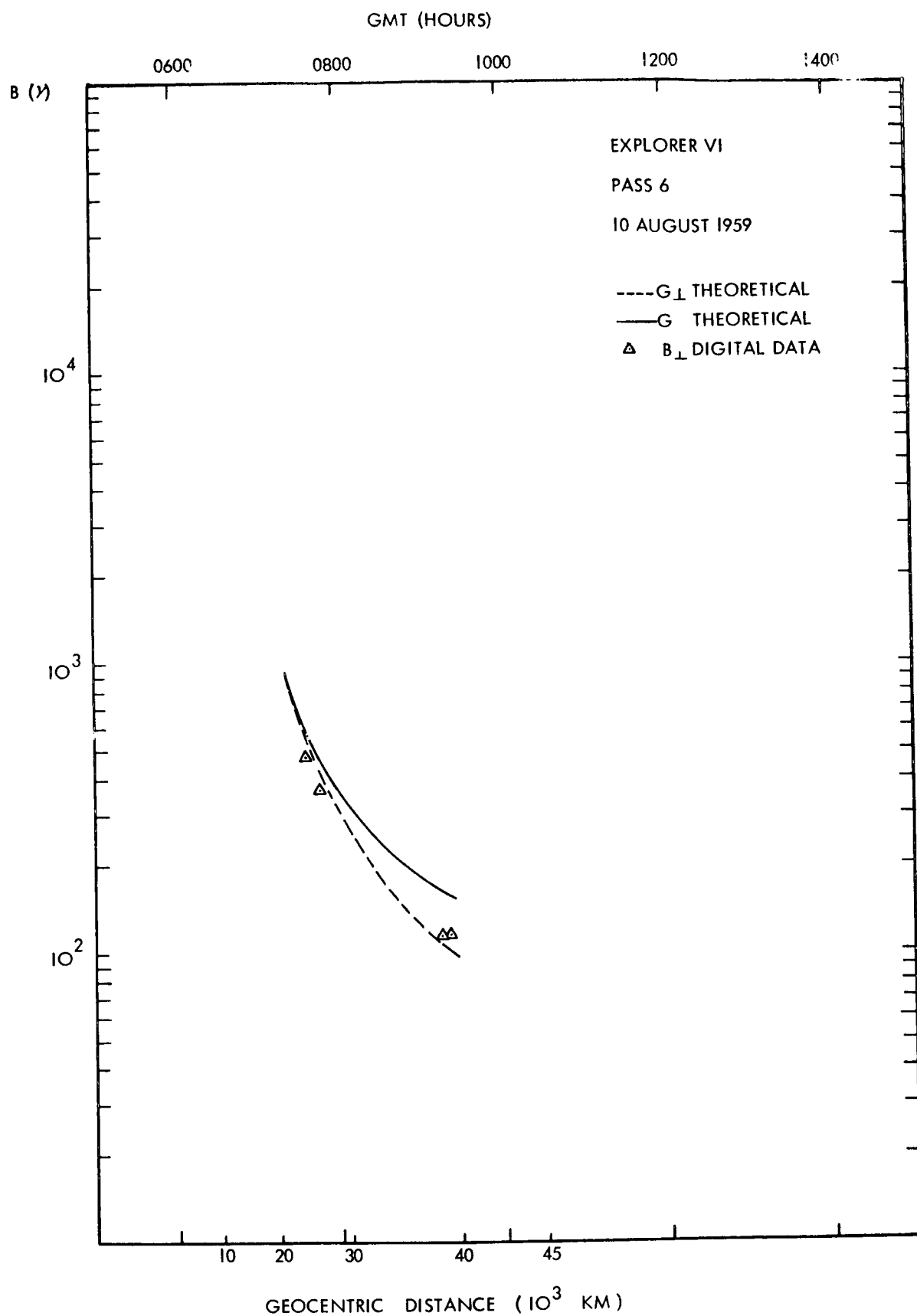
DATA COMPENDIUM:
FIELD MAGNITUDE

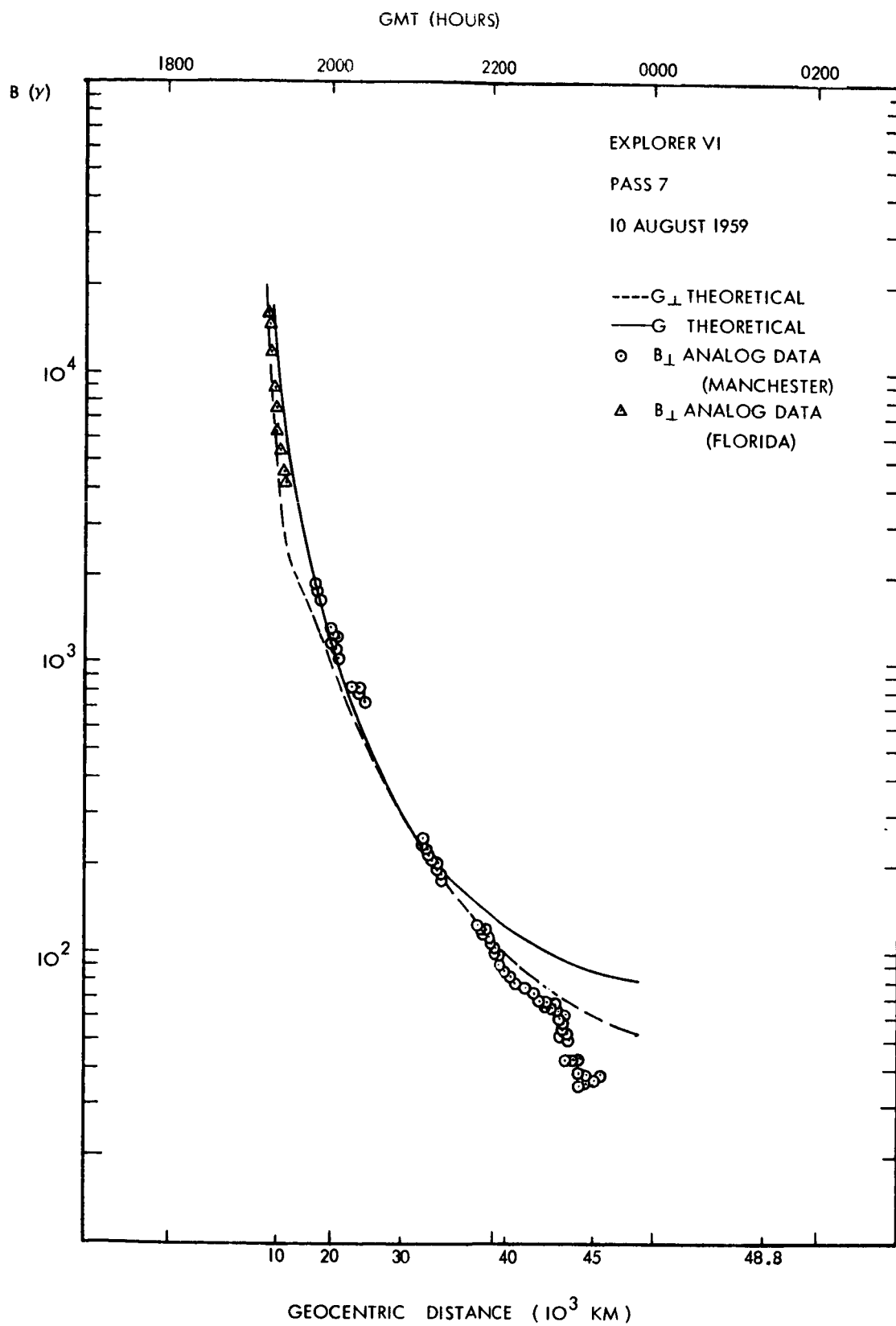


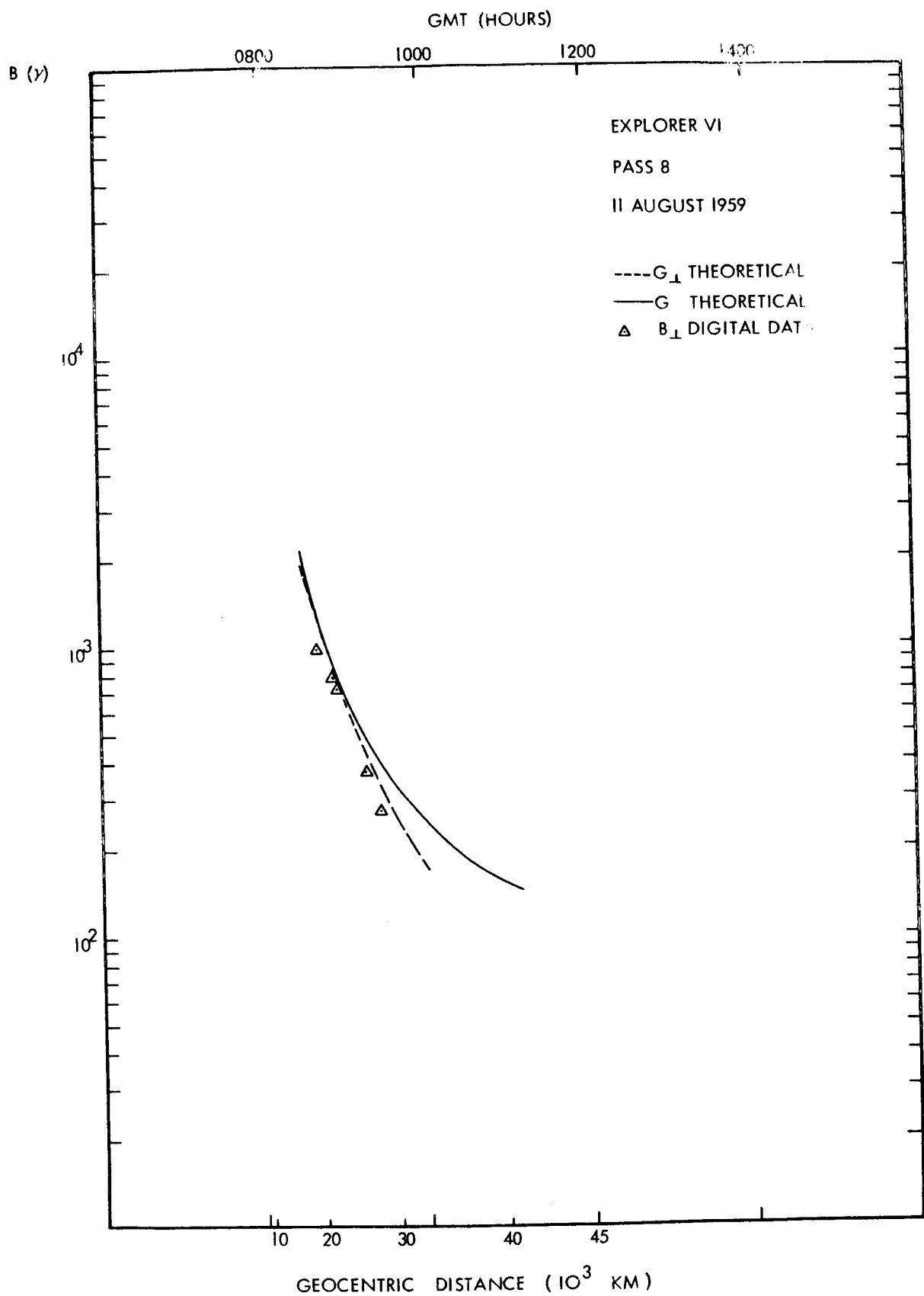


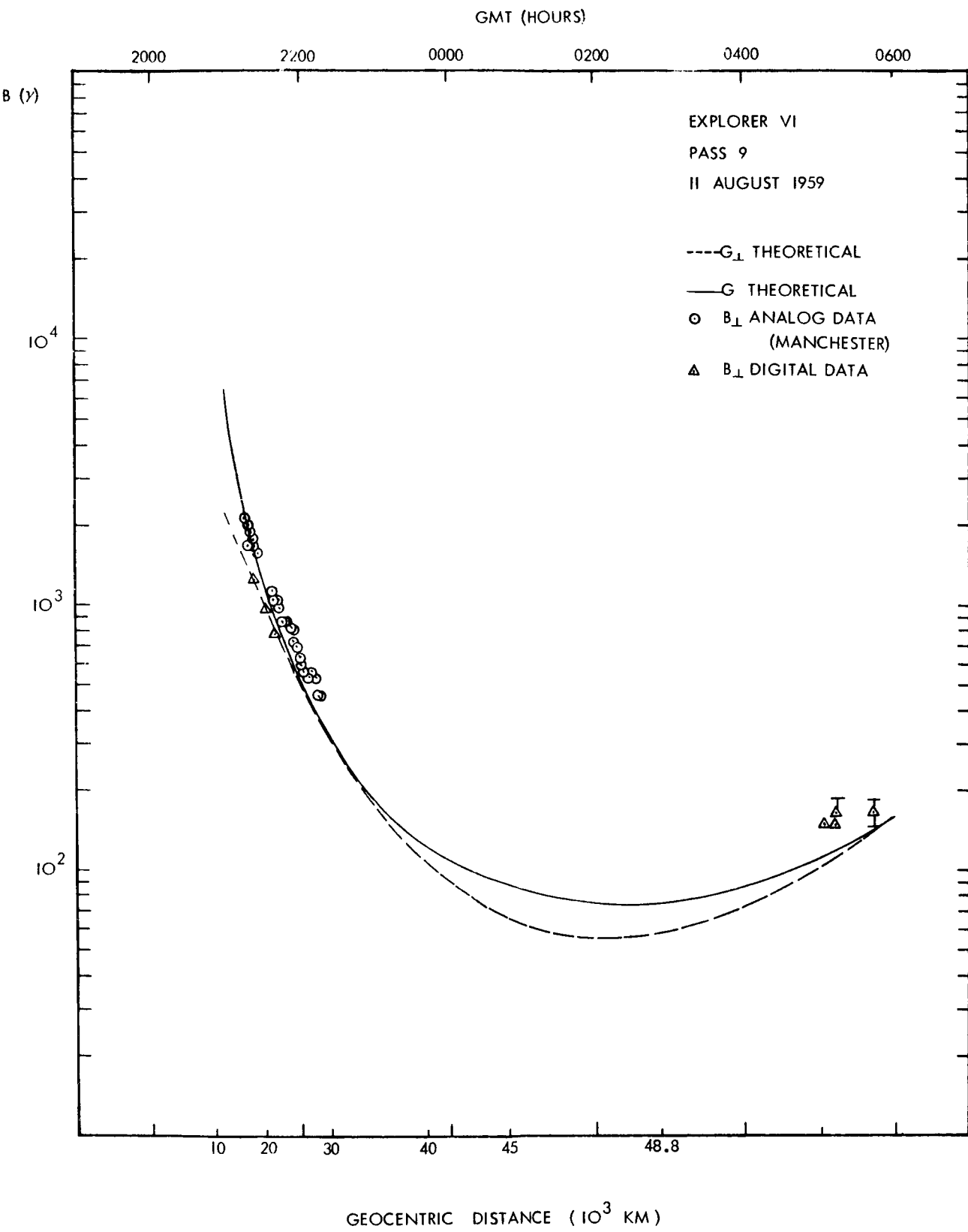


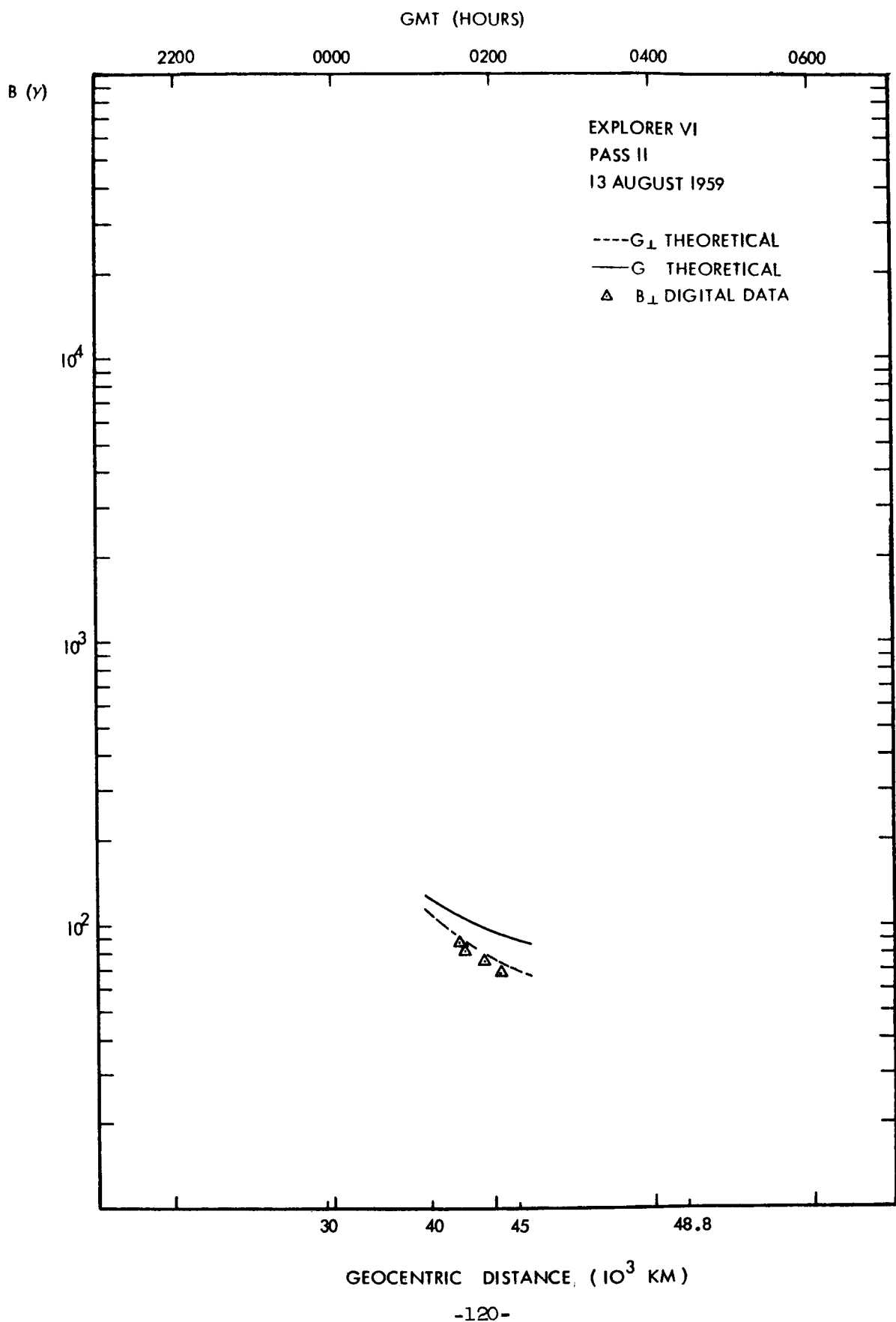


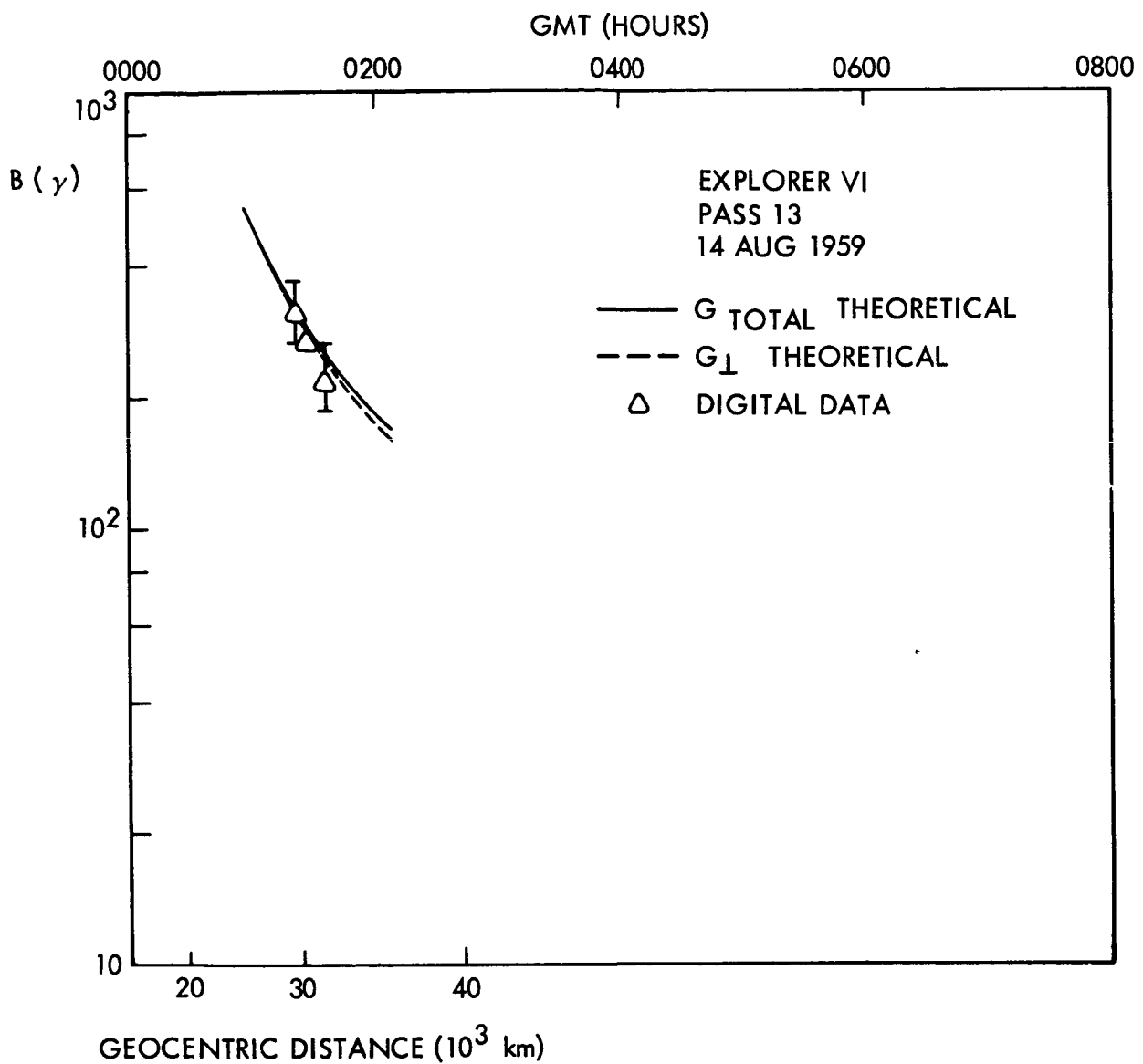


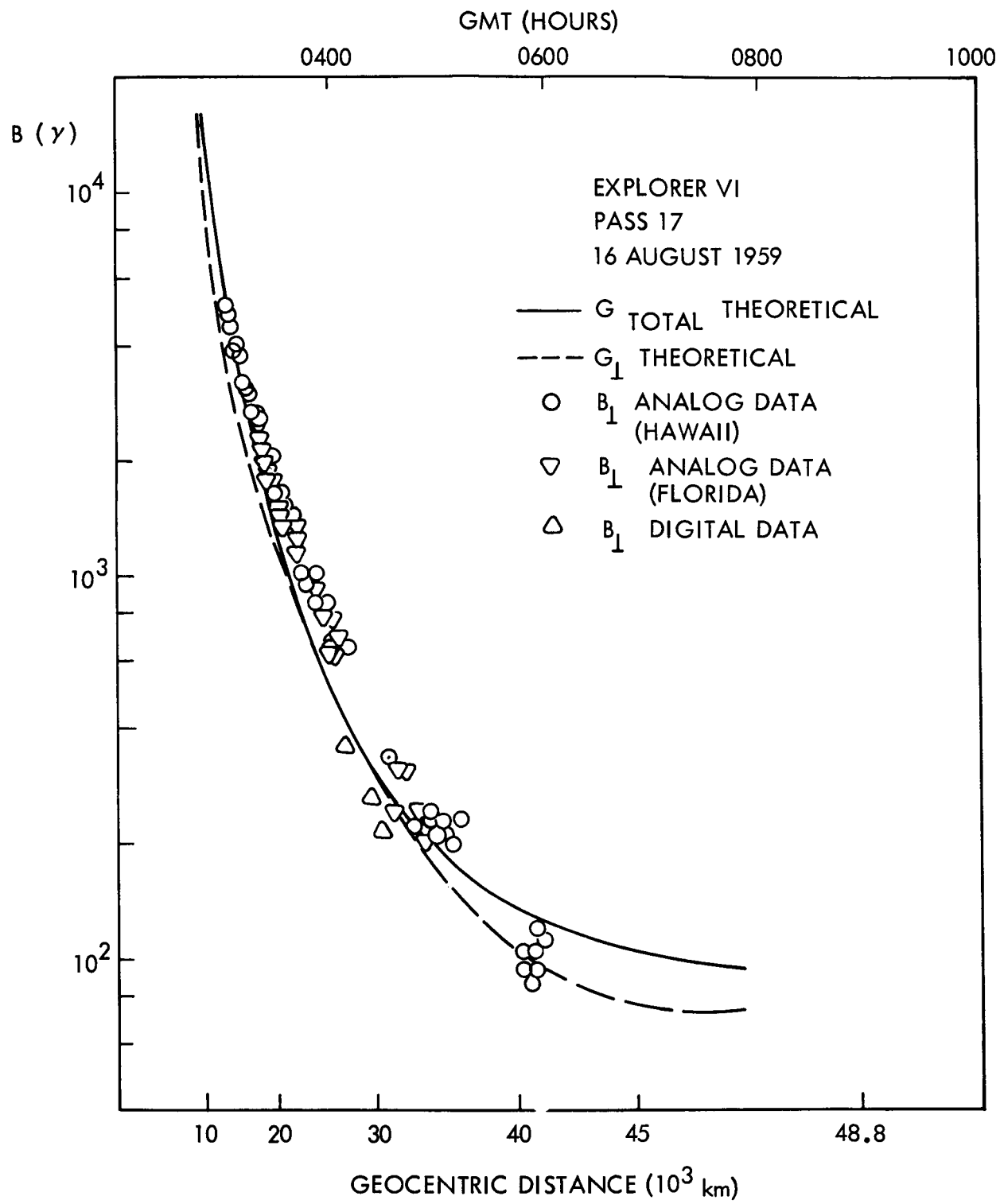


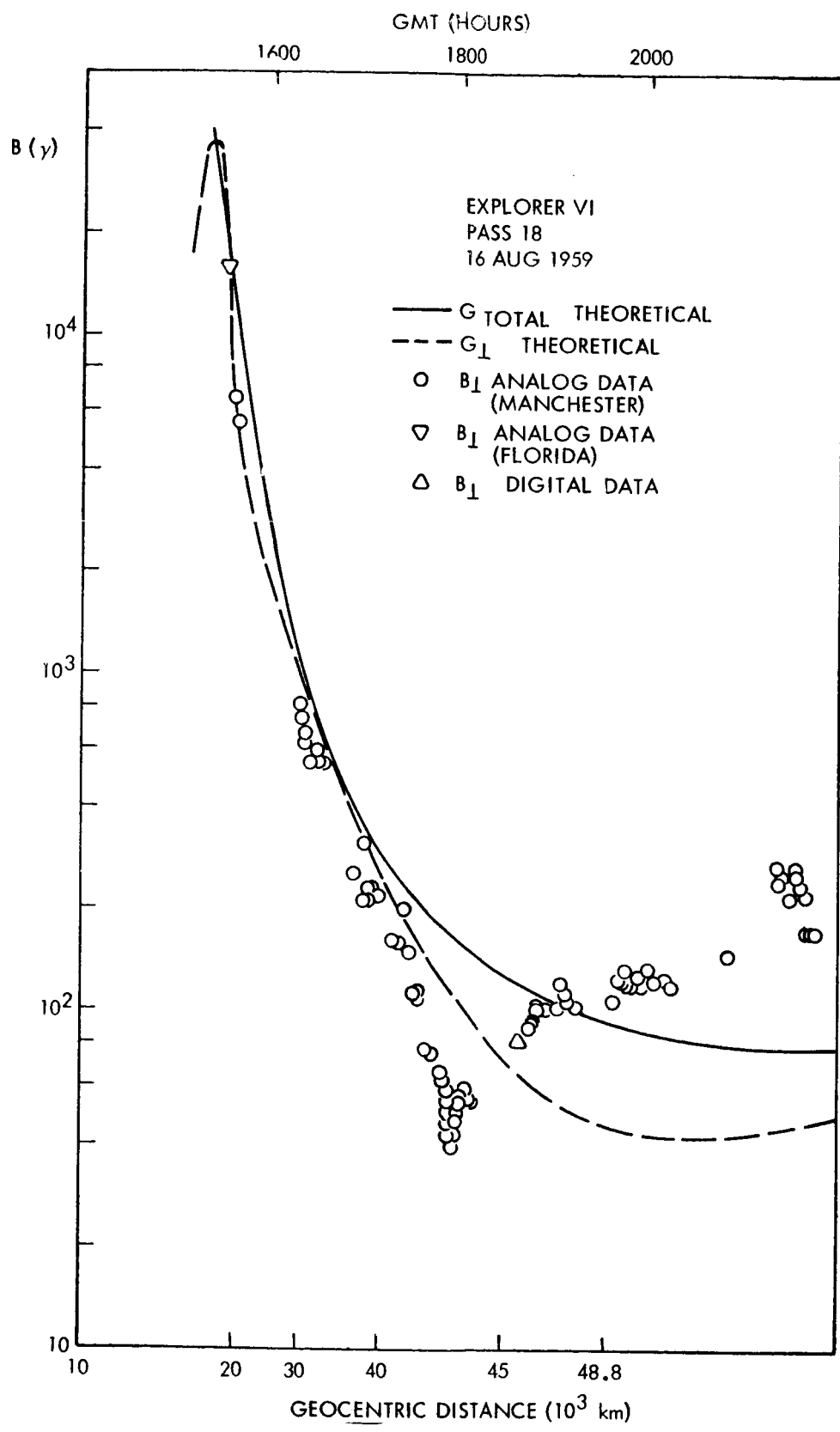


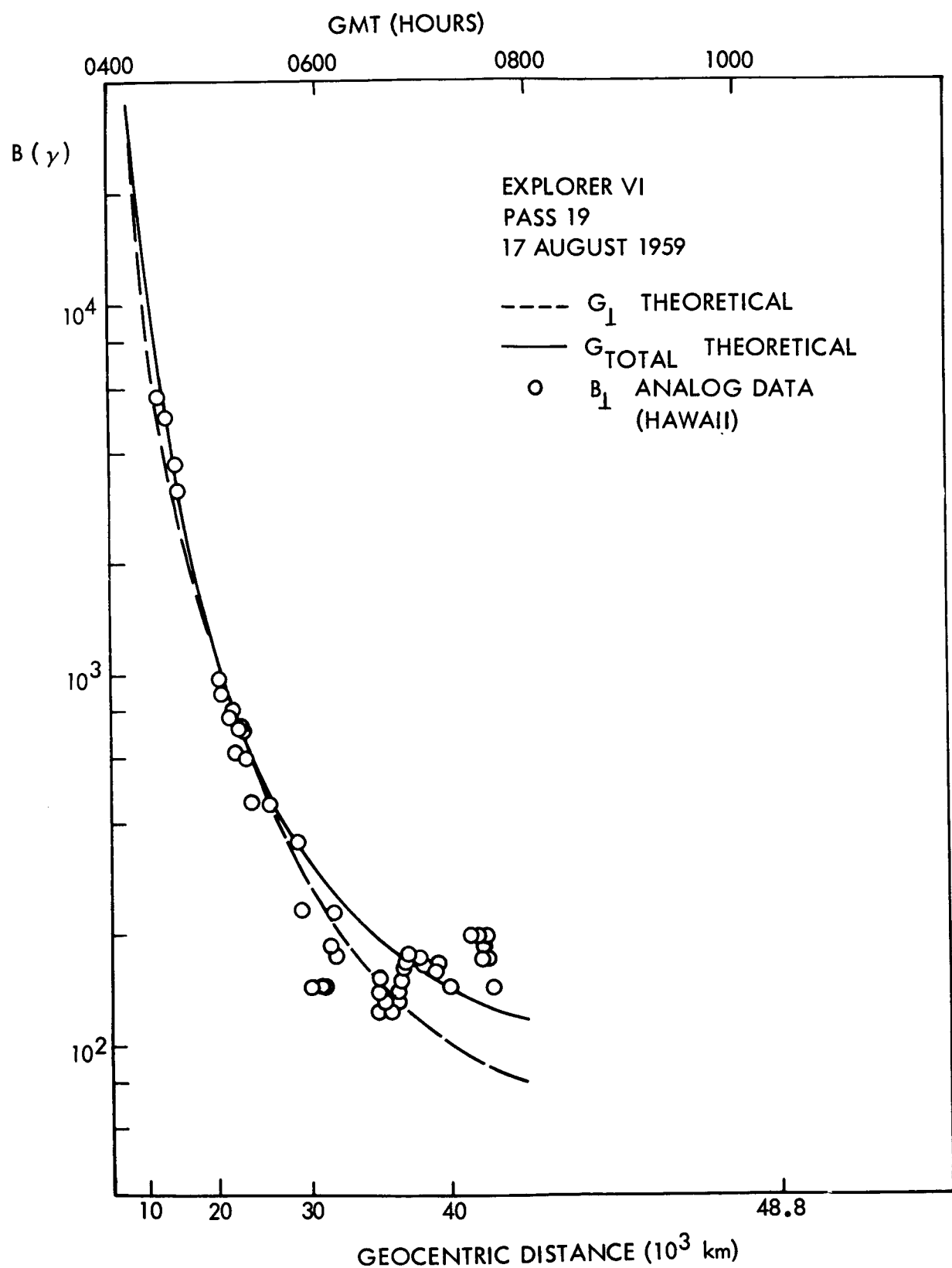


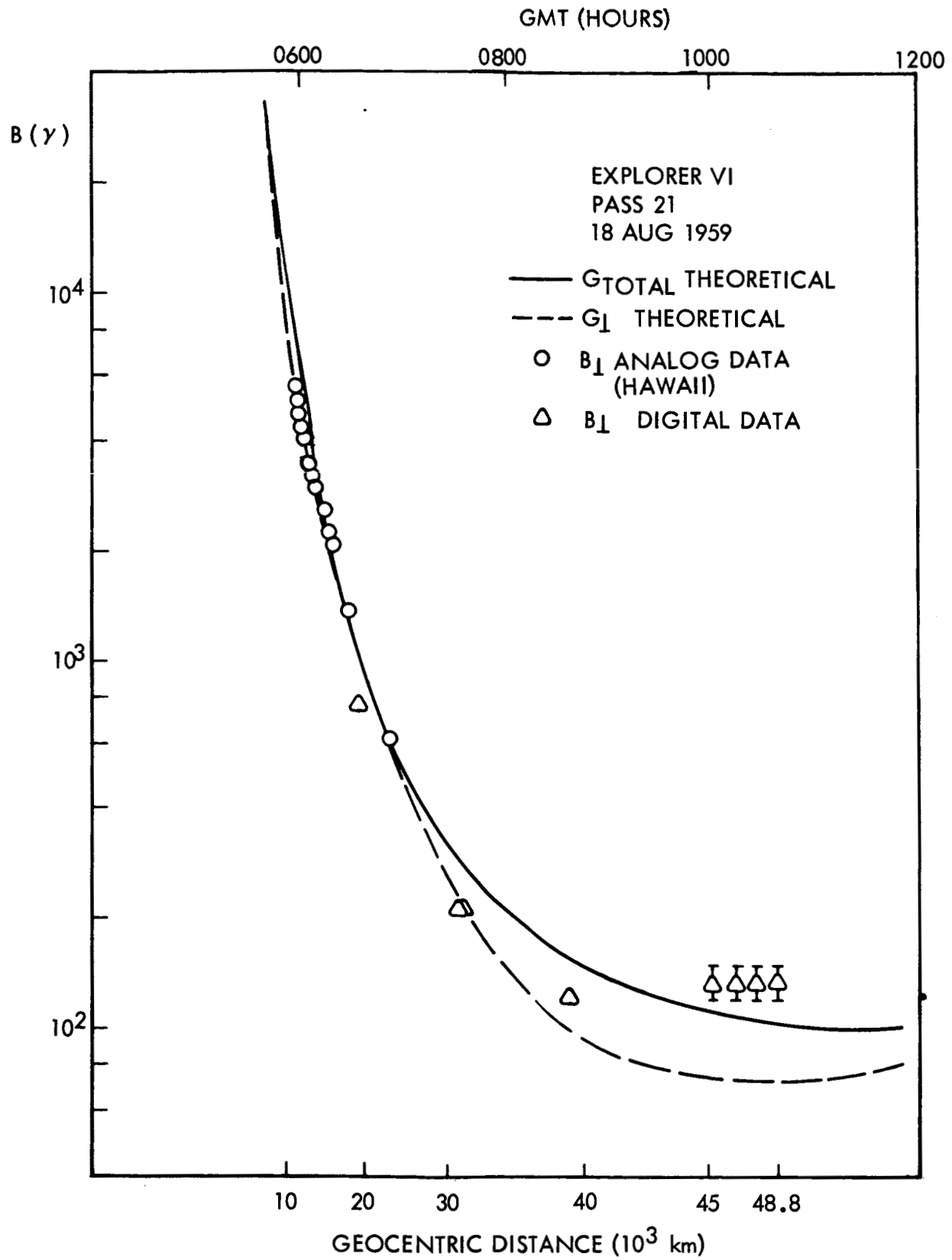


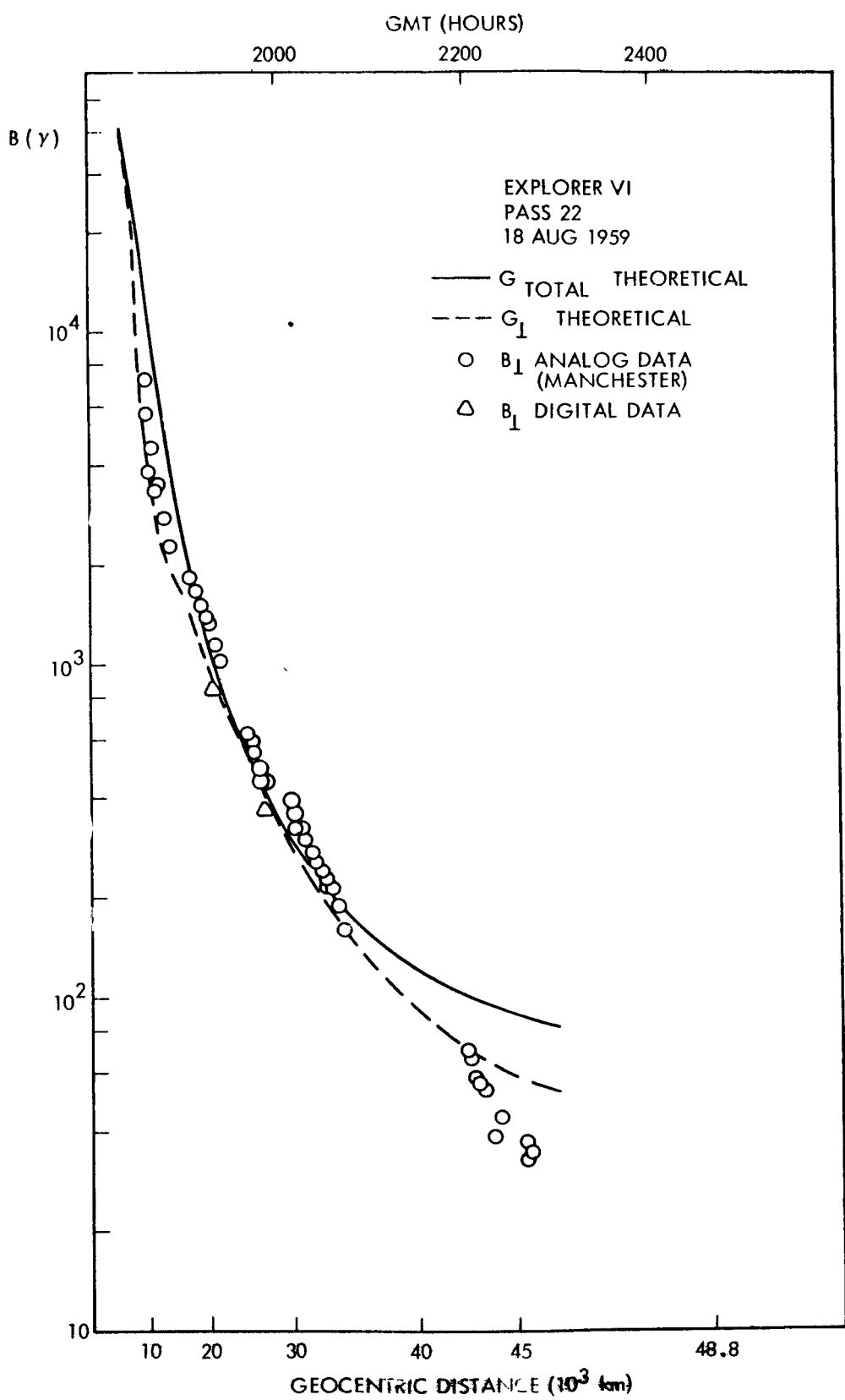


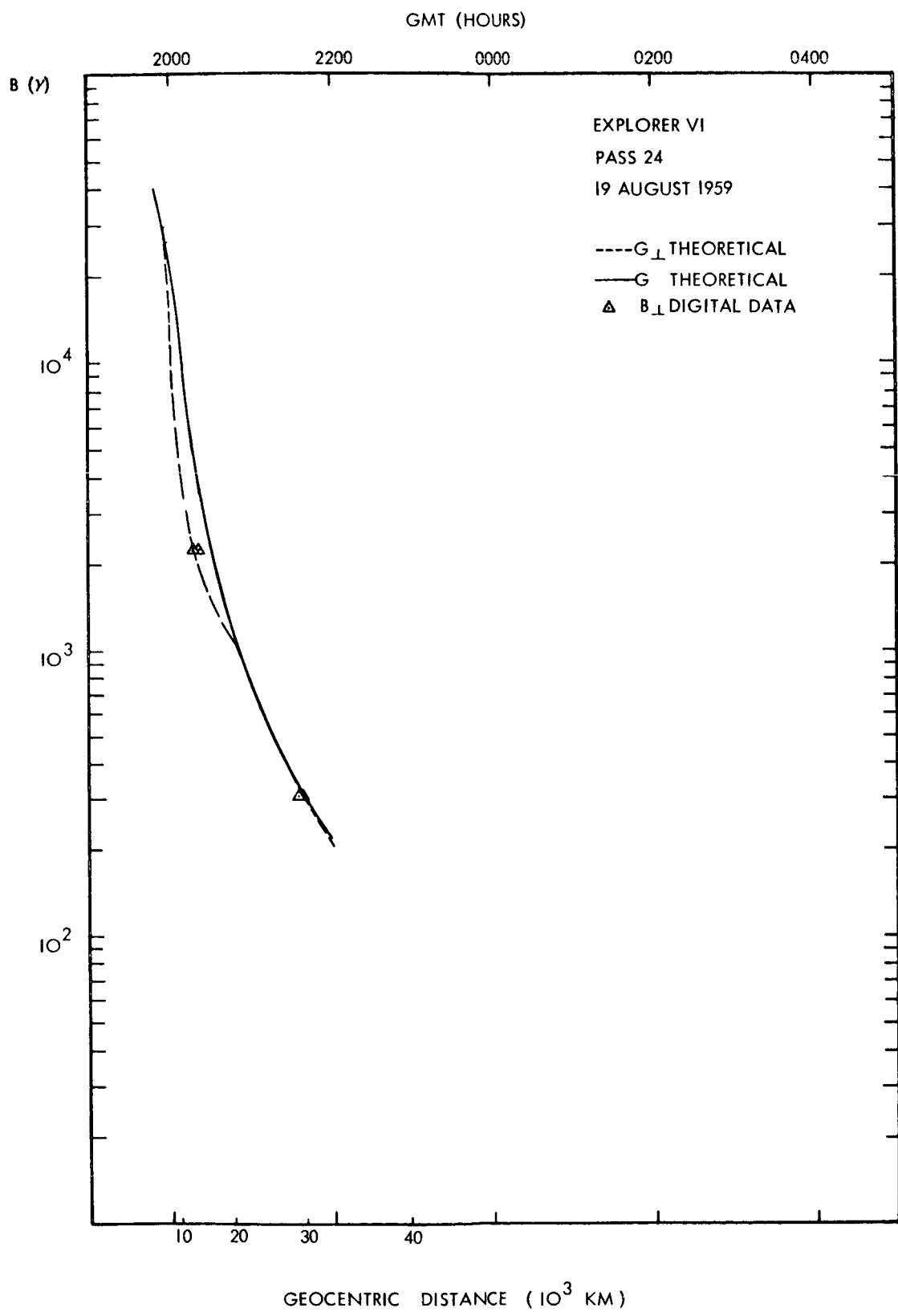


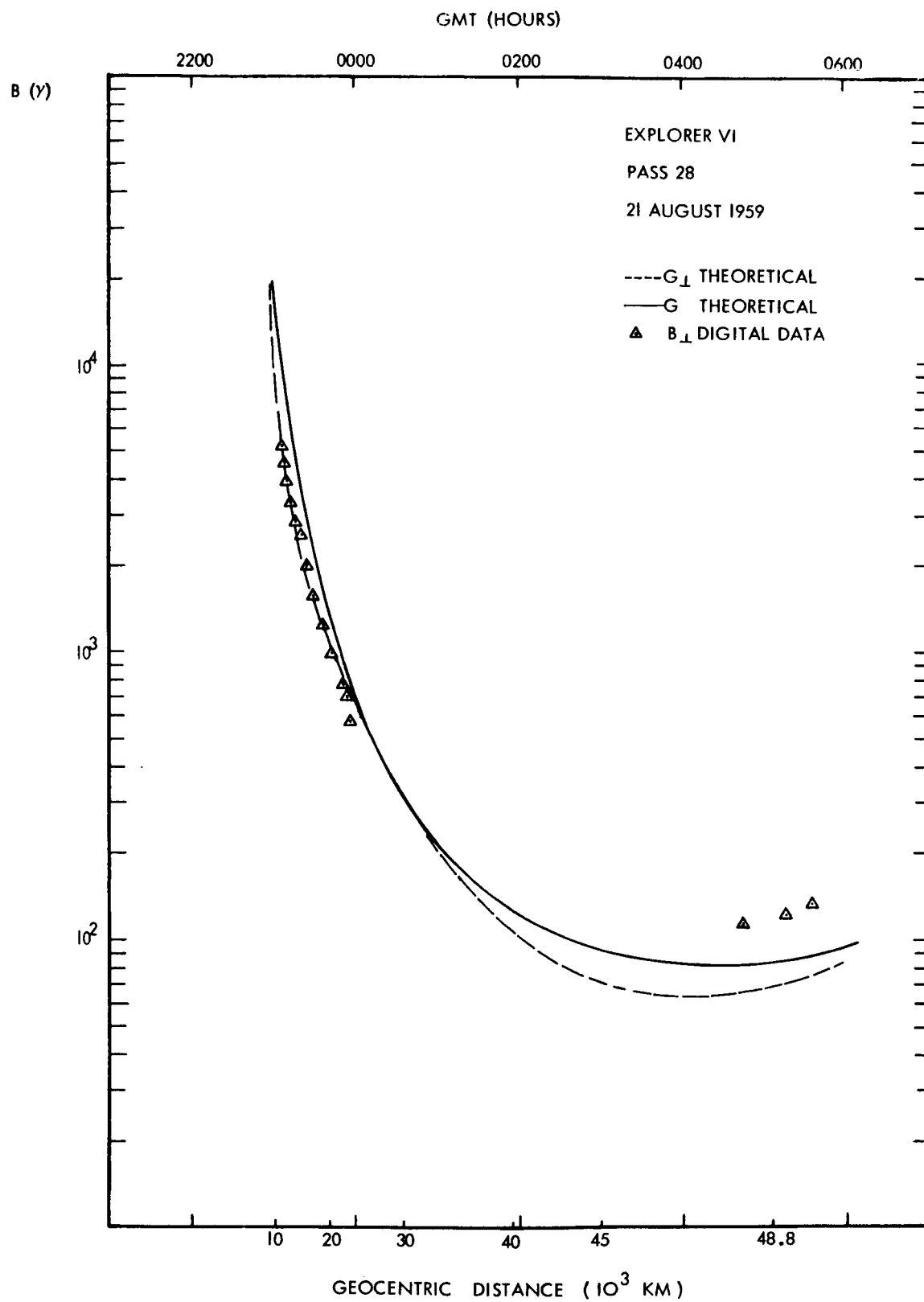


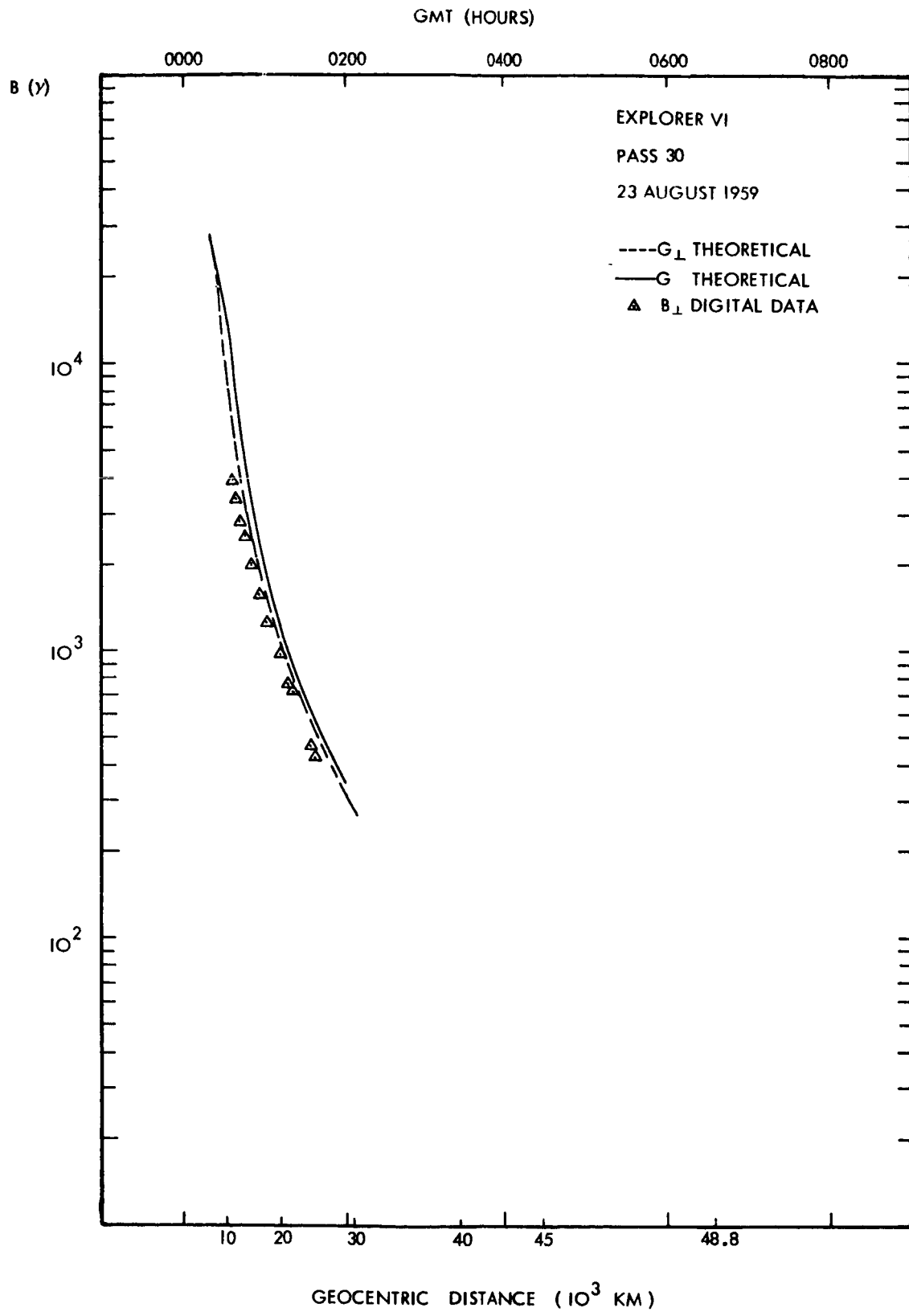


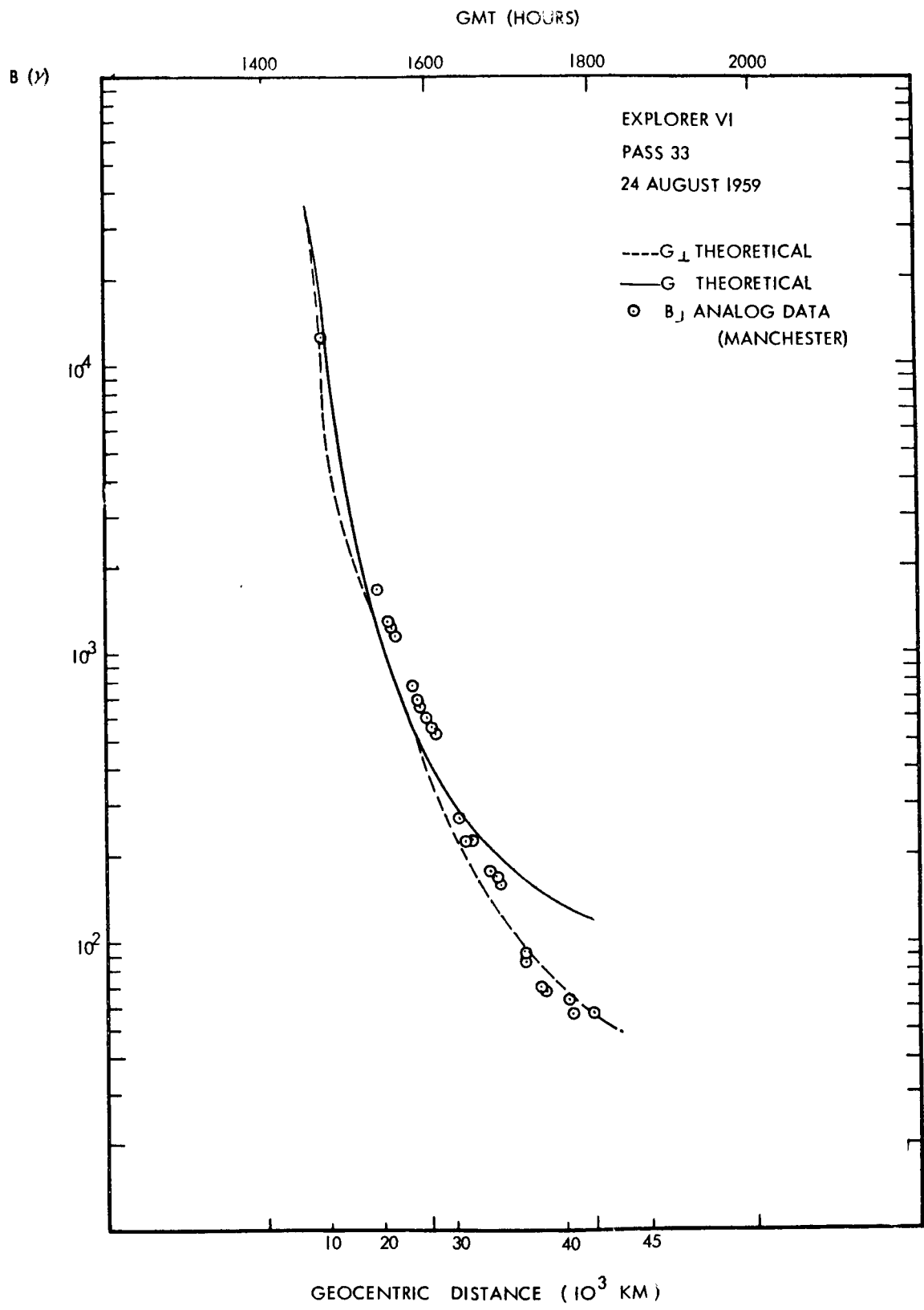


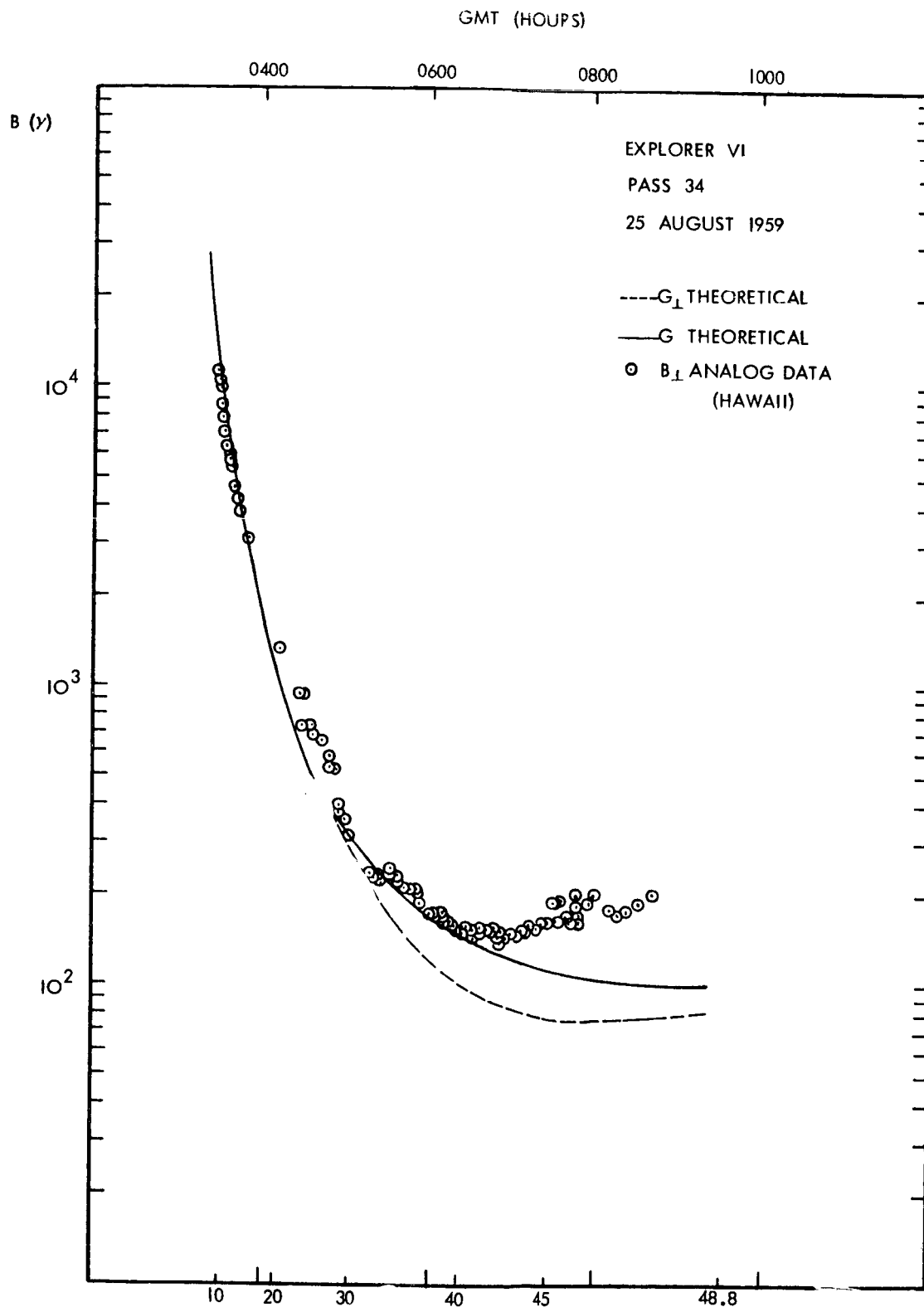




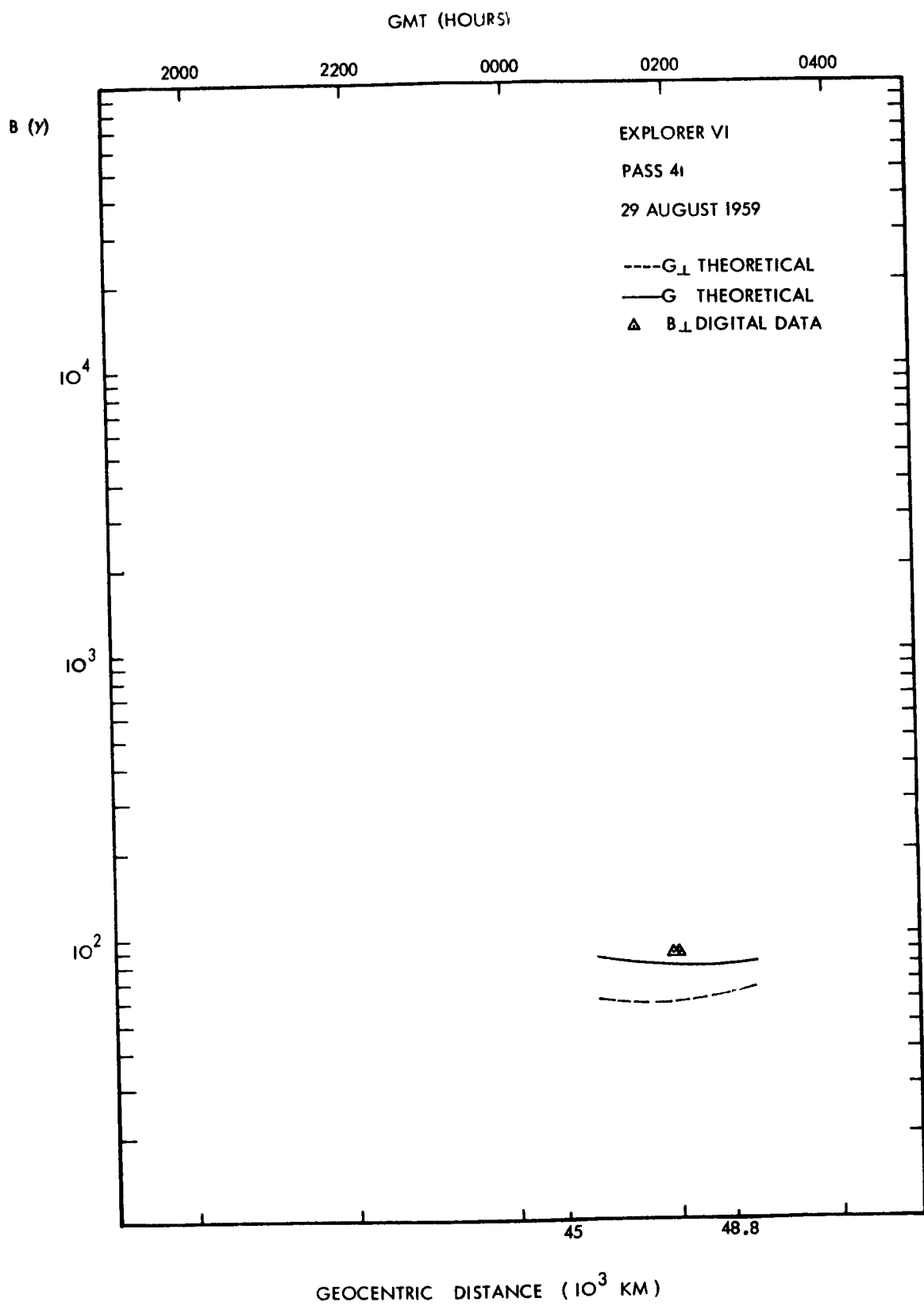


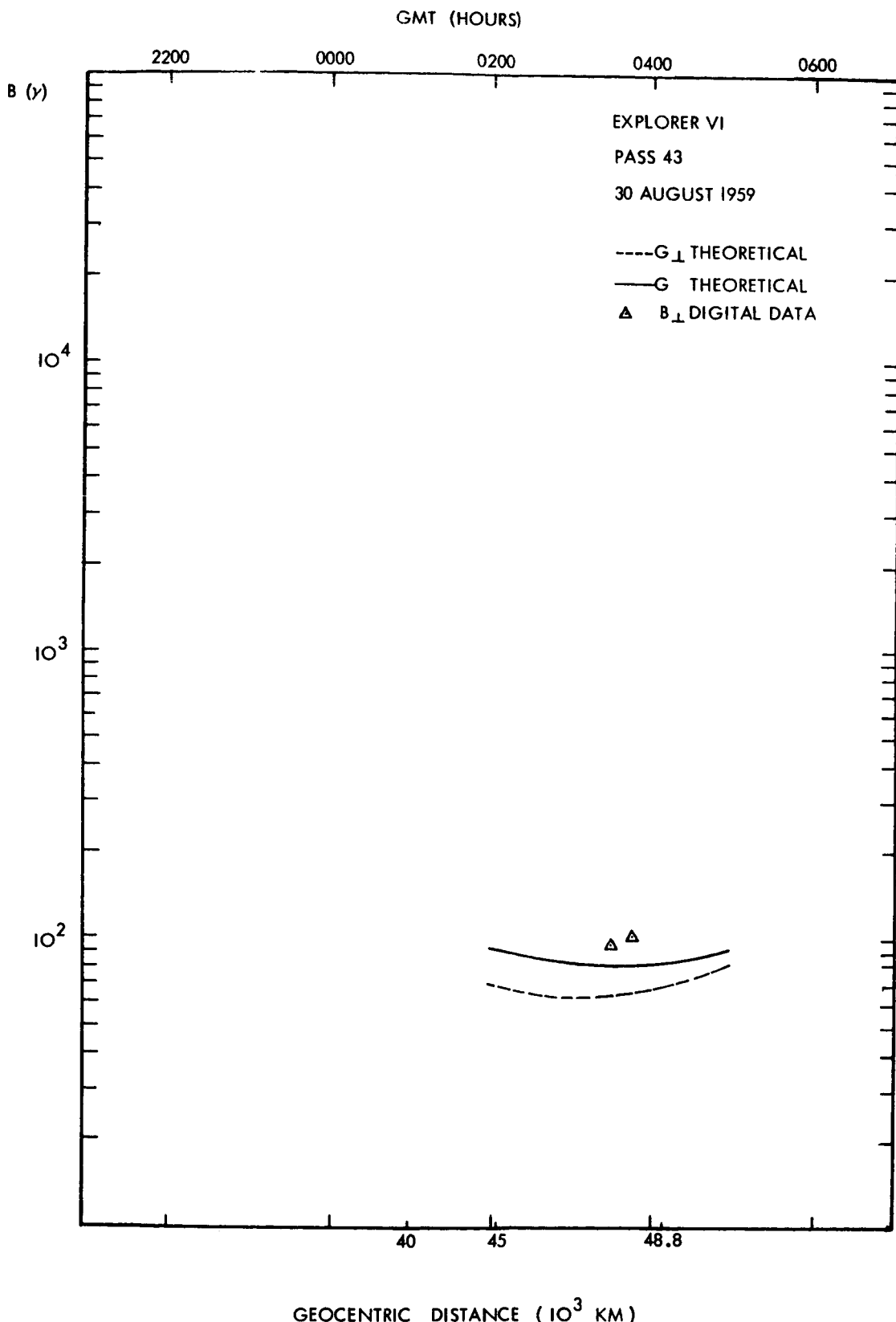


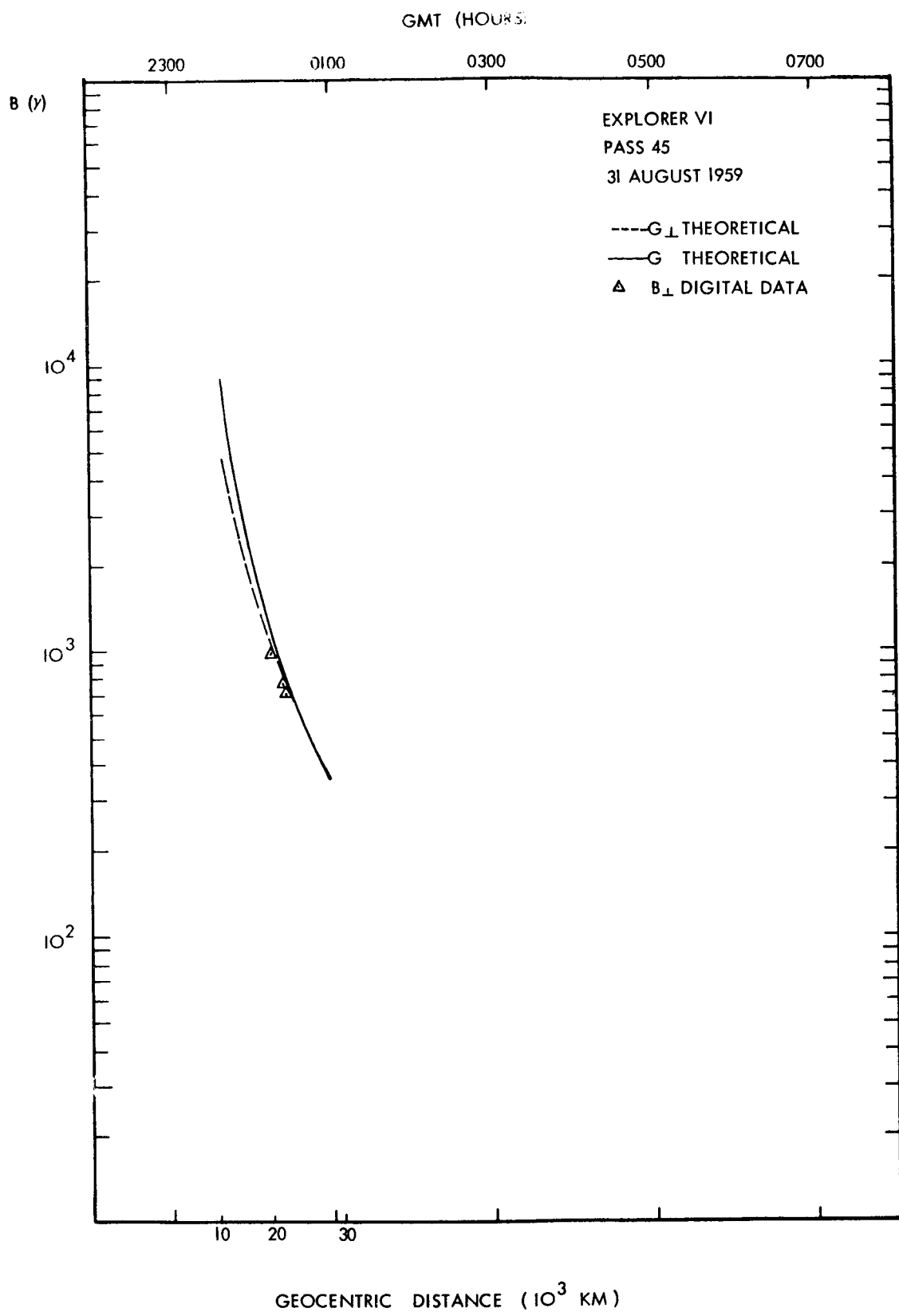


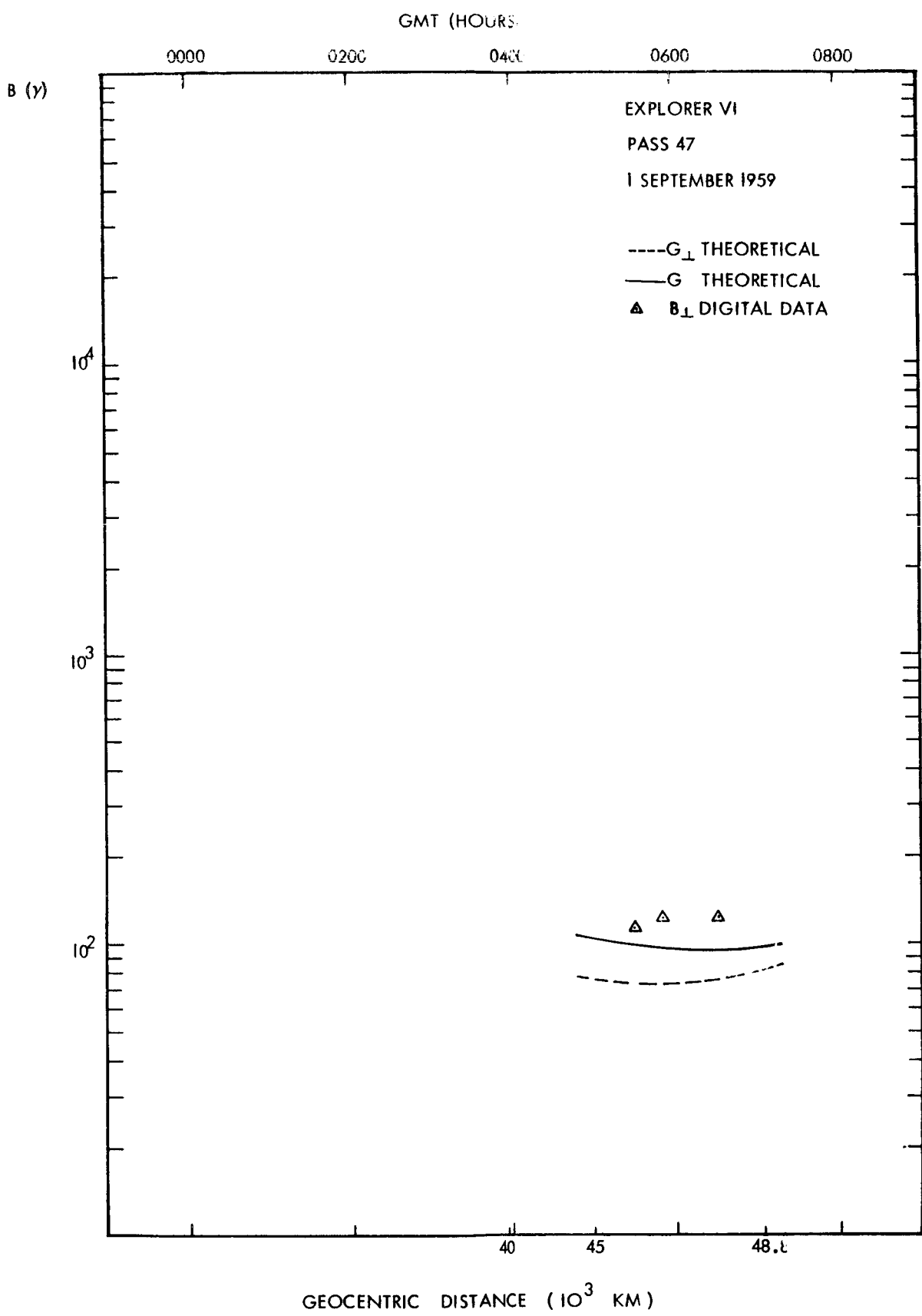


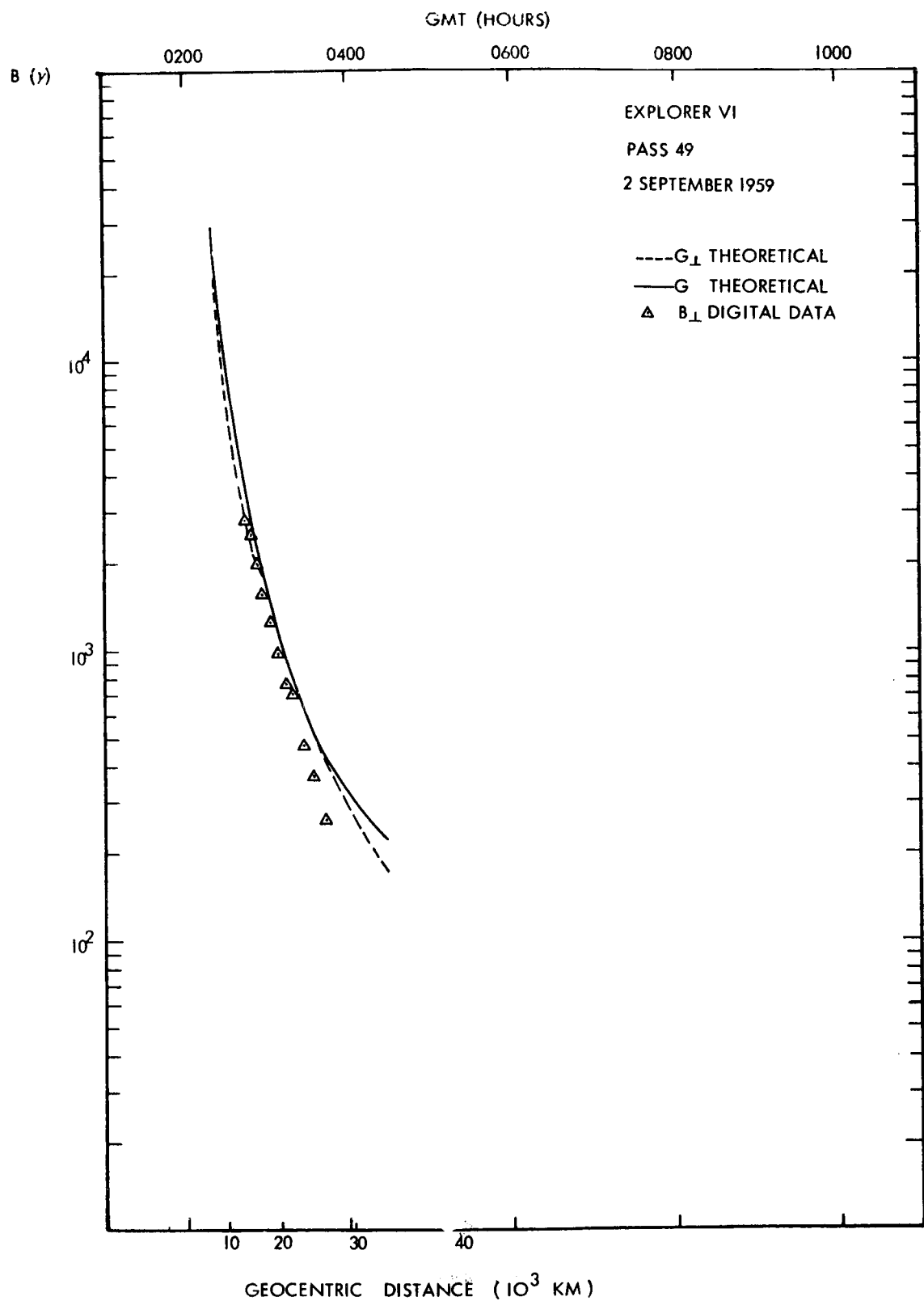
GEOCENTRIC DISTANCE (10^3 KM)

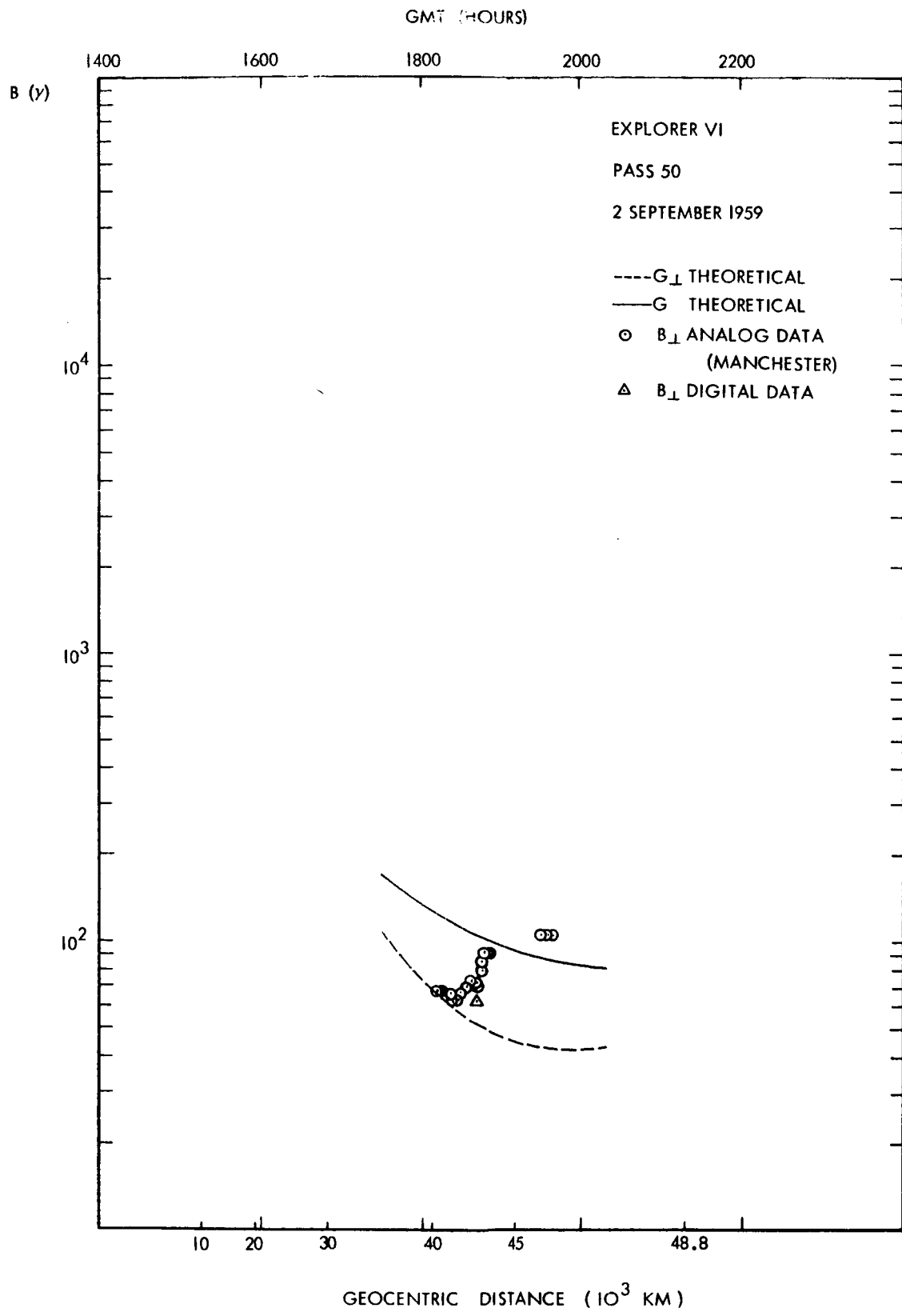


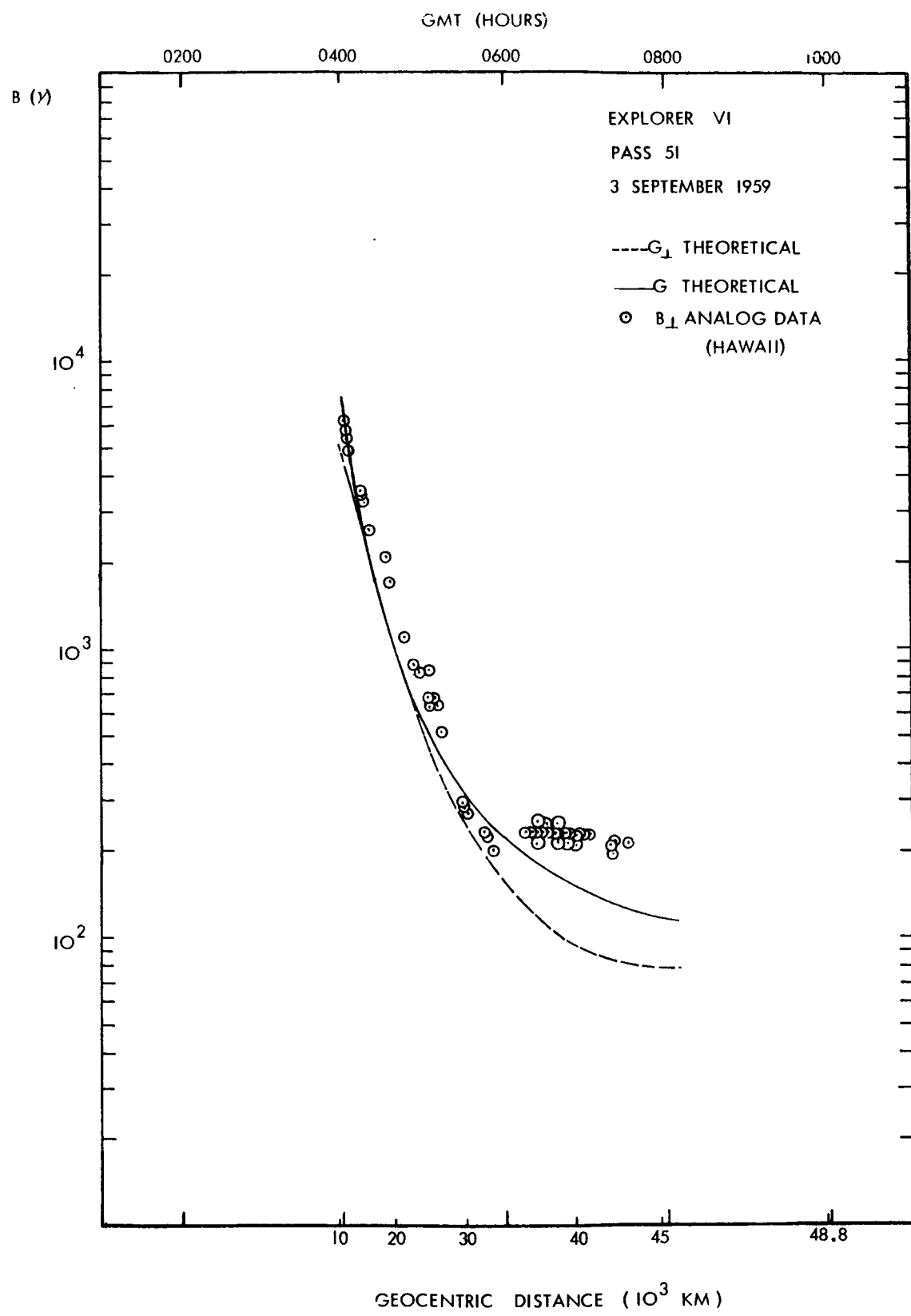


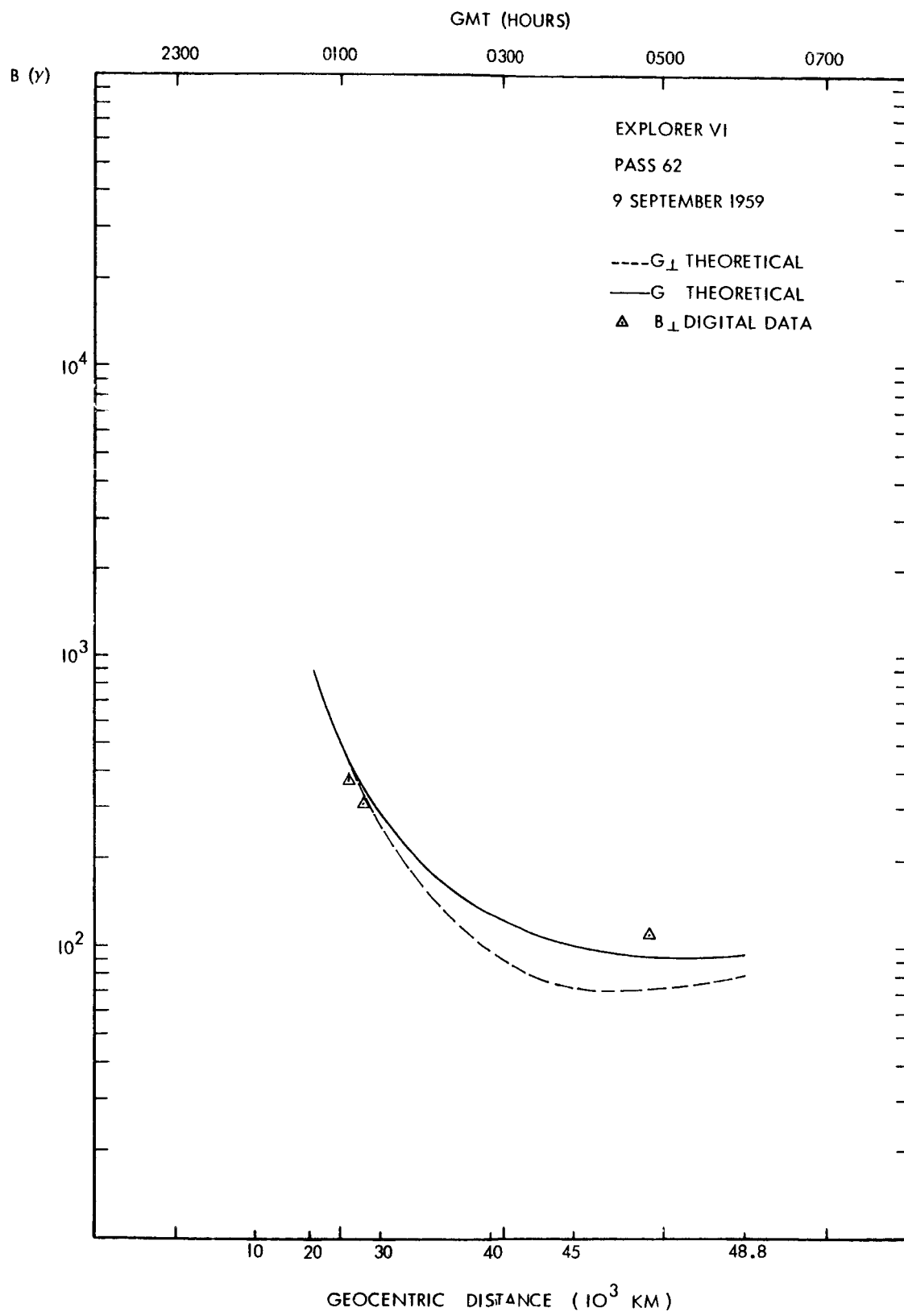


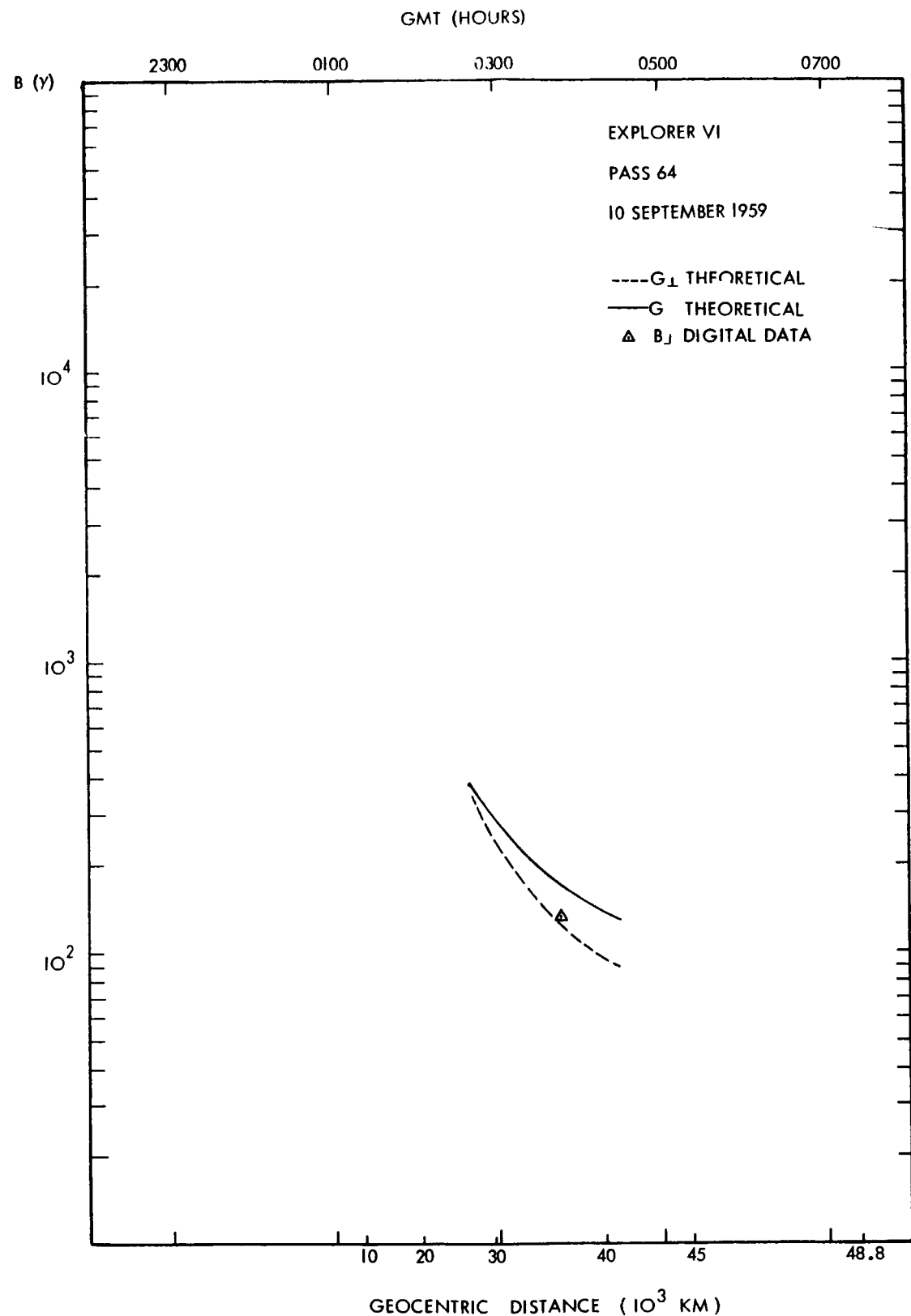






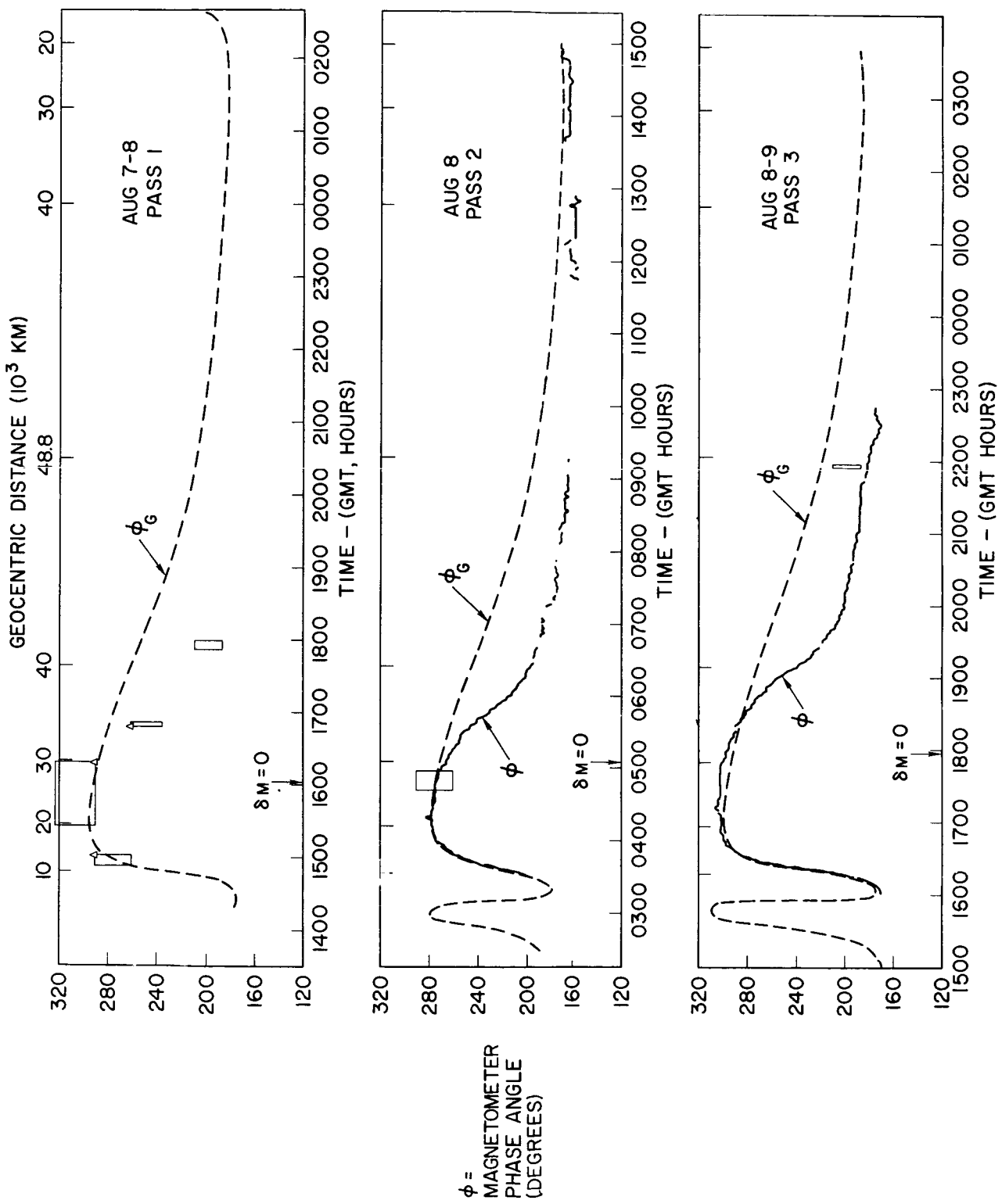


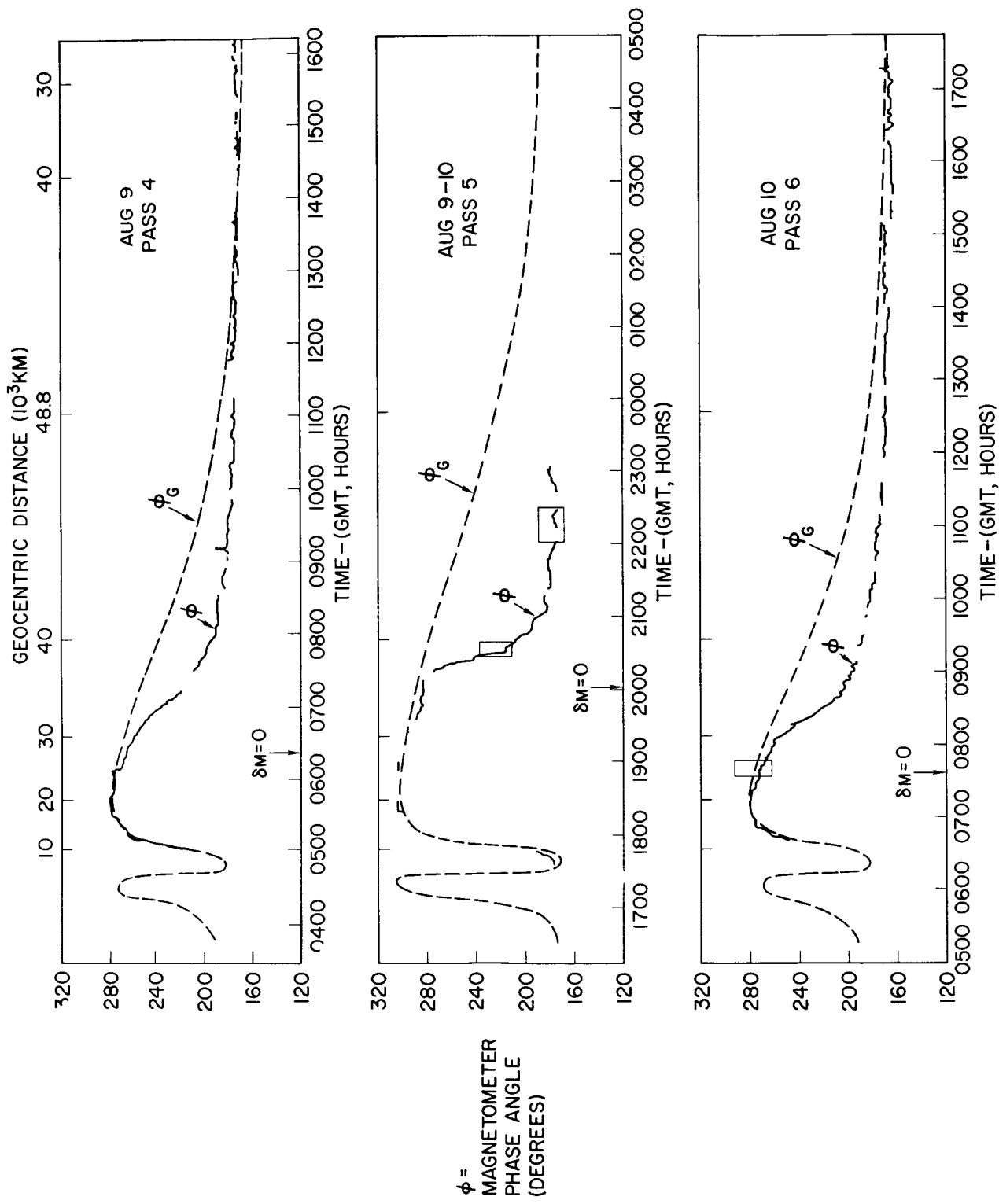


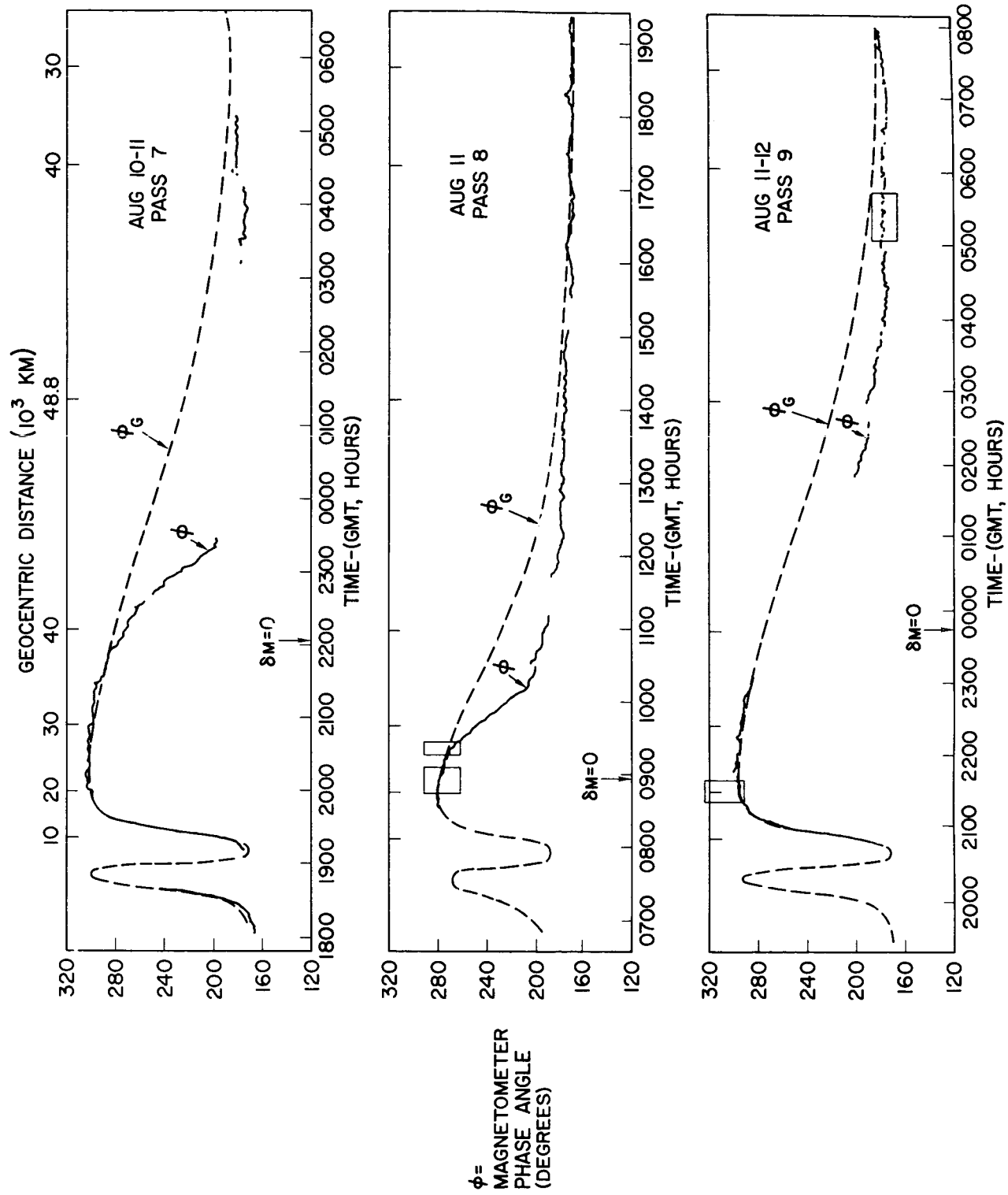


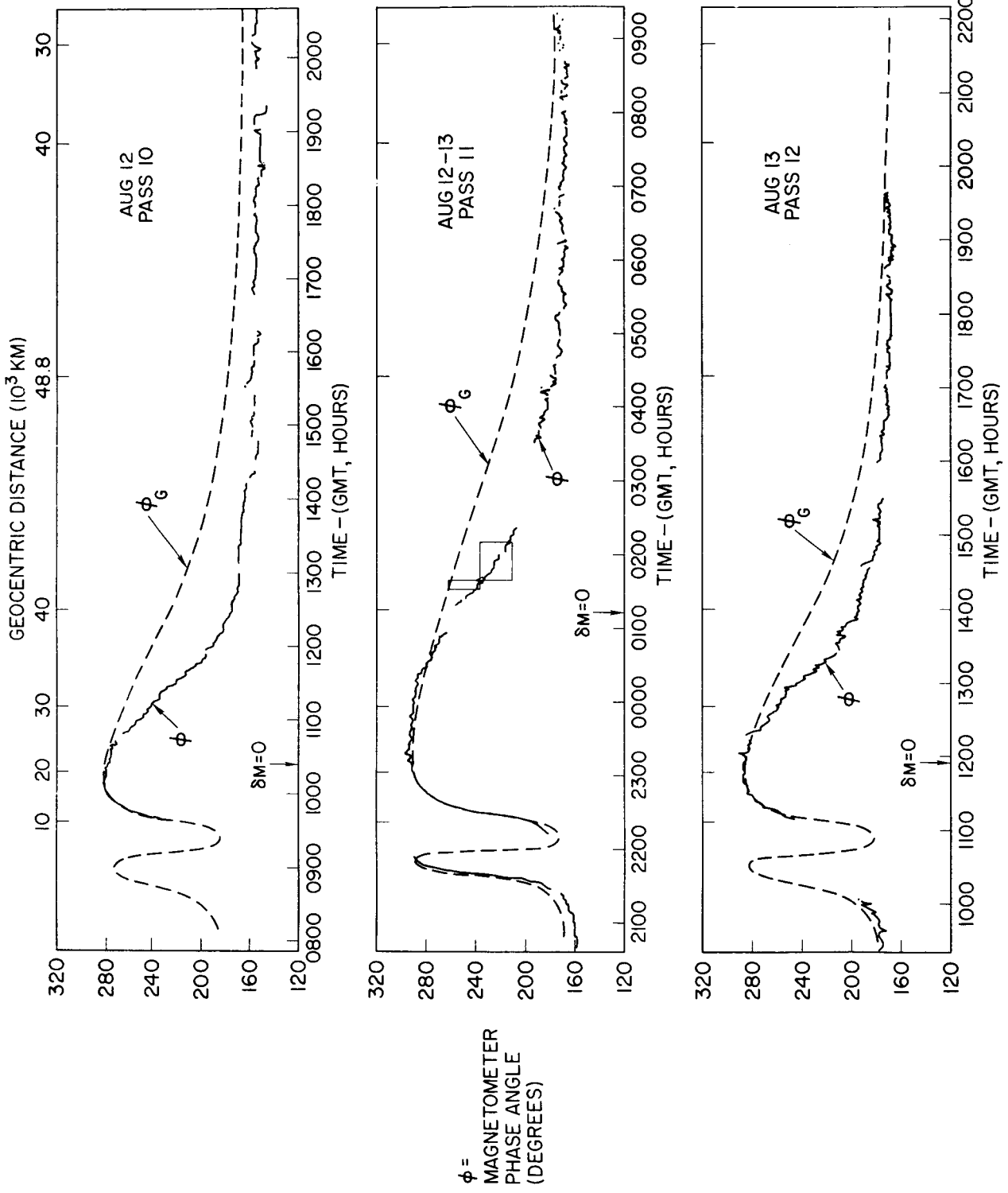
DATA COMPENDIUM:

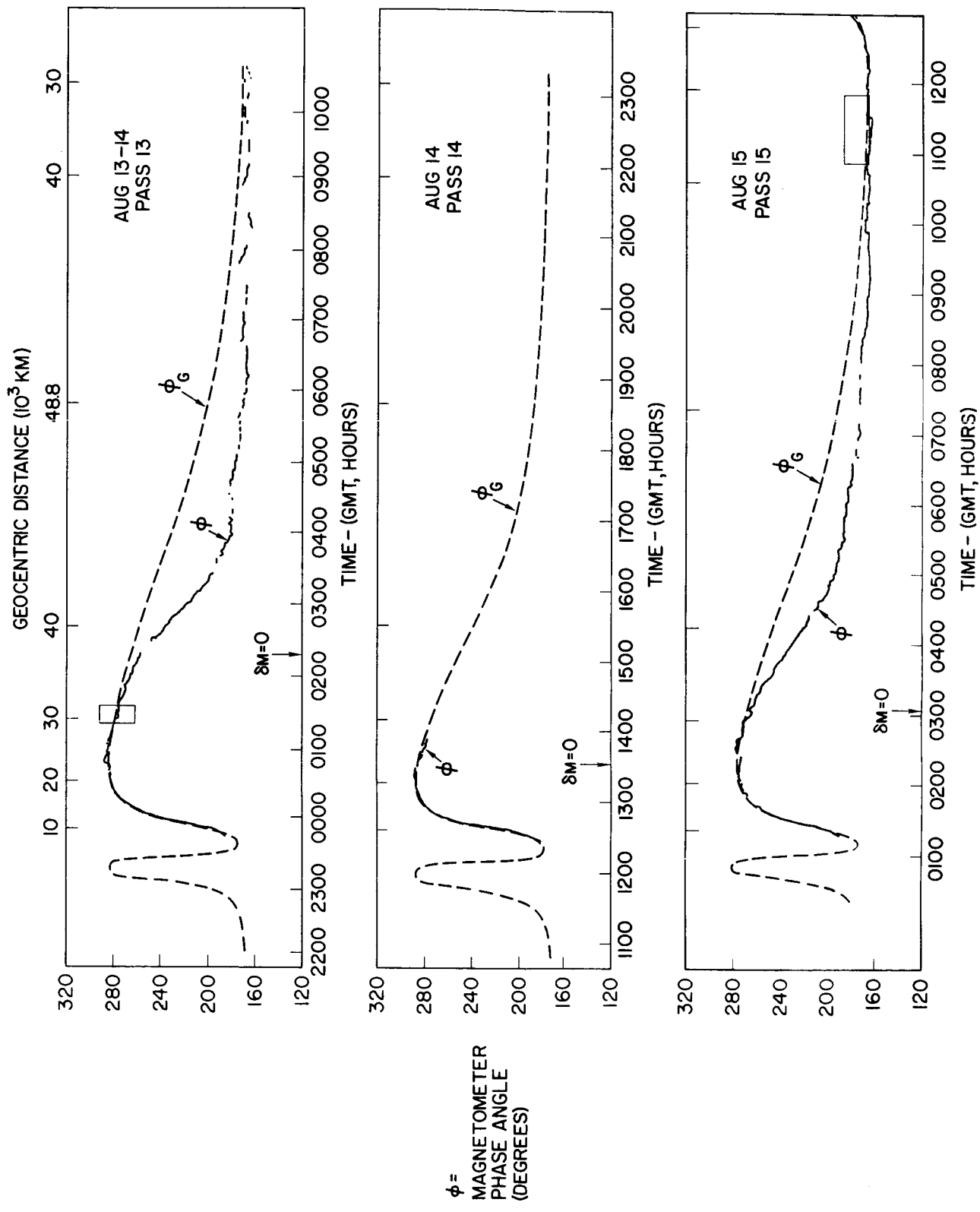
PHASE ANGLE

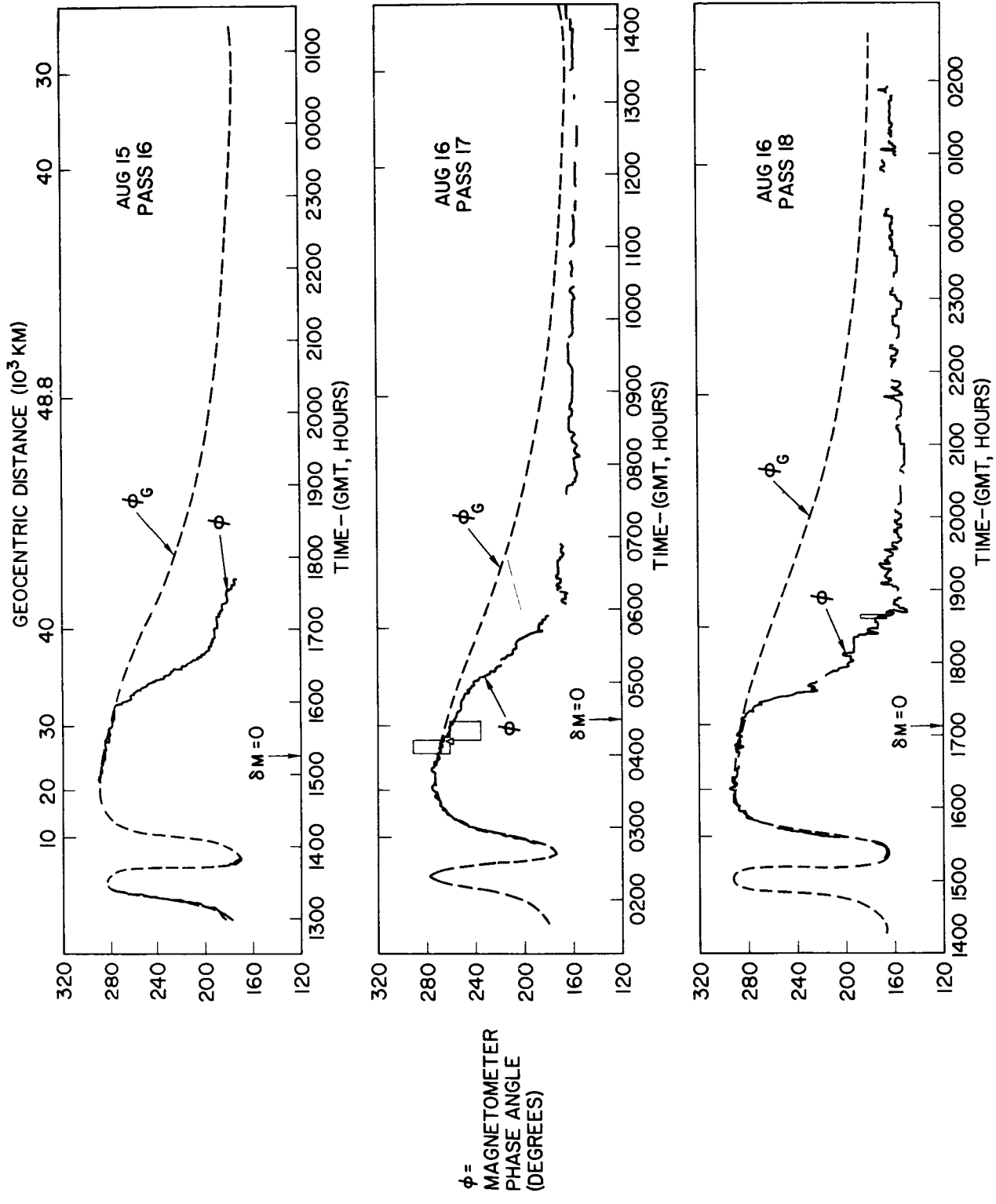


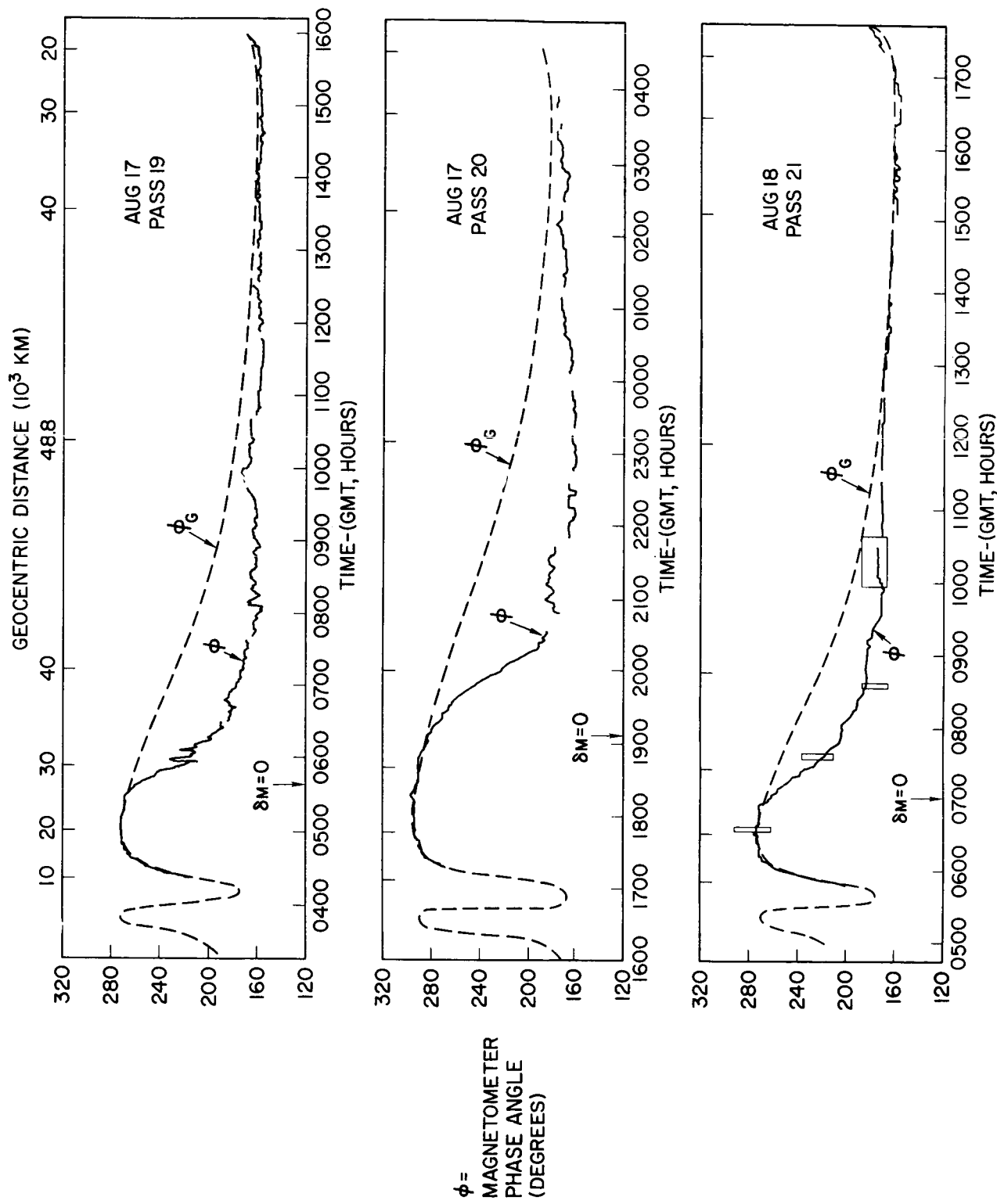


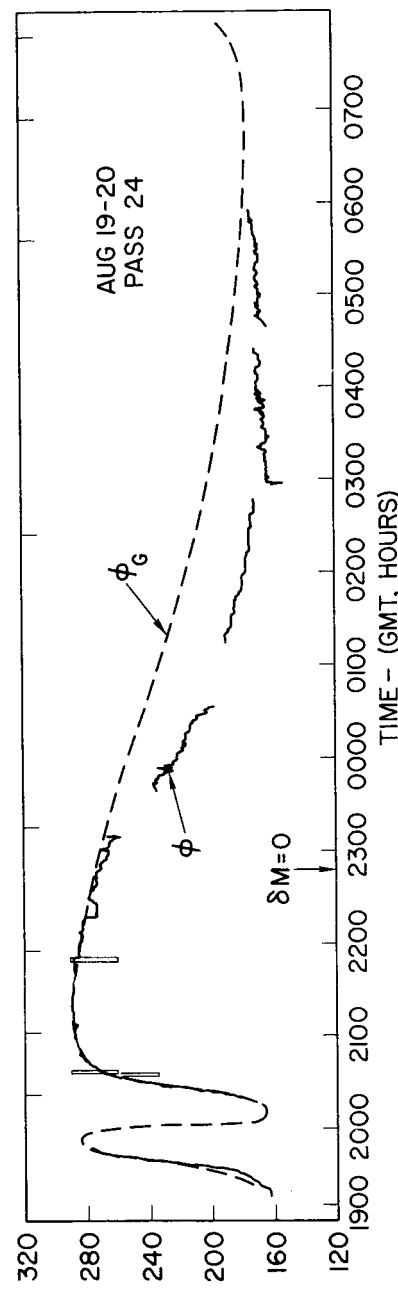
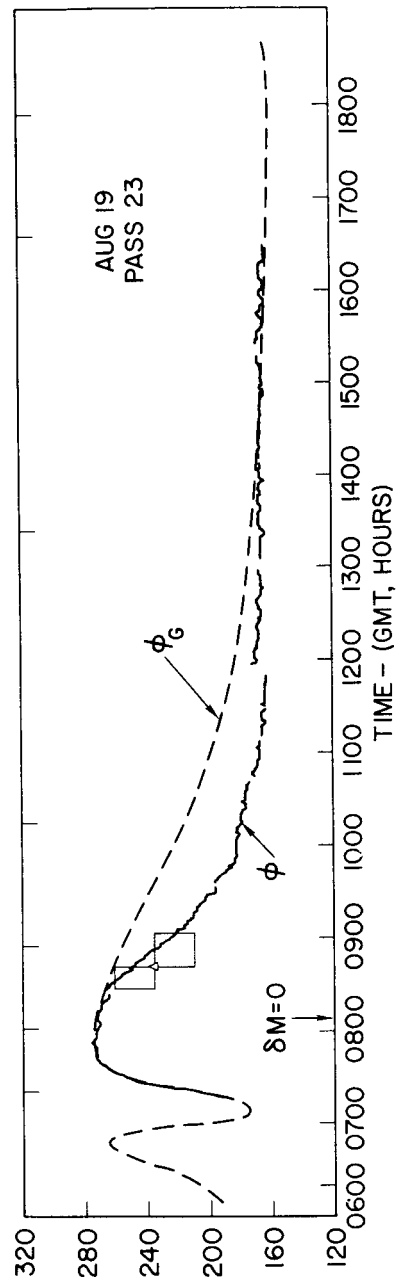
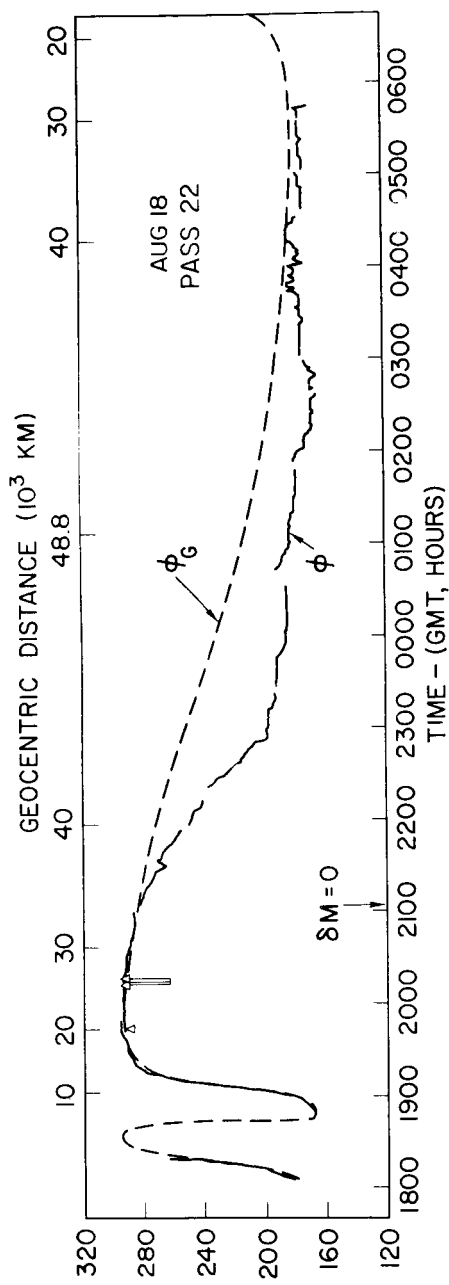




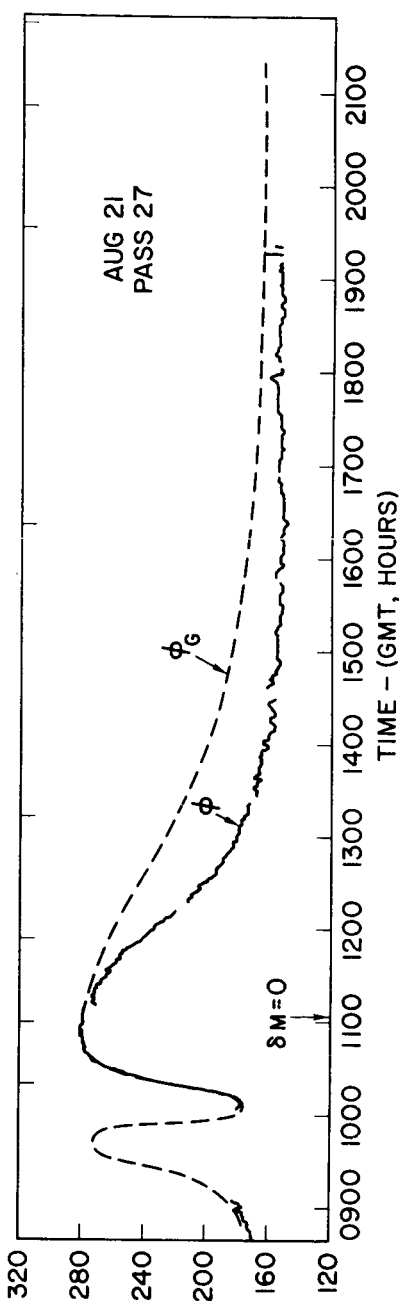
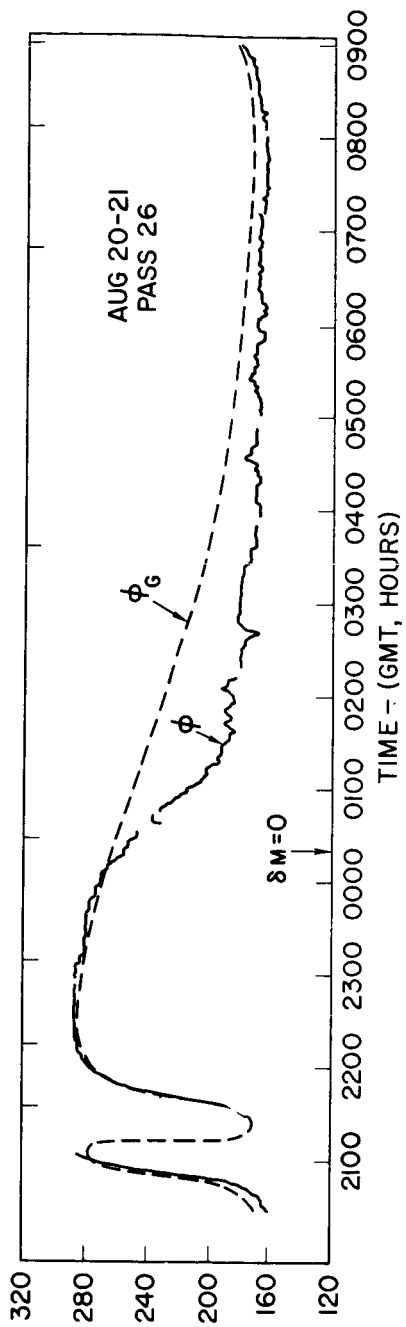
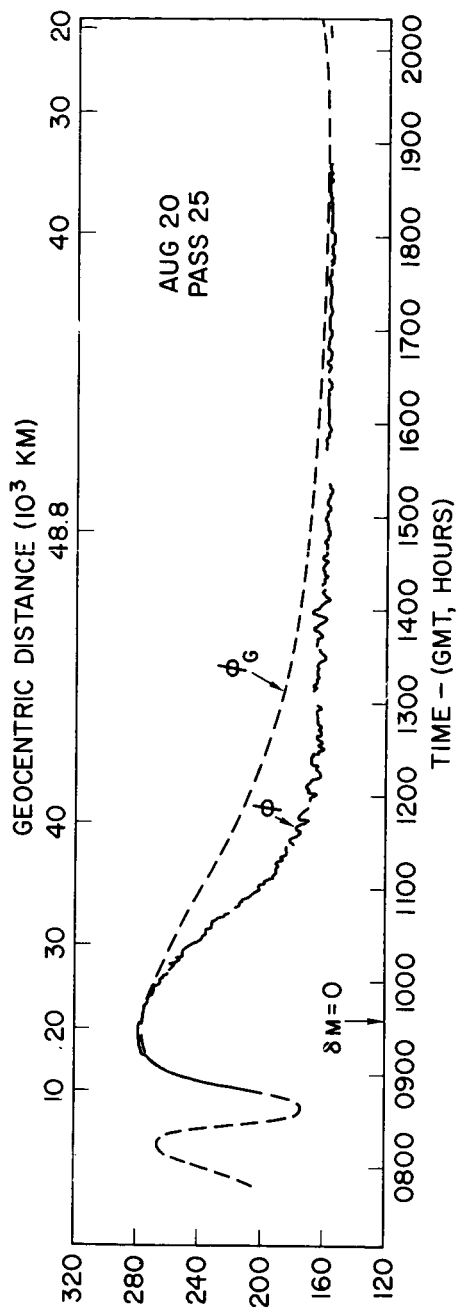




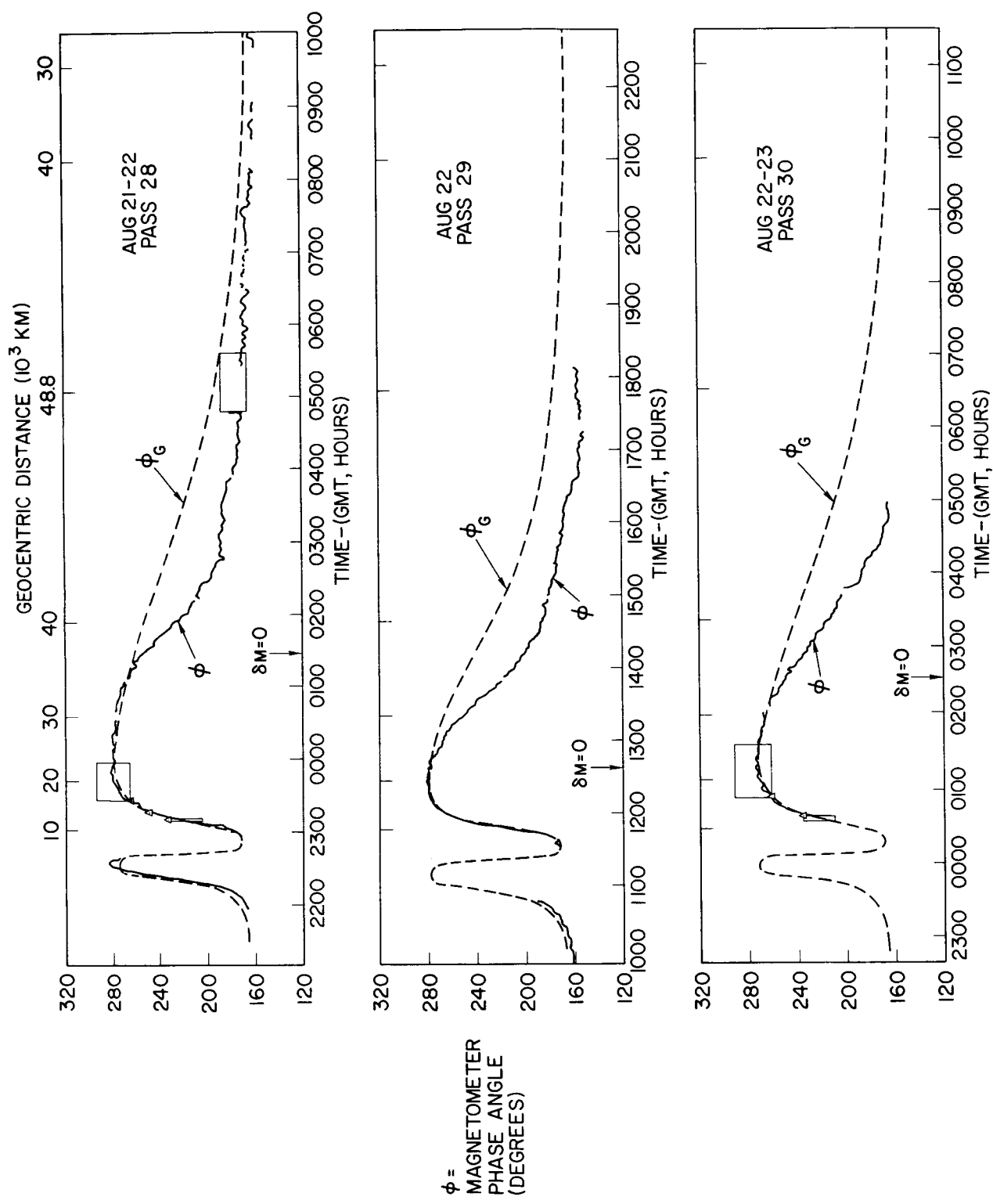


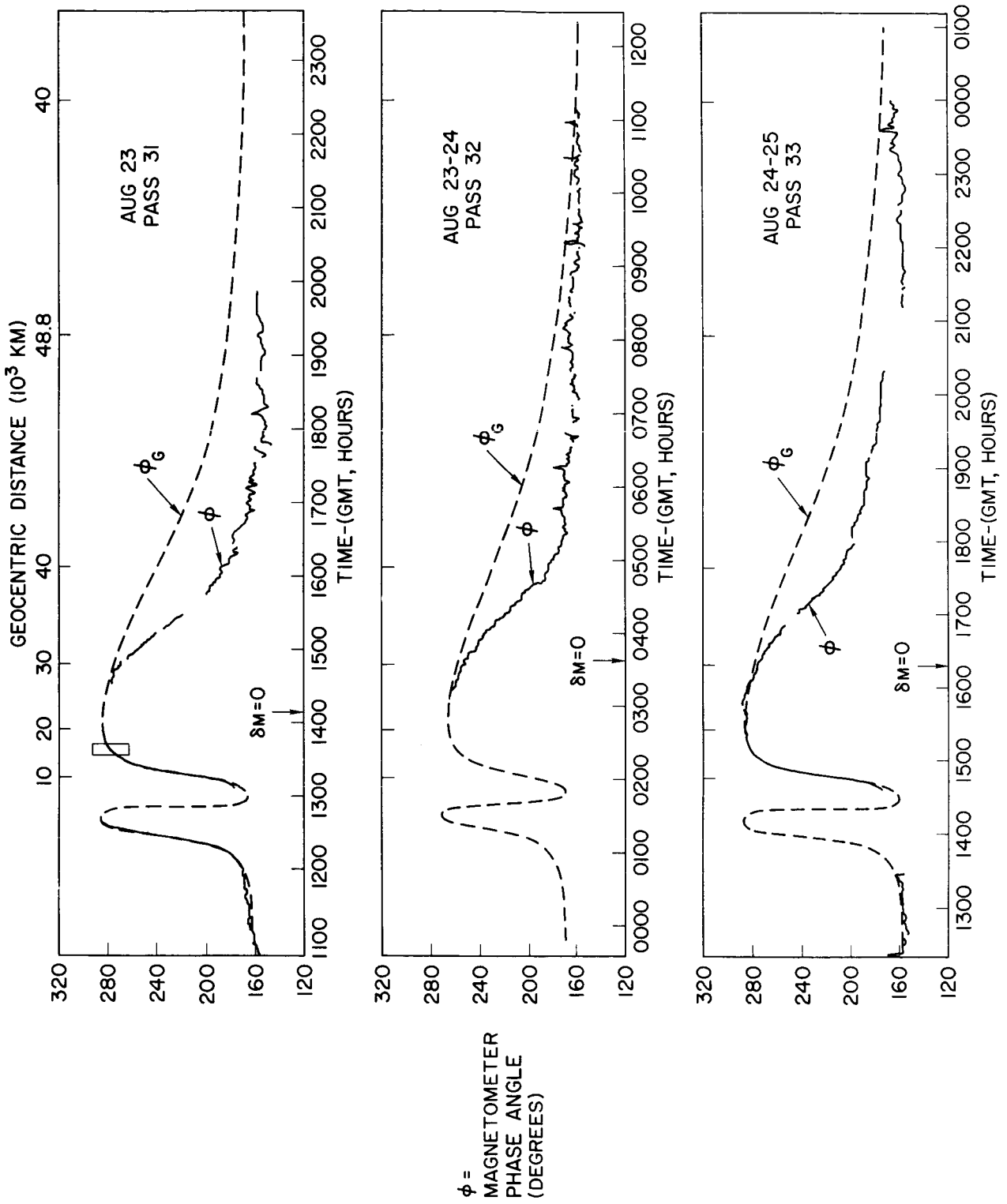


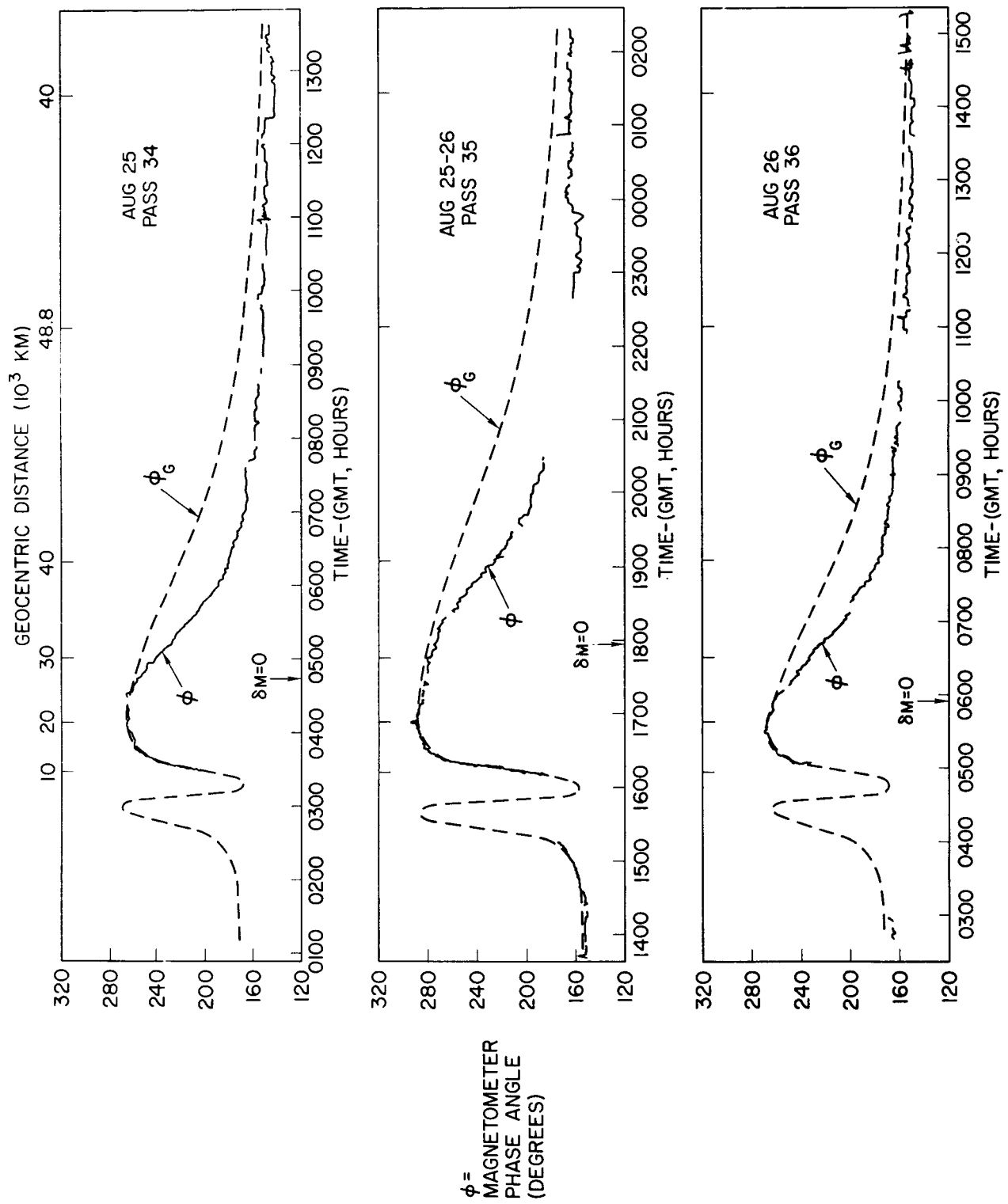
ϕ =
MAGNETOMETER
PHASE ANGLE
(DEGREES)

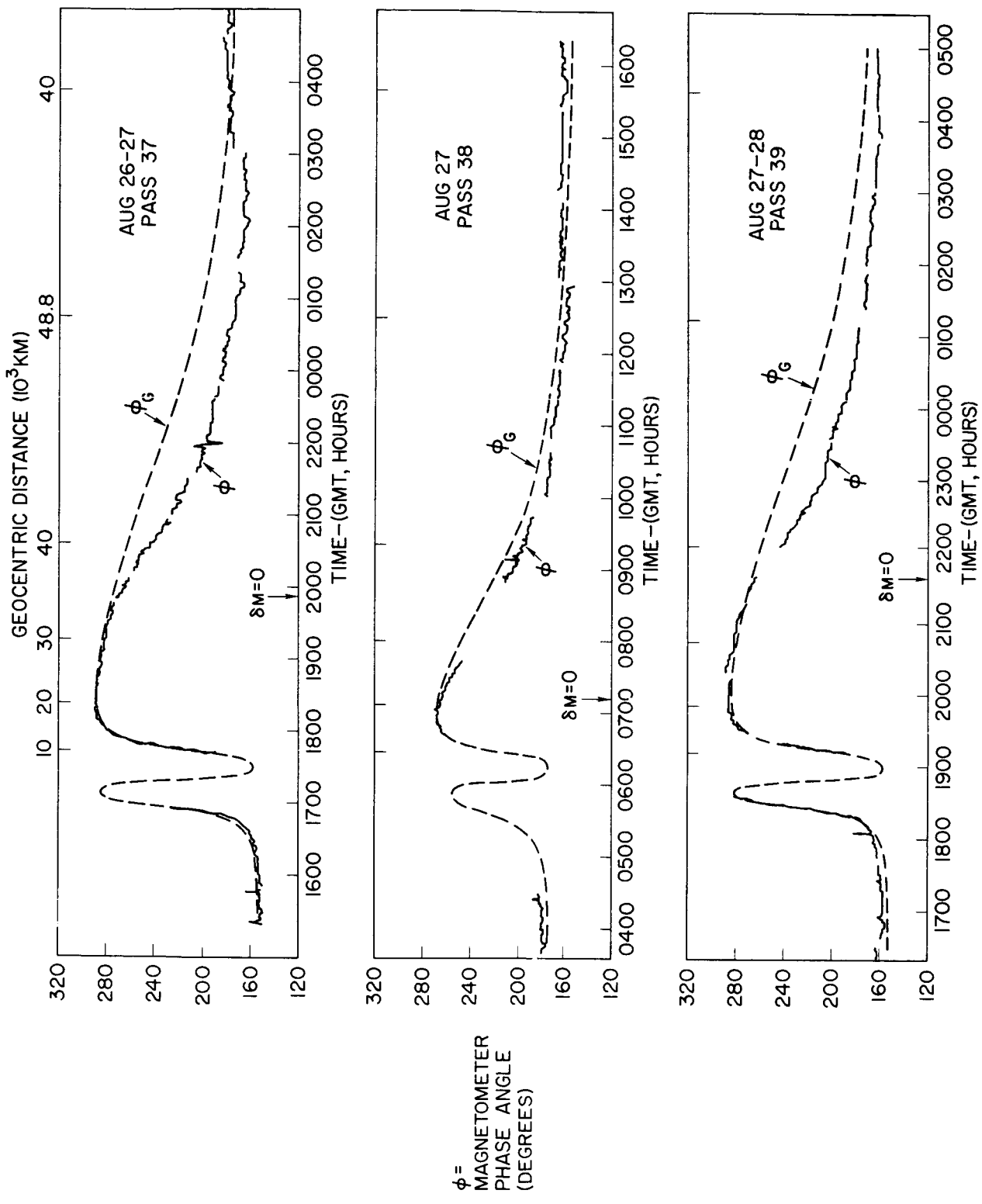


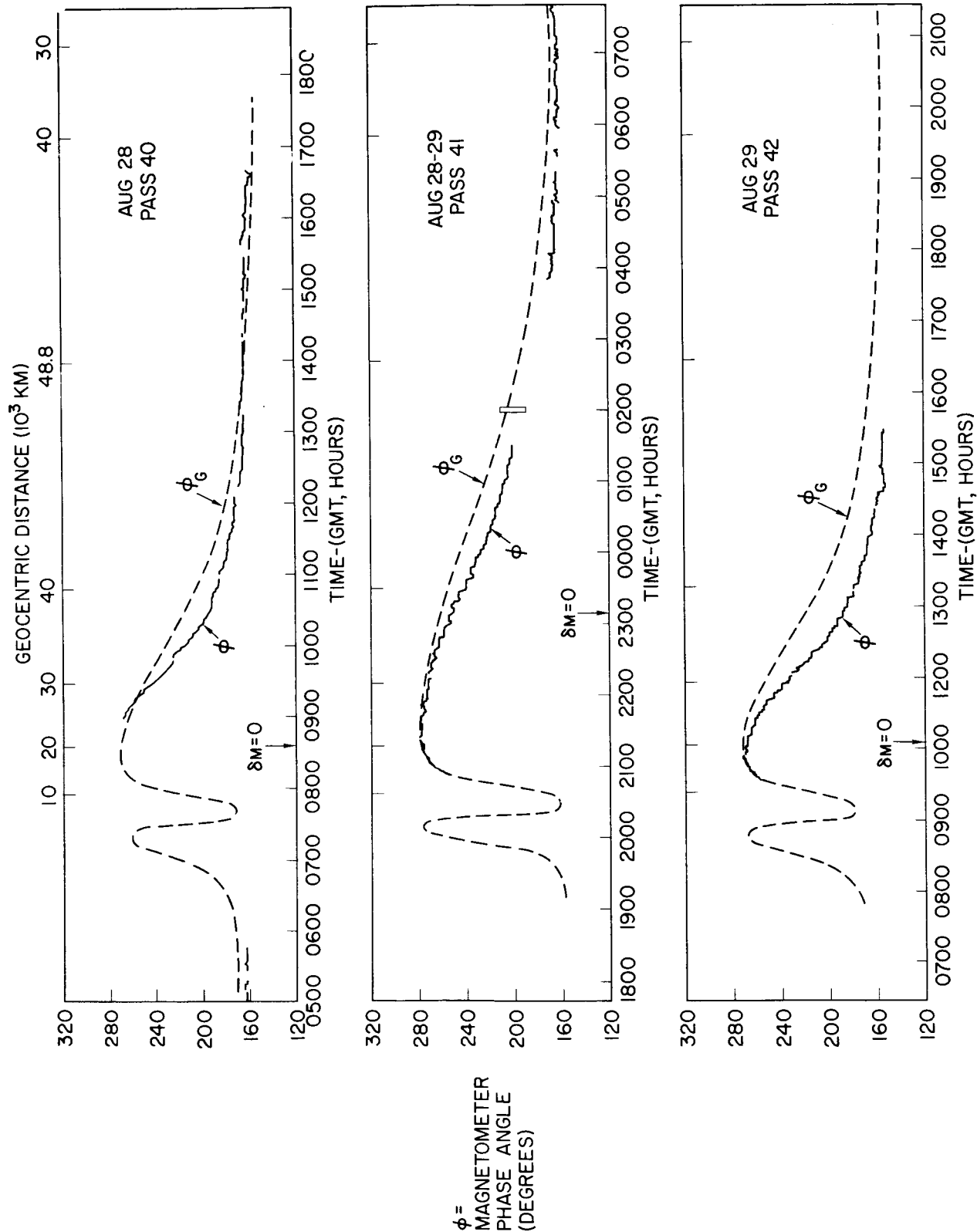
ϕ =
MAGNETOMETER
PHASE ANGLE
(DEGREES)

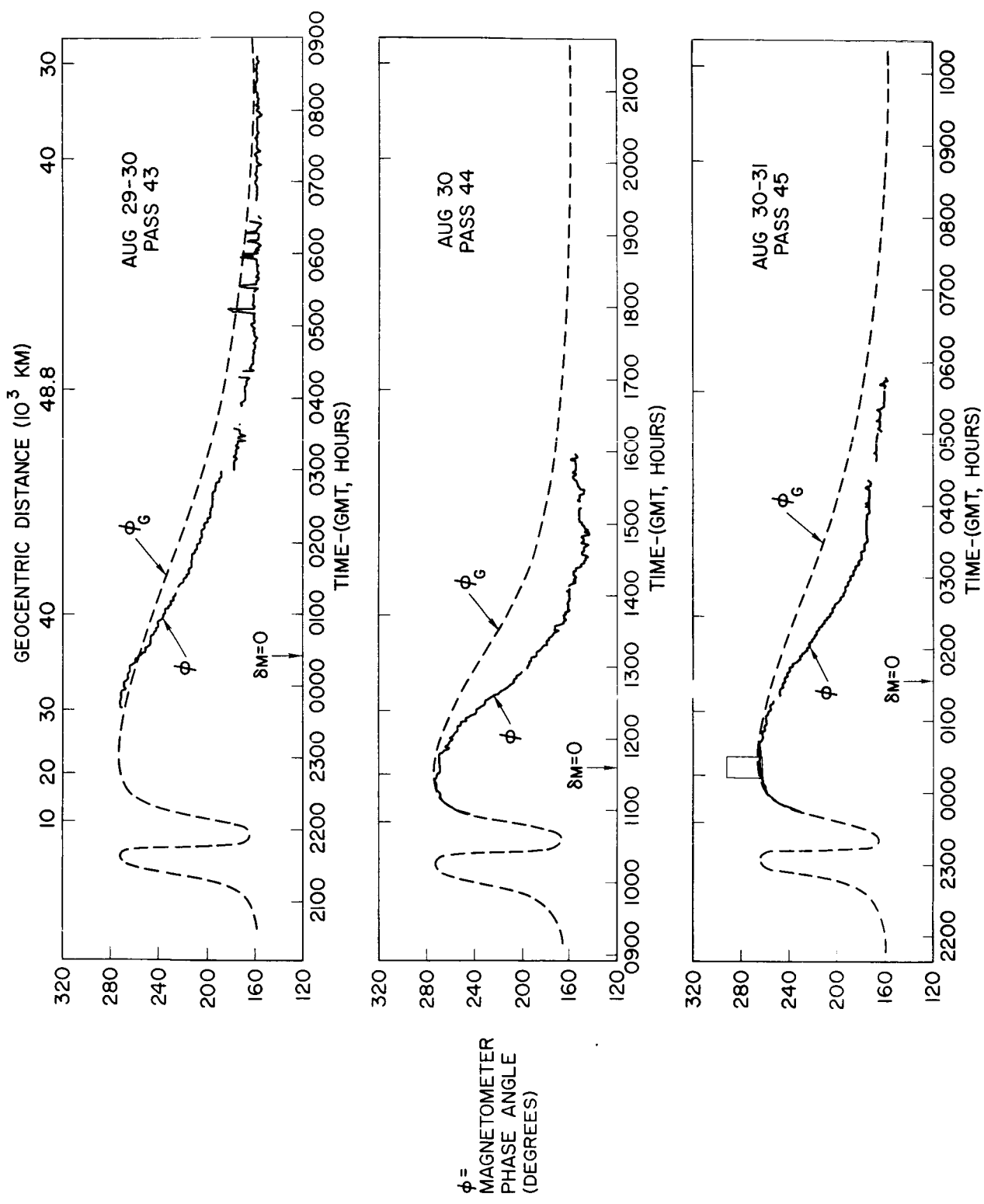


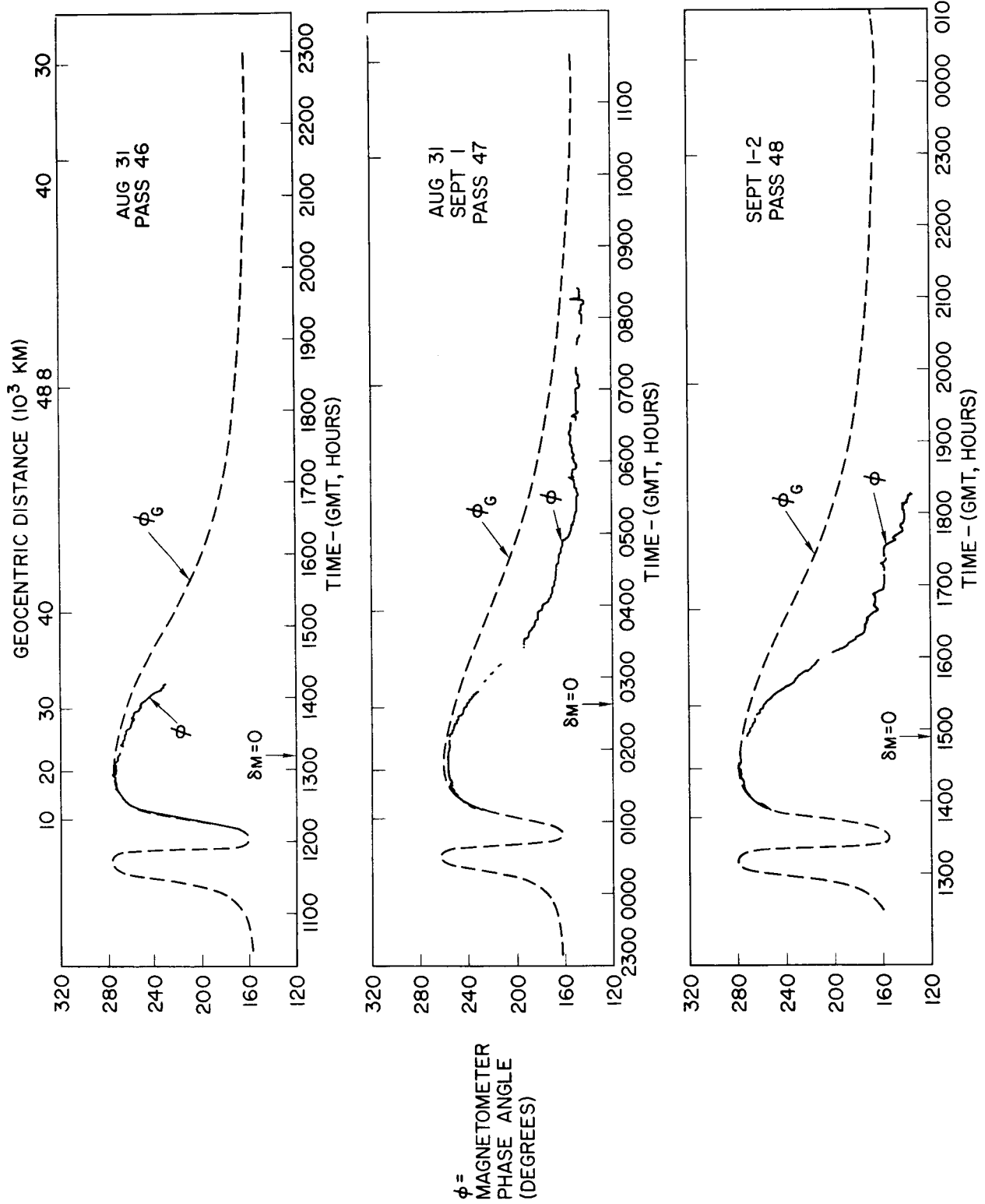


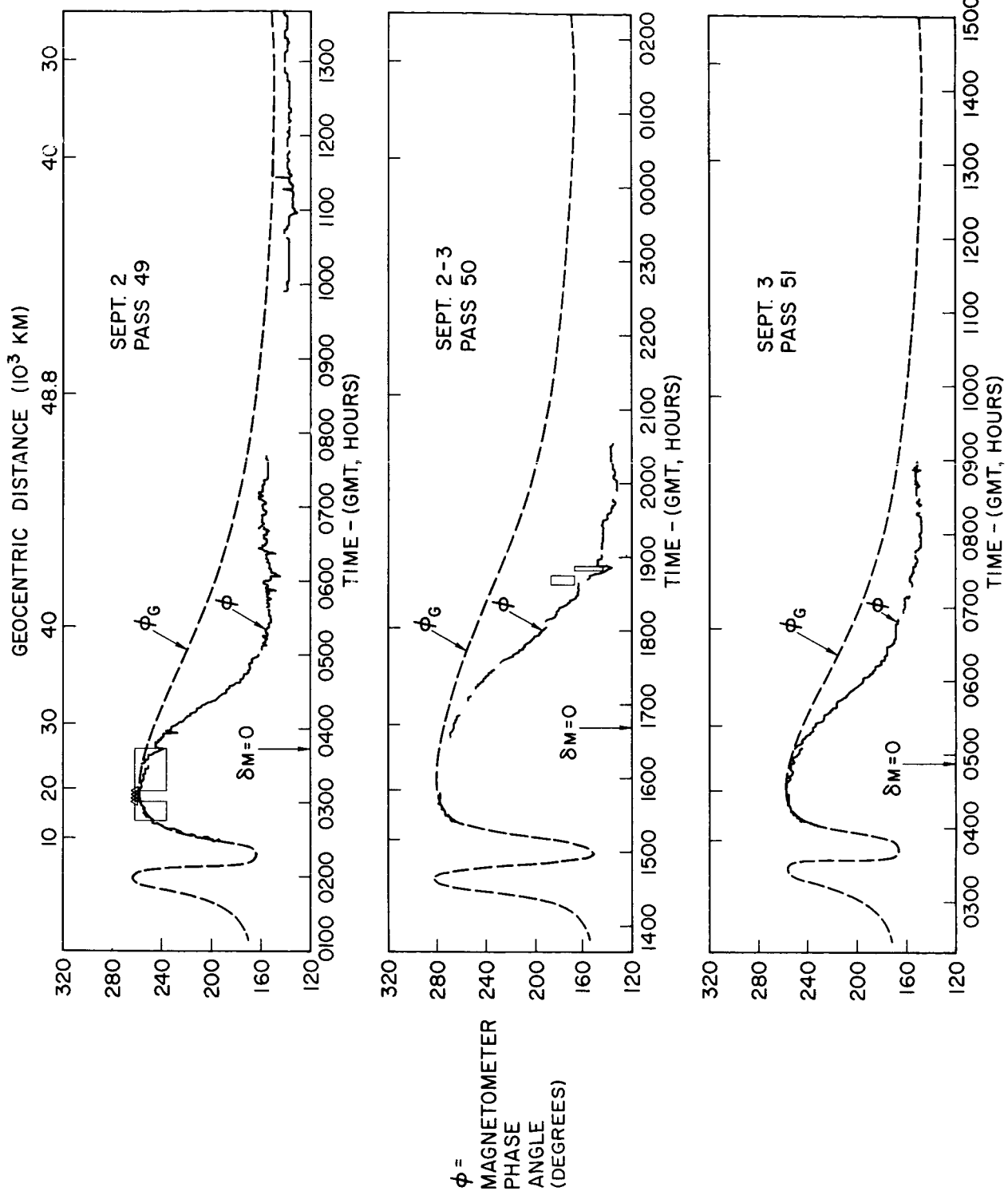


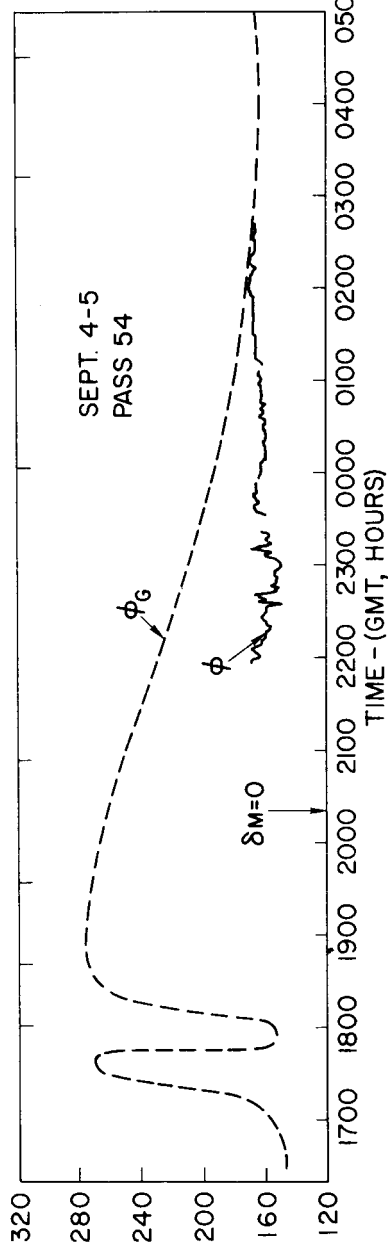
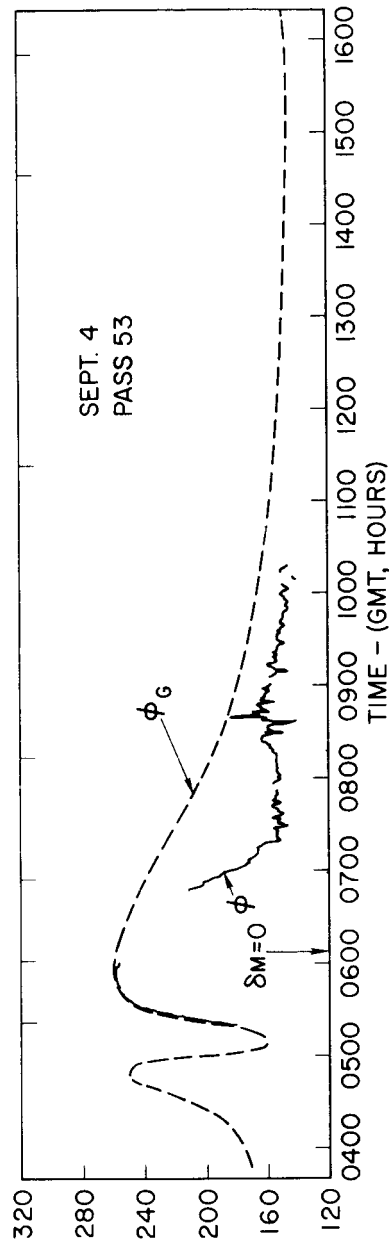
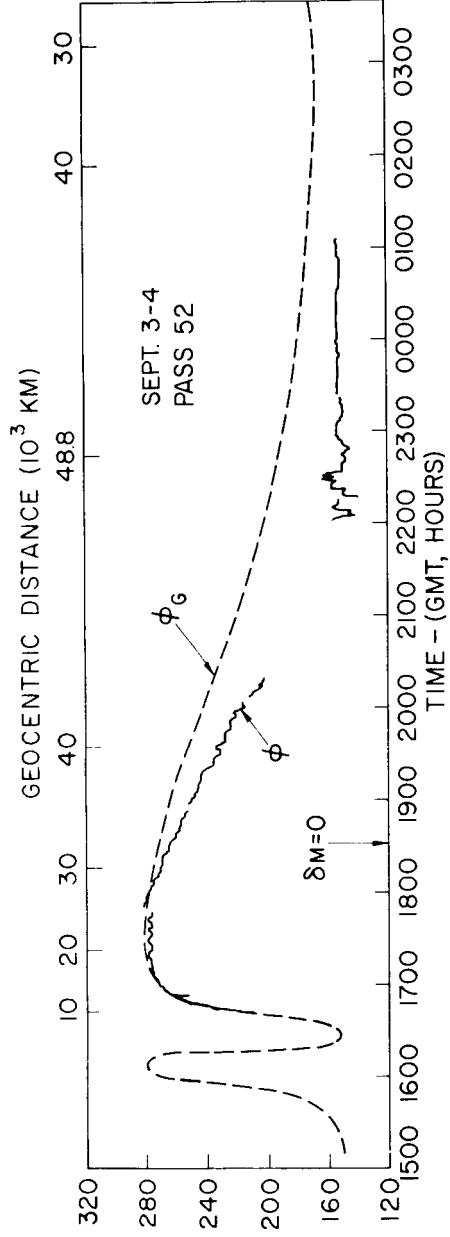




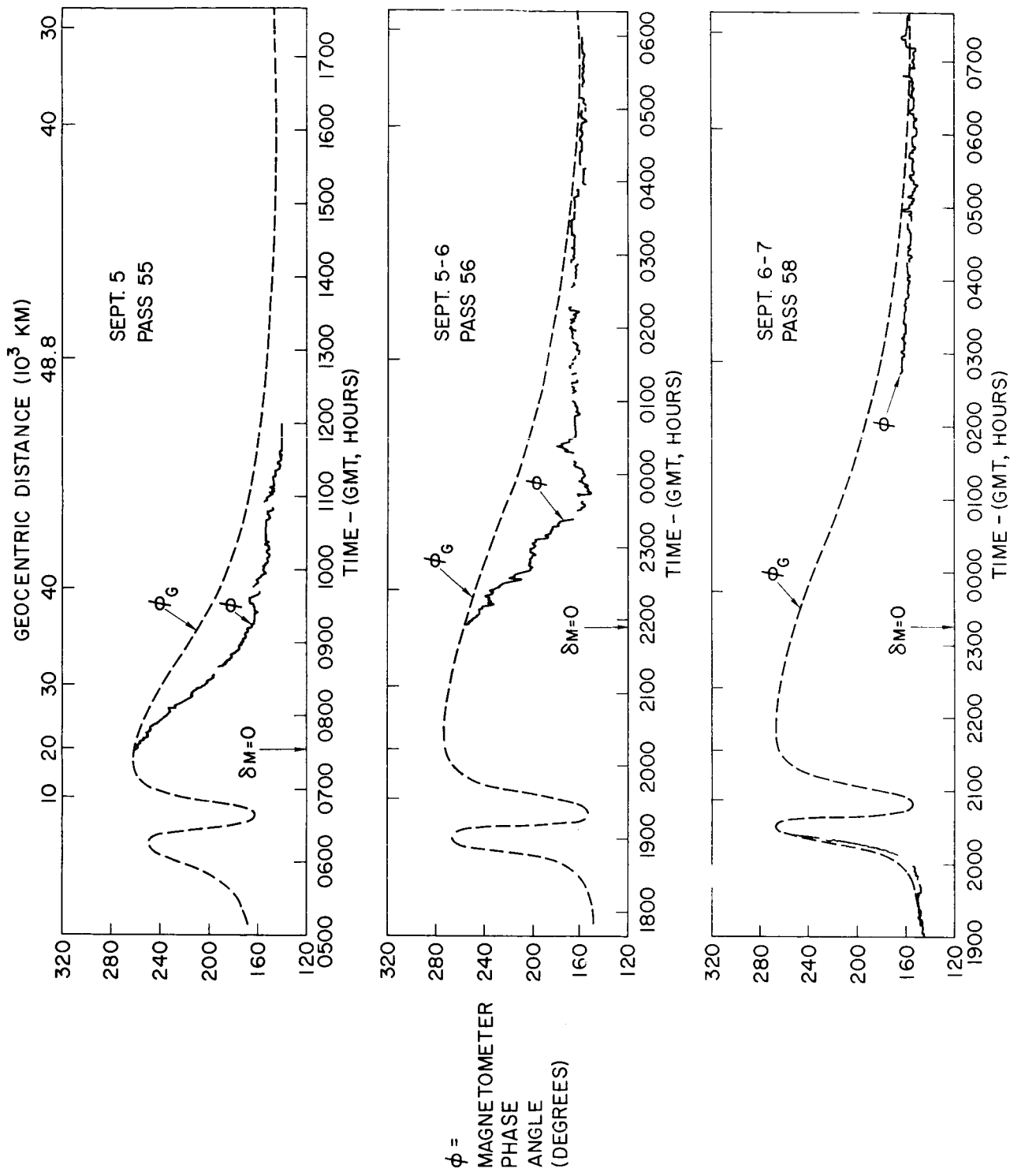


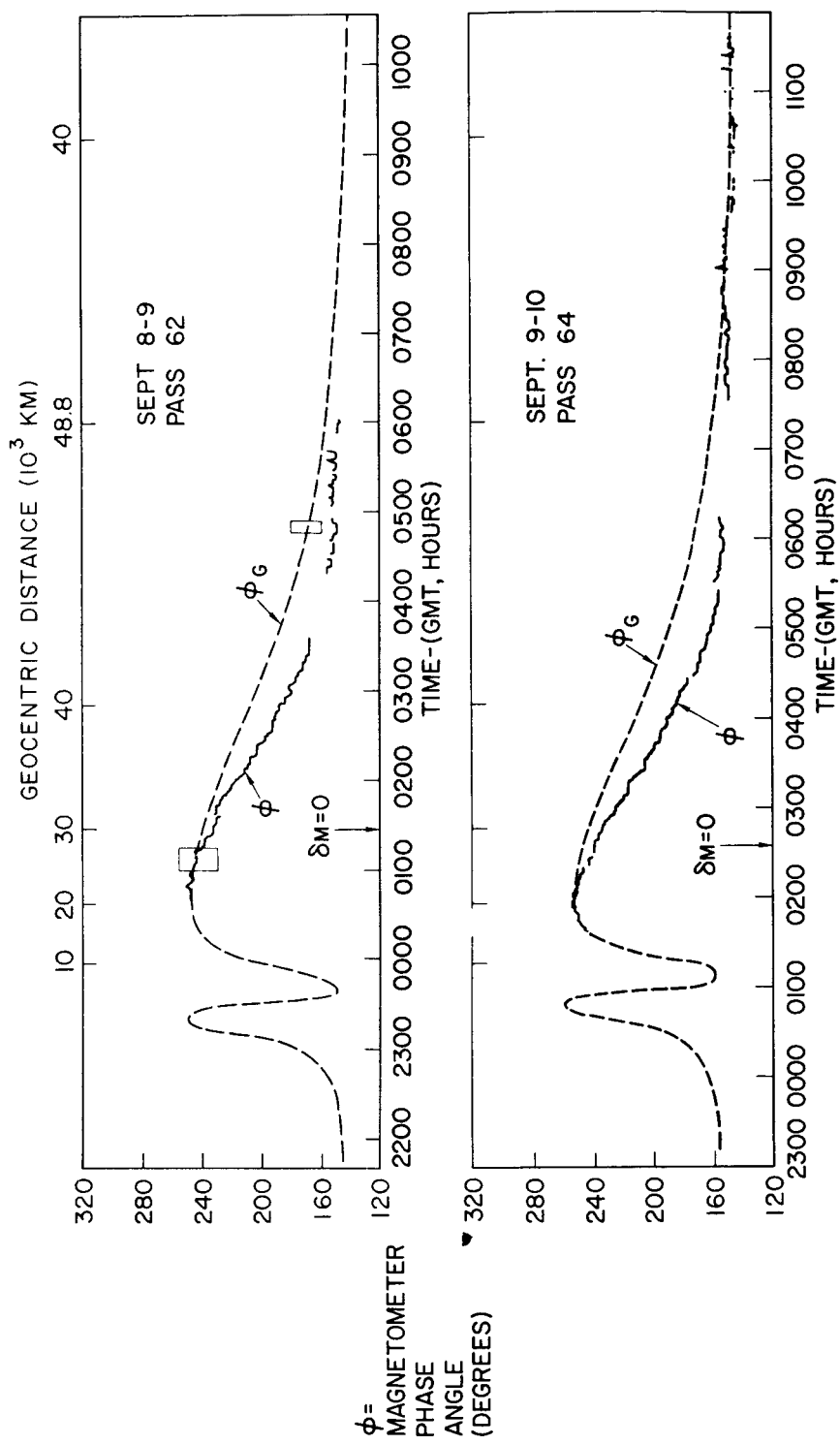






ϕ =
MAGNETOMETER
PHASE
ANGLE
(DEGREES)





Appendix

Computation of B_+ and ϕ

1. We assume that the spacecraft coordinates are given in the non-rotating, earth-centered system (X, Y, Z). Z lies along the earth's rotation axis and points north. X and Y lie in the geographic equatorial plane with X directed toward the vernal equinox. We assume also that the components of the field vector in geographic coordinates (B_r , B_λ , B_δ , where r is the radial distance and λ and δ are geographic longitude and latitude) are known. If B is the geomagnetic field, B_r , B_λ , and B_δ can be derived from formulae given in reference 3 or 6.

2. The magnetic field can be transformed into the inertial reference frame:

$$\begin{pmatrix} B_X \\ B_Y \\ B_Z \end{pmatrix} \begin{pmatrix} \cos\delta \cos\epsilon & -\sin\epsilon & -\sin\delta \cos\epsilon \\ \cos\delta \sin\epsilon & \cos\epsilon & -\sin\delta \sin\epsilon \\ \sin\delta & 0 & \cos\delta \end{pmatrix} \begin{pmatrix} B_r \\ B_\lambda \\ B_\delta \end{pmatrix}$$

where δ is the spacecraft latitude

and ϵ is $\tan^{-1} \frac{Y}{X}$.

3. Let the three orthogonal axes of the spacecraft reference frame be $\hat{\eta}, \hat{\xi}, \hat{\zeta}$, where $\hat{\zeta}$ is directed along the satellite spin axis. We assume the components of the spin axis in inertial space (ξ_X, ξ_Y, ξ_Z) are known, since the direction of the spin axis is an inertial invariant. Let \hat{s} be a unit vector in the earth-sun direction. The components s_X, s_Y, s_Z , given in the Nautical Ephemeris (7), can be normalized to give s_X, s_Y, s_Z . Thus,

$$s_X = \frac{s_X}{\sqrt{s_X^2 + s_Y^2 + s_Z^2}} \quad \text{etc.}$$

4. The matrix, $[\beta]$, transforms B_X , B_Y , B_Z into the satellite reference frame:

$$\begin{pmatrix} B_x \\ B_y \\ B_z \end{pmatrix} = \begin{pmatrix} \beta_{11} & \beta_{12} & \beta_{13} \\ \beta_{21} & \beta_{22} & \beta_{23} \\ \beta_{31} & \beta_{32} & \beta_{33} \end{pmatrix} \begin{pmatrix} B_X \\ B_Y \\ B_Z \end{pmatrix}$$

where

$$\beta_{31} = \xi_X$$

$$\beta_{32} = \xi_Y$$

$$\beta_{33} = \xi_Z ,$$

$$\begin{pmatrix} \beta_{21} \\ \beta_{22} \\ \beta_{23} \end{pmatrix} = \frac{1}{\sqrt{1 - (\xi \cdot s)^2}} \begin{pmatrix} \hat{i} & \hat{j} & \hat{k} \\ \xi_X & \xi_Y & \xi_Z \\ s_X & s_Y & s_Z \end{pmatrix}$$

$$\text{with } \xi \cdot s = \xi_X s_X + \xi_Y s_Y + \xi_Z s_Z ,$$

and

$$\begin{pmatrix} \beta_{11} \\ \beta_{12} \\ \beta_{13} \end{pmatrix} = \begin{pmatrix} \hat{i} & \hat{j} & \hat{k} \\ \beta_{21} & \beta_{22} & \beta_{23} \\ \xi_X & \xi_Y & \xi_Z \end{pmatrix}$$

These relations state that one coordinate coincides with the spin axis direction, the second coordinate is orthogonal to the spin axis direction (i.e. it lies in the equatorial plane of the satellite) and the sun-satellite direction, and the third forms the remaining member of a right-handed set.

5. The transverse component is

$$B_{\perp} = \left[B_{\eta}^2 + B_{\phi}^2 \right]^{1/2},$$

and the phase angle is

$$\phi = \tan^{-1} \frac{B_{\phi}}{B_{\eta}}.$$

Space Technology Laboratories, Inc.
Redondo Beach, California
November 1962